Leibniz-Institut
für Festkörper- und
Werkstoffforschung
Dresden

Annual Report 2013

Contents

Flashback to 2013

This Annual Report 2013 of the IFW presents a typical cross section of our scientific activities in the past year, highlighting main results in the first part and giving a somewhat more systematic overview of results obtained in our five Research Areas in its second part. In the back part this report contains the full list of published scientific articles and invited talks held by IFW researcher in 2013, along with other lists of PhD theses, patents, conferences and guest scientists. The very first pages of the Annual Report are devoted to a flashback on the institutes live in 2013: highlights, events and important developments beyond scientific results.

The year 2013 was a time of hard strategic work in the IFW: Present and upcoming personnel changes in the Institute's management, the forthcoming evaluation by the Leibniz Senate and recent developments of research politics and funding surroundings on local, national and European scale continue to drive a broad and intense discussion on a newly defined positioning of the IFW Dresden and on the further development of our research program. The Scientific Advisory Board and the Board of Trustiees are accompanying the strategy process which is not yet completed.

Concerning the personnel changes Prof. Dr. Jürgen Eckert took over the position of IFW's Scientific Director on April 1, 2013 from Prof. Dr. Ludwig Schultz, who has been responsible for the scientific work of the IFW Dresden since 2008. He remains the director of the IFW-Institute of Metallic Materials until a successor is appointed which is expected for autumn 2014. The Saxon Minister of Science and Arts, Prof. Dr. Sabine von Schorlemer, the Leibniz President Prof. Dr. Karl Ulrich Mayer and the Rector of the Dresden University of Technology Prof. Dr. Hans Müller-Steinhagen were present at the inauguration ceremony of the new Scientific Director and highly appreciated not only the merits of the departing and the new directors but also the outstanding scientific achievements and the innovative performance of the IFW both as a main player within the Dresden and Saxon research networks and as one of the largest Leibniz Institutes.

The IFW benefits a lot from well-established regional networks, especially from the close and fruitful cooperation with the Dresden University of Technology which is one of Germanys Universities of Excellence. A new form of cooperation between TU Dresden and

Change of office of the Scientific Director:
From Ludwig Schultz(left) to Jürgen Eckert (middle)

Conferring the honorary doctorate
to Lothar Dunsch

IFW goes international at the
Long Night of Sciences

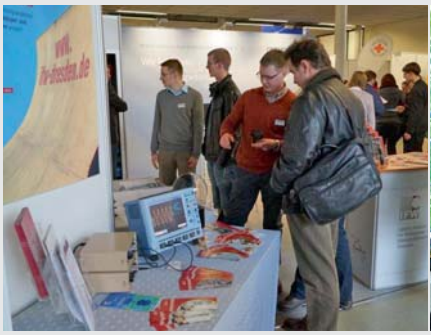

IFW was established in 2013 with the formation of the Centre for Transport and Device (CTD) as a joint institution on faculty level at TU Dresden. On the part of the university it involves the faculty of science, the faculty of mechanical science and engineering, and the faculty of electrical and computer engineering. The IFW is the main non-university partner of the CTD and contributes specialized laboratories and expertise for low-temperature facilities and characterization methods. The scientific focus of CTD is on emergent materials that are going to be fabricated, experimentally investigated, theoretically modelled and tailored into nanoscale electronic devices. Further the IFW is involved in the Cluster of Excellence "Center for Advancing Electronics Dresden (cfAED)" which addresses the advancement of electronic information processing systems ranging from Silicon nanowires and organic electronics up to large-scale heterogeneous information-driven engineering. Equally the cooperation with the Chemnitz University of Technology has been further strengthened by close cooperation in a number of joint projects including the Cluster of Excellence MERGE „Technologies for Multifunctional Lightweight Structures". The IFW is the central partner of the DFG Research Group "Molecular Spintronics" which joins all four Saxon universities (TU Dresden, TU Chemnitz, Leipzig University and TU Bergakademie Freiberg) and has been approved for a second funding period beginning from 2013.

As a Leibniz Institute the IFW is budgeted by the federal government and the German federal states in equal parts. However, an important index of quality is the amount of third party project funding. The level of third party funding in 2013 amounts to 13 Mio. Euro – a level at the forefront of the Leibniz Association. Most of this project funding was acquired in a highly competitive mode from the DFG and the EU. In particular the grants of three Emmy Noether Research Groups by the DFG show the competitive capability of the IFW. Among the large number of third party funded projects are three DFG-Priority Programs that are coordinated by the IFW, further four DFG-Priority Programs where the IFW participates, as well as three DFG Research Groups where the IFW participates. As in the previous years the IFW has been very successful in initiating EU projects and participating in them. Though quite time consuming these project applications have very positive effects on networking the IFW with other European groups. Eight of our 17 EU projects running in 2013 are coordinated by the IFW. Concerning the "Pakt für Forschung" the IFW was successful with its new proposal on "Tailored manipulation of fluids in functionalized highly integrated micro- and nanoscale fluidic systems". After having

Guests from South Korea visiting the IFW's cleanroom

IFW presentation at the fair "KarriereStart"

IFW contributed to and coordinated the new video clip on professional training in Leibniz Institutes

been awarded two ERC starting grants in 2012, IFW researchers could continue their success with this highly prestigious European funding program in 2013. Prof. Dr. Jürgen Eckert received an ERC Advanced Grant with a proposal on metastable alloys and Dr. Carmine Ortix received an ERC FET young researcher grant for research using curved nano-membranes for topological quantum computation.

Essentially publicly funded, the IFW is obliged to make its research results public. 382 publications in scientific journals and conference proceedings report on the IFW's research results on the year 2013. In 287 invited talks the Institute's scientists presented their work at other places around the world. 13 patents were issued for the IFW, and applications for 13 more patents have been made. This all indicates the attested high level on which the Institute carries out its research.

The IFW continued its large efforts to make scientific work accessible for the general public and to inspire young people to study science or engineering also in 2013. The IFW took part in many joint actions like the lecture series "Physics on Saturday", "Junior Doctor" or the Summer University of the TU Dresden. The Dresden Long Night of Sciences took place for the eleventh time in 2013, and again, the IFW offered an ample program which attracted about 4000 visitors. Besides these big events we organize almost weekly lab-tours for various visitor groups, from school classes through official representatives to guests from foreign organizations. Especially the IFW's superconducting test facility SpuraTrans in Dresden-Niedersedlitz has proved very popular among visitors, be it representatives from companies, students groups or politicians.

With respect to the infrastructural development we have put large efforts during the last years into the realization of a new annex building with special laboratory areas and additional office space. Now we are looking forward to the completion of construction works and the move-in of the first research groups in beginning of 2014.

2013 was again a yielding year with respect to prizes and honors awarded to members of the IFW. A full list of prizes awarded to members of the IFW is included at the end in this Report. Among them is the prestigious Junior Research Award of the Leibniz Association for Dr. Kristina Tschulik. In 2013 the IFW has been honored as being among one of the best training places for professional graduation in our region. Marco Naumann

successful completion of vocational training at IFW

hands-on experiments with superconductivity and magnetism

Presentation of the IFW Research Award to Denys Makarov

was awarded a prize for the best results in professional graduation of all physics laboratory assistant trainees in Germany. Furthermore, three scientists of the IFW have been appointed to professorships at universities in 2013: Prof. Dr. Bernhard Holzapfel accepted a call to the Karlsruhe Institute of Technology, Dr. Sabine Wurmehl refused a call to University of Colonia and Dr. Jens Freudenberger is being negotiating with TU Bergakademie Freiberg. Eight IFW members have been awarded the status of Honorary or Associated Professors at Universities in Chemnitz, Freiberg, Bucharest, Timisoara, Bratislava and Seoul.

A crucial part of the IFW's identity is its vivid life including the cultivation of the scientific dialogue, family-friendly working conditions, intercultural diversity and the support of sportive and cultural activities. In 2013 the IFW was re-audited as a family-friendly institution and received the certificate "Beruf und Familie". The IFW organizes a series of workshops, colloquia and talks to foster the scientific dialogue and, along the way, allow for social and communication aspects of cooperation. An important meeting for all scientists of the IFW is the yearly two-day program session where all scientists discuss and adjust the research program for the following year. Also the annual IFW Winter School contributes to the scientific communication among all IFW groups and to the training of young scientists in special topics of the IFW research program.

The positive development of the IFW is being fostered continuously by the engagement of colleagues and partners from universities, research institutes and industry, our Scientific Advisory Board and the Board of Trustees as well as the funding organizations. We would like to thank all of them for their support and cooperation.

Dresden, January 2014

Prof. Dr. Jürgen Eckert
Scientific Director

Hon. Prof. Dr. h. c. Rolf Pfrengle
Administrative Director

Presentation of the Audit "Beruf und Familie"

Ongoing construction work for the new annex building during 2013

Kids program during the Long Night of Sciences at IFW

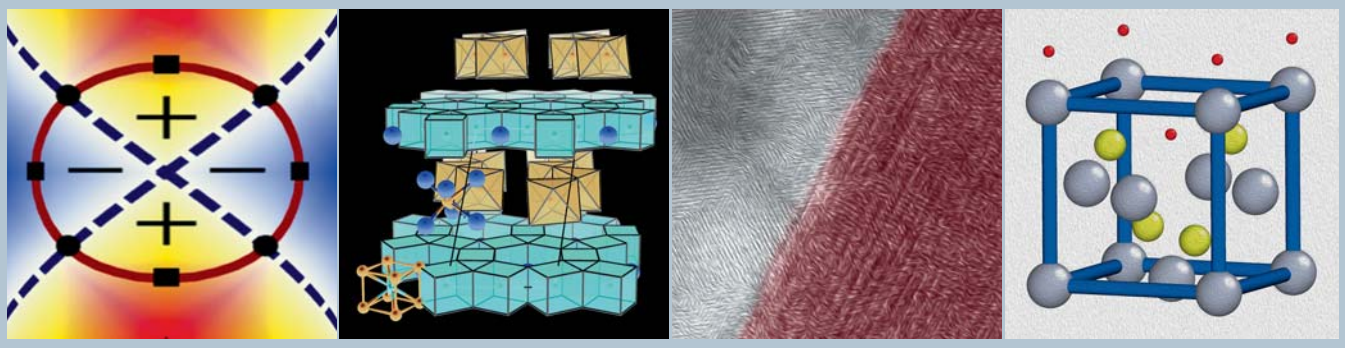

Highlights 2013

Highlights

Fe-based superconductors cannot live with or without magnetism

S. Haindl

The diversity in physical properties and the large number of different compounds (classified into families of 11-, 111-, 122-, 1111, etc.) let Fe-based superconductors quickly promote to a hot topic in modern condensed matter physics. Their discovery within the last decade inspired scientists to improve their understanding about the mechanism of high temperature superconductivity as well as about the complex coupling between structural and electronic degrees of freedom in a solid. During the second funding period of the DFG Priority Programme new projects at IFW Dresden try to unravel the secrets of superconducting pairing in Fe-based superconductors. The most challenging experiment - the design of a phase sensitive test for Fe-based superconductors - is currently an essential topic in collaboration with the University of Tübingen.

Probing the Superconducting Pairing Mechanism

Almost hundred years after the discovery of superconductivity, the new material class of Fe-based superconductors (Fe-pnictides, Fe-chalcogenides) reinforced a core topic of condensed matter physics: the loss-free transport of electrical current that arises from a pairing interaction between electrons below a critical temperature. The remarkable observation in the Fe-based superconductors is their extraordinary high critical temperature (up to 66 K) despite the vicinity of magnetic order. This excitement within the superconductivity community has often been commented as the transition from the '*cuprate*' to the '*iron age*'. Despite the huge amount of experimentally collected data the puzzle remains: On the one hand the magnetic order competes with superconductivity, on the other hand it is speculated that the magnetic order mediates the pairing interaction leaving behind a fingerprint in the theoretically proposed $s\pm$ symmetry of the order parameter.

A primary goal in the understanding of the Cooper pairing mechanism, that is believed to be triggered by spin fluctuations, is the investigation of the generic electronic phase diagram of the new materials. Coupling between structural (lattice), spin, and orbital degrees of freedom results in a highly complex electronic phase diagram showing an antiferromagnetic spin-density wave state, as well as a nematic phase in vicinity to a superconducting one that appears upon doping in most Fe-based superconductors. Therefore, the control of the doping content plays a crucial role in sample fabrication. Especially, in Co-doped $BaFe_2As_2$ films grown on Fe buffered substrates it turned out to be more difficult than expected. Surprisingly, the examination of the electronic phase diagram on the basis of $Ba(Fe_{1-x}Co_x)_2As_2$/Fe/MgO thin films revealed higher critical temperatures, T_c, in the under- and over-doped regime (Fig. 1a). On the one hand, this observation manifests the sensitive balance between concurrent mechanisms: spin density wave and superconductivity contest for the same electronic states at the Fermi level in underdoped 122 materials. On the other hand, stoichiometry control is a major issue for thin film fabrication.

In the supervised diploma thesis of Kurth *et al.* [1] disorder (presumably caused by As vacancies) and dopant inhomogeneities (Fig. 1b) were discussed as the main candidate responsible for an enhancement in T_c. For the underdoped region, the arguments follow the theoretical predictions that a weakening of the spin-density wave results in the increase of the superconducting transition.[2] Since the investigated films show As

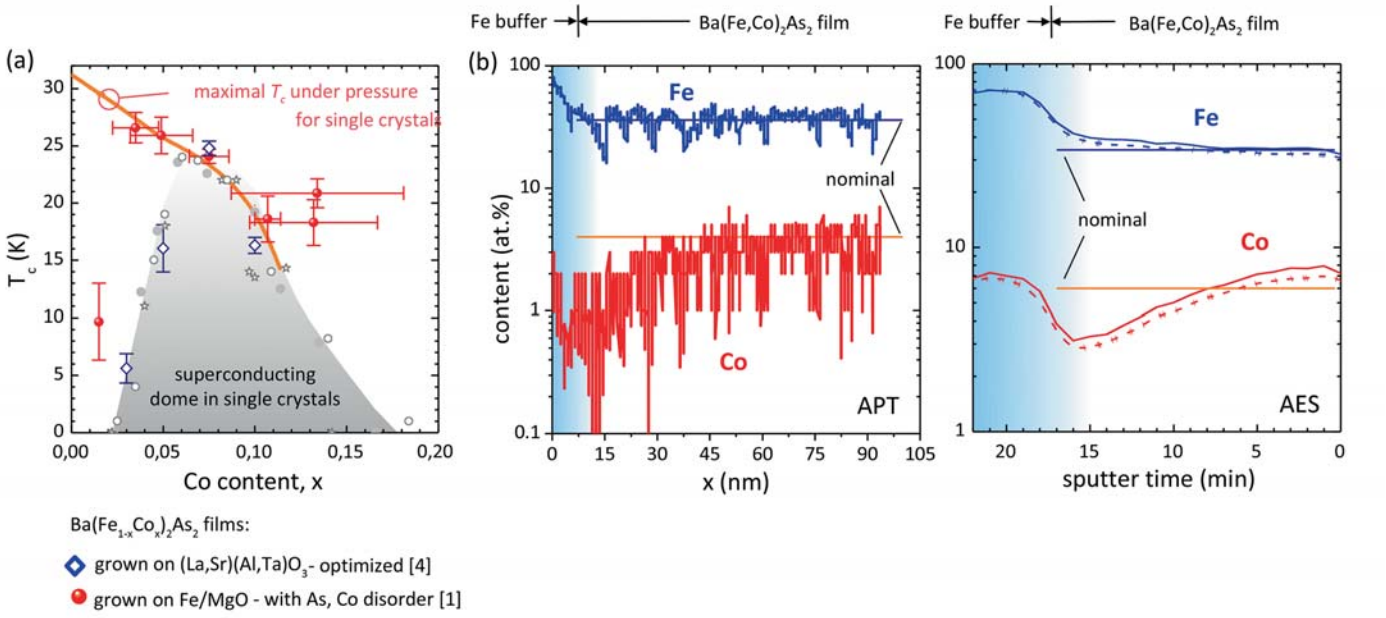

Fig. 1: (a) Comparison of the superconducting transition in thin films grown on Fe-buffered MgO substrates (red symbols), [1] in optimized films grown on (La,Sr)(Al,Ta)O_3 substrates (blue symbols), [4] and in single crystals (grey symbols). [5] The orange curve indicates the maximal T_c of Ba(Fe$_{1-x}$Co$_x$)$_2$As$_2$ single crystals under hydrostatic pressure as given in [6]. **(b)** Atomic Probe Tomography (APT) for a Ba(Fe$_{0.85}$Co$_{0.10}$)$_2$As$_2$ thin film grown on Fe/MgO and Auger Electron Spectroscopy (AES) for a Ba(Fe$_{0.85}$Co$_{0.15}$)$_2$As$_2$ thin film grown on Fe/MgO confirm the inhomogeneity in Co-content along the film thickness. (Figures taken from [7].)

deficiency, As vacancies may give rise to a strong impurity scattering potential, or, lead to the formation of magnetic moments (as discussed at IFW Dresden by S.-L. Drechsler an co-workers already for oxypnictides), both being able to suppress the spin density wave for the underdoped case.[2,3]

Similarily, pressure experiments on single crystals show an enhancement in T_c in underdoped Ba(Fe$_{1-x}$Co$_x$)$_2$As$_2$ compounds.[6] A thin strained layer thus be also responsible for the observed results but, unfortunately, effects of disorder and strain in the films cannot be disentangled experimentally, and there is no study so far that quantifies the influence of strain in pnictide thin films.[7]

Focus on Landmark Studies

The above example for Co-doped $BaFe_2As_2$ thin films demonstrates the technical difficulties in stoichiometry control of the dopant and also of volatile components like As. In contrast, large efforts in optimization of the growth conditions were undertaken at the Tokyo Institute of Technology (blue symbols in Fig. 1a). It is not a surprise that film growth of the more complex oxypnictides is still a greater challenge. An *all-in-situ* pulsed laser deposition growth of oxypnictides failed so far, but the room-temperature deposition of oxypnictides on $LaAlO_3$ substrates with a subsequent heat treatment under vacuum conditions resulted in polycrystalline and even epitaxially grown films of the 1111 family.

The successful growth of F-doped LaOFeAs and (La,Sm)OFeAs thin films based on a *two-step* process enabled fundamental research on this highly interesting compound. Temperature dependence of the upper critical field and its anisotropy were discussed on the basis of a *two-band* model.[8] Furthermore, in collaboration with Brookhaven National Laboratory time resolved infrared spectroscopy indicated large quasi-particle relaxation times typically observed in *s-wave* superconductors.[9] This experiment, however, is not able to distinguish between a pure *s-wave* state and the anticipated *s*± symmetry of the superconducting order parameter, which is an ongoing debate.

In order to test the superconducting order parameter symmetry, phase-sensitive tests have to be performed that are able to probe the phase-shift of magnitude π for *s*± symmetry, similar as it was observed in a milestone experiment for cuprate superconductors. In the latter case, the *d-wave* symmetry of the order parameter caused a π-shift in phase sensitive measurements.

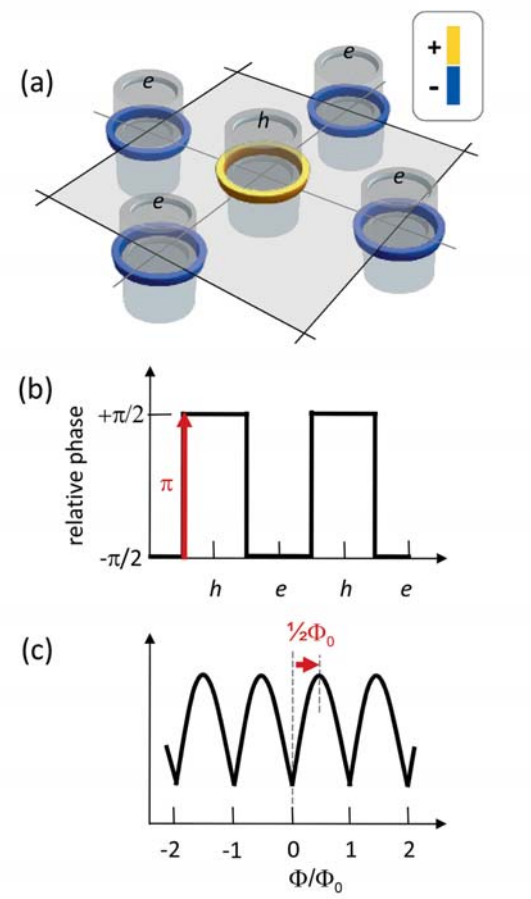

Fig. 2: (a) Schematic sketch of the $s\pm$ symmetry of the superconducting gap around hole (orange denoting +) and electron (blue denoting –) Fermi surfaces. **(b)** The relative phase shift between the superconducting gap around hole and electron band jumps by π. **(c)** Expected maxima positions of the critical currents dependent on the magnetic flux obtained in an appropriate SQUID interferometry experiment.

At present no distinctive phase sensitive experiment has been carried out for Fe-based superconductors. Thus, a direct observation of the $s\pm$ symmetry would be a key breakthrough and immidiately validate main theoretical concepts. Furthermore, it is speculated that the superconducting pairing may also deviate from the $s\pm$ symmetry in certain compounds. For example, *d-wave* symmetry was proposed for the purely hole doped KFe_2As_2, whereas *p-wave* symmetry appeared as candidate in LiFeAs. In a recently granted project within the DFG priority programme (SPP 1458) phase sensitive tests will be designed on Fe-based superconductors in collaboration between IFW Dresden and University of Tübingen. (Fig. 2)

Epitaxial Thin Film Growth Re-Examined

Despite the fact that Fe-pnictides and Fe-chalcogenides play a pivotal role in superconductivity research, prospects for their commerzialization turned out to be too little, not at least because of the lack of reproducibility in thin film fabrication and their still moderate success competing with properties of conventional superconductors or cuprates already in use. A closer inspection of thin film growth efforts and feasibility studies reveals certain drawbacks of the new superconductors for their commercialization that is often ignored due to the tendency of an unrealistic optimism. An invited comparative review [7] demonstrates the gap between the often *claimed* application potential and functional device realization in discussing key parameters of functional superconducting films and their difficult control.

In an ESF Exploratory Workshop organized in 2011 power applications and Josephson junction devices for Fe-based superconductors were evaluated as promising future routes. However, at present, a coated conductor technology based on Fe-pnictides and Fe-chalcogenides is still an exotic scenario since the critical current densities of the new superconductors neither exceed those of already applied materials nor do these compounds expand the range of device (for example, magnet) operation or reduce fabrication/operation costs. A similar assessment can be given for Josephson junction based devices. The fabrication of thin film junctions based on the new superconductors is a tremendous challenge. Nevertheless, it may be worth to test the electronic application potential for the new superconductors.

Turning the focus on fundamental experiments using thin film material, the review [7] also points out the many different problems concerning phase homogeneity, stoichiometry and impurities that document their yet insufficient control. An APT analysis of $Fe/Ba(Fe_{1-x}Co_x)_2As_2$ heterostructures demonstrates the detrimental influence of high deposition temperatures on the 122 phase stoichiometry resulting in spatial elemental concentration inhomogeneities (Fig. 3). In addition, the reported magnetic impurities

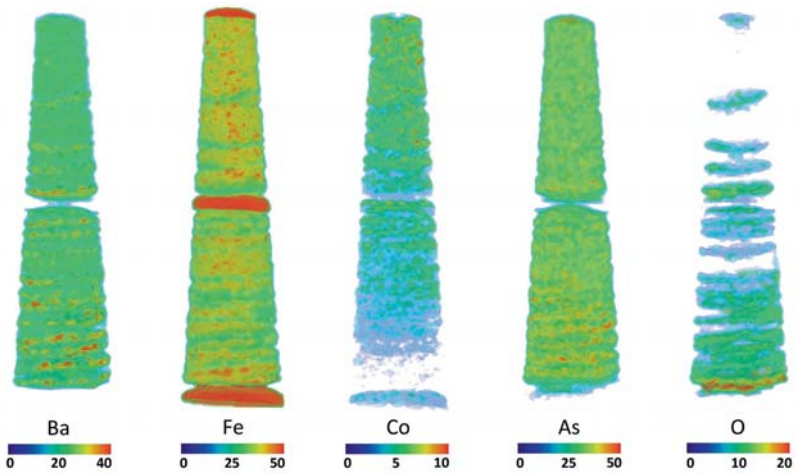

Fig. 3: Atomic Probe Tomography (APT) efforts in analyzing thin film stoichiometry: Spatial elemental inhomogeneities in the heterostructure of $Ba(Fe_{1-x}Co_x)_2As_2/Fe/Ba(Fe_{1-x}Co_x)_2As_2/Fe$. (Fig. taken from [7].)

in Fe-pnictide and Fe-chalcogenide thin films certainly mask any correct interpretation of superconducting pairing mechanism or symmetry. In a current DFG project the frontiers of film growth of Fe-based superconductors are pushed forward in order to obtain more insight in their electronic properties and how to tailor them.[10]

Acknowledgments: AES on thin films was carried out by S. Oswald (IFW Dresden). L. Wilde and S. Kölling (Fraunhofer IPMS – Center for Nanoelectronic Technologies Dresden) measured films by APT.

[1] F. Kurth *et al.*, Supercond. Sci. Technol. 26 (2013) 025014; F. Kurth, Diploma thesis TU Dresden (2012)
[2] D. J. Singh *et al.*, Physica C 469 (2009) 886; R. M. Fernandes *et al.*, PRB 85 (2012) 140512(R)
[3] K. Kikoin, *et al.*, arXiv: 1210.6536
[4] T. Katase *et al.*, Supercond. Sci. Technol. 25 (2012) 084015
[5] J.-H. Chu *et al.*, Phys. Rev. B 79 (2009) 014506; N. Ni *et al.*, Phys. Rev. B 78 (2008) 214515; F. L. Ning *et al.*, Phys. Rev. Lett. 104 (2010) 037001
[6] E. Colombier *et al.*, Supercond. Sci. Technol. 23 (2010) 054003
[7] S. Haindl *et al.*, Rep. Prog. Phys. 77 (2014), accepted for publication
[8] S. Haindl *et al.*, Int. J. Mod. Phys. B 27 (2013) 1330001
[9] X. Xi *et al.*, PRB 87 (2013) 180509
[10] S. Borisenko, Nature Mat. 12 (2013) 600

Funding: The continuous research at IFW Dresden on Fe-based superconducting thin films is led by German Research Foundation (DFG) under projects HA5934/1-1, HA5934/3-1, HA5934/4-1. European Science Foundation (ESF) is acknowledged for funding the Exploratory Workshop on Physics and Technology of Iron Pnictide Thin Films in 2011. Current collaborations are funded by DFG projects HA5934/3-2 and HA5934/5-1.

Resonant Inelastic X-Ray Scattering as a Probe of the Phase and Excitations of the Order Parameter of Superconductors

P. Marra, S. Sykora, K. Wohlfeld, J. van den Brink, J. Geck

The capability to probe the dispersion of elementary spin, charge, orbital, and lattice excitations has positioned resonant inelastic x-ray scattering (RIXS) at the forefront of photon science. Here we develop the scattering theory for RIXS on superconductors, calculating its momentum-dependent scattering amplitude. Considering superconductors with different pairing symmetries, we show that the low-energy scattering is strongly affected by the superconducting gap and coherence factors. This suggests RIXS as a tool to disentangle pairing symmetries and to probe the elementary excitations of unconventional superconductors.

Resonant inelastic x-ray scattering (RIXS) [1] is an established spectroscopic technique and in a number of cases theoretical considerations have preceded and stimulated these experimental advances. Being a photon-in–photon-out spectroscopy, both the energy $\hbar\omega$ and the transferred momentum $\mathbf{q}$ of the scattered photon are measured and therefore direct information on the dispersion of excitations becomes available. Compared to the available spectroscopic methods, such as scanning-tunneling spectroscopy (STS), photoemission spectroscopy, optical spectroscopy, or inelastic neutron scattering, RIXS uniquely combines the advantages of bulk sensitivity and availability of momentum resolution while at the same time requiring only small sample volumes. The energy resolution of RIXS is designed to reach 11 meV at the Cu L edges at the NSLS-II (Brookhaven National Laboratory) presently under construction [2]. This brings the RIXS energy resolution well into the regime of the energy gap of cuprate superconductors, which stretches out to 119 meV for mercury-based high Tc systems [3]. Consequently, the fundamental question arises of how the superconducting (SC) state leaves its fingerprints in RIXS spectra—in particular, whether and how RIXS is sensitive to the phase and amplitude of the SC gap and to quasiparticle excitations.

In a recent study [4], we have investigated the RIXS cross section for a superconducting material considering the so-called direct RIXS process at the transition metal (TM) ion L edges, in which the incoming photon resonantly excites the core shell **2*p*** electron into the **3*d*** shell which consequently decays into an outgoing photon and a charge, spin, or orbital excitation in the electronic system [5]. In this case we could bring the RIXS cross section in the form $I_e(\mathbf{q},\omega) = |W_e^c|^2\chi^c(\mathbf{q},\omega) + |W_e^s|^2\chi^s(\mathbf{q},\omega)$ where $\chi^{c,s}$ is the charge (spin) dynamical structure factor (DSF). Thereby, the amplitude of the RIXS form factors W_e^c and W_e^s can be tuned by properly adjusting the experimental conditions in RIXS. This implies that RIXS at L edges can measure either spin or charge DSF depending on the chosen polarization, which is a unique feature of RIXS spectroscopy. In our work [4], we have considered the case of Cu ions in lattices with tetragonal symmetry, i.e., the one

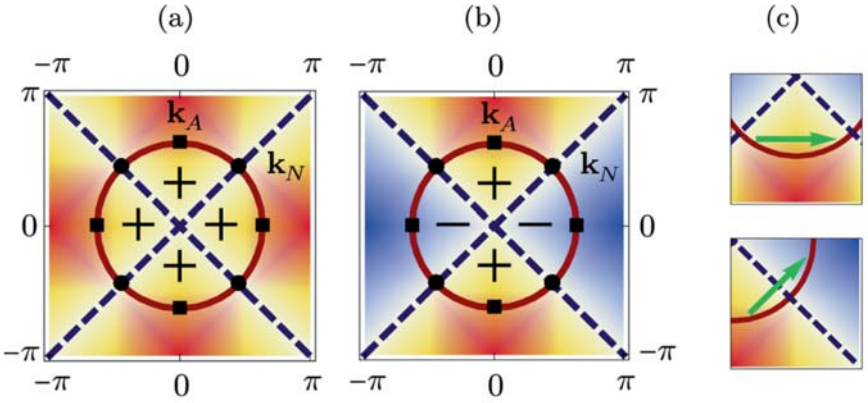

Fig.1: (a-c) Order parameters of an anisotropic *s*-wave **(a)** and *d*-wave **(b)** superconductor with an isotropic Fermi surface (solid line). The order parameter vanishes (has maxima) at the nodal points $\mathbf{k}_N$ (antinodal points $\mathbf{k}_A$). **(c)** Particle-hole excitations with and without sign reversal in the case of *d*-wave pairing.

which has direct relevance to the high T_c superconductors. Our main aim in this context was to establish how a variation of the phase of the SC order parameter is reflected in the spin and charge DSF. For this we considered two elementary types of pairing: (i) a *d*-wave pairing with $\Delta^d_{\mathbf{k}} \sim (\cos k_x - \cos k_y)$ and (ii) an anisotropic *s*-wave pairing with $\Delta^s_{\mathbf{k}} = |\Delta^d_{\mathbf{k}}| \sim |(\cos k_x - \cos k_y)|$, i.e., two pairing symmetries which differ from each other only in the SC order parameter phase. Maps of the considered gap functions and the Fermi surface are shown in Fig. 1.

The calculated quasiparticle spectra for the above two pairing symmetries are shown in Fig. 2(a) for a fixed and relatively large momentum transfer $q = k_F$, where k_F is the Fermi radius. Note that direct RIXS at the L edge in 2D cuprates allows momentum transfers $q \lesssim 0.87\pi$ [6], and therefore one is able to access momentum transfers of the order of k_F. Clearly, the spectral weight at $\hbar\omega = 2|\Delta|$ in the charge DSF is enhanced in the *s*-wave case. On the other hand, for the *d*-wave case the sign reversal leads immediately to a suppression of the DSF, which is confirmed by the dotted curve in Fig. 2(a). Note that due to the gap being equal in magnitude for both cases, the obtained effect is entirely due to phase changes of the SC order parameter along the Fermi surface.

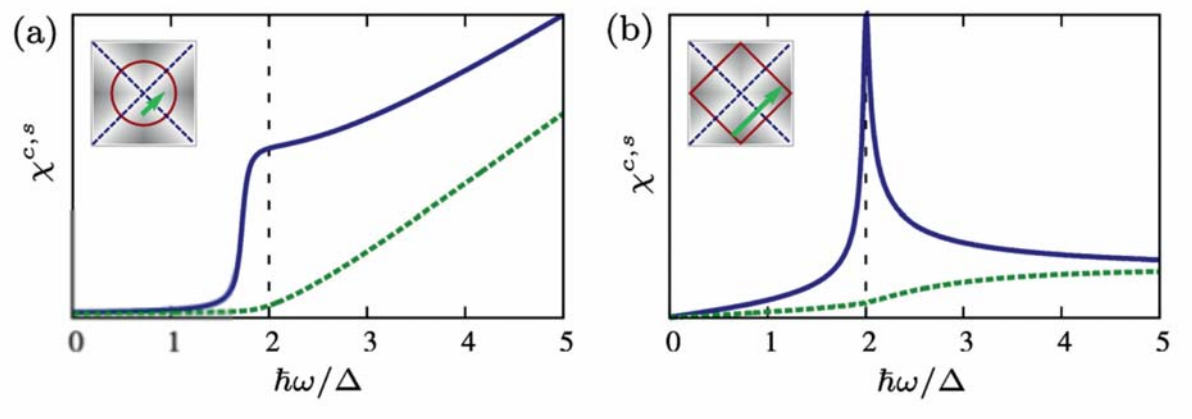

Fig. 2: Dynamical structure factor (DSF) in a SC for an isotropic **(a)** and for a nested Fermi surface **(b)** with transferred momentum $\mathbf{q} = (k_F, k_F)/\sqrt{2}$ and $\mathbf{q} = (\pi, \pi)$, for charge excitations (χ^c) with anisotropic *s*-wave (solid line) and *d*-wave (dashed line), and for spin excitations (χ^s) with *d*-wave (solid line) and anisotropic *s*-wave (dashed line).

In two-dimensional unconventional superconductors the conduction electrons show a tendency to Fermi-surface nesting with a typical nesting vector $\mathbf{Q} = (\pi,\pi)$. In Fig. 2(b) the scattering intensity as a function of energy for the two pairing symmetries considered above is shown again, but now for a perfectly nested cuprate-like Fermi surface (see inset), with a transferred momentum equal to the nesting vector. Now a coherence peak in the anisotropic *s*-wave pairing case appears due to the nesting effect. However, this peak is strongly suppressed in the *d*-wave case in the charge DSF as well as in the anisotropic *s*-wave case in the spin DSF due to the presence of sign preserving excitations.

To highlight its strong dependence on the order parameter phase, we show in Fig. 3 the DSF for a fixed energy $\hbar\omega = 2|\Delta|$ as a function of momentum $\mathbf{q}$ in the entire Brillouin zone, both for the anisotropic *s*-wave and the *d*-wave pairing, for a perfectly nested Fermi surface. Clearly, coherence peaks are visible in the spin DSF in the *d*-wave case for any of the nesting vector while they are strongly suppressed in the anisotropic *s*-wave case. Thus, the inherent phase sensitivity of RIXS enables to fully disentangle sign reversing and sign preserving excitations. This can be done in RIXS by tuning the polarization dependence in the form factors W^c_e and W^s_e.

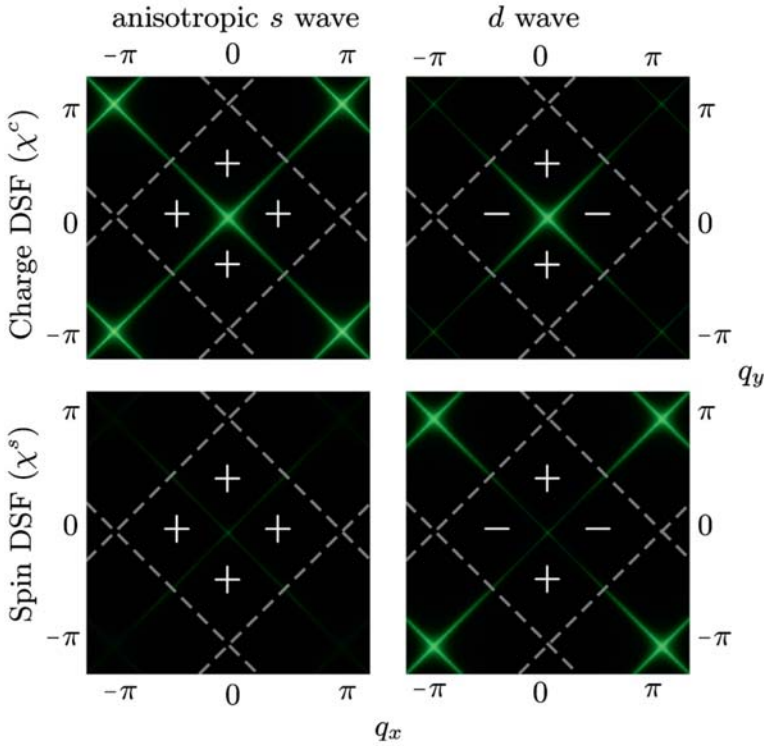

Fig. 3: Charge (χ^c) and spin (χ^s) DSF at fixed energy $\hbar\omega = 2|\Delta|$, as a function of transferred momentum for an anisotropic *s*-wave and a *d*-wave SC with a nested Fermi surface.

In conclusion we have shown that RIXS, in contrast to other well-known two-particle spectroscopies, is directly sensitive to the spin and to the charge DSF of a superconductor. This leads directly to a strong sensitivity of the RIXS spectra with respect to the symmetry of the order parameter. This, together with the recent experimental successes of RIXS, including, in particular, the major enhancements in resolution and pioneering study of hole doped cuprates[7], establishes the potential of RIXS as a versatile and practical spectroscopic technique to investigate the fundamental properties of superconducting materials.

[1] W. Schülke, Electron Dynamics by Inelastic X-Ray Scattering (Oxford University Press, Oxford, England, 2007)
[2] Brookhaven National Laboratory, Conceptual Design Report National Synchrotron Light Source II, 2006
[3] G. Yu, et al., Nat. Phys. 5, 873 (2009)
[4] P. Marra, S. Sykora, K. Wohlfeld, J. van den Brink, Phys. Rev. Lett. 110, 117005 (2013)
[5] L. J. P. Ament, et al., Rev. Mod. Phys. 83, 705 (2011)
[6] L. Braicovich, et al., Phys. Rev. B 81, 174533 (2010).
[7] M. Le Tacon, et al., Nat. Phys. 7, 725 (2011).

Funding: DFG

Exploring the application potential of Sm1111 thin films in high magnetic fields

K. Iida, J. Hänisch, F. Kurth, E. Reich, V. Grinenko, R. Hühne, L. Schultz, B. Holzapfel, C. Tarantini[1], J. Jaroszynski[1], S. Ueda[2], M. Naito[2], A. Ichinose[3], I. Tsukada[3]

The oxypnictide superconductor SmFeAs(O,F) is an attractive material among the Fe-based superconductors due to its highest transition temperature of 56 K. In order to exploit this new material for superconducting applications, the knowledge and understanding of its electro-magnetic properties, also in high magnetic fields, are needed. Recent success in fabricating epitaxial SmFeAs(O,F) thin films asks for exploring their transport properties. We measured high critical current densities of over 10^5 A/cm^2 at 45 T and 4.2 K for both main field orientations, which is favourable for high-field magnet applications. Additionally, by investigating the flux pinning mechanism, we observed a dimensional crossover between the superconducting coherence length and the FeAs interlayer distance near 35 K, indicative of quasi-2D superconductivity and possibly intrinsic Josephson junctions at low temperatures that can be employed in electronics applications such as terahertz radiation sources and superconducting Qubits.

Among the Fe-based superconductors, the highest superconducting transition temperature T_c of 56 K has been reported in SmFeAs(O,F)[1]. This new material class shows very high upper critical fields together with a moderate anisotropy ranging from 4 to 7 [2], which is promising for high-field magnet applications. Hence, several attempts on SmFeAs(O,F) wire fabrication by powder-in-tube technique (PIT) have already been reported [3]. Epitaxial thin films, on the other hand, are favourable for electronics applications as well as optical properties investigations due to their geometry. Recent success in fabricating high-quality epitaxial Fe-based superconducting thin films enables investigating their physical properties and exploring application possibilities. Whereas the high-field transport properties of FeSe-based superconductors (11 system) and MFe$_2$As$_2$-based superconductors (M = Ba, Sr,...; 122 system) have been studied in detail, low-T transport critical current properties of the oxypnictide thin films have not been reported before due to the absence of high quality films. Recently, *in situ* prepared LnFeAs(O,F) (Ln = Nd and Sm) epitaxial thin films with T_c exceeding 50 K have been realised by molecular beam epitaxy (MBE)[4,5]. In a close international collaboration, we investigated various in-plane transport properties of epitaxial SmFeAs(O,F) thin films grown by MBE on CaF_2 (001) single crystalline substrates [4] in magnetic fields up to 45 T [6]. The film investigated here is around 80 nm thick and shows a very sharp texture with both in-plane and out-of-plane mosaicity of less than 0.6°. A TEM image (Fig. 1) reveals a sharp interface and a relatively clean microstructure, except some FeF_2 nanoparticles (not shown here).

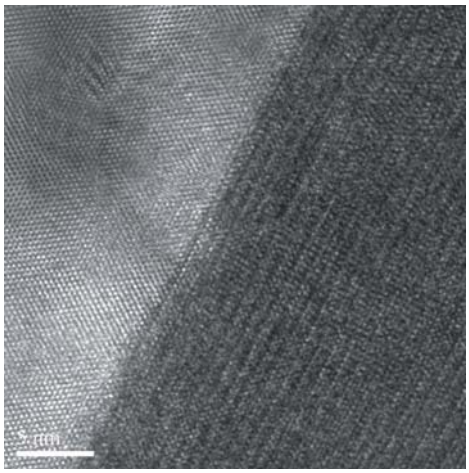

Fig. 1: High-resolution TEM image of the SmFeAs(O,F)/CaF_2 thin film in the vicinity of the interface between substrate (left) and film (right).

The superconducting transition temperature T_c (defined as 90% of the normal state resistivity) of this sample is 54.2 K. Figures 2a and 2b show so-called Arrhenius plots of resistivity for both crystallographic directions measured in static fields $\mu_0 H$ up to 45 T. For both directions, the transition is shifted to lower temperatures with increasing H, as shown in the inset of Fig. 2b. Significant broadening of the transition is observed for H$\|$c, which is reminiscent of high-T_c cuprates. Such broadening originates from enhanced thermally activated vortex motion for H$\|$c. In contrast, T_c as well as its transition width for H$\|$ab is less affected by H. The activation energy $U_0(H)$ for this thermally activated vortex motion [7] is given by the slope of the Arrhenius plots on the assumption of linear temperature dependence of U_0. $U_0(H)$ (Fig. 2c) shows a power law ($\sim H^{-\alpha}$) for both crystallographic directions in the range of $1\,T \leq \mu_0 H \leq 10\,T$ (viz. 20 T for H$\|$ab) with an exponent α close to 0.5 as expected for strong, plastic pinning. In higher fields, the exponent α is close to 1, and U_0 drops rapidly towards zero for $H \rightarrow H_{irr}(0)$.

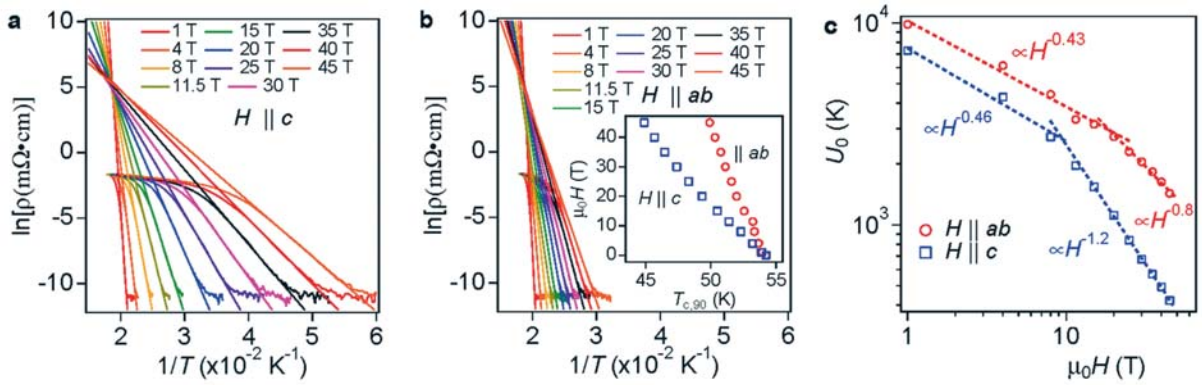

Fig. 2: Temperature dependence of resistivity ρ in Arrhenius representation at various magnetic fields Hllc **(a)** and H||ab **(b)**. Inset: $\mu_0 H_{c2}$(T) for both directions (criterion: 90% $\rho_n(T_c)$). **(c)** Field dependence of the activation energy U_0 for H||c and H||ab.

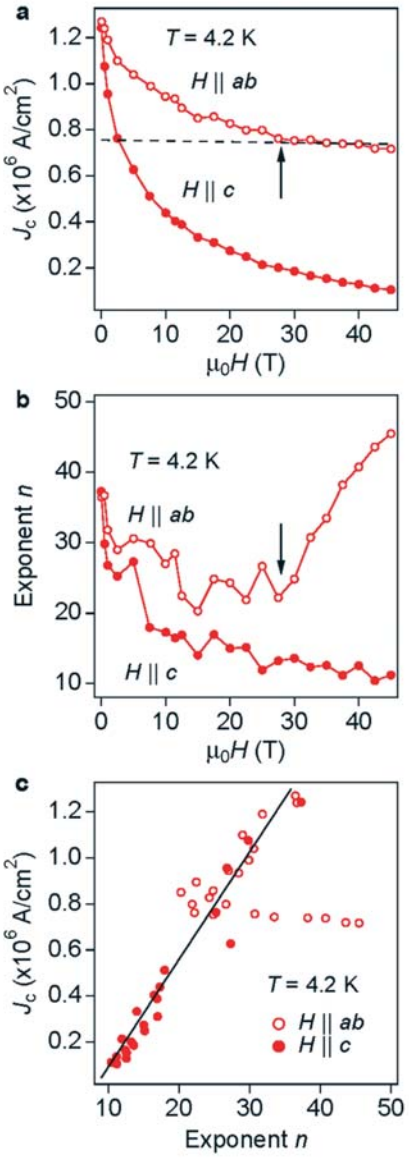

Fig. 3: Field dependence of the critical current density J_c **(a)** and of the corresponding n values **(b)** at 4.2 K up to 45 T. A crossover from extrinsic to intrinsic pinning is indicated by the arrow at around 30 K. **(c)** J_c-n scaling behaviour.

For all magnetic field strengths up to 45 T, the in-plane critical current density J_c for H||c is lower than for H||ab, as can be seen in Fig. 3a for T = 4.2 K. This tendency is observed for all temperatures. It is worth mentioning that a J_c value of over 100 kA/cm^2 was recorded even at 45 T applied ||c. This value is extremely promising for high-field magnet applications. J_c(H||ab) is decreasing gradually with H and shows an almost constant value of 740 kA/cm^2 for $\mu_0 H$ > 28 T. This behaviour can be explained by a combination of extrinsic pinning being dominant at lower fields (i.e. at normal precipitates and stacking faults) and intrinsic pinning at higher fields (i.e. due to a modulation of the Cooper pair density along *ab*-direction) [8]. The latter one can occur if the out-of-plane coherence length ξ_c is smaller than half the structural interlayer distance (here between neighbouring FeAs planes). This observation is known from strongly anisotropic 3D or quasi-2D cuprates, such as $YBa_2Cu_3O_{7-\delta}$ or $Bi_2Sr_2Ca_2Cu_3O_{10}$, respectively.

By analysing the *E-J* characteristics – from which J_c was determined – we obtain information on the pinning potential for $J \sim J_c$. *E-J* curves show a power-law relation $E \sim J^n$ ($n \sim U_p/kT$), which is explained phenomenologically on the assumption of a logarithmic current dependence of the pinning potential U_p for homogeneous samples [9]. Hence J_c should scale with n and, indeed, both show a similar field dependence for H||c, Figs. 3b,c. For H||ab, on the other hand, n and J_c show similar field dependence up to 28 T, whereas at larger fields n suddenly increases. This indicates a strong reduction of the flux creep rate and, hence, the onset of a second pinning mechanism. It is again due to the dominating intrinsic pinning at higher fields. In this B-T region, a full "lock-in" of the flux lines in the interlayers occurs. A maximum pinning force density F_p of 50 GN/m^3 at around 20 T for H||c has been observed, whereas F_p for H||ab was still increasing at the maximum available field of 45 T (F_p(45 T) > 300 GN/m^3). These values are comparable with pinning-enhanced $YBa_2Cu_3O_{7-\delta}$ at 65 K and P-doped $BaFe_2As_2$ at 5 K [10]. The irreversibility field H_{irr}||c at 4.2 K (up to which dissipationless current transport is possible) was roughly estimated from $F_p(H)$ as well as $H_{irr}(T)$ to be as high as 75 T.

Deeper insight into the flux pinning mechanisms is provided by angular dependence measurements, $J_c(\theta)$ and $n(\theta)$, where θ is the angle between H and the *c*-axis. This is summarised in Fig. 4 for three different temperatures. $J_c(\theta)$ at 30 K (Fig. 4a) shows an almost isotropic behaviour at 2.5 T of around 0.14 MA/cm^2 at angles θ up to 75°. Similar isotropic behaviour is seen at 6 T. These results suggest the presence of extended or *c*-axis correlated defects. The presence of the latter defects is ruled out by TEM investigation, since only relatively large FeF_2 particles are observed in the SmFeAs(O,F) matrix. As was pointed out recently [11], any defect of size larger than the out-of-plane coherence length will necessarily contribute anisotropically to *c*-axis pinning in anisotropic superconductors. Hence, the observed FeF_2 particles in combination with the intrinsic

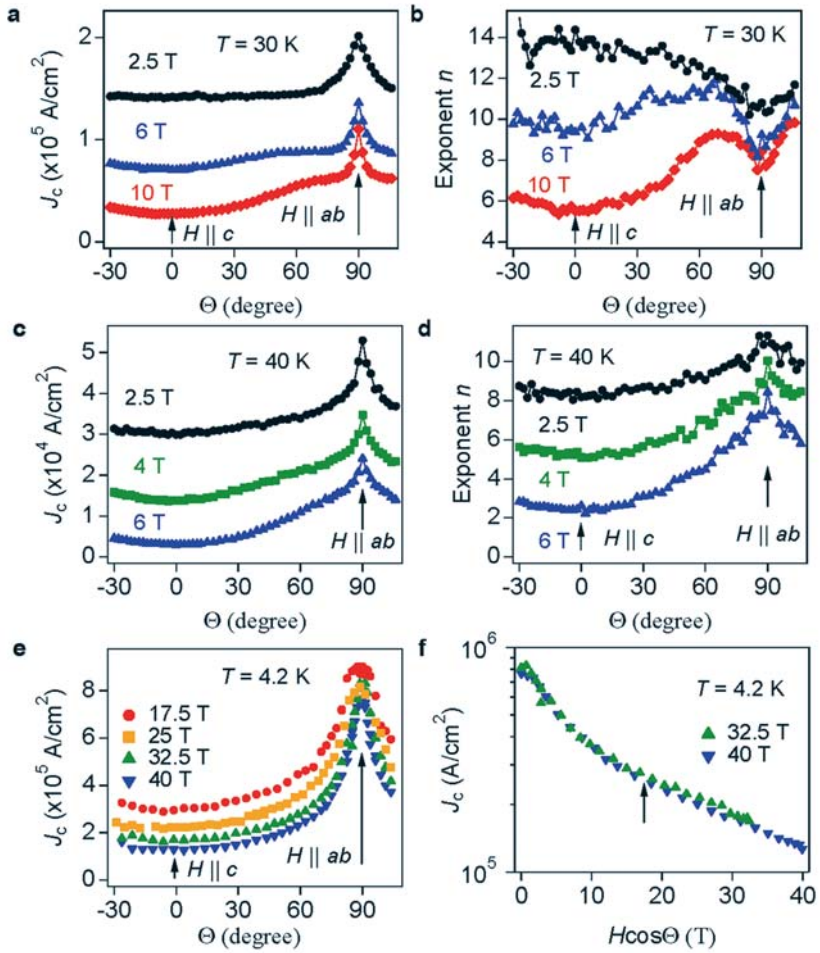

Fig. 4: Angular dependence of J_c and n for different applied magnetic fields at 30 K **(a, b)** and at 40 K **(c, d)**. **(e)** Angular dependence of J_c at 4.2 K under various applied magnetic fields up to 40 T. **(f)** Scaling of the angular dependent J_c measurements for $\mu_0 H$ = 32.5 T and 40 T. Below 17 T, both curves overlap as expected.

pinning (see below) may be responsible for this rather isotropic $J_c(\theta)$. For H||ab, a broad maximum of J_c is observed, and this peak becomes sharper with increasing field (Fig. 4a). However, the corresponding n values show a broad minimum for H close to *ab*-direction (Fig. 4b), which is the opposite behaviour to J_c. This is again a sign of intrinsic pinning and due to the thermal fluctuation of Josephson vortices, which leads to flux creep. The flux creep rate $S = -d\ln(J)/d\ln(t)$ and the exponent n are related as $S = 1/(n-1)$. When the applied field is close (but not too close) to the *ab*-plane, the flux lines are "trapped" by the interlayers. So-called staircase flux lines with possible flux line double-kink structures are generated, which are easily unpinned, leading to an increase in S or, *vice versa*, decrease in n. Similar behaviour has been observed in $YBa_2Cu_3O_{7-\delta}$ thin films [12,13] and recently at IFW on Fe(Se,Te) thin films [14]. This dip of n disappears at 40 K, although J_c still shows a broad maximum near *ab* (Figs. 4c and 4d). Hence, the "activation temperature" of intrinsic pinning lies between 30 and 40 K, which is in good agreement with the transition temperature between Abrikosov- and Josephson-like vortices in SmFeAs(O,F) single crystals [15]. Figure 4e shows $J_c(\theta)$ measured at 4.2 K in fields up to 40 T. A sharp peak is observed for H||ab with a J_c of around of 8×10^5 A/cm^2. For quasi-2D superconductors, where the superconducting layers are effectively decoupled (e.g., $Bi_2Sr_2CaCu_2O_{8-x}$), $J_c(\theta,H)$ is fully governed by the out-of-plane component of the applied magnetic field and can be scaled as $J_c(H\cos\theta)$. For our SmFeAs(O,F) thin film, the aforementioned condition is satisfied above 30 T applied parallel *ab*, at which the crossover field between extrinsic and intrinsic pinning is observed (see Fig. 3a). This sets a lower limit of total applied field (i.e. 30 T) and an upper limit for the c-axis component of H, $H\cos\theta$, for this scaling to be visible. For a total field of 32.5 T, that refers to roughly $H\cos\theta$ = 17 T, and, as can be seen in Fig. 4f, the scaling of the 32.5 T and 40 T curves does work well up to that value (arrow).

By comparing the interlayer distance and the out-of-plane coherence length at the dimensional crossover temperature $T_{cr} = \left(1 - 2\frac{\xi_c}{d}\right)$, we can estimate $\xi_c(0)$ to be roughly 0.3 - 0.4 nm ($T_{cr} \sim 30$ - 40 K, $d = 0.858$ nm). The ratio $\xi_c(0)/d_{FeAs} = 0.35$ - 0.47 explains the intrinsic pinning related to a quasi-2D system observed in this film. Via the normal state resistivity anisotropy of Sm1111 single crystals $\Gamma \sim 30$ [16], one can estimate the in-plane coherence length $\xi_{ab}(0)$ to be 1.7 - 2.2 nm. The evaluated superconducting coherence lengths for both crystallographic directions are in very good agreement with single-crystals values [17]. The presence of a dimensional crossover indicates the possibility of intrinsic Josephson junctions in SmFeAs(O,F). These can be used in superconducting electronics applications such as terahertz radiation sources and superconducting Qubits. And indeed, intrinsic Josephson junctions were reported for a $PrFeAsO_{0.7}$ single crystal [18].

For high-field magnet applications, a high J_c together with a low J_c anisotropy (i.e. $J_c(H||ab)/J_c(H||c)$) in presence of large magnetic fields is necessary. The present results are very promising, since J_c is over 10^5 A/cm^2 at 45 T for both crystallographic directions. Further increase in J_c is possible since the only appreciable defects in our SmFeAs(O,F) films are large FeF_2 particles. Improved pinning performance and, as a consequence, larger J_c could be realised by incorporating artificial pinning centres. Albeit the J_c anisotropy is increasing with H due to the finite density of large strong defects (FeF_2 particles) – which is also seen in the anisotropy of U_0, Fig. 2c –, this value is still low compared to high-T_c cuprates. For instance, the J_c anisotropy is about 3.6 at 30 T and 4.2 K in SmFeAs(O,F), whereas the corresponding value in $YBa_2Cu_3O_{7-\delta}$ is over 7, albeit the latter shows higher J_c than the former [19].

To conclude, we have explored intrinsic electro-magnetic properties of epitaxial SmFeAs(O,F) thin films prepared by MBE on CaF_2 (001) substrate by measuring field-angular dependence of transport properties up to 45 T. Our findings strongly support the presence of a competition between extrinsic pinning below ~ 30 T and intrinsic pinning above that value. We also determined a dimensional crossover at around $T = 30$ - 40 K, at which the out-of-plane coherence length becomes shorter than half the interlayer distance. This knowledge of SmFeAs(O,F) electromagnetic properties could stimulate future development of superconducting applications of this class of material.

[1] Ren, Z. A. et al. Chinese Phys. Lett. **25**, 2215 (2008).
[2] Lee, H. et al. Phys. Rev. B **80**,144512 (2009).
[3] Gao, Z. et al. Supercond. Sci. Technol. **21**, 112001 (2008).
[4] Ueda, S., et al. Appl. Phys. Lett. **99**, 232505 (2011).
[5] Uemura, H. et al. Solid State Commun. **152**, 735 (2012).
[6] Iida, K. et al. Sci. Rep. **3**, 2139; DOI:10.1038/srep02139 (2013).
[7] Yeshurun, Y. et al. Phys. Rev. Lett. **60**, 2202 (1988).
[8] Awaji, S.et al. Cryogenics **39**, 569 (1999).
[9] Zeldov, E. et al. Appl. Phys. Lett. **56**, 680 (1990).
[10] Miura M. et al. Nat. Commun. **4**, 2499, doi: 10.1038/ncomms3499 (2013).
[11] van der Beek et al. Supercond. Sci. Technol. **25**, 084010 (2012).
[12] Civale, L. et al. IEEE Trans. Appl. Supercond. **15**, 2808 (2005).
[13] Awaji, S. et al. Appl. Phys. Express **4**, 013101 (2011).
[14] Iida, K. et al. Phys. Rev. B **87**, 104510 (2013).
[15] Moll, P.J.W. et al. Nat. Mater. **12**, 134 (2012).
[16] Dubroka, A. et al. Phys. Rev. Lett. **101**, 097011 (2008).
[17] Welp, U. et al. Phys. Rev. B **83**, 100513(R) (2011).
[18] Kashiwaya, H. et al. Appl. Phys. Lett. **96**, 202504 (2010).
[19] Xu, A. et al. Supercond. Sci. Technol. **23**, 014003 (2010).

Cooperation: [1]Applied Superconductivity Center, NHMFL Tallahassee, USA
[2]Tokyo University of Agriculture and Technology, Koganei, Tokyo, Japan
[3]CRIEPI Yokosuka, Kanagawa, Japan

Funding: EU (7th Framework, IronSea and SuperIron), NSF (DMR-0654118), Japan Science and Technology Agency (SICORP)

Interband Quasiparticle Scattering in Superconducting LiFeAs Reconciles Photoemission and Tunneling Measurements

C. Hess, S. Sykora, T. Hänke, R. Schlegel, D. Baumann, V. B. Zabolotnyy,
L. Harnagea, S. Wurmehl, J. van den Brink, B. Büchner

Several angle-resolved photoemission spectroscopy (ARPES) studies reveal a poorly nested Fermi surface of LiFeAs, far away from a spin density wave instability, and clear-cut superconducting gap anisotropies. On the other hand a very different, more nested Fermi surface and dissimilar gap anisotropies have been obtained from quasiparticle interference (QPI) data, which were interpreted as arising from intraband scattering within holelike bands. Here we show that this ARPES-QPI paradox is completely resolved by interband scattering between the holelike bands. The resolution follows from an excellent agreement between experimental quasiparticle scattering data and T-matrix QPI calculations (based on experimental band structure data), which allows disentangling interband and intraband scattering processes.

Iron arsenides have the well-known property that experimentally observed factors such as Fermi surface (FS) nesting and the presence of van Hove singularities have a decisive impact on the type of spin fluctuations and on the superconducting ground state. In LiFeAs, angle resolved photoemission spectroscopy (ARPES) reveals an unusual, poorly nested, Fermi surface [1-4] and a strong momentum dependence $\Delta_i(\mathbf{k})$ of the superconducting gap. A model of the band structure which mimics these findings yields prevailing ferromagnetic fluctuations with an instability towards triplet superconductivity [5]. A much different normal state band structure which corresponds to a stronger nesting and other superconducting gap anisotropies $\Delta_i(\mathbf{k})$ have, however, recently been deduced from a spectroscopic imaging (SI) scanning tunneling microscopy (STM) study of the quasiparticle interference (QPI) of LiFeAs [6]. This finding is based on the central assumption that quasiparticles inducing the QPI are scattered only internally within separate holelike bands.

In a recent study [7], we have shown that this seeming ARPES-QPI paradox is completely resolved when interband scattering is taken into account. In particular, comparing the experimentally observed QPI pattern at small wave vectors with QPI calculations, which (i) are based on experimental band structure data and (ii) allow us to consider individual scattering processes separately, we find an excellent agreement between the experimental and calculated data when the mentioned interband scattering is taken into account, whereas intraband scattering alone fails to yield such an agreement. This explains the observed QPIs of Ref. [6] and that of another QPI study of LiFeAs [8] without having to resort to low-energy band structure models that contradict ARPES experiments.

LiFeAs is a *stoichiometric* superconductor, i.e. superconductivity emerges already without doping, at a relatively high critical temperature $T_c \approx 18$ K [9]. Unlike other iron arsenide superconductors, LiFeAs appears to be far away from a spin density wave (SDW) instability: All doping attempts lead to a decrease of T_c [10,11], and according to the ARPES studies [1-4], the FS of LiFeAs consists of two similarly sized electron-like FS sheets around the *X*-point (Throughout this report we refer to the one-Fe unit cell), and two hole-like FS sheets around the Γ-point arising from hole-like bands (labelled α and β, see Fig. 1). One of the two bands has a relatively large FS (β-band, $k_F \approx 0.4$ Å^{-1}, whereas the other is very small ($k_F \lesssim 0.1$ Å^{-1}) such that the corresponding α-band just touches the Fermi level yielding a structure close to a van-Hove singularity. Due to the lack of surface states [12], these findings and those from SI-STM are expected to be bulk representative, and in fact the ARPES electronic structure has been shown to be well consistent with bulk sensitive Hall effect results [13].

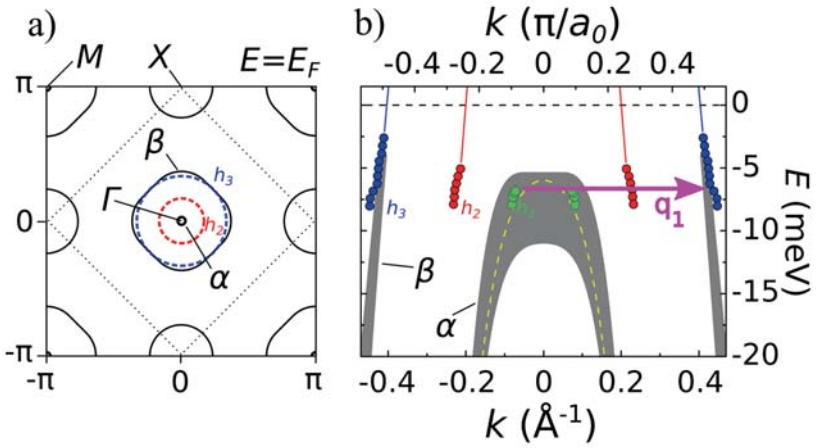

Fig. 1: a) Schematic illustration of the Fermi surface (FS) sheets of LiFeAs. Solid lines illustrate the approximate size of the FS sheets as observed by ARPES [1-4], dashed lines correspond to the hole-like FS resulting from the hole-like bands h_2 and h_3 as obtained from QPI by Allan et al. [6]. Note that Allan et al. extract the Fermi wave vectors along high-symmetry directions and that the shown FS sheets are respective isotropic two-dimensional extrapolations. The shown unfolded Brillouin zone (BZ) refers to the one-Fe unit cell. The BZ related to the two-Fe unit cell is indicated by dotted lines. **b)** LiFeAs band structure at negative energies. Circles represent the extracted quasiparticle dispersions E_k of the hole-like bands h_1, h_2, h_3 obtained in Ref. 6, where k is given by half of the length of the observed scattering vectors **q**. Grey shaded contours represent α and β bands as observed by ARPES [1-4]. The extended width of the α band indicates k_z dependence obtained from different photon energies [3]. The indicated dispersion shown as a dashed line corresponds to data obtained at a photon energy $h\nu = 20$ eV.

In their QPI study [6], Allan et al. used the extracted scattering vectors of the QPI to construct three hole-band dispersions along high-symmetry directions, where they assumed the observed scattering vectors to stem from intraband scattering. One of the resulting bands (labeled h_3 in Ref. 6) is consistent with the β-band observed in ARPES [1-4], and another (h_1) matches quite well the α-band (see Fig. 1). However, the third of the suggested bands (h_2) lacks such a correspondence since its Fermi wave vector, $k_F \approx 0.2$ Å^{-1} [6] neither matches that of the large nor the small hole-like FS observed in ARPES (see Fig. 1). Its length is, however much closer to that of the electron-like bands and thus is the one which would result in a stronger nesting.

As is evident in Refs. 6 and 8, a prominent feature of the Fourier transformed experimental QPI pattern at negative bias is a bright squarish contour at small $|\mathbf{q}| \leq \pi/2$. Fig. 2(a) shows our SI-STM data at $E = -6.8$ meV, which we have obtained on high-quality superconducting LiFeAs single crystals [14] in a home-built scanning tunneling microscope at $T = 5.8$ K (see Ref. 8 for details of the measurement and the full topographic and spectroscopic data set). The chosen energy value is significantly larger (> 1 meV) than the superconducting gap value [2,3,6,15]. Thus gap anisotropies do not play a strong role in the QPI pattern. The observed square structure can be straightforwardly understood by considering backscattering between the small (α) and the large (β) hole band [8]: due to the high DOS of the α-band and the relatively small momentum spread of this band at a given energy close to the band-top (see Fig. 1(b)), the corresponding scattering vectors (labeled $\mathbf{q}_1$) just map the constant energy contour (CEC) of the β-band (cf. Fig. 2(b)). In order to underpin this statement, we show in Fig. 1(b) that the diagonal $\mathbf{q}_1 = (h,h)$ with $h = (0.285 \pm 0.05) \cdot \pi/a$ [8] with a length $|\mathbf{q}_1| = \sqrt{2} \cdot (0.285 \pm 0.05)) \cdot \pi/a = (0.47 \pm 0.08)$ Å^{-1} (with $a = a_0/\sqrt{2} = 2.6809$ Å the shortest Fe-Fe distance, and $a_0 = 3.7914$ Å the in-plane lattice constant [9]) just connects states in the α and β bands along the Γ-M direction as observed at this energy by ARPES [1-4]. Ref. 6 reports a similar squarish structure, the size of which along the Γ-M direction Allan et al. used to extract the h_2-dispersion. In fact, we find that the diagonal $\mathbf{q}_1$ perfectly matches the reported $\mathbf{q}_{h2} \approx 0.28 \times 2\pi/a_0 = 0.46$ Å^{-1} at $E \approx -7$ meV [6]. This shows unambiguously that *i)* the present and the reported QPI patterns of Allan et al. are geometrically well consistent, and *ii)* as a consequence, the suggested h_2-band by Allan et al. does not describe a quasiparticle dispersion but has to be reinterpreted as the dispersion of the scattering wave vectors $\mathbf{q}_1$ which connect the α and β hole-like bands.

Having established this most important finding we corroborate it further by QPI simulations which we use to analyze the influence of the individual possible scattering processes separately. The calculation of the QPI intensity distribution arising from the local density of states is based on a standard T-matrix approach. Thereby the underlying electronic band structure of LiFeAs is modeled by a tight-binding approximation

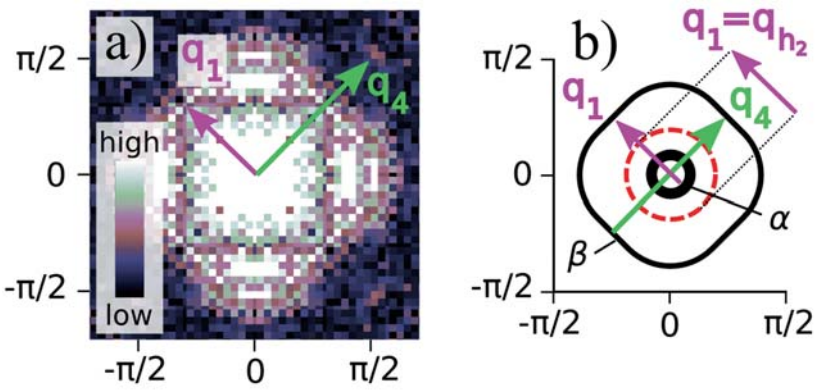

Fig. 2: a) Fourier transformed QPI data of LiFeAs at $E = -6.8$ meV [8]. **b)** Simplified constant energy contours (CEC) of the hole-like α and β bands at $E = -6.8$ meV. $\mathbf{q}_1$ represents interband scattering processes which connect states on both bands. It has the same length as $\mathbf{q}_{h2}$ (i.e., the diameter of the dashed h_2–CEC) reported in Ref. 6. $\mathbf{q}_4$ represents intraband scattering within the β band.

of the ARPES results of Refs. [1,3]. Furthermore, we have used the model $\Delta_k = 0.4$ meV + 6 meV × $\cos k_x \cos k_y$ which is able to account for the measured momentum dependence of the superconducting gap along the Fermi surface. Figure 3 shows calculated QPI patterns for bias voltage $E = -6.8$ meV. In order to identify the origin of the different features in the measured intensity distribution displayed in Fig. 2(a) we faded out specific scattering processes such that only intraband scattering within the two hole pockets α and β [panel (a)] and only interband scattering between α and β [panel (b)] entered the calculation separately. In panel (c) the intensities of both scattering types are summed up. Our numerical simulation confirms that the bright squarish structure described by vector $\mathbf{q}_1$ has to be assigned clearly to interband scattering. Moreover, its intensity is significantly larger than the intraband contributions. Comparison of Figs. 3(c) and 2(a) shows that the size and shape of most of the QPI features can be reproduced by our numerical simulation in excellent agreement with the experimental results.

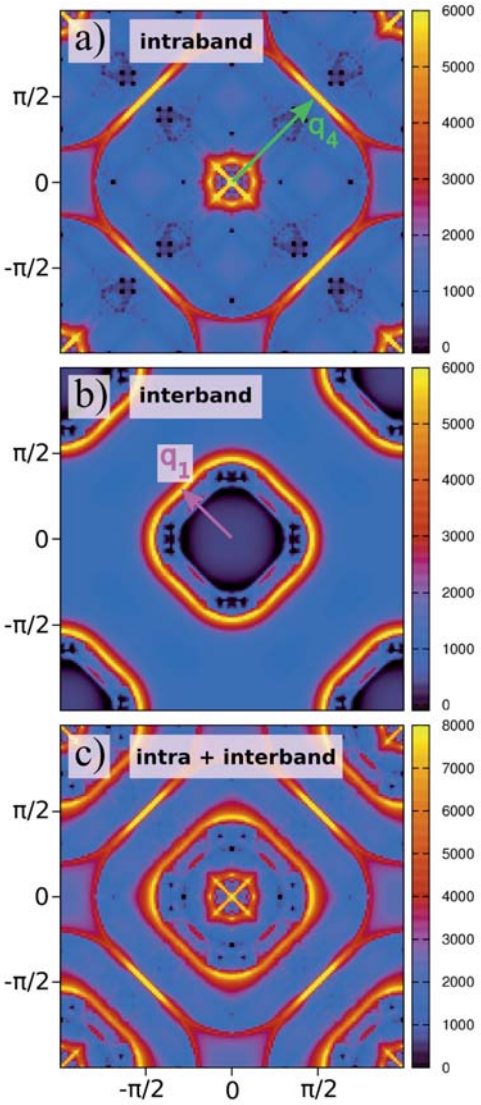

Fig. 3: (a-c) Numerical simulation of the QPI patterns using a T-matrix approach applied to a tight-binding model of the ARPES results [1,3] and anisotropic *s*-wave pairing (see text). **(a)** Only intraband scattering within the small holelike band α and the large holelike band β is considered. All scattering processes between α and β and those processes involving theelectron bands are suppressed in the calculation. **(b)** Only interband scattering between α and β is considered. **(c)** Contributions displayed in panels **(a)** and **(b)** are summed up in order to enable the comparison of the intensities. The scattering vectors $\mathbf{q}_1$, $\mathbf{q}_4$ (see Fig. 2) are indicated.

[1] S.V. Borisenko, et al., Phys. Rev. Lett. 105, 067002 (2010).
[2] K. Umezawa, et al., Phys. Rev. Lett. 108, 037002 (2012).
[3] S.V. Borisenko, et al., Symmetry 4, 251 (2012).
[4] A. A. Kordyuk, et al., Phys. Rev. B 83, 134513 (2011).
[5] P. M. R. Brydon, M. Daghofer, C. Timm, and J. van den Brink, Phys. Rev. B 83, 060501 (2011).
[6] M. P. Allan, et al., Science 336, 563 (2012).
[7] C. Hess, et al., Phys. Rev. Lett. 110, 017006 (2013).
[8] T. Hänke, et al., Phys. Rev. Lett. 108, 127001 (2012).
[9] J. H. Tapp, et al., Phys. Rev. B 78, 060505 (2008).
[10] S. Aswartham, et al. Phys. Rev. B 84, 054534 (2011).
[11] M. J. Pitcher, et al., J. Am. Chem. Soc. 132, 10467 (2010).
[12] A. Lankau, et al., Phys. Rev. B 82, 184518 (2010).
[13] O. Heyer, et al., Phys. Rev. B 84, 064512 (2011).
[14] I. Morozov, et al., Cryst. Growth Des. 10, 4428 (2010).
[15] T. Hanaguri, et al., Phys. Rev. B 85, 214505 (2012).

Funding: DFG

Nucleation of Martensite in Magnetic Shape Memory Alloys

R. Niemann, S. Kauffmann-Weiss, C. Behler, H. Seiner, O. Heczko, A. Backen, A. Diestel, U. K. Rößler, L. Schultz, S. Fähler

Magnetic Shape Memory (MSM) alloys can be used for large-strain actuator materials and in magnetocaloric regenerators of solid-state cooling devices. The energy efficiency of both applications depends strongly on the microstructure developing during a martensitic transformation. A martensitic microstructure that forms with as low elastic energy as possible and which contains only weakly pinned twin boundaries is optimal for application. We use the model system Ni-Mn-Ga in thin film geometry to study the nucleation and growth of martensite in-situ in the scanning electron microscope (SEM). We compare the results to theoretical models and explain why this multifunctional material shows a unique and beautiful microstructure.

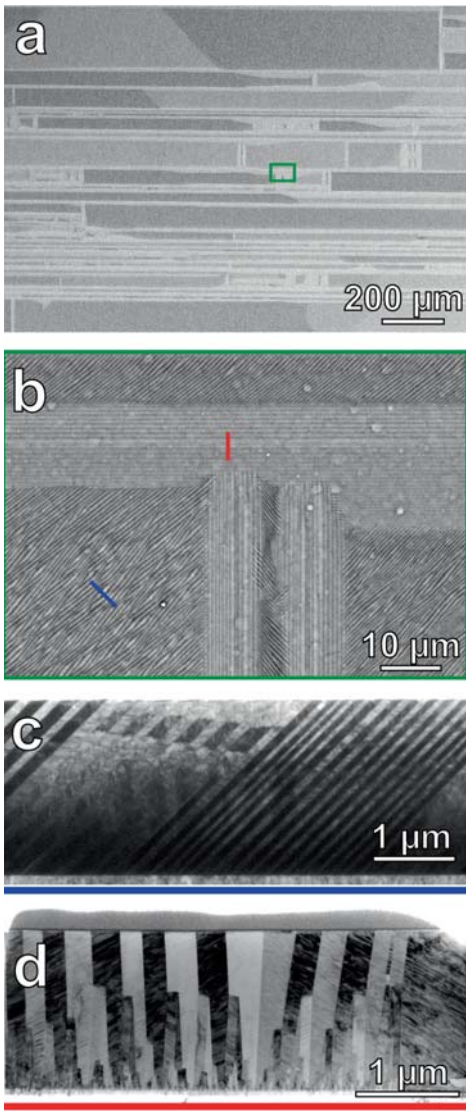

Fig. 1: (a) SEM micrograph (backscattered electron contrast) of an epitaxial Ni-Mn-Ga film in the martensitic state at room temperature. The surface has a beautiful and regular microstructure, similar to a painting by Mondrian. **(b)** A zoom-in at the marked area shows two different microstructures. All contrast comes from mesoscopic twin boundaries. **(c, d)** TEM micrographs at cross-sections along the lines marked in **(b)**.

MSM alloys exhibit a reversible phase transformation: a high temperature cubic phase (austenite) turns into a low temperature tetragonal phase (martensite) with lower volume. To accommodate stress at the phase boundary, the martensite splits into crystallographic variants that are connected by twin boundaries.

This phase transformation is the origin of a giant magnetocaloric effect if austenite and martensite have a different saturation magnetization. A magnetic field can reversibly induce the phase transition, which cools or heats the material [1]. The effect has maximum efficiency when the hysteresis of the phase transition is minimal. To identify origins of hysteresis losses, it is important to understand how the transformation proceeds. Another outstanding effect of MSM alloys is the magnetic field induced reorientation of variants. A low magnetic field of 0.1 T moves twin boundaries between variants, which leads to macroscopic strains in the order of 10 %. This process drastically depends on the type of twin boundary. Only mesoscopic low-symmetry twin boundaries ("Type II") are weakly pinned and can be moved by small fields [2]. They only exist in modulated martensites, which have an additional nanotwinned microstructure on the unit cell level. Accordingly, the modulated martensites are superior for most applications [3]. We will show that understanding the microstructure is important to enhance the functional properties. It is also a question of curiosity why the martensite forms beautiful symmetric patterns as shown in Fig. 1.

To study nucleation and growth of the martensite experimentally, we use epitaxially grown Ni-Mn-Ga films with thicknesses between 2 and 5 µm. They are deposited by sputtering from an alloyed target onto heated single-crystalline (100) oriented MgO substrates. The austenite phase of the Ni-Mn-Ga films has an epitaxial relationship (MgO(001)[100] || Ni-Mn-Ga(001)[110]) and undergoes a reversible martensitic phase transition around 330 K. We study the phase transformation in-situ by using a heated sample holder inside the SEM. The edges of all presented SEM micrographs are parallel to Ni-Mn-Ga $<110>_A$. Cross-sections of the films were analyzed by transmission electron microscopy (TEM).

A typical surface of a Ni-Mn-Ga film (Fig. 1a) exhibits a pattern similar to a painting by modern artist Mondrian: Elongated rectangular areas are separated by parallel stripes. Fig. 1b is a zoom-in to show the fine structure of the surface. Two different morphologies are observed on this length scale [4]: The first type of microstructure consists of bands aligned about 45° to the picture edges. They are not all parallel but form groups enclosing an angle of about 12° which leads to rhombus-like features. This microstructure also exhibits a characteristic zigzag surface topography which contributes to the contrast. In the cross-section (Fig. 1c) we see that these twin boundaries are inclined by 45° relative to the substrate.

The second type of microstructure consists of long stripes parallel to the picture edges. The individual stripes are about 1 µm wide, and form groups of up to 15 µm width. They

are up to 1 mm long, which is remarkable for an only 2 µm thick film. In atomic force microscopy they show almost no height contrast. In the TEM image of a cross-section (Fig. 1d) we see that these twin boundaries are either perpendicular to the surface or slightly inclined by ± 6° with respect to the surface normal.

At first glance, both microstructures appear to be completely different. They exhibit different surface morphology and topography and different orientations relative to the substrate. We follow the evolution of the microstructure by heating the film into the austenite (which has a smooth surface) and then switch to a temperature at which the transformation starts. This enables us to identify the first traces of martensite (nuclei) for both microstructures.

There are two distinct observations of the nucleus (Fig. 2). In one part of the sample, an almost diamond-shaped nucleus with four well-defined straight boundaries and sharp tips is observed (Fig. 2a). It is not symmetric along its main axis. A sketch of this nucleus is given in Fig. 2b. The boundaries between austenite and martensite are called habit planes. We calculated the orientation of these planes using Wechsler-Lieberman-Read-Theory (WLR). This theory uses only the lattice constants of both phases and assumes that only stress-free interfaces form. WLR theory also tells us that the observed diamond consists of four martensitic variants connected by twin boundaries along its axes.

Nuclei of different shape are observed in another part of the same sample (Fig. 2c). They are needle-like with sharp tips (sketched in Fig. 2d). The needle shape can again be explained by four martensitic variants with four habit planes. Often, two tips are observed on one end. We assume that in this case two needles have formed next to each other.

How do the observations of two nuclei with different shape and orientation fit together? It is important to take into account that we just observe the surface of the film, which is a 2-dimensional cross-section through the nucleus. Following WLR theory, a 3-dimensional nucleus consists of eight martensitic variants enclosed by eight habit planes and looks like a very long and thin octahedron with an aspect ratio of about 40:5:1. The eight martensitic variants are all connected by twin boundaries. This object is sketched in Fig. 2e in two different orientations relative to the austenitic film on the substrate. This directly illustrates how the two different surface observations arise: The top one in blue is a cut along the long axis – this leads to the needle observed at the surface. The green one is oriented by 45° to the film normal – the surface cuts this object in a way that the object appears as a kite.

Now we will analyze how the morphology with twin boundaries diagonal to the picture edges evolves from the diagonal nucleus (Fig. 2a). An overview of an austenite-martensite mixture during an early stage of the phase transition is shown in Fig. 3a. We can identify three steps of the transformation. The first stage is observed near the bottom left corner. It is the primary nucleus described above. In the next stage near the center of the image, we observe a long parallelogram (sketched in Fig 3c). Compared to a diamond nucleus, two of the martensite variants (green and red) have grown along their habit plane. The size of the blue and the purple variant remains unchanged. In this way, the

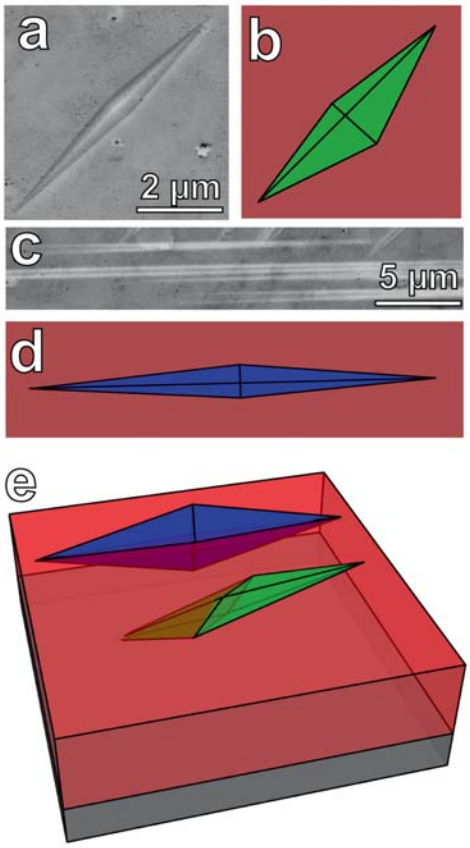

Fig. 2: SEM micrographs of a Ni-Mn-Ga film at the onset of the martensitic transformation (338 K) and models of the nuclei calculated by WLR theory. **(a)** The first trace of martensite is a diamond-shaped object with well-defined straight borders surrounded by single-crystalline cubic austenite. **(b)** Geometric sketch of this object consisting of four martensitic variants. **(c)** In another part of the sample, the first sign of martensite is a needle-like object, schematically sketched in **(d)**. **(e)** Sketch of the actual 3-dimensional nucleus model in two different crystallographic orientations. The observations **(a)** and **(c)** are the surface traces of this object.

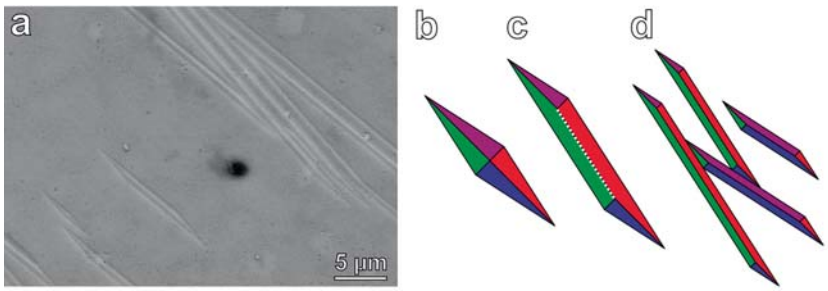

Fig. 3: (a) SEM image of martensitic structures enclosed by an austenite matrix. Three nucleation and growth stages of martensite can be identified. **(b)** Sketch of the diamond nucleus consisting of four martensitic variants. **(c)** A parallelogram evolves from a nucleus by growth of only the red and the green variant. The white dashed line marks a highly mobile (type II) twin boundary that forms inside the parallelogram. **(d)** Differently oriented parallelograms meet and result in the final martensitic microstructure.

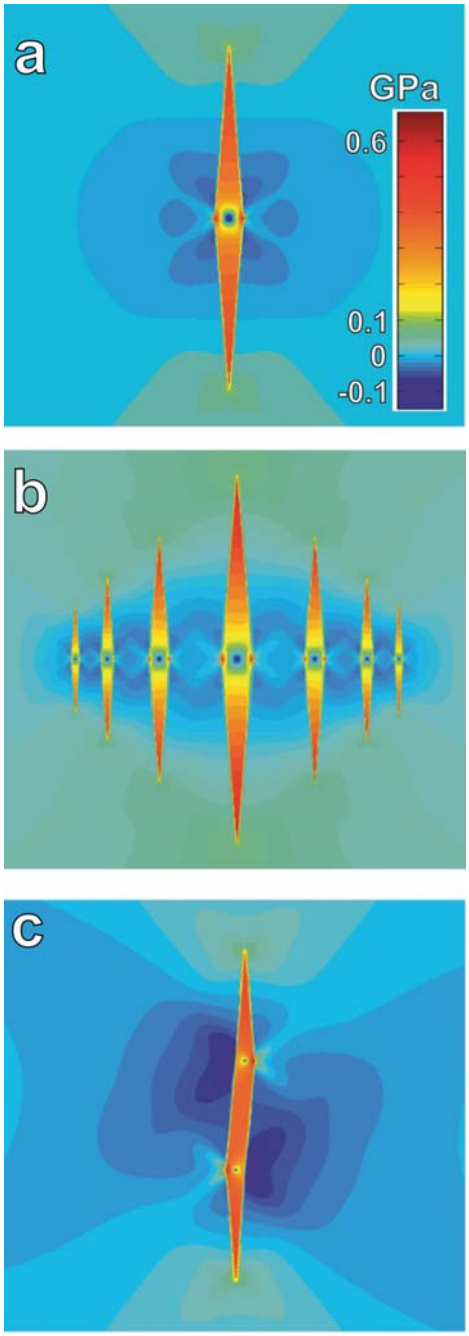

Fig. 4: Finite element method calculation of the volumetric stress **(a)** inside and outside a primary martensitic nucleus. The center point is highly stressed. Local minima outside the diamond promote auto nucleation. **(b)** Arrangement of nuclei created by auto nucleation. **(c)** Volumetric stress inside and outside a parallelogram-shaped martensitic plate.

volume of martensite can increase while all habit plane orientations stay constant. Inside this parallelogram, a new interface has formed between the green and the red variant (white dotted line). Calculations show that this is a highly mobile (type II) twin boundary.

In the final step, sketched in Fig. 3d, differently oriented parallelograms meet. They do not cross each other. Instead, a parallelogram stops growing when it touches already transformed martensite. This stage is called "coalescence". The transformation can only proceed by introducing more nuclei, until the final martensitic microstructure (Fig. 1) is reached.

Up to this point, we used a purely geometric model of the nucleus. However, the nucleus will also generate an elastic field in the surrounding austenite. We analyzed this by calculating the volumetric stress using a finite element method (FEM, Fig. 4) which considers the anisotropic elastic constants of martensite and the volume difference between both phases. Maxima of compressive stress are observed far from the obtuse corners of the nucleus (Fig. 4a). The martensite, which has a lower volume compared to austenite, could favorably form a new nucleus there. This auto nucleation process (Fig. 4b) leads to a chain of parallel oriented nuclei. FEM also shows the origin of the parallelogram formation: The center of the nucleus is highly stressed. The stress is reduced when the diamond evolves into a parallelogram (Fig. 4c) where the diamond center splits up into two points with lower elastic energy.

To conclude, we studied the martensitic phase transformation in thin films of the multifunctional alloy Ni-Mn-Ga. In situ observations in the SEM and additional TEM are combined with modeling. The different stages of the transformation, including nucleation, auto nucleation and coalescence, and also the final martensitic microstructure can be explained by WLR theory and FEM calculations. The transformation relies on a high number of nuclei, since the transformation stops whenever growing parallelograms of martensite meet. The volume change during the transformation promotes auto nucleation but also contributes to hysteresis losses. We observed a high density of type II twin boundaries in the final microstructure. They have a high energy [5] which increases hysteresis losses in magnetocaloric applications. However, these weakly pinned twin boundaries are very convenient when the material is used for actuation. In perspective, our results will allow to optimize the behavior of these active materials by designing or training these materials to generate specific microstructures, e.g. by controlling the distribution of martensite nuclei.

[1] S. Fähler et al. Adv. Eng. Mat. **14** (2012) 10
[2] L. Straka et al. Acta Mat **59** (2011) 7450
[3] R. Niemann et al. Adv. Eng. Mat. **14** (2012) 562
[4] A. Backen et al. arXiv:1311.5428 (2013)
[5] A. Diestel et al. Appl. Phys. Lett. **99** (2011) 092512

Cooperation: Czech Academy of Sciences Prague, TU Chemnitz, TU Dresden, U Duisburg-Essen
Funding: DFG (SPP1239 and SPP1599)

Electric field control of magnetism in an electrolyte

K. Leistner, L. Reichel, S. Oswald, M. Richter, H. Schlörb, S. Fähler, L. Schultz

Reversible control of magnetism in nano- and microstructures by electric fields is of key interest for novel high density magnetic data storage and multifunctional microsystems like sensors or actuators. At the electrode/electrolyte interface, a multitude of potential dependent electrode processes allow modifying the electrode surface: Double layer charging, ad- and desorption, and electrochemical reactions. Triggered by an external voltage, these processes alter the surface structure, electronic structure, or even composition and microstructure, and thus strongly affect the magnetic properties. Exemplarily, we demonstrate large voltage induced changes of saturation magnetization, coercivity and magnetic anisotropy in ultrathin FePt, CoPt and FePt/Fe composite films in an electrolyte. This concept can be applied to various metal/electrolyte systems promising the development of "smart magnetic materials" with variable voltage dependent magnetic behaviour.

Though the interdependence of magnetism and electricity had already been described by Maxwell in 1861, it took more than a century until it was realized that the coupling between magnetic and electric polarization in solid matter may exponentiate the application potential of polarized materials. To date, there are two main material classes exhibiting magnetoelectric effects: magnetic semiconductors and insulating multiferroics. They usually exhibit low Curie temperatures, or, in case of two-phase multiferroics, are constrained by thick, rigid substrates. Thus, alternative approaches are sought to address the growing demand on multifunctional nanosystems. For example, in nanostructured materials surface effects become increasingly important. This allows expanding the class of materials exhibiting magnetoelectric effects towards metals with high Curie temperature. Whereas in the bulk of metals the free electrons shield any electric field, this does not hold for the surface atomic layers. An elegant way to apply an electric field to a metal surface is to use it as an electrode in an electrolyte and charge the electrochemical double layer. Accordingly, e.g. the mechanical properties of metallic nanoparticles [1] and the coercivity in ultrathin magnetic films [2] can be tuned in an electrolyte by an external voltage.

In order to enhance and understand electric field effects of metals in an electrolyte, we investigated 2 nm thick ferromagnetic metallic films. Large effects are expected in the vicinity of a critical point as e.g. spin reorientation or the transition from ferro- to superparamagnetism. There, the magnetoelectric effect may allow toggling between

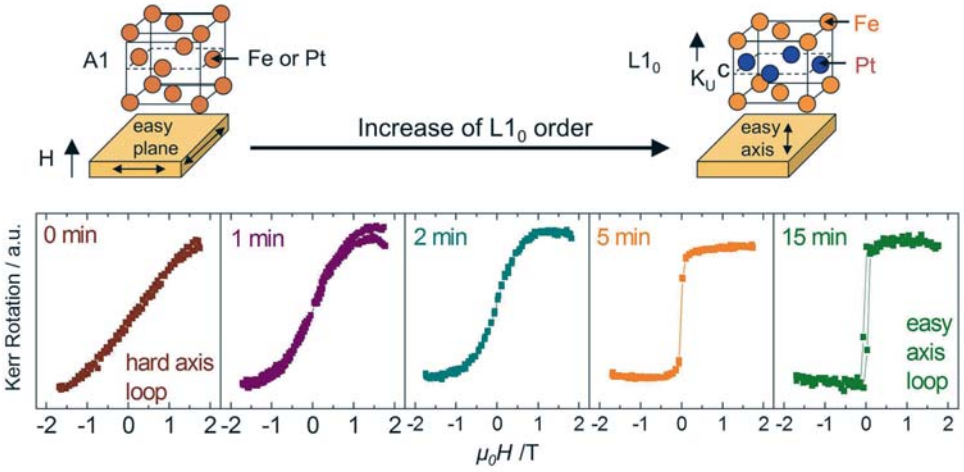

Fig. 1: Adjusting the critical point between shape anisotropy and magnetocrystalline anisotropy. By increasing the annealing times t_A from 0 to 15 min at 450°C the chemical order of 2 nm thick FePt films gradually changes from A1 to L1$_0$. This leads to a transition from in-plane to out-of-plane easy axis.

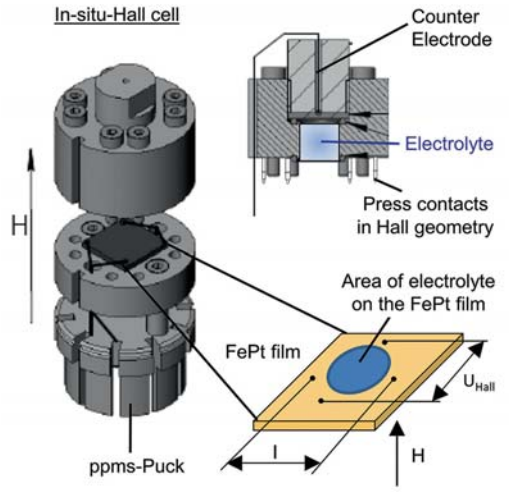

Fig. 2: In situ Hall cell (Ø 23 mm) for use in a Physical Property Measurement System (PPMS) and Hall contact geometry.

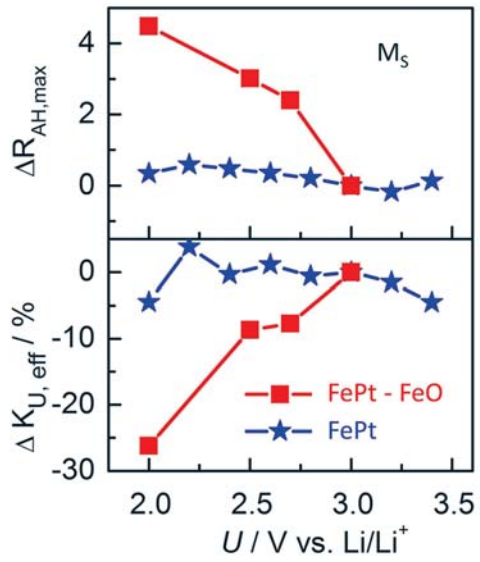

Fig. 3: Influence of external voltage U on saturation magnetization M_S and effective perpendicular anisotropy $K_{U,eff}$ for a 2 nm composite FePt/Fe-O (red) and for a single phase FePt film (blue) charged in 0.1 M $LiPF_6$ in DMC/EC (1:1). The change of maximum anomalous Hall resistance $R_{AH,max}$ is a measure for the saturation magnetization.

two magnetic states. In our case of textured (001) FePt films, the critical situation is established by the transition from an in-plane magnetic easy axis towards a perpendicular magnetic easy axis by tuning the $L1_0$ order parameter (Fig. 1). Without sufficient annealing the isotropic A1 FePt phase is present and the easy axis lies in-plane due to dominating shape anisotropy. Prolonged post annealing time leads to formation of the $L1_0$ phase and competing perpendicular magnetocrystalline anisotropy. The transition can be followed in Fig. 1 by the changes in the magneto-optical Kerr hysteresis curves from rotational to switching processes.

Films with intermediate magnetic properties (2 min post annealing) are then charged in an electrolyte. For charging, a Li based nonaqueous electrolyte is chosen, allowing for a large potential window of 1.2 V for non-destructive charging of FePt films [4]. The magnetic measurements in these ultrathin films exploit the anomalous Hall effect. In contrast to conventional magnetometry, the Hall measurement has a favourable scaling behaviour with decreasing film thickness. To probe the magnetic hysteresis during electrochemical charging, a powerful electrochemical in situ Hall cell has been designed (Fig. 2) [4]. Besides the detection of electric field effects at the electrode/electrolyte interface, this newly constructed cell also allows to monitor carrier density and velocity in electrochemical environments and to investigate the first stages of electrochemical deposition of magnetic materials.

These ingredients allowed to realize voltage induced switching between two magnetic states in FePt films. Large and reversible changes are observed in FePt films exhibiting a natural iron oxide component, but not for purely metallic FePt films (Fig. 3). At high voltages, a high perpendicular anisotropy state is present. At low voltages, the moment increases but perpendicular anisotropy decreases. The observed 5 % change of saturation magnetization and 25 % anisotropy change strongly exceed literature values on charged FePt [2]. Surface sensitive X-ray photoelectron spectroscopy revealed that the chemical state of Fe changes during the charging process [3]. The magnetic changes are thus coupled to reversible oxidation/reduction processes in the natural iron oxide layer on the surface of FePt. Similar reversible reactions on transition metal oxides in Li based electrolytes are researched in the field of supercapacitors and Li ion batteries [5] – one proposed reaction for our case is $Fe_3O_4 + 8\ Li^+ + 8\ e^- \leftrightarrow 3\ Fe^0 + 4\ Li_2O$.

Such a potential-induced modification of the surface iron oxide layer significantly affects the overall magnetization because ultrathin FePt films are used. The 2 nm films considered here consist of about five Fe/Pt layers. Thus, reversible oxidation/reduction of a single Fe layer may considerably reduce/enhance the magnetization of the film. Also the magnetocrystalline anisotropy of ultrathin films is very sensitive to structural or chemical modifications. It is therefore conceivable that chemical modification of a single atomic layer may alter the magnetocrystalline anisotropy of a 2-nm magnetic film by as much as 25%, as observed here. For thicker composite films, a potential induced change of anisotropy based on electrochemical modification of the surface layer can be discussed within the concept of exchange coupling between hard and soft magnetic phases. In general, two phase magnetic exchange coupling significantly reduces the effective anisotropy in comparison to the isolated hard magnetic phase. This has been exploited irreversibly already for hard magnetic FePt nanocomposites coupled to soft magnetic Fe [6]. For our approach this means that an external potential may be used to switch between a magnetic exchange coupled compound (e.g. FePt/Fe) with low anisotropy and an FePt(001)/Fe-O film with nonmagnetic surface oxide layer and higher anisotropy. An enhanced effect is indeed achieved by adding an Fe-O layer intentionally. An artificial FePt/Fe-O composite was prepared by subsequent PLD of 0.4-nm Fe on top of a 2 nm FePt film, followed by oxidation in ambient conditions. Figure 4 shows that this results in a substantially increased reversible change in magnetization of about 13 %.

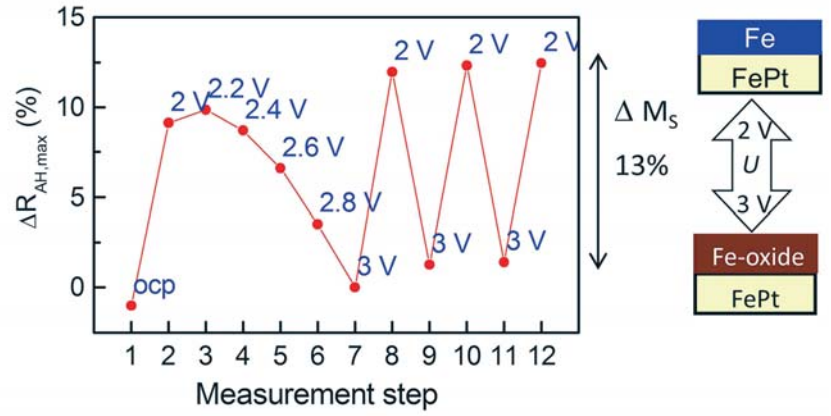

Fig. 4: Increased electric field effect for a 2 nm composite FePt/Fe-O sample with additional Fe-O layer. The change of the maximum anomalous Hall resistance $R_{AH,max}$ is plotted for several measurement steps involving voltages of and in between 2 and 3 V in 0.1 M $LiClO_4$ in DMC/EC (1:1).

Electric field effects in an electrolyte were also investigated also for $L1_0$ CoPt films, where even higher magnetoelectric effects are expected [7]. For $L1_0$ CoPt the critical ordering temperature is about 500 K lower as for FePt and thus the driving force for ordering is significantly lower. Thus, one key challenge is to achieve order in ultrathin CoPt films. We could realize high order in pulsed laser deposited 3 nm thick films at very high and very low deposition rates. This rate dependent ordering is due to an initial short range order formed by surface diffusion during the deposition step [8]. Charging $L1_0$ CoPt/Co-O films in an electrolyte leads to large voltage induced changes of coercivity of up to 200 % (Fig. 5) [9]. The changes are only partially reversible and can be explained by double layer charging and reduction/oxidation processes.

Our approach exploits the strong correlation between surface condition, electrochemistry and magnetism. Whereas up to now, mostly physical parameters as temperature and magnetic fields have been used to adjust magnetic properties we demonstrated that reversible control of magnetism can also be achieved by electrochemical reactions. Whereas pure electronic charging promises moderate variation of the magnetic properties of one phase, this is different for electrochemical reactions. Electrochemically induced phase transformation may even enable to switch magnetism on or off. This concept can be extended to various materials and metal/oxide combinations and also thicker exchange coupled composites to tailor magnetoelectric properties in a broad manner.

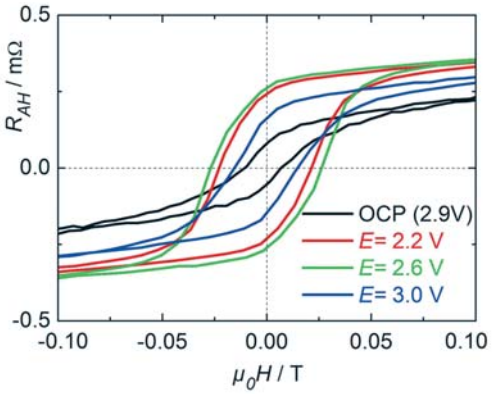

Fig. 5: In situ magnetic hysteresis of 3 nm thick CoPt/Co-O film in $LiClO_4$ in DMC/EC (1:1) at different voltages (ocp – open circuit potential).

Acknowledgements: We thank N. Lange, J. Wunderwald und K. Duschek (IFW Dresden, HTW Dresden) for their experimental work within this project, U. Besold for thin film preparation by pulsed laser deposition, and the department Forschungstechnik for help during the construction of the in situ cell.

[1] H.-J. Jin and J. Weissmüller, Science 332 (2011) 1179
[2] M. Weisheit, S. Fähler, A. Marty, Y. Souche, C. Poinsignon, and D. Givord, Science 315 (2007).349
[3] K. Leistner, J. Wunderwald, N. Lange, S. Oswald, M. Richter, H. Zhang, L. Schultz, and S. Fähler, Phys. Rev. B 87 (2013) 224411
[4] K. Leistner, N. Lange, S. Oswald, F. Scheiba, S. Fähler, H. Schlörb, and L. Schultz, Electrochim. Acta 81 (2012) 330
[5] P. Poizot, S. Laruelle, S. Grugeon, L. Dupont, and J.-M. Tarascon, Nature 407 (2000) 496
[6] A. Breitling, T. Bublat, and D. Goll, Phys. Status Solidi RRL 3 (2009) 130
[7] H. Zhang, M. Richter, K. Koepernik, I. Opahle, F. Tasnadi, and H. Eschrig, New J. Phys. 11 (2009) 043007
[8] L. Reichel, S. Fähler, L. Schultz, K. Leistner, J. Appl. Phys. 114 (2013) 093909
[9] L. Reichel, S. Oswald, S. Fähler, L. Schultz, K. Leistner, J. Appl. Phys. 113 (2013) 143904

Cooperation: TU Chemnitz
Funding: DFG project LE 2558/1-1

$Bi_{14}Rh_3I_9$ – the first synthesized member of a new class of matter

B. Rasche, A. Isaeva, M. Ruck, S. Borisenko, V. Zabolotnyy, B. Büchner, K. Koepernik, C. Ortix, M. Richter, and J. van den Brink

Commonly materials are classified as either electrical conductors or insulators. The theoretical discovery of topological insulators (TIs) in 2005 has fundamentally changed this dichotomy [1]. In a TI, spin-orbit interaction generates a non-trivial topology of the electronic band-structure dictating that its bulk is insulating, while its surface is (semi-)metallic. The first TI candidate material put forward [2] – graphene – is of limited practical use since its weak spin-orbit interactions produce a band-gap of only 0.01 K (1 μeV) [3]. Recent reinvestigation of Bi_2Se_3 and Bi_2Te_3, however, have firmly categorized these materials as strong three-dimensional TIs [4]. We have synthesized the first bulk material belonging to an entirely different, weak, topological class, built from stacks of two-dimensional TIs: $Bi_{14}Rh_3I_9$ [5]. Its Bi-Rh sheets are graphene analogues, but with a honeycomb net composed of $[RhBi_8]$-cubes rather than carbon atoms. The strong bismuth-related spin-orbit interaction renders each graphene-like layer a TI with a 2400 K band-gap.

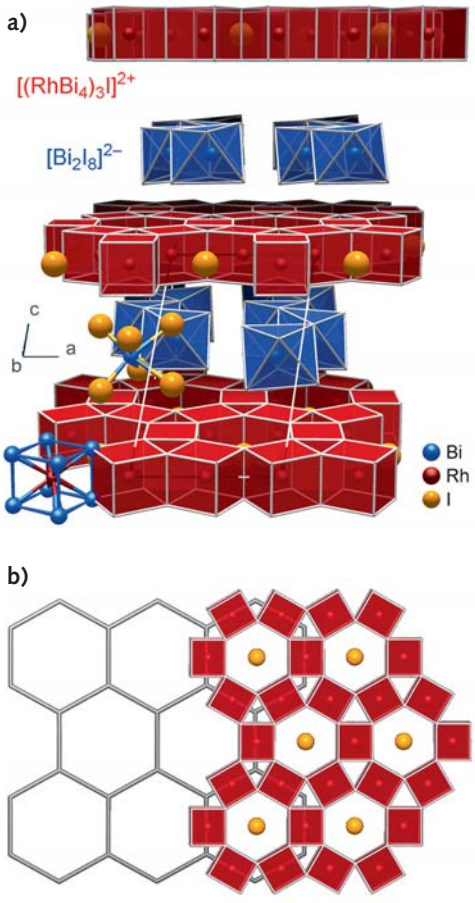

Fig. 1: Structure of $Bi_{14}Rh_3I_9$ and its relation to graphene. **a**, Triclinic crystal structure of $Bi_{14}Rh_3I_9$. Insulating layers of $[Bi_2I_8]^{2-}$ zigzag chains separate the intermetallic $[(RhBi_4)_3I]^{2+}$ layers that consist of hexagonal nets of edge-sharing $RhBi_8$ cubes. **b**, Honeycomb lattice of graphene scaled by a factor 3.8 overlaid with the structure of the intermetallic layer.

Topological insulators (TIs) are recently discovered states of matter and thus of the most fundamental scientific interest. On the other hand, they are promising candidates for future spintronic applications including quantum computing [6] due to the specific nature of their surface states: theory predicts that the propagation direction of TI surface electrons is robustly linked to their spin orientation [7]. In spite of their conceptual richness, a lack of equivalent advances in producing new classes of TI materials has led materials synthesis to concentrate largely on further perfecting and varying the materials class of bismuth-based chalcogenides Bi_2Se_3 and Bi_2Te_3, which are confirmed three-dimensional (3D) TIs [4], and HgTe films grown with utmost care by molecular beam epitaxy that under specific conditions form a 2D-TI [8].

We have synthesized $Bi_{14}Rh_3I_9$ from a stoichiometric melt of its elements. The resulting thin black platelets are air-stable and can be easily cleaved. We could show this material to be the first member of an entirely new class of stacked 2D-TIs, i.e., the bulk phase of a *weak* 3D topological insulator [5].

The crystal structure was determined by single-crystal X-ray diffraction and exhibits an alternating stacking of 2D bismuth-rhodium networks and insulating spacers (Fig. 1a). The former, further denoted as the intermetallic layer, can be understood as a decorated honeycomb network. It has the same hexagonal p6/mmm layer group symmetry as a graphene sheet. A lattice scaling of about 3.8 in Fig. 1b makes this structural equivalence prominent. Whereas the nodes of a graphene sheet host carbon atoms, in the intermetallic layer of $Bi_{14}Rh_3I_9$ the nodes of the net are found in the centres of triangular-prismatic voids. These appear in the hexagonal arrangement of Bi cubes that are centred by Rh atoms. This arrangement can also be seen as a kagome-type net with the Rh atoms of edge-sharing cubes at the nodes of the net. The hexagonal-prismatic voids are filled with iodide anions. As a result, an overall composition of $[(RhBi_4)_3I]$ can be assigned to the intermetallic layer. all together establishing a quasi-2D bimetallic network. The spacer layer consists of BiI zigzag chains weakly interacting with the intermetallic layers. The whole sandwiched structure of $Bi_{14}Rh_3I_9 = [(RhBi_4)_3I]^{2+}[Bi_2I_8]^{2-}$ can be characterized as salt-like in stacking direction.

The fact that the weakly coupled intermetallic layers have the same structural symmetry as graphene sheets suggests similarities in the electronic structure between graphene and $Bi_{14}Rh_3I_9$. Indeed, a scalar relativistic band-structure calculation for $Bi_{14}Rh_3I_9$, where the spin-orbit coupling (SOC) is effectively switched off, reveals the presence of two point-like Fermi surfaces (also called Dirac points, DPs) in the triclinic Brillouin

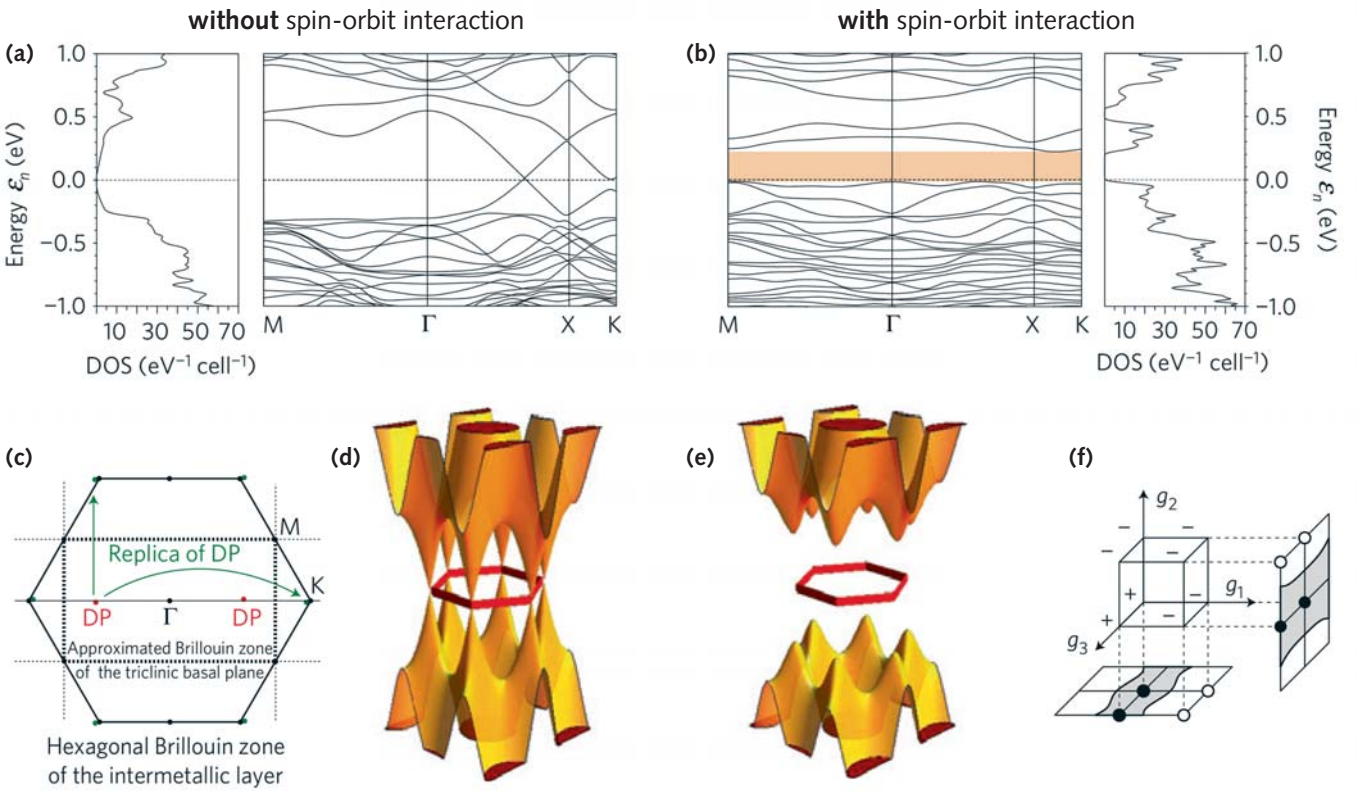

zone. These are considered as indicators of a non-trivial topology of the bulk band structure which will show a gap as soon as SOC is taken into account. Fig. 2a displays the scalar relativistic band-structure with one of the mentioned band crossings. Unfolding the triclinic zone to a hexagonal one, we observe that the DPs appear very close to the K point at the edge of the hexagonal Brillouin zone, precisely where they are in graphene (Fig. 2c). The very weak hopping of electrons between the layers causes a minor dispersion perpendicular to the plane, rendering the calculated band structure quasi-2D.

However, for a proper understanding of the electronic band structure one needs to go beyond calculations in scalar relativistic approximation. Whereas the SOC in graphene is very weak (it is expected to open a gap on an energy scale of 0.01 K [3]) bismuth is known for its strong SOC that can stabilize topologically non-trivial electronic states. As we are thus dealing with graphene-like DPs in the presence of strong SOC, the mechanism proposed in Ref. [2] to stabilize a topologically non-trivial quantum spin Hall state will be in action full-force in the intermetallic layers of $Bi_{14}Rh_3I_9$. Indeed, a full relativistic band-structure calculation yields a calculated band-gap of 210 meV, corresponding to 2,400 K, see Fig. 2b.

To confirm the topological nature of the resulting insulating state we implemented the direct calculation of the four topological Z_2 invariants [9] ν_0; (ν_1, ν_2, ν_3) in the full-potential local-orbital (FLPO) band-structure code, being developed at IFW [10]. This calculation is based on an analysis of the wavefunction parity eigenvalues at the eight time-reversal invariant points of the band-structure, as illustrated in Fig. 2f. Owing to the stacking of the quasi-2D intermetallic planes, one expects $Bi_{14}Rh_3I_9$ to be a weak TI. We indeed find ν_0; (ν_1, ν_2, ν_3) = 0; (0, 0, 1). The fact that $\nu_0 = 0$ and $\nu_3 = 1$ proves that $Bi_{14}Rh_3I_9$ is a weak topological insulator – the first synthesized material in this topological class – and confirms that the intermetallic planes form sheets of quantum spin Hall states that are stacked along the c axis. On surfaces perpendicular to the normal [001] and therefore parallel to the intermetallic planes, which are the natural cleaving planes of the material, topological surface states will thus be absent. At any other surface an even number of Dirac cones appears, each having a strongly anisotro-

Fig. 2: Electronic structure of $Bi_{14}Rh_3I_9$ without and with spin–orbit interaction. **a**, Scalar relativistic band-structure of triclinic $Bi_{14}Rh_3I_9$. On the line Γ – X a Dirac cone is present. **b**, Full relativistic band-structure where the spin-orbit interaction opens up a gap of 210 meV (shaded area). **c**, Projections of the Dirac points (DP, red) onto the two-dimensional Brillouin zone (dashed lines) of the triclinic basal plane. Replication of the DP (green) to the neighbouring Brillouin zones yields positions close to the K points of the unfolded hexagonal Brillouin zone (solid lines). **d**, **e**, Illustration of the Dirac cones in the situation without spin–orbit interaction **(d)** and the topological gap induced by the spin–orbit interaction **(e)**. **f**, Parity eigenvalues at the eight time-reversal invariant points in the 3D Brillouin zone, where g_3 corresponds to the direction perpendicular to the Bi–Rh planes. The parity eigenvalues lead to the topological invariants ν_0; (ν_1, ν_2, ν_3) = 0; (0, 0, 1). Projected parities on the planes perpendicular to g_1 and g_2 illustrate the presence of topological edge states on these surfaces.

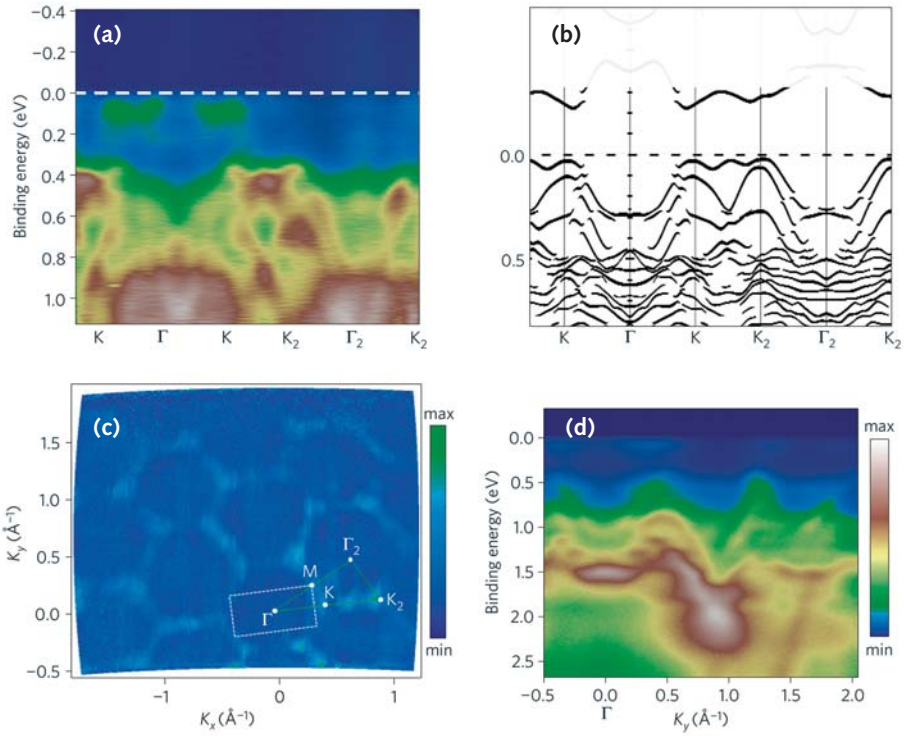

Fig. 3: Band-structure as measured by angle-resolved photoemission [12] compared to the calculated one. A small amount of electron doping brings the Fermi-level into the conduction band, so that the topological band-gap becomes clearly visible. **a**, Momentum–energy intensity plot along the high-symmetry Γ – K direction of the unfolded Brillouin zone. **b**, Unfolded full relativistic band-structure along the same direction. **c**, Momentum distribution at 0.4 eV binding energy integrated within a 50 meV window. White dashed lines show the trigonal, surface projected Brillouin zone. **d**, Typical momentum–energy distribution taken along the cut that corresponds to $k_x = 0$ in **c**.

pic group velocity due to the quasi-2D of the bulk band-structure. The metallicity of these surface states is stable against disorder, which, as for strong topological insulators, does not act as a source of localization [11].

The theoretical band structure can be tested by angle-resolved photoemission spectroscopy (ARPES), which in particular can provide the experimental value of the electronic band-gap, if by slight electron doping the Fermi level of the material is shifted into the conduction band. The ARPES spectra in Fig. 3a, d are consistent with the material being slightly n-doped.

We compare the ARPES results with the full relativistic band-structure calculations in the unfolded Brillouin zone selecting the Γ – K high-symmetry direction (Fig. 3a, b). The agreement between experimental data and calculations is remarkable. First, the observed gap, as determined considering the distance between the features of the integrated spectral weight, is 270 meV, which is consistent with the relativistic band-structure. Also the number and behaviour of the dispersing features clearly seen in ARPES intensity plots are essentially captured by the bands projected to the hexagonal Brillouin zone. Prominent examples are small differences between the points Γ and Γ_2 and structures on the line K – K_2.

This agreement confirms experimentally the validity of the calculated band-structure and, thus, of the calculated topological invariants. As a consequence spin-locked topological surface states will be present at any crystal face that is not parallel to the (001) plane. Such faces, however, do not correspond to natural cuts of the crystal and the associated surface roughness has prevented us so far from observing these spin-polarized surface states by ARPES on, for instance, (100) surfaces. In principle, (spin-polarized) scanning tunnelling microscopy and spectroscopy should be able to directly probe these states at step edges of the natural (001) cleaving plane.

Finally, the momentum distribution of ARPES intensity at 400 meV binding energy, just below the calculated Fermi level of $Bi_{14}Rh_3I_9$, clearly shows a hexagonal pattern (Fig. 3c), as is expected from the band-structure calculations where the top of the valence band is formed by a dispersive feature that is relatively flat between the K points. The hexagonal pattern justifies the unfolding of the Brillouin zone carried out to facilitate the comparison to ARPES. At the same time its slight irregularity reflects the overall triclinic crystal symmetry.

The hexagons observed in ARPES emphasize the structural and electronic similarities of $Bi_{14}Rh_3I_9$ to graphene. The compelling difference with graphene is that the large SOC drives $Bi_{14}Rh_3I_9$ electronically into a topologically insulating state, corresponding to a 3D stack of 2D quantum spin Hall states, which is very different from the strong topological insulator states observed so far in bulk materials such as Bi_2Se_3 or Bi_2Te_3 and which is predicted to leave marked signatures on electronic transport through its spin-polarized, stacked quasi-1D topological surface states [11].

Acknowledgement: We acknowledge the help of Setti Thirupathaiah, Timur Kim and Janek Maletz at the ARPES beamline. We thank Martin Kaiser for his contributions in solving the crystal structure. We are indebted to ZIH TU Dresden for the provided computational facilities.

[1] C. L. Kane and E.J. Mele, Phys. Rev. Lett. **95** (2005) 146802.
[2] C. L. Kane and E. J. Mele, Phys. Rev. Lett. **95** (2005) 226801.
[3] H. Min *et al.*, Phys. Rev. B **74** (2006) 165310.
[4] Y. Xia *et al.*, Nature Phys. **5** (2009) 398402; Y. L. Chen *et al.*, Science **325** (2009)178181.
[5] B. Rasche *et al.*, Nature Mat. **12** (2013) 422.
[6] A. R. Akhmerov, J. Nilsson, and C. W. Beenakker, Phys. Rev. Lett. **102** (2009) 216404.
[7] C. Wu, B. A. Bernevig, and S.-C. Zhang, Phys. Rev. Lett. **96** (2006) 106401.
[8] C. Brüne *et al.*, Phys. Rev. Lett. **106** (2011) 126803.
[9] L. Fu and C. L. Kane, Phys. Rev. B **76** (2007) 045302.
[10] K. Koepernik and H. Eschrig, Phys. Rev. B **59** (1999) 1743; http://www.fplo.de/.
[11] Z. Ringel, Y. Kraus, and A. Stern, Phys. Rev. B **86** (2012) 045102.
[12] S. V. Borisenko, Synchrotron Radiat. News **25** (2012) 611.

Cooperation: Department of Chemistry and Food Chemistry, TU Dresden, Germany; Max Planck Institute for Chemical Physics of Solids, Dresden.
Funding: DFG grants BO 1912/3-1, BO 1912/2-2, and ZA 654/1-1.

Yet the surface matters: anisotropy and location of topological surface states

F. Virot, R. Hayn, M. Richter, and J. van den Brink

Topological insulators (TI) form a fancy class of materials which are insulating in their interior but posses semi-metallic, spin-polarized surface states [1]. Surface states of conventional metals or insulators are sensitive to the surface topography and chemistry and can be suppressed, e.g., by oxidation. At variance, the recently discovered TI are characterized by topological invariants which are *determined by the bulk* electronic structure and *account for the existence* of „topological" surface states. These states cannot be suppressed by surface modification unless bulk properties are affected. We investigated to what extend surface topography and chemistry can modify the dispersion and the spatial location of the topological surface states. This was done for the model system β-HgS, but our conclusions are of general nature. We suggest how the spin-transport can be improved in view of envisaged spintronic applications and point to possible difficulties in the observation of topological states by surface-sensitive techniques.

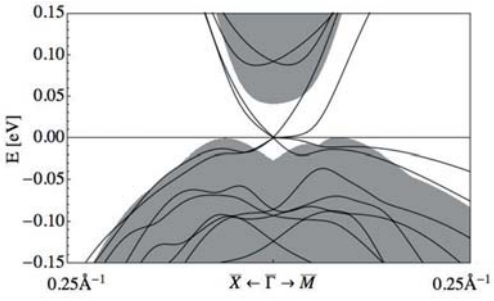

Fig. 1: Band structure of a 5 nm thick (001) HgS slab (lines) close to the Γ point along two specific directions, superimposed to the HgS bulk band structure (gray area) projected to the (001) surface. The topological surface states cross at the ***k***-point Γ, where they also cut the Fermi level thus forming a point-like Fermi surface. Close to the crossing, the dispersion is linear („Dirac cone"). The dispersion anisotropy shows up between the two pairs of occupied or unoccupied bands along the direction Γ – M. One band of each pair belongs to the top, the other to the bottom of the slab, which has no mirror plane parallel to the surface. Both bands are interchanged if the ***k***-direction is rotated by π/2.

Metacinnebar, β-HgS, was recently suggested by us to be a strong three-dimensional topological insulator with a very anisotropic dispersion of the surface states at the (001) facet [2], see Fig. 1. Such an anisotropy strongly enhances the spin relaxation time in comparison with an isotropic situation and is therefore a benefit or even a precondition for the envisaged spintronic applications of TIs [3].

Our suggestion [2] that β-HgS would be a TI was based on an electronic structure obtained in the so-called local-density approximation. Using more elaborate approximations, other authors confirmed [4] or disproved [5] this suggestion. It should be noted that the conclusions on the surface states and their anisotropy that we present here are independent of how such debates are settled. We consider β-HgS as a model system to illustrate the principle of topological surface state engineering [6, 7] by the controlled chemical and crystallographic modification of these states which should be applicable to TIs in general. In particular, we address the following questions:

(1) Can the dispersion of the topological surface states be influenced by surface decoration or by the choice of the facet?

(2) Where in space are these states located and how can the location be modified?

To this end we performed electronic structure calculations using the full-potential local-orbital (FPLO) code, developed at IFW [8]. The surface of β-HgS was simulated by 5 -7 nm thick slabs separated by about 2 nm thick vacuum layers in a three-dimensional supercell geometry. The left part of Fig. 2 shows the reconstructed (001)-surface of HgS, decorated with two H-atoms per surface unit cell. Mercury termination is assumed for the (001) facet since we found this termination in our calculations to be the most stable one in agreement with experimental observations. To satisfy the stoichiometry, every second Hg atom has to be removed from this facet giving rise to a c(2×2) reconstruction. Calculations were performed without and with H-decoration. In the latter case, the *z*-coordinates of the H atoms were varied in order to find their stable position. To investigate the influence of the growth direction, we further calculated the electronic structure of the (110) surface, which is another common facet of the zincblende structure. No reconstruction takes place at this facet, shown in the right-hand part of Fig. 2.

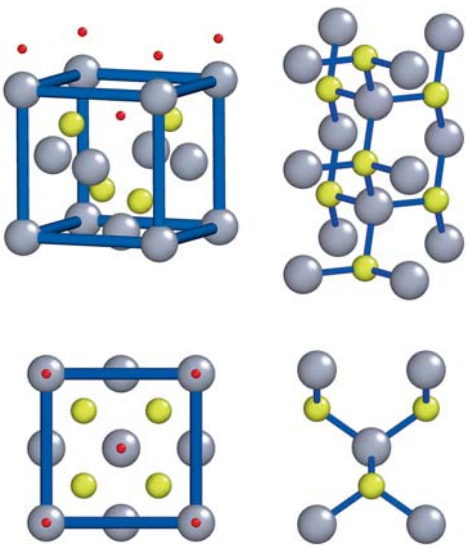

Fig. 2: Left panel: Conventional elementary cell of β-HgS (zincblende structure) with H-decorated surface in perspective view and top view onto the (001) surface (Hg, large gray spheres; S, medium-size yellow spheres). At the Hg-terminated surface, every second atom is removed. H atoms (small red spheres) are added in one of the calculations to saturate the dangling bonds. **Right panel:** Perspective and top views of the (110) surface.

Let us focus our attention first to the location of the topological surface states, Fig. 3, since this information will turn out to be important for the understanding of their dispersion anisotropy. The figure shows density profiles of the surface states at the ***k***-point Γ, where they cross the Fermi level. We notice that the three profiles differ considerably among each other. In the two cases of pristine surfaces, the amplitudes are maximum at the surface and the states decay exponentially with decay lengths of 1 nm for HgS (001) and 2 nm for HgS (110). The former facet has twice as many dangling bonds per surface unit cell than the latter. Since the dangling bonds substantially contribute to the formation of the topological surface states, see the left panel of Fig. 4, the decay length is the smaller the more dangling bonds are available. If the dangling bonds are partly saturated by deposition of hydrogen, they become covalently split (Fig. 4, right panel) and their weight is removed from the vicinity of the Fermi level. As a consequence, the density profile belonging to H-HgS (001) shows a dip at the very surface and a maximum 1 nm underneath. With a following exponential decay at 1 nm length scale, Fig. 3, about 15 atomic layers contribute to these surface states.

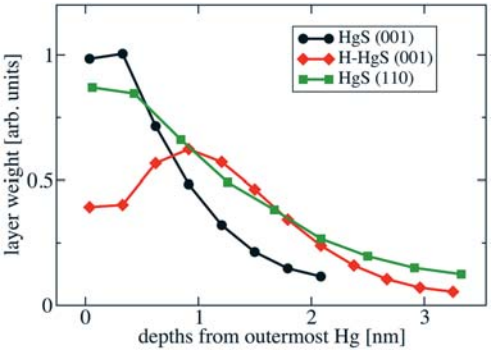

Fig. 3: Layer-resolved weights of the topological surface states at Γ. The orbital weights are summed over all four states (top and bottom of the slab) and over one HgS atomic double layer [one $(HgS)_2$ double layer for (110)]. In the case of H-passivated HgS, the H-weights are included in the surface double layer.

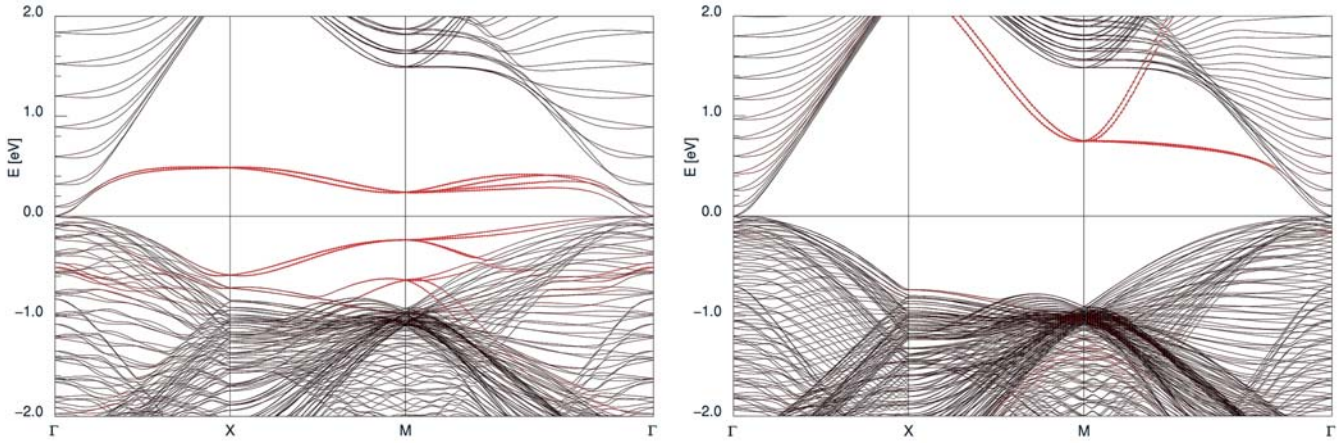

Fig. 4: Band structures of (001) β-HgS slabs. The size of the red dots on the bands denotes the band weight projected to the outermost HgS_2 (H-HgS_2) layers and also marks the almost dispersionless dangling-bond states. The Fermi level is at zero energy. **Left panel:** slab of 5 nm thickness with clean surfaces. **Right panel:** slab of 7 nm thickness with surfaces passivated by hydrogen.

We now turn to the dispersion of the surface states and compare Fig. 1 with Fig. 5. What we find is that the strongly anisotropic dispersion close to the crossing point at Γ, obtained in Ref. [2] for the undecorated (001) facet (Fig. 1), is almost completely suppressed at the (110) facet (left panel of Fig. 5) and largely reduced by H-decoration of the (001) facet (right panel).

The strong anisotropy in the case of the pristine (001) surface can be understood from a combination of two facts: (i) The 4-fold rotoinversion symmetry of the zincblende structure is broken at its surface, see Fig. 6 (left panel). The remaining C_2-axis allows an anisotropy to exist; (ii) This possibility becomes effective by the location of the surface states weight at the outermost atomic layers which makes these states strongly susceptible to the low-symmetry crystal field.

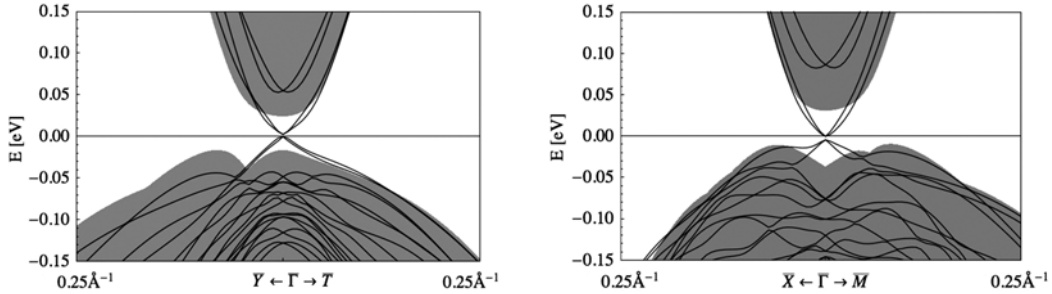

Fig. 5: Left panel: band structure of a 7 nm thick (110) HgS slab (lines) close to the Γ point along two specific directions, superimposed to the HgS bulk band structure (gray area) projected to the (110) surface. The topological surface states show almost isotropic dispersion at the Fermi level. **Right panel:** the same for a 7 nm thick H-passivated (001) HgS slab. Here, the dispersion is slightly anisotropic.

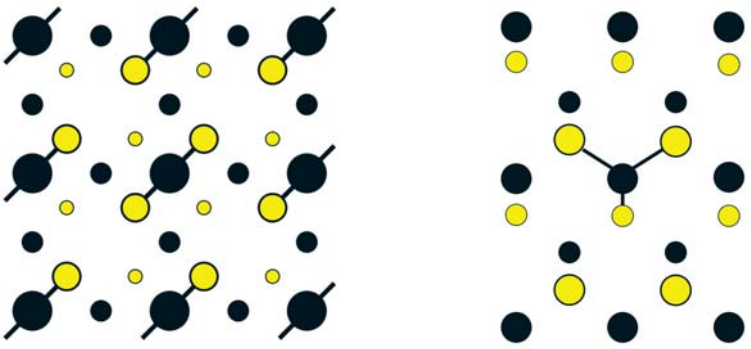

Fig. 6: Left panel: Top-view of the reconstructed (001) surface. The size of the circles indicates the distance from the surface, which is formed by Hg-squares (big black balls). The bonds of the surface atoms to S-neighbors in the second atomic layer (yellow) are denoted by lines.
Right panel: Top-view of the (110) surface with two visible HgS-layers and indicated bonds of the central Hg atom.

The symmetry at the (110) surface, right panel of Fig. 6, is not higher than at (001), but the states show a much smaller anisotropy in their dispersion. This can partly be explained by their larger decay length. In addition and at least equally important, each atom at the (110) surface is threefold coordinated with bonds forming a regular tripod. The related local threefold axes stick out of the surface plane at an angle of 54.7°. In contrast, chains of bonds dominate the local symmetry at the (001) surface, providing a much stronger second-order ligand field as it is present in the (110) case.
Going back to the (001) surface, we find that decoration with hydrogen almost completely destroys the beneficial anisotropy of the dispersion. Here, the broken symmetry has very little effect since the maximum amplitude is located 1 nm, i.e. seven atomic layers, beneath the surface. We note that the inelastic mean free path of electrons at energies between 15 and 350 eV is smaller than 1 nm. Thus, surface decoration may also mask the surface states in photoemission experiments.

We have shown in conclusion, that surface termination and decoration can play a crucial role for topological insulators. For example, surface passivation destroys the dispersion anisotropy of the topological states at the (001) surface of β-HgS. This strongly reduces the relation between spin relaxation time and scattering time and, thus, the spin conductivity. A careful surface preparation and an appropriate choice of the facet are needed to achieve a high spin conductivity which is required for spintronic applications. An intended generation of anisotropy, e.g. by anisotropic surface decoration, might further improve this quantity.
The location of topological surface states is sensitive to the surface condition. This may considerably influence the related signal intensity in surface-sensitive observation techniques like scanning-tunneling microscopy or photoemission.

Acknowledgement: We thank C. Ortix, K. Koepernik, and M. Ruck for discussion.

[1] C. L. Kane and E. J. Mele, Phys. Rev. Lett. **95** (2005) 146802; B. A. Bernevig, T. L. Hughes, and S.-C. Zhang, Science **314** (2006) 1757.
[2] F. Virot, R. Hayn, M. Richter, and J. van den Brink, Phys. Rev. Lett. **106** (2011) 236806.
[3] V. E. Sacksteder *et al.*, Phys. Rev. B **85** (2012) 205303.
[4] R. Sakuma *et al.*, Phys. Rev. B **84** (2011) 085144.
[5] A. Svane *et al.*, Phys. Rev. B **84** (2011) 205205.
[6] D. Soriano, F. Ortmann, and S. Roche, Phys. Rev. Lett. **109** (2012) 266805.
[7] F. Virot, R. Hayn, M. Richter, and J. van den Brink, Phys. Rev. Lett. **111** (2013) 146803.
[8] K. Koepernik and H. Eschrig, Phys. Rev. B **59** (1999) 1743; http://www.fplo.de/.

Cooperation: Institut de Matériaux, Microélectronique et Nanosciences de Provence, Faculté St. Jérôme, Université Aix-Marseille, France; Centre de Cadarache, Institut de Radioprotection et de Sûreté Nucléaire, PSN-RES/SAG/LETR, France.
Funding: GENCI-CINES (Grant c2012096873) for HPC.

Novel class of $SrTiO_3$-based heterostructures

R. Giraud, J. Dufouleur, B. Büchner

Oxygen vacancies play a fundamental role in the electronic properties of oxide heterostructures. At the interface between the band insulator $SrTiO_3$ and another oxide insulator, they can contribute to a charge accumulation layer on the $SrTiO_3$ side, creating a two-dimensional electron gas (2DEG) of massive quasi-particles. Besides, such defects can also alter the lifetime of electrons confined in $SrTiO_3$ close to the interface, and therefore their mobility. Here, we reveal that the electron mobility in a novel type of oxide heterostructure, the spinel/perovskite γ-$Al_2O_3/SrTiO_3$, can be significantly enhanced with respect to state-of-the-art 2DEGs at the $LaAlO_3/SrTiO_3$ interface. With an electron mean free path increased by a factor ten at low temperatures, the phase coherence length of such a high-mobility 2DEG should now reach the micron scale. Therefore, this result is a milestone towards the study of quantum coherent transport in nanostructures patterned from oxide heterostructures.

In transition-metal oxide heterostructures, a two-dimensional electron gas (2DEG) can form at the interface between two insulators [1, 2]. Since this metallic state is induced by charges delocalized in the 3*d* band of transition-metal ions, electrons are strongly correlated, and electronic interactions can induce new electronic phases in 2D, showing ferromagnetic or superconducting correlations. Such striking physical properties were revealed at the interface between two band insulators, in the archetype oxide heterostructure $LaAlO_3/SrTiO_3$ [3, 4]. Although the growth conditions required to achieve the 2D nature of the metallic interface are now well understood, the origin of charges accumulated at the interface is still a matter of debate. In $SrTiO_3$-based epitaxial heterostructures, two mechanisms responsible for charge generation were clearly identified: i) the charge transfer induced by a built-in electric potential due a polar discontinuity at the interface [1, 5], and ii) the electrical doping due to randomly-distributed oxygen vacancies, acting as double donors in $SrTiO_3$ [6, 7].
The γ-$Al_2O_3/SrTiO_3$ system corresponds to a ***novel type of oxide heterostructures for which regularly-ordered defects generate a charge accumulation layer at the interface***. This new concept of spatially-controlled oxygen vacancies, organized in a quasi two-dimensional array close to the interface (see Fig.1), may be fundamental to reveal some new properties of interface 2DEGs. Indeed, we recently discovered seemingly specific properties, such as the strongly-enhanced electron density and mobility [8] or the giant magnetic susceptibility of the 2DEG. Besides, such heterostructures may have the potential to drive new developments in oxide nanoelectronics: i) the electron mobility is now high enough to study the quantum coherent transport of strongly-correlated electrons in laterally-patterned nanostructures; ii) the O-vacancy ordering could favor the orbital ordering of Ti 3d-states, a necessary condition to search for topological phases induced by electronic interactions [9].

An important issue to consider in oxide heterostructures based on $SrTiO_3$ is the nature of the oxide overlayer which induces a 2DEG at the interface, on the $SrTiO_3$ side. Initially only evidenced with single-cristalline polar materials, like $LaTiO_3$ and $LaAlO_3$, it was recently shown that many other oxides, including amorphous $LaAlO_3$ or Al_2O_3, can induce a metallic state at the interface with $SrTiO_3$ [10, 11]. In absence of a strong polar discontinuity, the most-likely mechanism to create delocalized charges in $SrTiO_3$ is the massive creation of oxygen vacancies close to the interface. A drawback of these disorder-induced 2DEGs is their rather low Hall mobility, which remains smaller than about $10^2\,cm^2/Vs$. An interesting way to circumvent this limitation is to favor a self-organization of oxygen vacancies close to the interface. This is indeed likely to happen for a specific matching of different oxygen sub-lattices in an epitaxial heterostructure.

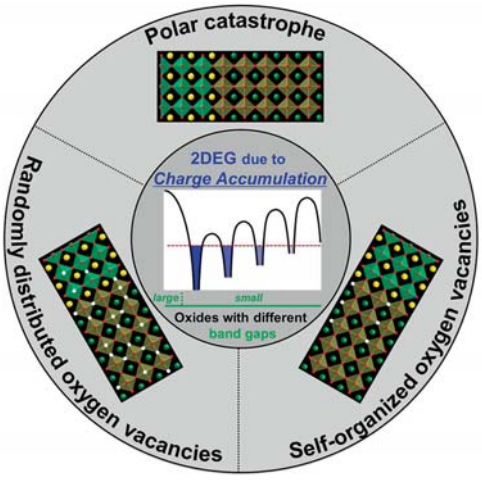

Fig. 1: Schematic representation of the different categories of oxide heterostructures giving a 2DEG at the interface with $SrTiO_3$ (the $LaAlO_3/SrTiO_3$ heterostructure is used for the sketch). The built-in potential in a polar oxide overlayer can induce a charge transfer to the interface (polar catastrophe), but charges can also origin from oxygen vacancies (white dots), which can be randomly or regularly distributed close to the interface.

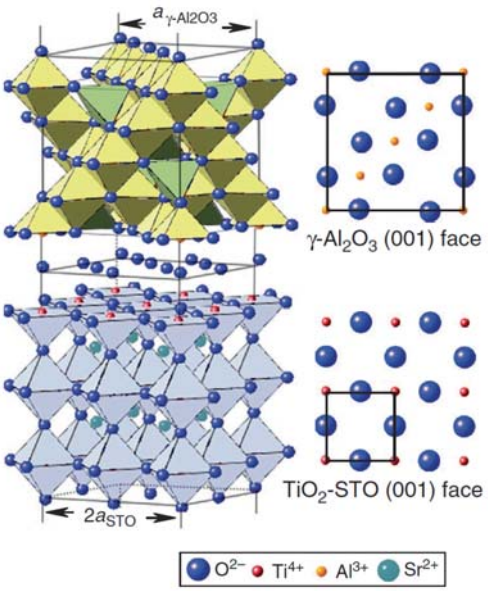

Fig. 2: Crystalline structure of the (001) γ-Al_2O_3/$SrTiO_3$ heterostructure, showing the matching of the oxygen sub-lattice in the TiO_2 and AlO_2 planes. The connectivity between oxygen octahedra remains unknown. After [Chen2013].

Quite so, we recently evidenced an unprecedented high Hall mobility in excess of 10^5 cm^2/Vs at the γ-Al_2O_3/$SrTiO_3$ heterointerface [8], for which the gamma phase of alumina has a lattice parameter of its oxygen sub-lattice twice larger than the one of $SrTiO_3$. This value of the Hall mobility is about ten times larger than the highest electron mobility ever achieved in best $LaAlO_3$/$SrTiO_3$ heterostructures, and it is even higher than those found for optimized bulk-doped $SrTiO_3$ samples [12].

In collaboration with Dr. Y. Chen and Dr. N. Pryds, at the Technical University of Denmark, we studied the transport properties of this new type of oxide heterostructure, the spinel/perovskite γ-Al_2O_3/$SrTiO_3$, the crystalline structure of which is depicted in Fig. 2. Its specific structural property is the very good lattice matching of oxygen sub-lattices. Indeed, the lattice constant of the spinel a[γ-Al_2O_3] = 7.911 Å is nearly twice that of the perovskite a[$SrTiO_3$] = 3.905 Å, which favors the epitaxial growth of γ-Al_2O_3 on $SrTiO_3$. Importantly, our colleagues in Denmark found that the TiO_2 and AlO_2 planes have a similar ordering of anions, which allows them to grow an epilayer of γ-Al_2O_3 directly onto a TiO_2-terminated $SrTiO_3$ substrate, after some surface preparation, by pulsed-laser deposition [8]. The epitaxial growth is achieved at the subunit cell level, with a layer-by-layer growth of neutral molecular blocks similar to the two-dimensional growth mode of Fe_3O_4 on MgO [13]. This results in a very high quality of the heterointerface, with enhanced electrical properties compared to $LaAlO_3$/$SrTiO_3$ heterostructures.

The electrical properties of the γ-Al_2O_3/$SrTiO_3$ heterointerface were systematically studied at the TU Denmark by van der Pauw measurements, and the influence of the thickness of the γ-Al_2O_3 epilayer was investigated in detail. As summarized in Fig. 3(a,b), our collaborators found a metallic state for a thickness exceeding two unit cell (2uc), as well as a strong enhancement of both the carrier density and Hall mobility in a narrow range between 2uc and 3uc. Such a threshold for the onset of the metallic phase is not surprising for a 2DEG, since its intrinsic electrostatic properties put some constrains on the band bending on the $SrTiO_3$ side of the interface (roughly, enough charges need to accumulate so that electrostatic screening becomes efficient to bend the bands on an energy scale comparable to half the band gap of bulk $SrTiO_3$). However, the optimum in the density and mobility found around 2.5uc is more intriguing. This tends to point at the subtlety of the charge-transfer mechanism, and possibly at the influence of local strains and distortions of the octahedra. Most important, the Hall mobility in optimized 2DEGs was found to exceed by one order of magnitude the best values ever achieved with $LaAlO_3$/$SrTiO_3$ heterostructures, and the very high carrier density cannot be explained by the polar catastrophe.

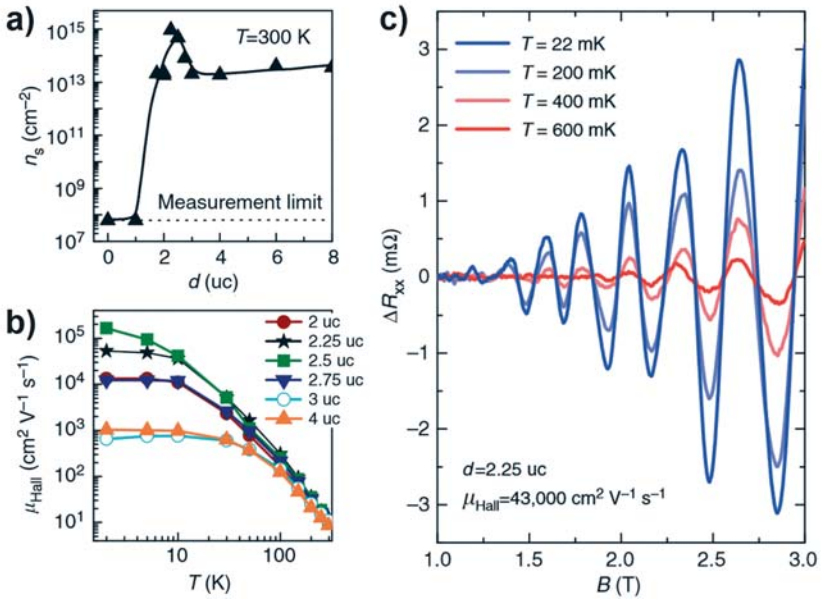

Fig. 3: (a) Evolution of the sheet carrier density n_s, obtained from Hall measurements, as a function of the thickness d of the γ-Al_2O_3 overlayer (in unit cell, uc). **(b)** Temperature dependence of the Hall mobility, obtained from the conductivity and the carrier density, for heterostructures with different values of *d* (controlled at the level of 1/4 th of a unit cell). **(c)** Temperature dependence of the low-field SdH oscillations revealed at very low temperatures for the sample with *d* = 2.25 uc, giving a quantum mobility of about 7200 cm^2/Vs. This mobility is directly related to the mean free path, whereas the Hall mobility is connected to the typical length scale for backscattering. After [Chen2013].

To better understand the electrical properties of a 2DEG, a very efficient way is to measure Shubnikov-de Haas (SdH) oscillations, *i.e.* the nonmonotonic field-dependence of the resistivity due to the formation of Landau levels. It directly gives important informations about the carrier density/mobility of different electronic bands, and their effective mass. Besides, the study of the angular dependence of quantum oscillations, when tilting the magnetic field with respect to the sample plane, gives some additional information about the dimensionality of delocalized charges. Due to the very large effective mass of quasi-particles delocalized in the Ti-bands in oxide 2DEGs, the damping of SdH oscillations with temperature is very strong, so that measurements must be performed at very low temperatures, well below 1K.

By measuring the magneto-transport properties at very low temperatures ($T > 20$ mK), we directly confirmed the very high mobility of a single band contributing to the 2D electron gas formed at this new oxide heterointerface. This can be directly seen in Fig. 3(c) from the onset of SdH oscillations at rather small magnetic fields ($B > 1$T). From the temperature-dependence of the oscillations, the effective mass of charge carriers can be extracted at a given magnetic field. Besides, the field-dependence of the oscillations' amplitude (Dingle plot) gives access to the total scattering time, which reveals an improvement larger than one order of magnitude with respect to other well-known $SrTiO_3$-based 2DEGs (details can be found in [8]). A direct consequence is that the mean free path is remarkably long, of about 200 nm in optimized $LaAlO_3/SrTiO_3$ heterostructures. This gives a lower bound for the phase coherence length $L\phi$, which is actually expected to exceed the micron scale (according to the ratio between the Hall mobility and the quantum mobility, of about 6). Such an unprecedented long value of $L\phi$ should now allow us to investigate the quantum coherent transport of strongly-correlated electrons in laterally-patterned nanostructures. Indeed, the physics of artificially-built mesoscopic conductors was not studied so far due to a much too small phase coherence length, *i.e.* below 200 nm for optimized $LaAlO_3/SrTiO_3$ heterostructures [14].

[1] Ohtomo, A. and Hwang, H. Y., *Nature* **427** (2004) 423.
[2] Mannhart, J. *et al.*, *MRS Bulletin* **33** (2008) 1027.
[3] Brinkman, A. *et al.*, *Nature Mater.* **6** (2007) 493.
[4] Reyren, N. *et al.*, *Science* **317** (2007) 1196.
[5] Okamoto, S. & Millis, A. J., *Nature* **428** (2004) 630.
[6] Kalabukhov, A. *et al.*, *Phys. Rev. B* **75** (2007) 121404.
[7] Herranz, G *et al.*, *Phys. Rev. Lett.* **98** (2007) 216803.
[8] Chen, Y. *et al., Nature Comm.* **4** (2013) 1371.
[9] Rüegg, A. and Fiete, G. A., *Phys. Rev. B* **84** (2011) 201103.
[10] Chen, Y. *et al.*, *Nano Lett.* **11** (2011) 3774.
[11] Lee, S. W. *et al.*, *Nano Lett.* **12** (2012) 4775.
[12] Son, J. *et al.*, *Nature Mater.* **9** (2010) 482.
[13] Reisinger, D. *et al.*, *Appl. Phys. A* **77** (2003) 619.
[14] Rakhmilevitch, D. *et al.*, *Phys. Rev. B* **82** (2010) 235119.

Cooperation: Yunzhong Chen, Nini Pryds (TU Denmark)

Charge and spin transfer at phthalocyanine interfaces

S. Lindner, B. Mahns, B. Büchner, M. Knupfer

Surface and interface studies help to understand the fundamental processes at the corresponding interfaces. In the field of organic molecular materials, many fascinating phenomena can occur at hetero-interfaces, and their importance bridges the entire range from fundamental aspects to application in organic devices. Recently, we have studied a number of organic hetero-interfaces within the family of phthalocyanines. Intriguingly, at a particular phthalocyanine interface we discovered an interaction that is characterized by charge *and* spin transfer between the molecules at the interface, which leads to new physical properties. This might even be an initial representative of a fascinating novel material class.

The addition or the removal of charge as a successful tool to modify physical properties plays an important role in fundamental and applied science. In the field of molecular solids, charge transfer has a long-standing and successful history and prominent examples can be found in, e.g., the classes of organic conductors, as well as superconductors [1-4]. So-called charge transfer salts have been manufactured and demonstrated interesting and often unexpected physical properties ranging from metallicity and superconductivity over complex phase diagrams including charge density and spin density wave phases to highly correlated materials (Mott insulators) [1,3]. Intriguingly, even the formation of a two-dimensional metallic layer has been reported as a consequence of charge transfer between the two insulating organic molecular crystals (TTF and TCNQ) [5,6]. Most recently, superconductivity was reported for some alkali intercalated molecular solids built from hydrocarbons such as picene, which renewed interest in the study of charge transfer materials and variations of their physical properties upon charging [7,8].

In view of more applied aspects, charge transfer has also been investigated and exploited in order to improve or engineer the performance of organic electronic devices. For instance, it has been shown that the inclusion of organic dopants in organic semiconductors can significantly enhance charge carrier injection from electrodes and the modification of electrode surfaces with particular organic layers accompanied by charge transfer allows tuning of hole injection barriers at such junctions [9,10].

Within the huge family of π-conjugated molecular materials which are also considered in organic (opto-)electronic devices, transition metal phthalocyanines offer an additional degree of freedom via the incorporation of the transition metal in the center of the molecule. The transition metals provide a magnetic moment, which results in an interesting combination of organic semiconductors plus magnetism. This has intriguing aspects in view of the development of a spin electronic based on organics [11, 12].

In general, metal phthalocyanines are rather stable against e.g. heat, light, moisture or oxygen, and they have been applied already in organic light-emitting diodes (OLEDs) [13], organic photovoltaic cells [13–15], organic field-effect transistors (OFETs) [16, 17] and even first organic spintronic devices [18, 19].

Within our research activities on organic heterojunctions, we have recently combined selected phthalocyanines that should allow for charge transfer at the respective interface. An important criterion to be considered in order to render charge transfer feasible is the relative size of the ionisation energies and the electron affinities of the involved molecules. This is outlined in Fig. 1. In detail, charge transfer becomes likely when the ionisation energy of the donor (molecule 1) approaches the electron affinity of the acceptor (molecule 2). Following this conjecture we have chosen the two phthalocyanines MnPc and F_{16}CoPc. We have grown well ordered interfaces with the molecules lying flat on the substrate (Au or Ag single crystals) and also parallel to each other at the organic interface.

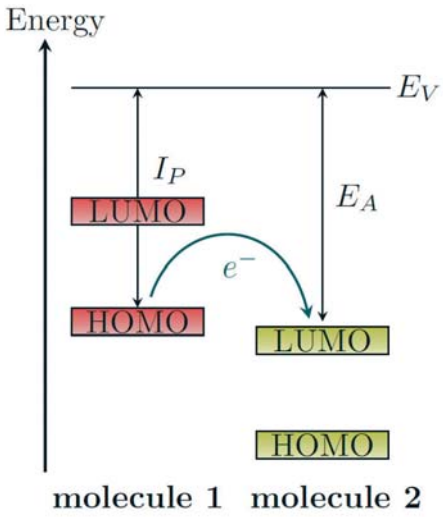

Fig. 1: Schematic energy level alignment for an organic semiconductor heterojunction with charge transfer. An important condition for charge transfer is fulfilled when the ionisation energy (I_P) of molecule 1 approaches the electron affinity (E_A) of molecule 2. HOMO means highest occupied molecular orbital, whereas lowest occupied molecular orbital is abbreviated LUMO.

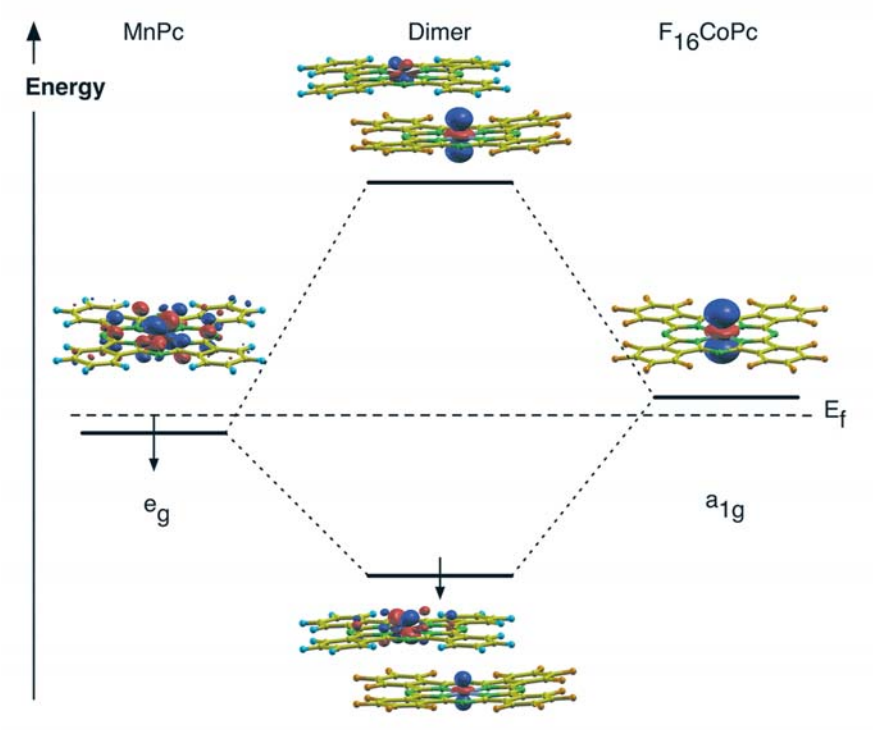

Fig. 2: Interaction of the MnPc and F_{16}CoPc states in the MnPc-F_{16}CoPc dimer close to the Fermi-level. The Mn $3d_{xz}$ and the Co $3d_{z^2}$ orbitals hybridize to form a two-level system.

Using photoelectron spectroscopy studies and calculations based on density functional theory (DFT) we have unambiguously demonstrated that the interface between MnPc and F_{16}CoPc is characterized by a sizable charge transfer between the two molecular species [20]. Importantly, the charge transfer occurs between the two transition metal centers only, with no visible contribution from the organic ligands. The interaction is due to a local hybrid where the Co $3d_{z^2}$ orbital of F_{16}CoPc and the Mn $3d_{xz}$ orbital of MnPc are involved forming a two-level hybrid system as is schematically shown in Fig. 2. As only the lower of the two hybrid states is occupied, the charge is directly transferred to the Co $3d_{z^2}$ orbital. This clearly distinguishes the charge transfer from many other molecular materials where the two π-conjugated organic systems are involved.

Intriguingly, this peculiar charge transfer path harbors another remarkable property, it is related to a change of the molecular magnetic moments. Every change of the charge state of the transition metal centers changes the occupancy of the associated 3d electronic levels, and thus also the total spin or magnetic moment of these orbitals. In other words, the transfer of charge between the transition metal centers at the MnPc/F_{16}CoPc interface is accompanied by a transfer of spin.

Our results are of importance for the application of such interfaces in organic electronic devices since charge transfer considerably affects the energy level alignment and the transport behavior of the respective heterojunction. Moreover, MnPc and F_{16}CoPc may also be able to form a (bulk) charge transfer salt, purely made from phthalocyanines with potentially novel and unexpected physical properties. Since the transfer of charge is also connected to a transfer of spin and the hybrid system has a net spin of S = 2, such compounds could also be termed spin-transfer materials with future applications in the area of spintronics.

In a first step towards bulk materials, we have demonstrated that thin films consisting of MnPc/F_{16}CoPc dimers can directly be formed via co-evaporation [21]. The resulting phthalocyanine blend is characterized by the existence of a new electronic excitation at 0.6 eV, which was confirmed by the DFT calculations. The calculations show that the new signal is caused by a dipole allowed transition between the hybrid states of the above

mentioned two level system. These results indicate that the interaction between the two molecules is strong enough to show the electronic characteristics of the interaction even in a co-evaporated film. The low energy gap excitation suggests that such mixed films might be applicable as small band gap organic semiconductors. Finally, since it is reasonable to assume similar interaction for other flat transition metal complexes, the molecule pair described here might be an initial representative of a fascinating incipient material class.

Acknowledgements: We thank R. Hübel, S. Leger and M. Naumann for technical assistance.

[1] N. Toyota et al., Low-Dimensional Molecular Metals, Springer Berlin, 2007.
[2] P. Batail et al., Chem. Rev. 104 (2004) 4887.
[3] L. Ouahab et al., Organic conductors, superconductors and Magnets, Kluwer Academic, 2004.
[4] O. Gunnarsson et al., Alkali-doped fullerides, World Scientific, Singapore, 2004.
[5] H. Alves et al., Nat. Mater. 7 (2008) 574.
[6] S. Wen et al., Chem. Commun. 46 (2010) 5133.
[7] R. Mitsuhashi et al., Nat. 464 (2010) 76.
[8] M. Xue et al., Sci. Rep. 2 (2012) 389.
[9] N. Koch et al., PRL 95 (2005) 237601.
[10] K. Walzer et al., Chem. Rev. 107 (2007) 1233.
[11] S. Sanvito et al., Nat. Phys. 6 (2010) 562.
[12] S. Sanvito et al., Nat. Mater. 10 (2011) 484.
[13] N. R. Armstrong et al., Macromol. Rapid Commun. 30 (2009) 717
[14] P. Peumans et al., Appl. Phys. Lett. 79 (2001) 126.
[15] B. P. Rand et al., Prog. Photovolt. 15 (2007) 659.
[16] M. M. Ling et al., Org. Electron. 7 (2006) 568.
[17] V. Dediu et al., Solid State Commun. 122 (2002) 181.
[18] W. J. M. Naber et al., J. Phys. D, Appl. Phys. 40 (2007) 205.
[19] A. Zhao et al., Science 309 (2005) 1542.
[20] Lindner et al., PRL 109 (2012) 027601.
[21] Lindner et al., J. Chem. Phys 138 (2013) 024707.

Cooperation: Institute of Theoretical Physics, TU Bergakademie Freiberg; Institute of Semiconductor Physics, TU Chemnitz
Funding: DFG FOR 1154

Combining shape memory crystals and metallic glass in the Cu-Ti-Ni-Zr system

S. Pauly, P. Gargarella, K. K. Song, K. Kosiba, B. Escher, U. Kühn, and J. Eckert

Bulk metallic glasses (BMGs), or synonymously amorphous alloys, are generally similarly unforgiving when being loaded uniaxially like silicate glasses. Both families of glasses tend to fail catastrophically without any appreciable plastic strain, which is a direct consequence of their structure. The damage tolerance of amorphous alloys, however, can be significantly improved when ductile crystals are introduced into the glass. Especially interesting in this respect are shape memory crystals because the deformation-induced martensitic transformation in these crystals leads to an overall work hardening of the composites. So far "shape memory BMG composites" have been limited to compositions based on CuZr. Here, this approach is extended to novel Cu-Ti-Ni-Zr alloys.

Simply put, in BMG composites the crystals represent heterogeneities in the amorphous structure, which interact with the evolution and propagation of shear bands. These shear bands are the carriers of plastic strain in metallic glasses [1] and are generally confined to a few dozens of nanometres [1]. The multiplication of shear bands in the presence of the crystalline phase enhances the overall macroscopic strain in the composite and reduces the intrinsic brittleness of monolithic metallic glasses [2].

Several alloy compositions are known to form composites consisting of a soft β-type phase and a glassy matrix and they are all based on the elements Ti and/or Zr [3-5]. Unfortunately, these BMG matrix composites suffer from work softening since the hardening in the crystalline phase is not sufficient to compensate for the softening that occurs in the glass [1,6,7]. Yet, when the crystalline phase is a shape memory phase the situation changes. The martensitic transformation, which takes place in the crystals, results in very pronounced hardening combined with an increase in plasticity [7,8]. To date only Cu-Zr-based alloys are known to be able to precipitate a shape memory phase and at the same time to contain a sufficient glass-forming ability to render the formation of these shape memory BMG composites possible [8].

In the search for new compositions we have concentrated on the Cu-Ti-Ni-Zr system because it is known to vitrify upon quenching [9,10] and, moreover, the shape memory phase B2 Ti(Cu,Ni) can precipitate [11]. In order to narrow the number of suitable compositions down, the $\lambda+\Delta h^{1/2}$ criterion [12] was employed to predict the glass-forming ability in the pseudo-ternary TiCu-TiNi-CuZr system (Fig. 1a). This criterion considers the topological instability (λ) and electronic effects (Δh) [12] according to:

$$\lambda = \sum c_i \left| \frac{r_i^3}{\sum_A n_j r_j^3} - 1 \right|, \text{ and} \qquad [1]$$

$$\Delta h = (\Delta\phi)^2 - 5.7(\Delta n_{ws}^{1/3})^2, \qquad [2]$$

where c_i and r_i are the molar fraction and the atomic radii of the solute element and n_j and r_j are the number and atomic radii of each element in the compound, respectively. $\Delta\phi$ and Δn_{ws} are the average difference of the work function and of the electron density between the different elements of the alloy [12].

The resulting $\lambda+\Delta h^{1/2}$ map is shown in Fig. 1a. Brighter regions correspond to larger $\lambda+\Delta h^{1/2}$ values, which in turn indicate a higher glass-forming ability. In total nine different compositions were synthesized and analyzed regarding thermal stability, phase formation and mechanical properties as indicated in Fig. 1a. These thermal data as well as values found in literature were additionally combined to plot isolines of the so-called γ_m-parameter ($\gamma_m = (2\,T_x - T_g)/T_l$) ($T_x$: crystallization temperature, T_g: glass transition temperature, T_l: liquidus temperature) [13], which is known to be a reliable

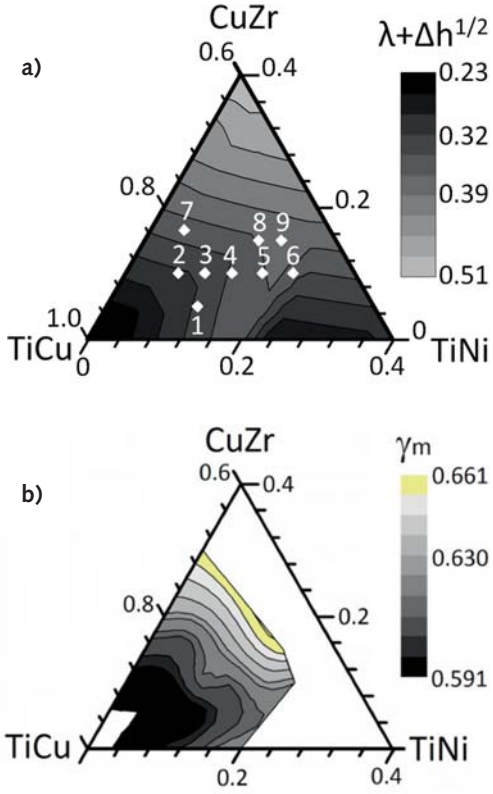

Fig. 1: (a) $\lambda+h^{1/2}$ criterion and **(b)** the γ_m-parameter ($\gamma_m = (2T_x - T_g)/T_l$) ($T_x$: crystallization temperature, T_g: glass transition temperature, T_l: liquidus temperature) in the pseudo-ternary TiCu-TiNi-CuZr system. Towards the CuZr-rich side the glass-forming ability increases and the predictions seems to correlate well with the experimental data. The different compositions chosen in this work are indicated in the maps.

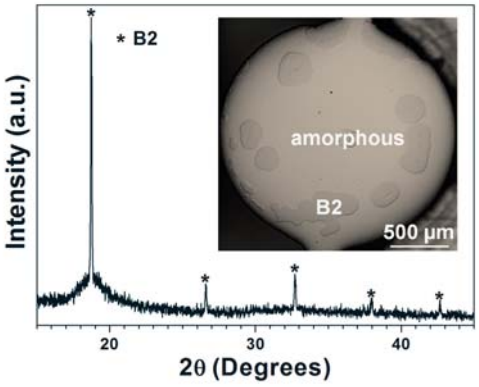

Fig. 2: X-ray diffraction pattern of the $Ti_{45}Cu_{41}Ni_9Zr_5$ rod with a diameter of 2 mm. Sharp Bragg peaks of the B2(Cu,Ni)(Ti,Zr) phase overlap with a broad maximum coming from the amorphous phase. The inset is the microstructure of this sample as seen in the optical microscope. The slightly darker crystals have sizes on the order of several hundred micrometres and are heterogeneously distributed.

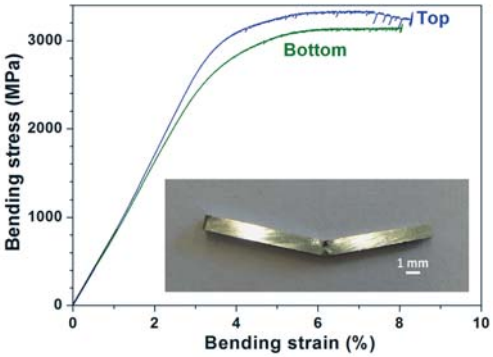

Fig. 3: Bending stress vs. bending strain for a $(Ti_{0.45}Cu_{0.41}Ni_{0.09}Zr_{0.05})_{99}Si_1$ BMG composite. The top and bottom part of an as-cast plate were investigated and both exhibit yield strengths above 2000 MPa and fracture strains around 8%. The inset shows a sample after the bending test, which did not fracture.

indicator of the glass-forming ability. The comparison between the predicted and experimental data shows a satisfying agreement. The tendency to vitrify increases for CuZr-rich alloys.

In the following we focus on $Ti_{45}Cu_{41}Ni_9Zr_5$ (alloy 5) and its slight modification $(Ti_{0.45}Cu_{0.41}Ni_{0.09}Zr_{0.05})_{99}Si_1$ because they are in the regime where the B2 NiTi phase is expected to form. The addition of minor amounts of Si has been reported to improve the glass-forming ability and therefore also quinary alloys were produced. Fig. 2 represents an X-ray diffraction pattern of an as-cast $Ti_{45}Cu_{41}Ni_9Zr_5$ rod with a diameter of 2 mm and superimposed on the broad maximum coming from the amorphous phase are sharp Bragg reflections. These can be allocated to a B2 structure (B2(Cu,Ni)(Ti,Zr)), which means the present composite indeed constitutes a shape memory BMG composite. Due to the large solubility of Cu in the NiTi phase [11] the B2 phase is a solid solution. The inset of Fig. 2 displays the resulting microstructure. The spherical crystals with typical sizes of several hundred micrometres are distributed heterogeneously in the matrix.

The mechanical properties of all Cu-Ti-Ni-Zr alloys were evaluated under compressive loading and it can be shown that the samples have high strengths (up to about 1700 MPa) and large plastic strains (up to 24%) [14]. Both yield strength and plastic strain as well as the work-hardening behaviour depend on the crystalline volume fractions in a similar way as reported for CuZr-based alloys [15].

The relatively high deformability of the $(Ti_{0.45}Cu_{0.41}Ni_{0.09}Zr_{0.05})_{99}Si_1$ alloy can be inferred from Fig. 3, which depicts the bending stress-strain curve of a specimen taken from the top and the bottom of an as-cast plate. The material yields at stresses above 2000 MPa and the fracture strain reaches around 8%. The material is so tough that it does not fail during the test as shown in the inset and instead bends significantly. Hence, the present alloys not only exhibit enhanced mechanical properties but, more importantly, prove that the deformation behaviour of these shape memory BMG composites seems to follow the same mechanisms regardless of composition or constituent phases. In other words, the concept of shape memory BMG composites can be extended to a variety of alloy systems and thus seems to be universally applicable.

[1] A.L. Greer et al. Mater. Sci. Eng. R. 74 (2013) 71.
[2] J. Eckert et al. J. Mater. Res. 22 (2007) 285.
[3] C.C. Hays et al. Phys. Rev. Lett. 84 (2000) 2901.
[4] D.C. Hofmann et al. Nature 451 (2008) 1085.
[5] D.C. Hofmann et al. PNAS 105 (2008) 20136.
[6] C.A. Schuh et al. Acta Mater. 55 (2007) 4067.
[7] D.C. Hofmann. Science 329 (2010) 1294.
[8] S. Pauly et al. Acta Mater. 57 (2009) 5445.
[9] S.J. Pang et al. Intermetallics 15 (2007) 683.
[10] H. Men et al. Mater. Trans. 46 (2005) 2218.
[11] G. Cacciamani et al. In: Effenberg G, Ilyenko S, editors. Light Metal Ternary Systems: Phase Diagrams, Crystallographic and Thermodynamic Data, vol. 11A4.
[12] M.F. De Oliveira. J. Appl. Phys. 111 (2012).
[13] S. Guo et al. Intermetallics 18 (2010) 883.
[14] P. Gargarella et al. Acta. Mater. (2014) accepted.
[15] S. Pauly et al. Appl. Phys. Lett. 95 (2009) 101906.

Cooperation: Federal University of São Carlos (UFSCar), University of São Paulo, TU Kaiserslautern, DESY Hamburg, ESRF Grenoble.
Funding: DAAD, CNPq (Brazil), CSC (China), DFG.

Nanomembranes for energy storage devices

C. Yan, J. Deng, W. Si, X. Sun, Y. Chen, S. Oswald, S. Baunack, and O. G. Schmidt

Lithium-ion batteries (LIBs), as a class of energy storage devices, are currently attracting great attention for applications in portable electronic devices and electrical vehicles. Needs for significant improvements in LIBs have emerged as one of the foremost challenges that the world is facing today. Electrochemically active nanomembranes may provide the key to improve performance of electrode materials for LIBs. Despite significant progress, the electrodes are still far from commercialization. Therefore, new strategies for building advanced nanomembrane electrodes with ultrafast power rates and long lifespans are urgently needed. Here, we present novel directions for nanomembrane-based anode research by rolled-up nanotechnology and highlight the advantages of this technology in improving the performance of LIBs.

The demand for highly efficient lithium-ion batteries to power diverse electric devices is growing fast. Thus, the search for new electrode materials has become an urgent task in building next generation lithium-ion batteries, so as to meet the ever-growing requirements for high capacity and high power density. Bending and rolling is commonly employed in nature to release strain in films to maintain structure stability. Rolled-up nanotechnology has proven to be an intriguing approach on the micro-/nanoscale for various promising future applications and concepts. Recently, we reported a novel "swiss roll" shape micro-structure composed of multilayer Ge and Ti nanomembranes (Fig. 1A) with superior reversible capacity by rolled-up nanotechnology [1]. Ge and Ti nanomembranes were deposited onto a silicon wafer via electron beam evaporation method and the tubular micro-structures were fabricated via the release of the intrinsic strain accommodated in the nano-bilayer, which then results in a self-rolling delamination process. The whole process is highly efficient and also minimizes the whole system energy that leads to good volume tolerance during repeated charge/discharge cycles. With this "swiss roll" shape material, we created a microbattery of about 25 μm in diameter and 400 μm in length. The high conductivity, fast lithium ion diffusion and excellent reversibility of the microbattery were evaluated by direct measurement on a single microbattery via a mini-circuit. The proof of concept in this work paves the way for integration of microbatteries with other micro-devices for on- and off-chip applications. With the same method, we present a new type of tubular configuration (Fig. 1B) made from naturally rolled-up C/Si/C trilayer nanomembranes [2]. A high capacity of ~2000 mAh g^{-1} can be retained at a current density of 50 mA g^{-1} without discernible decay, and the capacity can keep ~1000 mAh g^{-1} even after 300 cycles at 500 mA g^{-1} with almost 100 % capacity retention. The trilayer structure design provides a stable conductive network and prevents Si pulverization and aggregation during cycling, thus guaranteeing superior electrochemical performance. Moreover, the intrinsic strain accommodated in multi-layer nanomembranes is efficiently released by self-winding and thus offers a minimization of the system energy. As an extension to rolled-up nanotechnology, we employed this method to fabricate sandwich-stacked SnO_2/Cu hybrid nanosheets as multichannel anodes for lithium-ion batteries (Fig. 1C) with the use of carbon black as inter-sheet spacer [3]. The sandwich-stacked SnO_2/Cu hybrid nanosheets exhibit significant improvement in cyclability compared to SnO_2 and SnO_2/Cu hybrid nanosheets. By employing a direct self-rolling and compressing approach, a much higher effective volume efficiency is achieved as compared to rolled-up hollow tubes. In addition to the nanosheets, with thin film nanotechnology, we introduced a new concept to fabricate on chip, all solid-state and flexible micro-supercapacitors (Fig. 2A) based on MnO_x/Au multilayers [4], which are compatible with current microelectronics. Furthermore, the nature of the process allows the micro-supercapacitor to be integrated with other micro-devices, to meet the need for microscale energy storage. This

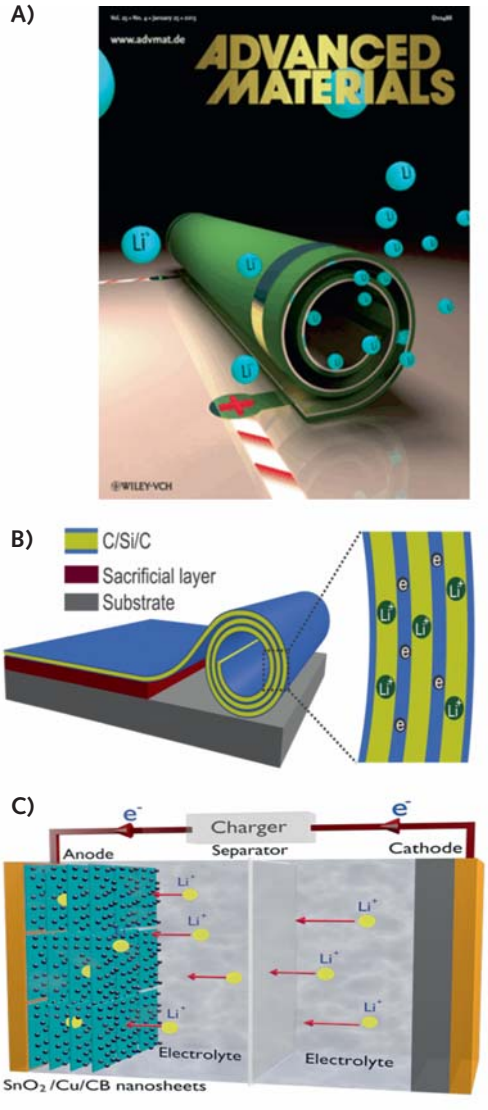

Fig. 1: (A) Schematic diagram of a novel "swiss roll" shape micro-structure composed of multilayer Ge and Ti nanomembranes; **(B)** Fabrication process of a new type of tubular configuration made from naturally rolled-up C/Si/C trilayer nanomembranes; **(C)** Sandwich-stacked SnO_2/Cu hybrid nanosheets as multiple channels for LIBs.

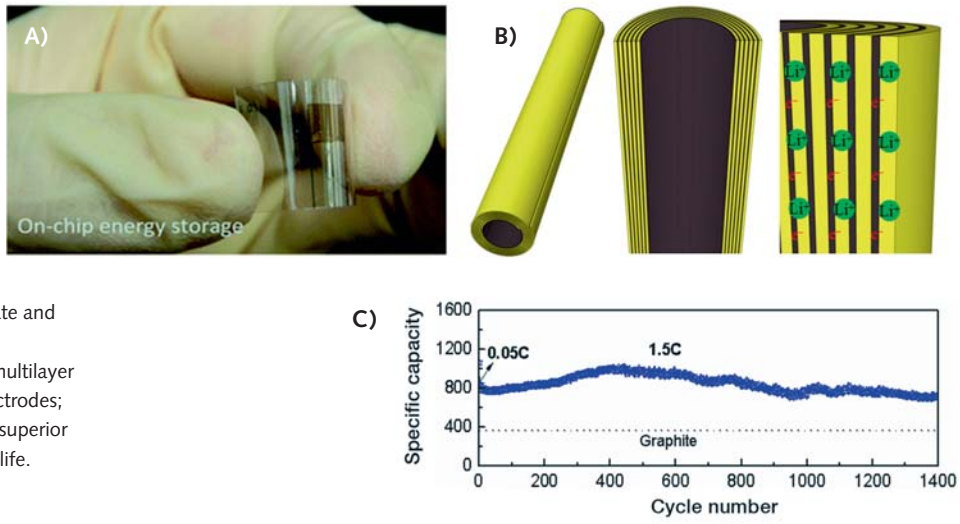

Fig. 2: (A) On chip, all solid-state and flexible micro-supercapacitors; **(B)** Fabrication process of the multilayer graphene/GeO_2 microtube electrodes; **(C)** NiO nanomembranes with superior power rate and ultralong cycle life.

synthesis approach presents a promising route to design electrodes with thin film nanotechnology for high performance energy storage devices.

In order to build advanced nanomembrane electrodes with ultrafast power rates and long lifespans, multilayer graphene/GeO_2 microtubes (Fig. 2B) were also fabricated to improve the electrochemical performance of LIBs [5], which reveals a high capacity of 919 mAh g^{-1} at 0.1 C and cycle life of 700 cycles at 1 C with over 100 % capacity retention. Even at a high cycling rate of 2 C, 85% of the original capacity is still retained after 1000 deep cycles. The observed high capacity combined with excellent structure stability and high rate capability is unprecedented in oxides-based composite electrodes. Our key strategy in this report is that GeO_2 multilayers work as the active layers for lithium ion storage, while the graphene serves as the electrically conductive and elastic layer and also as additional lithium storage sites. Such novel graphene-based tubular nanoarchitectures provide short Li ion pathways and high electrical and ionic conductivity, and hence exhibit much improved specific capacity, cycling performance and super rate capability. With rolled-up nanotechnology, we fabricate three-dimensionally "curved" NiO nanomembranes [6]. The curved NiO nanomembranes exhibit both superior power rate and ultralong cycle life when utilized as the anode material for LIBs (Fig. 2C). The electrodes deliver a high capacity of 721 mAh g^{-1} at 1.5 C (1 C = 718 mA g^{-1}) after 1400 cycles. Notably, even after cycling at an extremely high C-rate of 50 C (i.e., current density of 35 400 mA g^{-1}), the capacity is able to recover to the initial value when the current rate is set back to 0.2 C after 110 cycles. To the best of our knowledge, such high power rates and ultralong lifespans for nickel-oxide-based electrodes have not been reported previously. Our demonstrator with tubular and strain-relaxed structures fabricated by rolled-up nanotechnology are liable to improve the materials tolerance against stress cracking and are therefore promising candidates for increasing the stability of energy storage devices such as lithium ion batteries. More importantly, the process for rolled-up nanomembranes is compatible to industrial-level technologies like e-beam evaporation, sputtering deposition and atomic layer deposition, etc.

[1] C. Yan et al., Adv. Mater. 25 (2013) 539.
[2] J. Deng et al., Angew. Chem. Int. Edit. 125 (2013) 2382.
[3] J. Deng et al., ACS Nano 7 (2013) 6948.
[4] W. Si et al., Energy Environ. Sci. 6 (2013) 3218.
[6] Y. Chen et al., Adv. Energy Mater. 3 (2013) 1269.
[6] X. Sun et al., Adv. Energy Mater. 2013, DOI: 10.1002/aenm.201300912.

Funding: International Research Training Group (IRTG), Pakt project (No. 49004401)

Electro-mechanical control of quantum light

Y. H. Huo, J. X. Zhang, E. Zallo, F. Ding, and O. G. Schmidt

A future quantum network involves the manipulation of stationary quantum bits in each node, as well as the transmission of quantum information between the different nodes using flying qubits. Recent experiments have shown that the semiconductor quantum dots (QDs) are ideal candidates for both tasks. On one hand the electron and the heavy/light hole spins in the QDs can be initialized, addressed and manipulated with high rates, making them excellent two-level stationary qubits. On the other hand, the quantum information carried by the spins can be passed onto the radiatively emitted single photons or entangled photon pairs, thus generating the long-lived flying qubits. However, a stumbling block for this scenario has been the lack of precise control over the electronic and optical properties during the QDs growth, making the post-growth control indispensable. In the following we review two of our most recent progresses in this direction, which were achieved by using the unique electro-mechanical tuning technique developed in our group.

Photons travel fastest in nature and have long coherence times, thus they are considered ideal information carriers for the long distance quantum communications. The quantum bits (qubits) — a quantum analogue of the classical bits — can be encoded in the photon polarization degree of freedom, giving photons the name "flying qubits". Spins are natural two-level systems which fulfil the quantum superposition principle, and they are potential candidates for implementing the fast, single-qubit and two-qubit quantum gates. In *most* of the cases the spins are confined in certain material systems, in order to prevent the decoherence problem induced by the environment, thus giving spins the name "stationary qubits".

A quiet revolution has taken place in the past decade: advances in semiconductor materials growth and device fabrications have enabled experiments to be performed in the solid-state platform on the level of single photons and single spins.[1] Furthermore the exploitation of photon-spin interfaces, i.e., the photon-spin-photon conversions, opens up many exciting applications, for example, building a quantum repeater for the future quantum network. Semiconductor QDs are among the most successful test systems so far. Non-classical light, such as single photons and entangled photon pairs, can be generated via the electron-hole radiative recombination in the QDs, with their polarizations determined by the optical selection rules. Therefore the quantum information carried by the electron and the heavy/light hole spins are passed onto the emitted photons.

In the first part of this report we review the achievement of a wavelength tunable quantum light-emitting-diode (Q-LED), which generates single photons with a high speed of up to 0.8 GHz.[2] The all-electrically operated tunable Q-LED is the *first* among its kind, and represents an important step towards the realization of indistinguishable photons from remote electrically driven QDs. In the second part we review the electronic structure engineering of QDs via external strain fields.[3] The hole ground state is switched to light hole (LH) by applying elastic stresses to an initially unstrained QD, which facilitates the spin manipulation experiments with LH spins. We envision that both works will contribute significantly to the developments of semiconductor QD based qubits.

Part I: Self-assembled semiconductor QDs allow monolithic integration with electronic and photonic elements relying on mature semiconductor technologies. In particular, for the practical device application, epitaxially grown QDs can be easily embedded in a LED to achieve electrically driven single photon sources (SPSs), which could eliminate the use of the bulky laser system. However, an inhomogeneous spectral broadening of about 10 meV is commonly induced by random distributions in shape and composition of QDs during the self-assembled growth process. This gives rise to distinguishability of

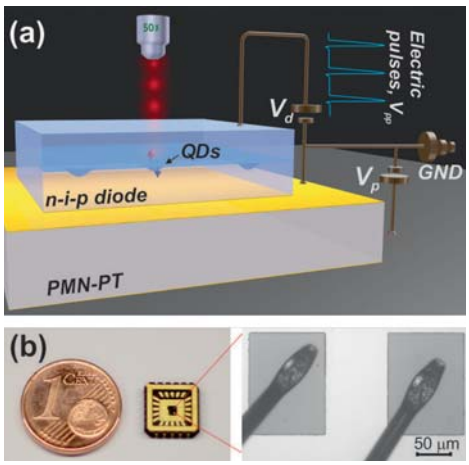

Fig. 1: A sketch of the nanomembrane-based strain-tunable Q-LED. **(a)** The *n-i-p* GaAs nanomembrane-based diode including self-assembled InAs QDs integrated onto a piezoelectric crystal, in which the strain field can modify the emission energy of photons emitted from the QDs. **(b)** Microscope images of the devices. The right side shows nanomembranes bonded on the PMN-PT crystal and the *n*-GaAs contacts formed by the electrical bonding of the aluminum wires on the top of the nanomembrane.

the photons from different QDs, and to date becomes the main obstacle to be overcome for the applications of self-assembled QDs in a quantum network.

A strain-tunable Q-LED is shown schematically in Fig. 1a, together with the microscope images of the device (see Fig. 1b). The electric contacts for the diode and the piezoelectric crystal are independent, and they share the same ground contact on the gold layer. With this configuration, electric fields can be independently applied to the diode and to the piezoelectric crystal without any cross-talk, therefore achieving an all-electrically simultaneous excitation and tuning of the QDs. Because the QDs are embedded in thin nanomembranes, the device facilitates the transfer of large strain fields from the PMN-PT crystal to the QDs and thus allows a broad tuning range of energy shift of the QD emission.[4, 5]

The device as shown in Fig. 1b is then mounted in a helium flow cryostat and all the experiments are carried out at 5 K. The electroluminescence (EL) is collected by a 50× microscope objective, which is placed on the top of the nanomembrane. The application of *Vp* to the PMN-PT results in an out-of-plane electric field *Fp* which leads to an in-plane strain in the nanomembrane. A broad tuning of the single photon emission of about 5 meV is achieved, see Fig. 2a.

For the single photon emission characterization we use a second-order time correlation setup,[2] and a typical result is shown in Fig. 2b. The periodic autocorrelation peaks together with the absent peak at zero-time delay provides the evidence of the trigged single-photon emission. The time separation between the neighboring peaks is 1.25 ns and coincides with the repetition rate of 0.8 GHz. We also prove that the triggered single-photon-emitting characteristic of this Q-LED is well maintained during the strain-controlled wavelength tuning. Together with the near-GHz operations, our device proposes a promising way to achieve indistinguishable single-photon emission from two remote Q-LEDs.

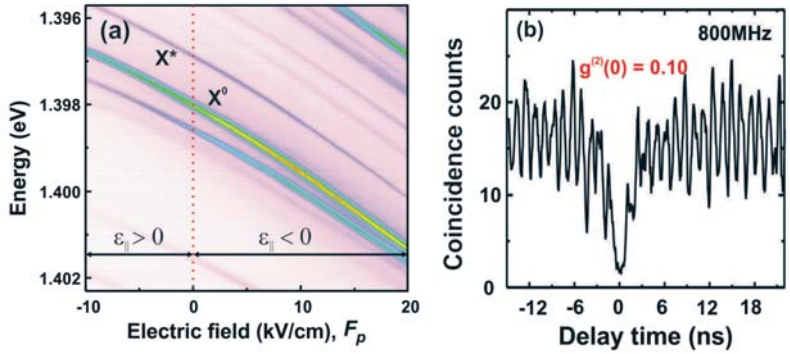

Fig. 2: (a) Tunable single QD emission under in-plane biaxial strain $\varepsilon_{\|}$. Large compressive ($\varepsilon_{\|} < 0$) or tensile strain ($\varepsilon_{\|} > 0$) can be obtained by applying different electric fields to the PMN-PT crystal along the z direction. The QD is under pulsed electric excitations. **(b)** Autocorrelation measurements of the single QD emission at an excitation repetition rate of 800 MHz. The pronounced anti-bunching dip at zero-time delay provides the evidence of the single-photon emissions.

Part II: Hole spins in QDs are receiving increasing attention, as decoherence due to hyperfine interaction with the nuclear spin bath should be reduced compared to electron spins. All experimental studies presented so far have been dealing with heavy-holes (HH). This is because quantum confinement and compressive strain in self-assembled QDs lifts the valence band degeneracy and leaves HH states energetically well above the LH states. However, using LHs instead of HHs would be beneficial for quantum information technologies, for example the coherent conversion of photons into electron-spins and the possibility to directly control the LH spin state via microwaves. For the realization of these and future proposals, the LH should be the ground state (GS), as any decay channel would reduce the coherence time. Here we address two open questions: Can we make high-quality QDs with a GS of dominant LH-type? How does the excitonic emission of such a QD look like?

Our successful answer to the first question is to use strain-engineering: starting from almost unstrained GaAs QDs in AlGaAs matrix with a conventional HH GS, we reverse the energetic order of the HH and LH bands by biaxial tensile stress. The process preserves the zero-dimensional character of the exciton. Our QDs are obtained by local droplet

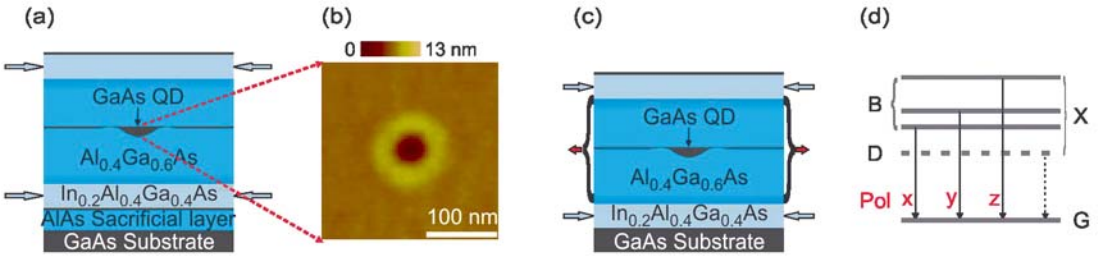

Fig. 3: A QD with LH exciton ground state. **(a)** Schematics of the GaAs QD heterostructure. The length of the horizontal arrows is proportional to the magnitude of in-plane strain in the layers. **(b)** AFM image of a representative "self-etched" nanohole on the AlGaAs surface prior to GaAs filling. **(c)** Schematics of the GaAs QD heterostructure after selective etching of the AlAs sacrificial layer. **(d)** Energy levels diagram and allowed dipole transitions with corresponding polarization directions. X indicates the neutral exciton, which consists of a dark (D) state and three bright (B) states decaying to the crystal ground state (G). "x" and "y" denote in-plane crystal directions [110] and [1-10] and "z" denotes the growth direction [001].

etching of nanoholes into an AlGaAs surface followed by GaAs-filling and AlGaAs overgrowth. A sketch of the heterostructure is shown in Fig. 3a. Compared to strained self-assembled QDs, GaAs/AlGaAs QDs are almost unstrained and their height, which influences the LH-HH splitting, can be controlled by adjusting the amount of GaAs used to fill the nanoholes. Since in-plane anisotropy of the confinement potential is expected to contribute to LH-HH mixing, the growth protocol is further optimized to obtain highly symmetric QDs (see Fig. 3b). Finally, to allow the LH to become the GS, a biaxial tensile strain of about 0.36% is induced on the QDs by embedding them into symmetrically pre-stressed membranes, which are then released from the substrate (see arrows in Fig. 3a and Fig. 3c.)

Due to the electron-hole exchange interaction, the exciton formed of electron and light hole should have three optically bright states ('B') polarized along [110], [1-10] and [001] crystal directions and one optically dark state ('D') as shown in Fig. 3d. This is different from HH exciton configurations, which include two bright states and two dark states. To verify whether the LH has been switched to the GS of the valence band, we excite μ-photoluminescence (μ-PL) with a focused laser beam parallel to the z direction and collect linear-polarization-resolved PL spectra of as-grown and tensile strained QDs along both z- and x- (cleaved edge) directions. The spectra for a representative as-grown QD are shown in Figs. 4a,b and are fully consistent with a HH exciton: two in-plane polarized bright-exciton states, B_1 and B_2. After the membrane undercut, the average QD-emission-energy red-shifts by about 50 meV due to the tensile biaxial strain, as illustrated by the spectra from another representative QD, shown in Fig. 4c,d. Most importantly all QD spectra measured so far display a new line located at ~ 430 μeV above the in-plane polarized doublet $B_{1,2}$. This line, indicated as B_z in Fig. 3d is linearly polarized along z. These observations are in line with our expectations for a LH exciton having three bright recombination channels: $B_{1,2}$ and B_z. See Ref [3] for more details.

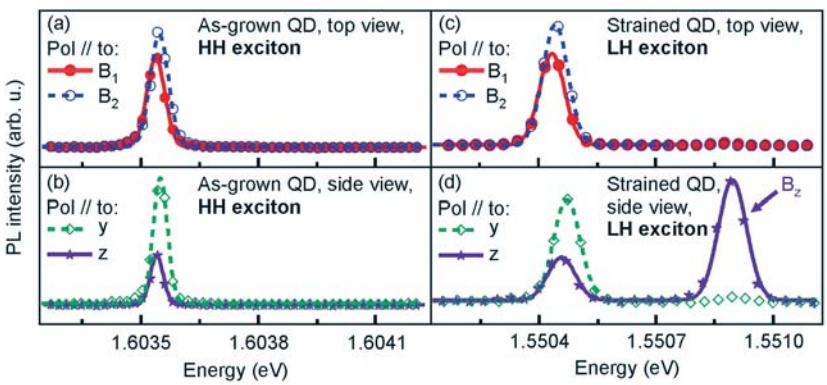

Fig. 4: μ-PL spectra of representative HH and LH excitons in single GaAs/AlGaAs QDs. **(a)** to **(d):** Spectra of neutral exciton along two perpendicular polarization directions in one representative as-grown QD **(a,b)** and one tensile strained QD **(c,d)**. Spectra are collected along the conventional z [001] direction in **(a)** and **(c)** and along x [110] direction from a cleaved edge in **(b)** and **(d)**. The solid (open) circles (B1 and B2) correspond to in-plane polarizations (x and y), solid stars correspond to out-of-plane polarization (z). Lines are Lorentzian fittings.

In conclusion we use the elastic stain engineering technique to control the quantum light emissions from semiconductor QDs. An all-electrically operated wavelength tunable Q-LED is demonstrated, with an excitation repetition rate up to 0.8 GHz. Also we have shown that the excitonic GS of self-assembled GaAs QDs can be switched from the common dominant HH to the LH type by strain fields. Our results will find immediate applications, such as electrically prepared flying qubits and LH-based stationary qubits, in a semiconductor-based quantum system for quantum communication technologies.

Acknowledgements: Valuable collaborations with B. Höfer, L. Han, S. Kumar are greatly appreciated. We thank B. Eichler, R. Engelhard, P. Atkinson, C. Deneke, D. J. Thurmer and S. Baunack for the technical support, also D. Grimm, B. Martin and S. Harazim for assistance in clean room maintenance.

[1] R. J. Warburton, Nature Mater. 12 (2013) 483.
[2] J. X. Zhang et al., Nano Lett. 13 (2013) 5808.
[3] Y. H. Huo et al., Nature Phys. (2013) doi:10.1038/nphys2799.
[4] F. Ding et al., Phys. Rev. Lett. 104 (2010) 067405.
[5] R. Trotta et al., Phys. Rev. Lett. 109 (2012) 147401.

Cooperation: 1. R. Grifone, D. Kriegner, R. Trotta, J. Stangl, G. Katsaros, and A. Rastelli, Institute of Semiconductor and Solid State Physics, Johannes Kepler University Linz, Austria; 2. B. J. Witek, N. Akopian, V. Zwiller, Kavli Institute of Nanosciene, Delft University of Technology, The Netherlands; 3. J. R. Cardenas, R. Singh, G. Bester, Max-Planck-Institute for Solid State Research, Germany

Funding: BMBF project QuaHL-Rep (No. 01BQ1032 and 01BQ1034), DFG FOR730, EU FP7 (No. 601126 210 - HANAS), China Scholarship Council (No. 2010601008).
Cooperation: Institute of Semiconductor and Solid State Physics, Johannes Kepler University Linz, Austria; Kavli Institute of Nanosciene, Delft University of Technology, The Netherlands; Max-Planck-Institute for Solid State Research, Stuttgart, Germany

Technological impact

Functional properties of Heusler compounds on the nanoscale – from fundamentals to applications

M. Gellesch, M. Dimitrakopoulou, M. Scholz, C. G. F. Blum, M. Schulze,
J. van den Brink, S. Hampel, S. Wurmehl, and B. Büchner

We have designed a new Heusler-based type of magnets, where Heusler nanocrystals are obtained by filling carbon nanotubes. The nanocrystals are chemically stable intermetallic single crystalline ferromagnetic Heusler nanoparticles. We have found a ground-breaking way to overcome the hurdles typically involved with intermetallic nanomaterials. Our exceptional approach allows us to tailor the properties of magnetocaloric, thermoelectric and shape-memory materials or the half-metallic ferromagnets, found among the family of Heusler compounds, in the form of chemically stable nanoparticles with well-defined size. These findings will set stage for the exploration of the functional properties of Heusler compounds on the nanoscale. Our studies will allow us to explore whether potential applications for the new functional properties of our nanocrystals exist and moreover how we can control the properties of the material towards such potential application.

Research on nanoscale materials is motivated by the observation that materials show a significant change in physical and chemical properties or even exhibit novel phenomena at nanometer dimensions due to a high surface-to-volume ratio and finite size effects [1-4]. One of the major driving forces of altered properties in nanoscale materials is their greatly enhanced surface to volume ratio. This, however, constitutes at the same time a challenge, as a large surface area can trigger rapid oxidation of metallic nanoscale objects [5]. This fundamental hurdle has so far obstructed the full exploitation of attractive bulk properties of metallic and intermetallic materials on the nanoscale, encompassing e.g. ferromagnets with high magnetic moments and record critical temperatures. A drawback of previously reported methods for the synthesis of Heusler nanoparticles is the broad distribution of diameters and a coating with undefined geometry [6]. While the coercive fields of common ferromagnetic materials (e.g. iron) can be enhanced by downscaling their size [e.g. 7], intermetallic systems like Heusler compounds offer the additional possibility to tune physical properties by varying compositions. However, reports on Heusler nanomaterials are scarce, few reports on nanoparticles [e.g. 6] and a single one on Heusler nanowires [8], - although Heusler materials constitute a huge class of highly functional materials [9].

In order to overcome the limitations of the known synthesis methods, we suggest an alternative and elegant approach based on nanoparticles encapsulated inside the hollow cavity of carbon nanotubes: In our experiments, we have filled multiwalled carbon nanotubes (CNT) with the intermetallic Heusler compound Co_2FeGa by extending a reported solution filling approach for carbon nanotubes [10]. Here we could verify that our synthesis method provides a ground-breaking way to overcome the hurdles typically involved with intermetallic nanomaterials.

The filling particles exhibit a characteristically ellipsoidal shape and possess a narrow size distribution with a mean diameter of $d_{NP} = 35 \pm 7$ nm (diameter perpendicular to the long tube axis). The particle diameter correlates with the mean diameter $d_{CNT} = 38 \pm 9$ nm of the inner cavity of the CNT, which indicates that the diameter of the nanoparticles may be directly controlled by an appropriate choice of CNT. Nanobeam electron diffraction reveals that the filling particles are single crystalline (Fig. 1). We observed the $L2_1$ lattice structure which coincides with the bulk one, giving evidence for a high structural integrity of the filling particles. It is remarkable that although the samples have been exposed to air for several months, we find no hints for oxidation of the filling

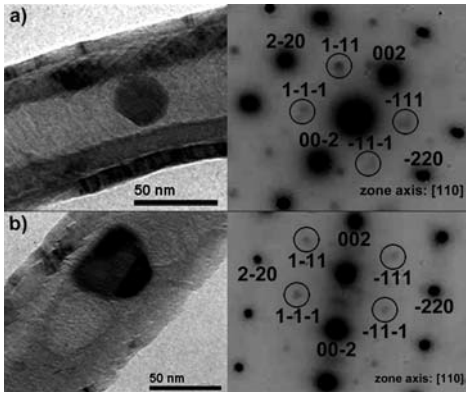

Fig. 1: Bright field TEM images and corresponding nanobeam electron diffraction patterns of individually Co_2FeGa particles inside carbon nanotubes as observed from a [110] zone axis. The diffraction patterns and in particular the presence of the 111 and 200 superstructure reflections are evidence for the single crystalline character and a high degree of structural order of the filling particles.

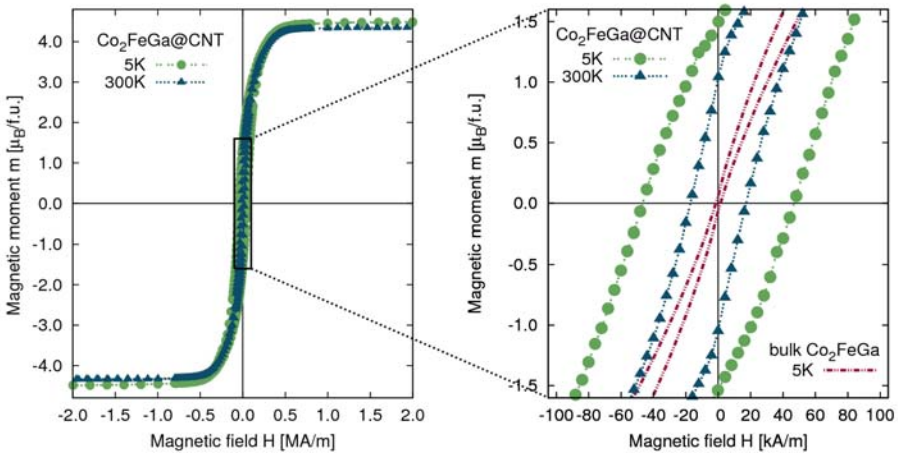

Fig. 2: (left panel) Hysteresis curves of carbon nanotubes filled with Co_2FeGa Heusler nanoparticles measured at a temperature of 5 K and 300 K. The right panel shows an enlarged view on the hysteresis curve in comparison with a polycrystalline bulk sample. Here the enhanced coercive field in Heusler-filled carbon nanotubes can be clearly identified.

particles, even at those close to the open tips of the CNT. This chemical stability is a great advantage, not only over unprotected intermetallic nanoparticles, but also over Heusler thin films and bulk Heusler compounds, where battling oxidation constitutes a permanent challenge [11]. The downscaling enhances the coercive field of the Heusler magnets more than 30-fold while preserving magnetic transition temperature (Fig. 2) and saturation magnetization of the respective bulk Heusler compounds (not shown).

Chemically stable intermetallic nanoparticles with tailored dimensions may be useful for many different technological applications. (i) The filled tubes can be embedded in different materials such as polymers, conventional metals or magnets. The alignment of embedded nanoparticles will most likely not change their nano- nor the microstructure, but it will add new functionalities, e.g. an enhanced magnetic anisotropy. Our composite material will have the additional advantage, apart from tuning the magnetic properties, of being very stable even at elevated temperatures compared to the pure magnetic material and will hence allow technical applications exceeding the conventional operating temperatures. (ii) Individual Heusler filled CNT may work as tips for magnetic force microscopy (MFM) where tailored magnetic properties might enhance the performance of MFM tips. Additionally, some Heusler compounds are predicted to be potential half-metallic antiferromagnets (also called compensated half-metallic ferrimagnets). Those materials exhibit 100% spin polarization but have no net magnetic moment. Such materials are considered as potential candidates for tips in scanning tunneling microscopy (STM).

Our findings will set stage for the exploration of the functional properties of Heusler compounds on the nanoscale. Several technological applications for the new functional properties of our nanocrystals are envisioned.

We thank G. Kreutzer, S. Gaß, T. Gemming, J. Thomas, and A. Wolter for support.

[1] G.C. Hadijipanyis, R.W. Siegel, Nanophase Materials: Synthesis, Properties, Applications, Kluwer Academic, London (1994).
[2] A.S. Edelstein, R.C. Cammarata, Institute of Physics, Philadelphia (1996).
[3] L.M. Liz-Marzan, P.V. Kamat, Nanoscale Materials, Kluwer Academic, (2003).
[4] G.A. Ozin, A.C. Arsenault. Nanochemistry, Cambridge (2005).
[5] A.-H. Lu et al., *Angew. Chem. Int. Ed.* **46**, 1222 (2007).
[6] L. Basit et al., *J. Phys. D Appl. Phys.* **42**, 084018, (2009).
[7] R.H. Kodama, *J. Mag. Mag. Mat.* **200,** 359 (1999).
[8] K.R. Sapkota et al., *J. Appl. Phys.* **111**, 123906 (2012).
[9] T. Graf et al., *Prog. Solid State Ch.* **39**, 1 (2011).
[10] M. Gellesch et al., *Cryst. Growth Des.* **13,** 2707 (2013).
[11] H.J. Elmers et al., *Phys. Rev. B* **67**, 104412 (2003).

Funding: AUDI AG, DFG, BMBF, DAAD, SSddV

Ultra-thin and flexible Hall Sensors for electrical machines and drives

M. Melzer, F. Bahr[1], D. Karnaushenko, D. Makarov, G. S. Cañón Bermúdez, J. I. Mönch, W. Hofmann[1], O. G. Schmidt

There is a trend in electronics towards becoming flexible, stretchable or printable, which allows electronic components to be arbitrarily reshaped after fabrication. This unique feature offers new unexplored functionalities for the markets of consumer electronics and eMobility. Already developed flexible magnetoresistive sensors typically reveal a maximum responsivity in the range of small magnetic flux densities of about several mT. However, they are not suitable for eMobility applications where detecting out-of-plane magnetic fields up to 2.2 T in small air gaps of less than 500 μm between rotor and stator of electrical machines is required. In this respect, we recently reported on the fabrication of a flexible and ultra-thin Bismuth Hall sensor on a conventional flexible printed circuit board (PCB) with a total thickness of 150 μm including cabling. These sensors were successfully integrated onto the curved surface of the stator poles of a magnetic bearing. We demonstrate that the magnetic flux density in the air gap of a two-axes active magnetic bearing can be monitored using flexible Bismuth Hall sensors.

In the rapidly developing market of eMobility there is a strong demand for novel sensor solutions fulfilling the specific requirements imposed by new tasks such as, e.g. the optimization of the eMotor design or the improvement of the dynamical performance (stiffness and damping) as well as a precise positioning accuracy of magnetic bearing systems. Both of these tasks require the measurement of the magnetic flux density of up to 2.2 T in curved and tiny air gaps (<500 μm) of electrical machines. In order to accomplish this task, sensor solutions based on the Hall effect have to be developed, which are ultra-thin (less than 200 μm thick) and flexible.

There are reports on flexible magnetoresistive sensors [1-3]. However, these sensors are typically applied for in-plane magnetic field measurements and reveal a maximum responsivity in the range of small magnetic flux densities of about several mT, which is not suitable for eMobility applications where detecting out-of-plane magnetic fields up to 2.2 T with high precision and reliability is required. For this field range, Hall effect sensors are the favorable choice, as they provide a linear voltage response up to high magnetic fields. We already reported on the fabrication of flexible metal-based Hall sensors with a thickness of 280 μm on ultra-thin Polyetheretherketone (PEEK) foils [4]. These flexible sensors can be bent down to radii of 5 mm and provide a reliable measurement of the magnetic flux density of up to 2.3 T. However, the demonstrated sensors were still too thick to fulfill the safety requirements for an application in electrical machines and drives.

Here, we fabricate Bismuth-based Hall effect sensors on commercially available flexible printed circuit boards (PCBs), which allow us to reduce the total thickness of magnetic field sensors down to 150 μm including contacts and encapsulation. The performance of these sensors is highlighted in the present work and their application for the measurement of magnetic flux densities in a magnetic bearing is discussed [5].

For the fabrication of Hall sensor elements, Bismuth films were deposited using magnetron sputtering at room temperature onto commercially available 150 μm thick double layer flexible Polyimide-based PCBs (Fig. 1(a, b)). These polymeric membranes reveal a good mechanical, thermal and chemical stability. Bismuth Hall sensors represent an interesting alternative to the conventional semiconductor-based magnetic field sensors mainly due to two reasons: (i) Bi has the largest Hall coefficient and thus largest sensitivity among all (half-) metals and (ii) it is rather easy in preparation and processing. Fabrication in brief: first, we deposit a 5-nm-thick Cr seed layer on the

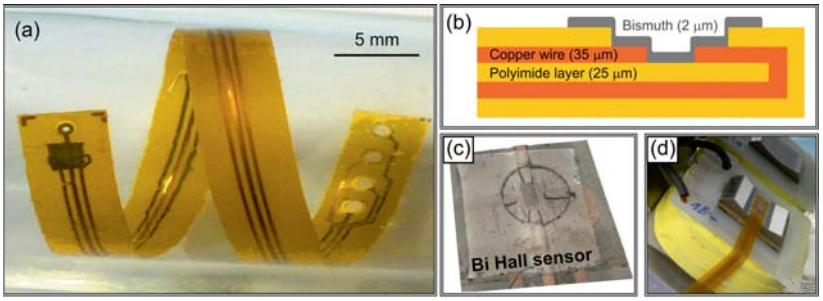

Fig.1: (a) Flexible Bismuth Hall sensors. **(b)** Schematics of the Hall sensor cross-section. **(c)** Confocal 3-dimensional microscopy imaging of the deposited Bi sensor elements. **(d)** Integration of the sensors at the stator pole of a magnetic bearing system.

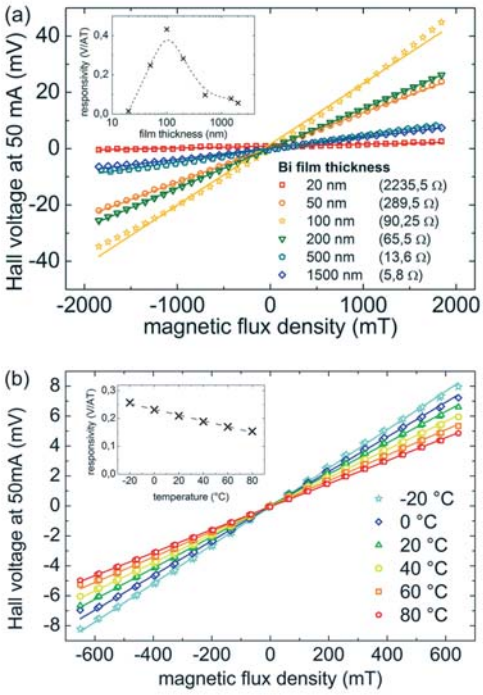

Fig. 2: Performance of the Hall sensors. **(a)** Impact of the Bi film thickness on the Hall response for the sensors prepared on PEEK foils. The legend contains information on the electrical resistance of the current-supplying contacts. The inset summarizes the responsivity of the sensor elements as a function of the Bi film thickness. **(b)** 2-μm-thick Bi Hall sensor prepared on flexible PCB measured at different temperatures. The inset summarizes the responsivity of the sensor with respect to the measurement temperature.

flexible PCB and Copper contacting pads (wire thickness of 35 μm) to assure a good adhesion of Bi films to the polymeric membranes. Afterwards, Bi layers are grown. Both Cr and Bi films are grown through the opening in the top layer of the flexible PCB as shown in Fig. 1(a-c).

In this respect, the electrical contacting of the Bi sensing element is directly established during the deposition process. The thickness of the Bi layers prepared on flexible PCBs is limited to 2 μm, which is thinner compared to the thickness of the top layer of the PCB (25 μm). Therefore, the total thickness of the sensor is determined by the initial dimensions of the flexible PCB and in this study is 150 μm. These flexible sensors can be mounted onto the non-planar surface of the stator poles of magnetic bearings as shown in Fig. 1(d). In order to optimize the sensor responsivity, a series of reference samples was prepared where extended Bi films of different thicknesses in the range between 20 and 1500 nm were deposited onto PEEK flexible foils. The electrical contacting in the Hall configuration was realized using contact pins with a distance of 6 mm. The responsivity is defined as the slope of the Hall response (Hall voltage vs. Magnetic flux density) normalized to the value of the supply current.

Fig. 2(a) shows the modification of the performance of the Bi Hall sensors prepared on PEEK foils with the thickness of the Bi film. As the current density is increasing with the decrease of the film thickness, the responsivity is increasing for thinner sensors reaching a maximum of about 400 mV/(A T) for the sensor with a 100-nm-thick Bi layer. However, the responsivity drops abruptly when the thickness of the Bi film is reduced below 100 nm. We attribute this finding to the modification of the morphology of the thin Bi films. Indeed, the scanning electron microscopy study (not shown) reveals a substantial increase of the granularity of the film for a small thickness of Bi below 100 nm. This modification of the film morphology results in a substantial increase of the sensor resistance as shown in the legend of Fig. 2(a). In addition, a grainy morphology leads to the reduction of the mechanical stability of the sensors. Therefore, although the maximum of the sensor responsivity is achieved for the 100-nm-thick Bi films, in the following experiments we will use 2-μm-thick Bi layers for the fabrication of the sensors on flexible PCBs. This results in a smaller responsivity of the sensors but substantially enhances their reliability with respect to the bending experiments and prevents a breaking of the electrical contacts at the sensor location.

Temperature dependence of the Hall response is one of the crucial parameters characterizing the performance of the sensor. Fig. 2(b) shows the series of Hall responses measured at different temperatures of the 2-μm-thick Bi film prepared on flexible PCB. As typically observed for the Hall effect, the responsivity of the sensors becomes smaller with an increasing temperature due to the mobility decrease of the charge carriers. The slope of the linear fit shown in the inset provides a value of the temperature coefficient of the sensor's responsivity of about -0.35 mV/(A T K). The temperatures in this investigation represent a realistic operation range for magnetic bearings. Hence, the flexible magnetic field sensors presented here would require an additional temperature compensation for magnetic bearings applications.

Table I summarizes the geometrical and electrical characteristics of the flexible Bi Hall sensors prepared on flexible PCB with the total sensor thickness of 150 μm. The elec-

trical properties are presented after the amplification of the initial sensor signal. With an amplification coefficient of 1000x, a sensor resolution at room temperature of 25 mT is achieved for a magnetic flux density of 2 T. In order to reduce disturbances, a supply current of 10 mA is used.

SENSOR CHARACTERISTICS

	Parameter	Value
Sensor dimensions	Area of the sensor element	4 mm²
	Active sensor area	1 x 1 mm²
	Bismuth film thickness	2 μm
	Total height	150 μm
Electrical parameters	Supply current	10 mA
	Electrical resistance	(20 ... 30) Ω
	Hall responsivity	≈ 0.1 V/(A·T)
	Sensor resolution	50 mT
	Signal-to-Noise ratio	32 dB
Other parameters	Operating temperature range	0 to 80 °C
	Temperature coefficient of responsivity	1 mV/(A·T·K)
	Minimum bending radius	10 mm

In the following, we employ the ultra-thin flexible Hall sensors to monitor the magnetic flux density inside narrow air gaps of < 500 μm in active magnetic bearings (AMBs). As the magnetic flux density is the relevant system variable for the magnetic force generation, the direct magnetic field measurement is thus of special interest to improve the performance of the AMBs. In order to analyze the functionality of the new sensor elements under real conditions, they have been integrated in a two-axes AMB setup (Fig. 3(a)). The radial bearing is operating with two stators and heteropolar flux paths for controlling as well as a certain homopolar bias magnetization. One sensor element was mounted on each of the four poles of stator 1 to measure the flux densities in both bearing axes. The rotor position is detected using a capacitive measurement system providing a resolution of about 50 nm. On a proof-of-concept level, we present the detection of the magnetic flux density inside the air gaps using calibrated flexible Hall sensors. Here, a conventional cascaded position control with subordinated current control is implemented for both bearing axes. Fig. 3(b) exemplifies the measured control flux density of one air gap with positioning the rotor in the mechanical center. By using control parameters realizing a stiffness of 1.6 N/μm and a damping ratio of D = 0.5, a positioning accuracy of ±0.25 μm is achieved. The Hall sensors provide a magnetic flux density signal with a noise amplitude of about 50 mT_{P-P}. The presented data reveals that the fabricated ultra-thin and flexible Bismuth Hall sensors are suitable for flux density measurements in magnetic bearing systems.

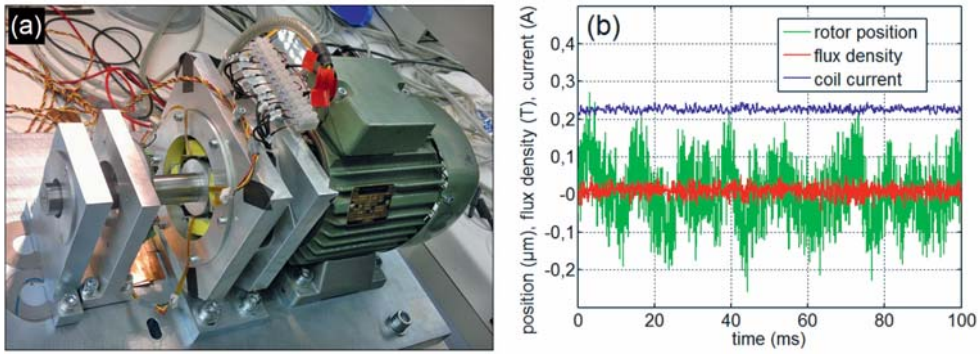

Fig. 3: (a) Test rig of a two-axes active magnetic bearing. **(b)** Monitoring of the control flux density for rotor positioning in the mechanical center using conventional cascaded position and current control: stiffness: 1.6 N/μm; damping ratio: D = 0.5.

Conclusion

We fabricated ultra-thin and flexible Bismuth Hall sensors on commercially available flexible PCBs. The total thickness of the sensor is 150 μm, which is limited by the dimensions of the flexible PCB. The Hall response of the sensors is optimized with respect to the thickness of the Bismuth film to be 400 mV/(A T) for the 100-nm-thick Bismuth layer. However, with the present design of the flexible PCB, 100-nm-thick Bi sensors are not stable mechanically. Therefore, for experiments in the AMB a 2-μm-thick Bi film was used. Our study also shows, that if the PCB design is improved, e.g. by an encapsulation of the Bismuth layer in the mechanical neutral plane, the sensitivity of the sensor can be substantially increased.

These sensors are thin enough to be successfully integrated on the curved surface of stator poles of a conventional two-axes permanent magnet bias AMB. The demonstrated reliable measurement of the magnetic flux density in the air gap of the magnetic bearing opens up the possibility to realize a flux based control using the measured flux density as a feedback signal.

These ultra-thin and flexible magnetic field sensors could enable the following AMB applications: the integration of the flux density measurement system can (i) boost the positioning accuracy of rotors in AMBs as required for high precision machining tools and (ii) enhance the reliability of the AMBs used for sub-see compressors by adding a redundant flux based control.

[1] S. S. P. Parkin, Appl. Phys. Lett. 69, 3092 (1996).
[2] Y.-F. Chen et al., Adv. Mater. 20, 3224 (2008).
[3] C. Barraud et al., Appl. Phys. Lett. 96, 072502 (2010).
[4] F. Bahr et al., Full paper in the proceedings of the 13th International Symposium on Magnetic Bearings – ISMB13, Arlington, Virginia, USA, 2012.
[5] F. Bahr et al., Full paper in the proceedings of the 1st Brazilian Workshop on Magnetic Bearings, Rio de Janeiro, Brazil, 2013.

Cooperation: [1]Elektrotechnisches Institut, TU Dresden
Funding: DFG (projects HO 1483/64-1, SCHM 1298/15-1), BMBF project Nanett (FKZ: 03IS2011F), European Research Council (ERC grant agreement no. 306277)

Multi-Analyser-Detector for Synchrotron Powder Diffraction at 60 keV Beam Energy

A. Horst, A. Berghäuser[1], M. Hinterstein[2], M. Knapp[3], D. Lindackers, H. Ehrenberg[3], J. Eckert

In order to perform high resolution measurements at the powder diffraction beamline P02.1 at PETRA III we developed a Multi-Analyzer-Detector. Here we describe the main challenges for the construction. Monolithic collimators and slits were machined from the Tungsten alloy Densimet by spark eroding to provide a high signal-to-noise ratio without signal contamination from stray radiation. The motorized individual crystal adjustment allows a high precision for the crystal orientation. A patent-registered system combining levers and spirals can achieve an accuracy of $5 \cdot 10^{-5}$° in a very compact construction.

Powder Diffraction is nowadays the workhorse in Material Science, crystallography and related fields for the investigation of materials properties [1,2,3,4,5]. The determination of the crystallographic structure and its change with physical and chemical parameters gives insight in how materials behave and how functional materials might be improved. Beside powerful and brilliant radiation sources like synchrotrons or sophisticated sample environments to mimic real operating conditions, the radiation detection system plays a crucial role to get the relevant information out of the experiment.
In the detector concept (Fig. 1) presented in this report, the scattered intensity is diffracted by secondary monochromators. In order to reduce the measuring time, multiple channels (10 channels separated by 1°) are used in parallel to either increase statistics or reduce the necessary angular scanning range. In order to enhance the available analytical spectra, a high energy Powder Diffraction beamline was implemented at PETRA III, working at 60 keV which allows the best tradeoff between high energy and high resolution. For high energies the separation of direct and diffracted beam as well as the avoidance of fluorescence and penetration of the construction material becomes challenging.
In cooperation with engineers and scientists from other institutions the IFW Forschungstechnik developed and built a detector system with 10 channels for the High Resolution Powder Diffraction Station P02.1 at the PETRA III Synchrotron in Hamburg.

MAD Design principles

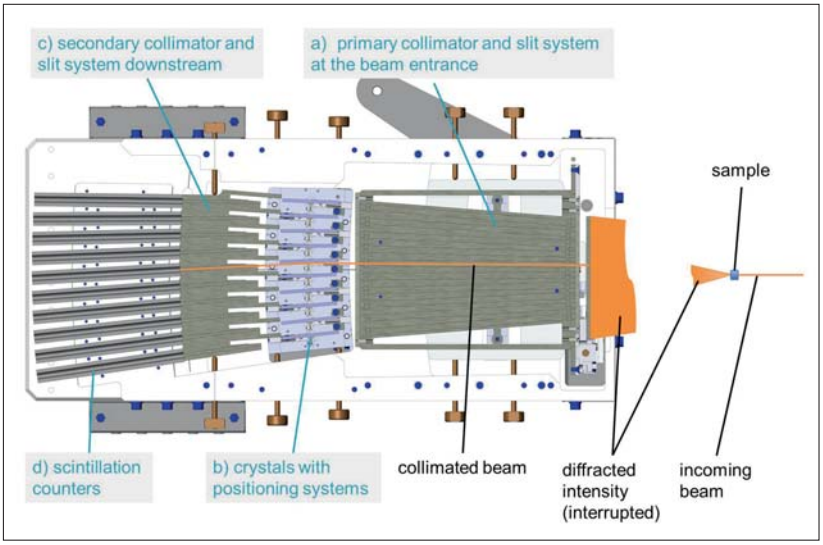

Fig. 1: Physical parts of the MAD with collimated and reflected beam after the crystal.

The detector consists mainly of the following components which are depicted in the sketch given in Fig. 1. The components are:
a) Primary collimator and slit system at the beam entrance (Densimet)
b) Crystals with positioning systems (silicon Si111 reflection)
c) Secondary collimator and slit system downstream the crystals (Densimet)
d) Scintillation counters (YAP)

After passing the sample the beam is collimated, then Bragg-reflected at the crystals and finally detected in the scintillation counters. With respect to the scattering performance the choice of crystals is limited. In order to maximize the scattered intensity and resolution as well as minimize variations between the channels the crystals were cut from the very same silicon wafer. With optimized dimensions the crystals were cut in 111 orientation, leading to a theoretical scattering angle of 3.7766° with respect to the incoming beam (Fig. 2). In order to get a sufficiently good signal to noise ratio, the scattered beam has to be well separated from either primary beam and any stray or fluorescence scattering.

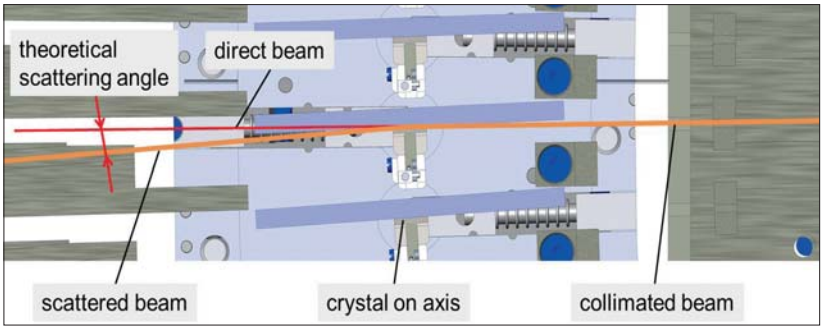

Fig. 2: Beam path in details.

With respect to the high beam energy highly absorbing materials have to be used as collimators and slits as for instance tungsten alloy (Densimet). In addition, the absorption edge of tungsten is right above 60keV and not critical. To avoid gaps in the collimator block and sources of stray radiation, the collimator blocks were machined out of one piece by spark eroding. A monolithic block of high accuracy and leak tight to high energy stray radiation was obtained. To individually adapt the acceptance of the channels, tungsten alloy (Densimet) slits with fixed width can be inserted at entrance and exit of the primary collimator block (Fig. 3).

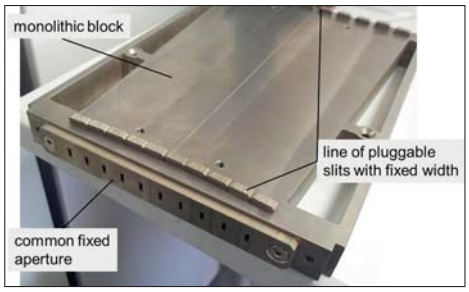

Fig. 3: Monolithic primary collimator with Densimet slits and fixed entrance blade.

The main components of the detector are the ten crystals operating as secondary monochromators and their positioning system. Since the Darwin width of a Si111 reflection at 60keV is about $2.5 \cdot 10^{-4}$° and for a proper centering about 10 data points are necessary, an angular resolution of 10^{-5}° is mandatory. At the same time the positioning system has to avoid strain on the crystal since this can deteriorate the lattice planes. The setup also has to be long term stable against drifts or thermal expansion, otherwise frequent realignment would be necessary. The offset angle between the crystals is set by machining and only a small angular range around the ideal position for fine adjustment of about +- 0.2° is necessary.

The technical solution for this is described in the following and Fig. 4: A stepper motor (running in full stepping to micro stepping mode) with a fixed 485:1 backlash reduced gear is attached via a stiff coupling to a spiral. A lever arm is pressed with low force on the side of the spiral and acting on the axis of the crystals. The connecting axis between motor and spiral is supported in a fine pitch thread, thereby feeding the spiral through the rotation. The motor is mounted on a linear slide and can follow this movement. With the combined feed and rotation the spiral changes its diameter on the lever arm and rotates lever arm and crystal. One complete turn of the spiral corresponds to 0.2° rotation of the crystal. With the stepper motor running in full step mode a final step resolution of 11640 steps/0.2° turn at the crystal axis can be realized, that is $1.7 \cdot 10^{-5}$° per step. To prevent any temperature effects the spiral and lever are machined from invar.

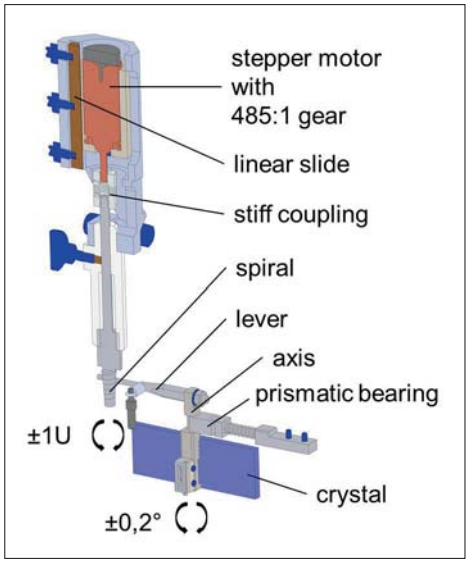

Fig. 4: Parts of the positioning system for the crystals.

The connection between crystal and its rotating axis is also delicate. Firstly, the surface of the crystal has to be centered in the axis of rotation, since offsets lead to non-linearities in the crystal alignment. Secondly, any strain introduced into the crystal by the

connection between axis and crystal has to be avoided since this could lead to symmetric or even asymmetric reflection broadening. In order to eliminate the influence of the tolerance of crystal thickness in positioning the reflecting side of the crystal in the rotation axis, the axis was glued to the front side of the crystal (the beam reflecting side) with glue that is stiff enough and does not shrink during hardening (Fig. 5). To avoid strain introduced through thermal effects the material of the axis was chosen the same as the crystal, silicon. By that, any temperature difference between assembly and operation will not lead to strain on the crystal. Machining of silicon is challenging. An electrically conducting silicon composition was used to be able to apply spark erosion. The silicon axis includes an adjustable edge-blade to absorb any non-scattered part of the beam.

To obtain a clearance free and self-inhibiting crystal axis, a spring loaded prism bearing was constructed.
The secondary collimator leads the scattered beam to the scintillator and absorbs the unscattered part in a beam dump (Fig. 6). For maximum efficiency the thickness of the scintillator crystal is optimized for 60 keV.

Figure 7: The accuracy of the crystal adjustment system was measured by means of an autocollimator system.

With the MAD a device was designed, which fulfills the target to perform high energy X-ray powder diffraction. The corresponding demands of collimating the diffracted intensity, high resolution in adjusting analyser crystals and long term stable working conditions were achieved.
The development led to a patent registration.

[1] P. L. Lee, D. Shu, M. Ramanathan, C. Preissner, J. Wang, M. A. Beno, R. B. Von Dreele, L. Ribaud, C. Kurtz, S. M. Antao, X. Jiao and B. H. Toby, *J. Synchrotron Rad.* **15** (2008) 427-432.
[2] N. Tartoni, S. P. Thompson, C.C. Tang, B. L. Willis, G. E. Derbyshire, A. G. Wright, S. C. Jaye, J. M. Homer, J. D. Pizzey and A. M. T. Bell, *J. Synchrotron Rad.* **15** (2008) 43-49.
[3] F. Gozzo, B. Schmitt, Th. Bortolamedi, C. Giannini, A. Guagliardi, M. Lange, D. Meister, D. Maden, P. Willmott, B. D. Patterson, *J. Alloys and Compounds* **362** (2004) 206-217.
[4] A. N. Fitch, *J. Res. Natl. Inst. Stan. Technol.* **109** (2004) 133-142.
[5] I. Peral, J. McKinlay, M. Knapp and S. Ferrer, *J. Synchrotron Rad.* **18** (2011) 842-850.

Cooperation: [1]University of Hamburg, [2]TU Dresden, [3]Karlsruhe Institute of Technology
Funding: BMBF project 05KS7OD2

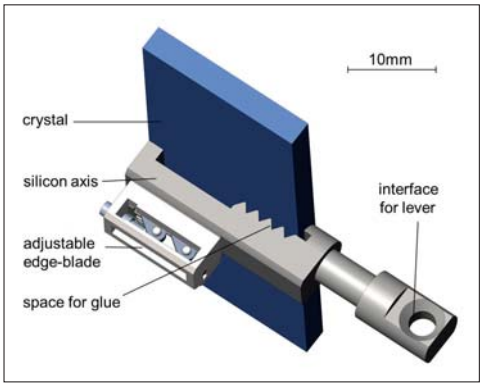

Fig. 5: Silicon axis with crystal and adjustable edge-blade.

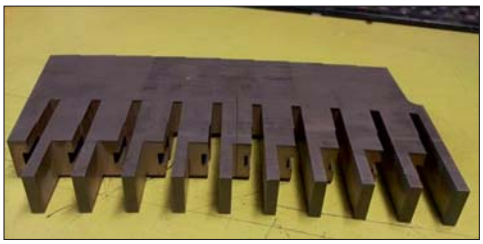

Fig. 6: Secondary collimator.

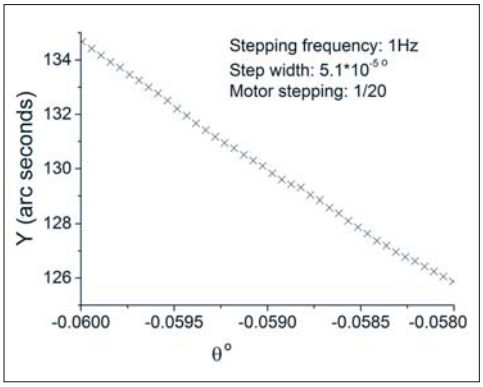

Fig. 7: Autocollimator measurement in dependence of crystal tilting. The step width corresponds to three full steps of $1.7 \cdot 10^{-5}$°.

A new Fullerene Generator with Adjustable "Active Gas Volume"

U. Biscop and F. Ziegs

The story of fullerenes started back in 1985 with the discovery of soccer ball shaped carbon by chemists Kroto, Smalley and Curl [1], when they unexpectedly found the C_{60} molecule by actually trying creating a soot atmosphere similar to interstellar dust. For this outstanding achievement they were awarded the Nobel Prize in Chemistry in 1996. This third modification of carbon was given the name "fullerene" in honor of the visionary designer Richard Buckminster Fuller (1895-1983).

The next breakthrough was made by a German-American team in 1990 which developed a high-output soot generator utilizing the principle of a DC-arc discharge evaporating graphite rods. This so called Krätschmer-Huffman method [2] realized mass production of C_{60} and larger fullerenes. With macroscopic amounts of the molecules at hand it was now possible to analyze their chemical and physical properties in detail.

Fullerene research in the IFW Dresden started in 1992 with an in-house built generator based on the Krätschmer-Huffman method. Continuous improvements of this technology made the Department Electrochemistry and Conductive Polymers of the IFW Dresden to one of the leading research groups in this field worldwide. Since then the main processing parameters for the synthesis of fullerene molecules – current intensity, atmospheric pressure, rod filling composition and geometry of the arc discharge – have been optimized. As a result of 20 years of research a new parameter was identified. This is where our new fullerene generator comes into play.

Experiments at one of the existing fullerene generators had shown that the active volume of the gas atmosphere surrounding the arc discharge influences the cage size of fullerenes as well as the structure of clusters inside the cage. The motivation for developing a new fullerene generator was to implement a mechanism inside the reaction chamber allowing controlling this "active gas volume" around the arc discharge. Finally, in November 2013 the IFW fullerene laboratory was enriched by a new generator for the synthesis of fullerenes. The generator was completely designed in-house by the Research Technology Division and the Department Electrochemistry and Conductive Polymers. Except the reaction chamber all specific parts and components were manufactured and assembled in the IFW's mechanical workshop. Its design is based on the original Krätschmer-Huffman chamber with radial feedthroughs for graphite rods. Since a pure gas atmosphere is required for the synthesis of fullerenes, the reaction volume has to be evacuated prior to experiments. Thus, the chamber was designed for high vacuum conditions, using a rotary slide pump in combination with a cold trap to remove oxygen and other residual gases from the chamber.

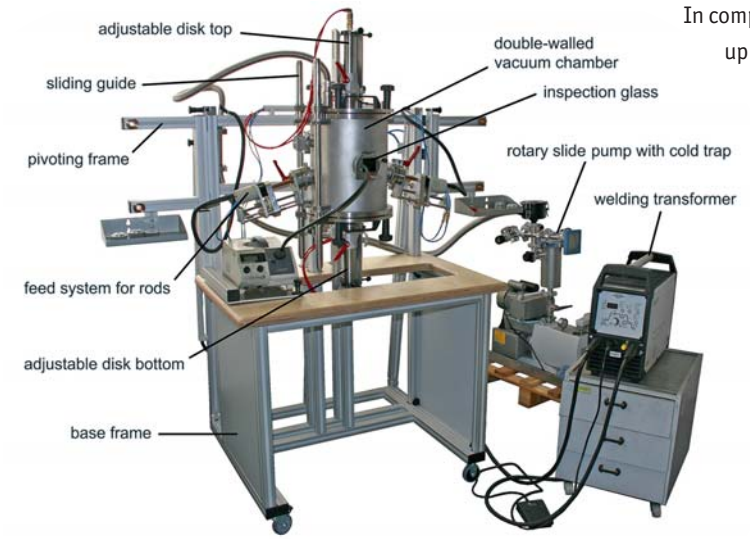

Fig. 1: The new generator with peripheral equipment. This picture illustrates the setup of the new generator and its peripheral components in the fullerene laboratory of the IFW Dresden.

In comparison to the already existing facilities the new generator comes up with three main features.

First the handling has been improved so that heavy-weight cover plates can remain in the base frame. Therefor a sliding guide in combination with pivoting frames was developed. Moreover, the generator itself is pivot-mounted in its center of gravity allowing easy access to the inside for removing the soot and cleaning the chamber.

Second the complete feed system of graphite rods was thoroughly redesigned. A manually driven gearbox in combination with a spindle drive uncouples the graphite rod rotary joints from forces resulting of the pressure difference between the inside of the chamber and atmospheric pressure. As a result a precise and constant rod infeed can be carried out by the operator. The

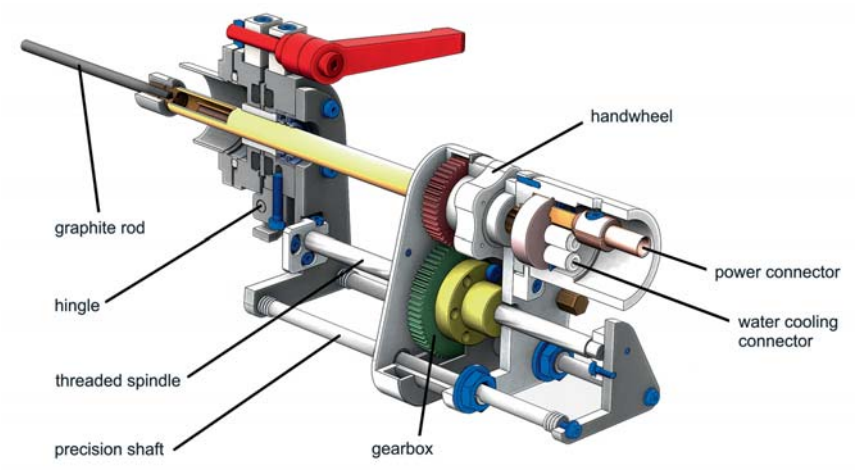

Fig. 2: New feed system for graphite rods. The combination of gearbox and pitch of the threaded spindle uncouples forces from pressure differences allowing comfortable and precise feed.

whole drive is already equipped with a clutch allowing motorized infeed at a further stage of extension. Thus, the future integration of the rod infeed into a closed loop is possible. Both spindle drives own two degrees of freedom in order to adjust both rods to a congruent focal point.

The rods can be adjusted within the range of +/- 1 degree to compensate their shape tolerances. Additionally, they can be rotated around their longitudinal axis. Another unique feature of the new feed system are the slightly upwards tilted feedthroughs. So by using mixed metal powder filled rods the main advantage is that this material cannot trickle out.

The third new feature - which can be seen as the outstanding highlight of the new generator – are the two symmetrical and adjustable disks. For the first time in fullerene synthesis they allow continuously variable adjustment of the important parameter "active gas volume" within a preset range in situ.

To ensure a controlled thermal gradient from the arc discharge towards the chamber's wall both disks are water cooled as well. Because of the ambitious design of the disk's internal structure the quality of welded seams has to meet highest standards. The disks themselves are completely made of stainless steel. Cooling water is supplied through coaxial welded tubes and distributed equally inside the disks, avoiding a radial temperature gradient. Both disks are placed in vacuum-tight slide bushings with rotary shaft seals. The disks can be individually or symmetrically adjusted by the operator within a range of 0 to 90 mm from the cover plates. As a consequence, the "active gas volume" surrounding the arc discharge can be varied by 60 percent.

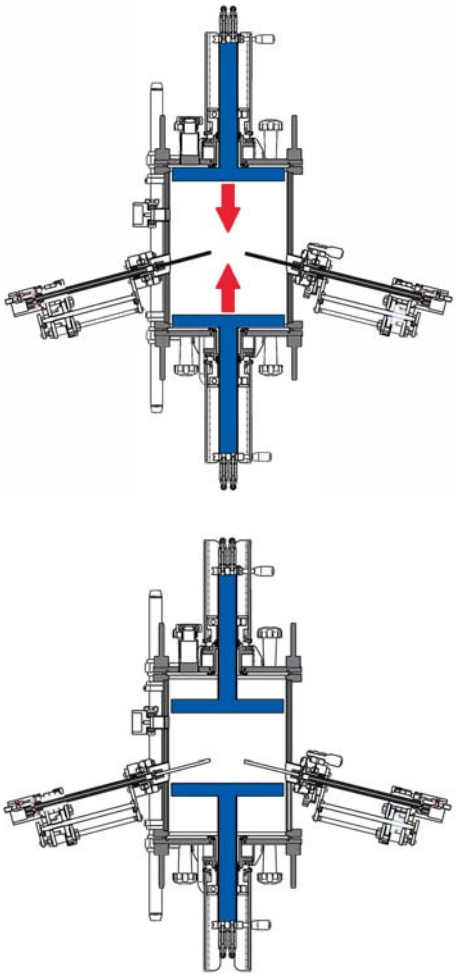

Fig. 3: Variable water-cooled disks to adjust the "active gas volume". Both disks can be adjusted separately to ensure a maximum degree of freedom for experiments.

In current fullerene research activities at the IFW special attention is paid to synthesizing and characterizing new structures with new magnetic, chemical, optical and charge transfer properties. By controlling the "active gas volume" it is expected to generate lots of unprecedented fullerenes for new fields of application to tie in with 20 years of successful fullerene research experiences.

The authors thank Prof. Dr. L. Dunsch, Prof. Dr. B. Büchner and Prof. Dr. D. Lindackers who initiated and put forward this project and gratefully acknowledge the valuable discussions with Dr.-Ing. R. Voigtländer and Dr.-Ing. T. Goedsche. Moreover the authors thank the whole team of the IFW's mechanical workshop for its commitment in the manufacturing and assembly of the generator and its peripheral components.

[1] H. W. Kroto, J.R. Heath, S. C. O' Brien, R. F. Curl, R. E. Smalley: C60: Buckminsterfullerene., *Nature* **318**, 162-163 (1985)
[2] W. Krätschmer: The story of making fullerenes., *Nanoscale* **3**, 2485-2489 (2011)

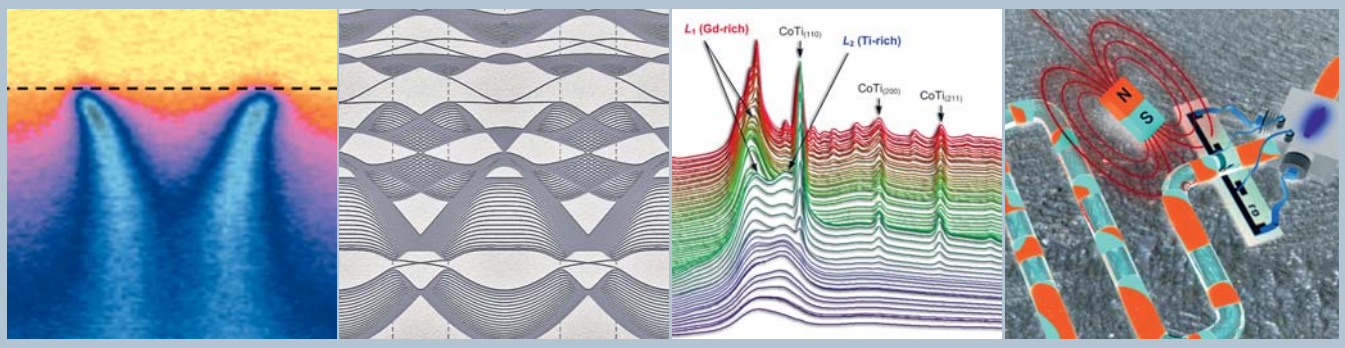

Reports from Research Areas

Research Area 1
Superconductivity and superconductors

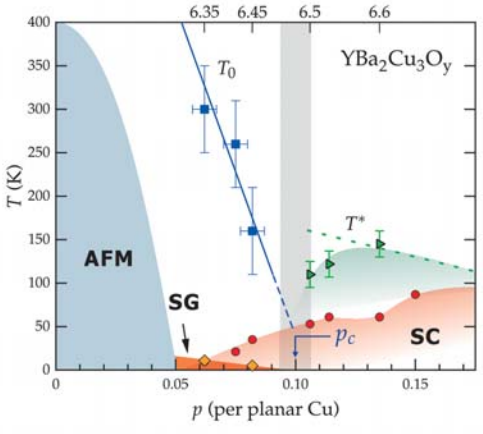

Fig.: Phase diagram of underdoped YBCOy in terms of hole concentration p. y values are shown on the top axis for convenience. T_0 and T* denote the onset temperatures of the static order with unknown nature and of the spin pseudogap, respectively. The dotted line drawn for T* is estimated from previously known NMR results.

Evidence of a critical hole concentration in underdoped $YBa_2Cu_3O_y$ single crystals revealed by ^{63}Cu NMR

S.-H. Baek, T. Loew[1], V. Hinkov[1], C. T. Lin[1], B. Keimer[1], B. Büchner, and H.-J. Grafe

The superconducting copper oxides (cuprates) in the underdoped regime feature unusual states of matter, such as a pseudogap (PG), density-wave order (stripes), and the coexistence of magnetism and superconductivity. Debates regarding the origin and the precise nature of those phases or related phenomena such as a reconstruction of the Fermi surface at a quantum critical point are still ongoing. In particular, interest in the underdoped $YBa_2Cu_3O_y$ has been revived in recent years. In order to elucidate the underlying physics in the highly underdoped region of $YBa_2Cu_3O_y$ ($y < 6.5$) on a microscopic level, we carried out a ^{63}Cu nuclear magnetic resonance (NMR) study of this compound. We show that a critical hole doping p_c exists in the p-T phase diagram of $YBCO_y$ beneath the superconducting (SC) dome at $p \sim 0.1$ (see Fig.), below which a static order sets in with a well-defined onset temperature. On the other hand, the spin pseudogap in the low-energy spin excitation spectrum was identified only near and above this critical hole concentration, suggesting that the spin pseudogap competes with this static magnetic order [1].

[1] S.-H. Baek et al., Physical Review B **86**, 220504(R) (2012)

Cooperation: [1]Max-Plank-Institut für Festkörperforschung, Stuttgart
Funding: DFG through FOR538 (Grant No. BU887/4) and SPP1458 (Grant No. GR3330/2)

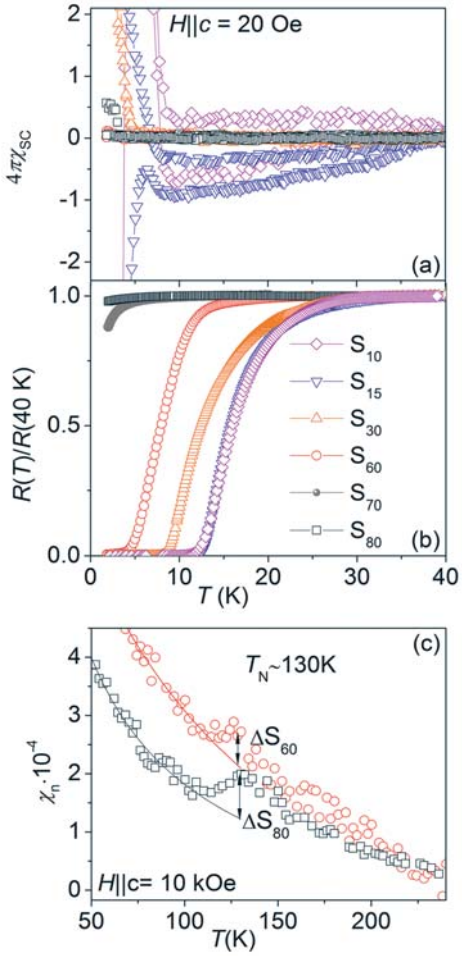

Strain-induced superconductivity in the parent compound $BaFe_2As_2$

J. Engelmann, V. Grinenko, K. Iida, F. Kurth, R. Hühne, J. Hänisch, M. Hoffmann, S. Oswald, L. Schultz, P. Chekhonin[1], W. Skrotzki[1], D. V. Efremov, B. Holzapfel

$BaFe_2As_2$ (Ba122) thin films with different thicknesses, d_{Ba122}, were prepared on Fe-buffered $MgAl_2O_4$ substrates using pulsed laser deposition. Below a critical thickness of $d_c \approx 30$ nm the Ba122 layers are heavily strained due to the lattice misfit to the substrate and show superconductivity (SC) with critical temperatures up to 35 K (see Fig. a, b) in contrast to non-superconducting unstrained thicker films. Bulk superconductivity with a $T_c \approx 10$ K was confirmed for the strained films by transport and magnetic measurements, whereas a so-called filamentary SC was found in the temperature range of $10\,K < T < 35\,K$. This filamentary SC is attributed to minor regions in the film with a slightly different strain state. Increasing d_{Ba122} results in a relaxation of the Ba122 layer leading to the extinction of SC and the occurrence of a spin density wave state as in typical single crystals of the parent compound Ba122 (see Fig. c). Based on these results, we conclude that structural modification is one of the key parameters for controlling the phase diagram of Ba122 and probably other Fe pnictides and chalcogenides. For further details see J. Engelmann et al., Nature Communications **4**, 2877 (2013); doi: 10.1038/ncomms3877.

Fig.: (a) Temperature dependence of the susceptibility for the Ba122 films having different thickness. **(b)** Temperature dependence of the normalized resistance for the Ba122 thin films (index represents the thickness of the Ba122 layer). **(c)** Thick Ba122 layers exhibit again the magnetic transition of bulk Ba122.

Cooperation: [1]TU Dresden
Funding: DFG (GRK1621), EU (SuperIron, IronSea)

Superconducting gap in $Ca_{1-x}Na_xFe_2As_2$ from angle-resolved photoemission spectroscopy

D. V. Evtushinsky, V. B. Zabolotnyy, L. Harnagea, S. Thirupathaiah, J. Maletz, S. Aswartham, S. Wurmehl, B. Büchner, and S. V. Borisenko

Unlike other types of high-temperature superconductors, iron-based compounds can be synthesized in form of various crystals, exhibiting a large variety of electronic band structures, magnetic responses, superconducting order parameters, and electronic properties in general. On the other hand, difficulties, related to the complexity of the electronic interactions in iron-based superconductors, hinder accurate and precise determination of the material structures in many cases.

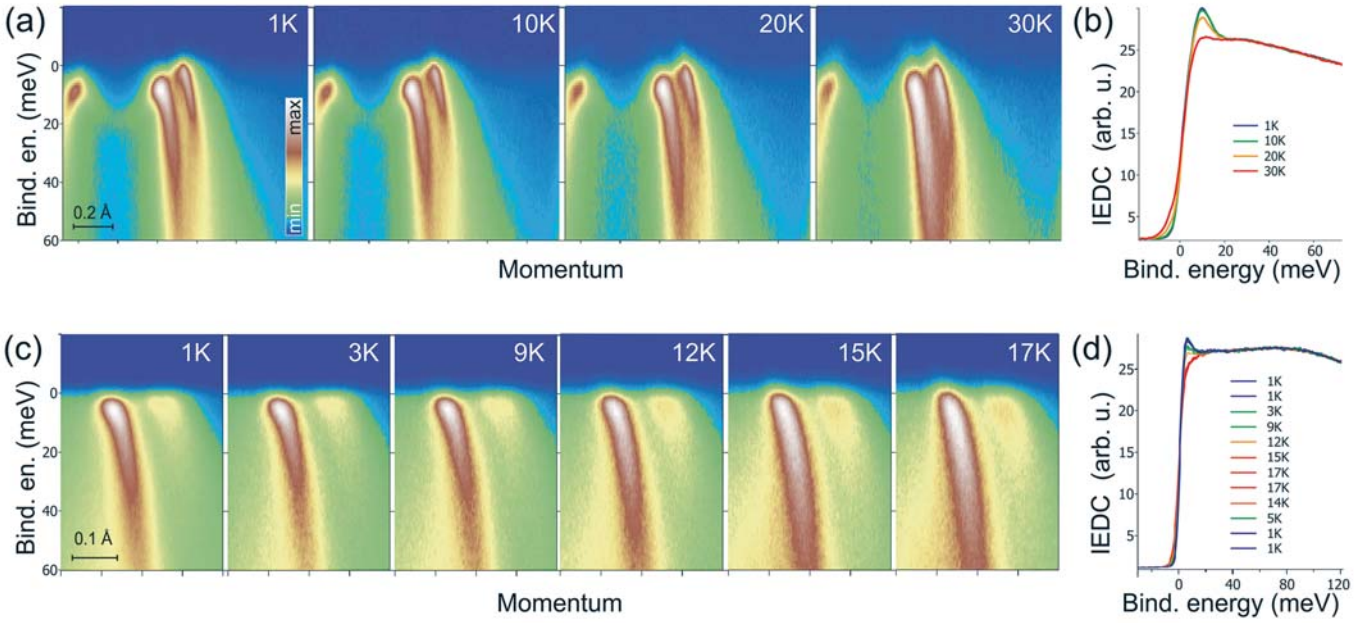

Synthesis of sodium-doped calcium iron arsenide of 122 crystalline structure, $Ca_{1-x}Na_xFe_2As_2$, offered another material for testing of numerous proposals as for the source of effective electron pairing in iron superconductors, the more a series of samples highly suitable for experimental studies were produced. Fig. 1 shows temperature-dependent angle-resolved photoemission spectroscopy (ARPES) measurements for samples with critical temperatures of 33 and 14 K. The energy-momentum cut, shown in panel (a), captures Fermi crossings of the inner and outer Γ barrels for a 33K-sample. Bending of the band dispersion is seen for both outer and inner Γ barrels with stronger effect for the latter. Panel (b) shows temperature dependence of the partial density of states, exhibiting growth of the coherence peak below T_c. Fit of the spectra measured at 1 K yields gap values of 7.8 meV for the inner band and 2.3 meV for the outer one. Panels (c) and (d) present similar data sets measured for a 14K-sample. The determined gap magnitudes are 3.5 for the inner and 1.9 meV for the outer bands. The gap distribution over the Fermi surface contours measured for $Ca_{1-x}Na_xFe_2As_2$ of different doping level is rather close to the results obtained earlier for other representatives of 122 class. In particular it implies that a two-gap behavior – one with magnitude close to the BCS prediction and the other much larger – is generic to many of iron-based superconductors. More information on these studies can be found in Ref. 1 and references therein.

[1] D. Evtushinsky et al., Phys. Rev. B **87**, 094501 (2013).

Fig.: (a) Temperature dependence of the energy-momentum cut passing through the Γ point for the sample with T_c = 33 K. Fermi crossings of both inner and outer Γ barrels are clearly visible.
(b) Temperature dependence of the partial density of states, exhibiting the development of the coherence peak below T_c.
(c) Temperature dependence of the cut passing through Γ point for the sample with T_c = 14 K.
(d) Corresponding partial density of states, measured by scanning temperature up and down.

Cooperation: MPI Stuttgart, TU Dresden
Funding: DFG grants No. BO1912/2-2, BE1749/13 and WU595/3-1

Does the high-energy anomaly in ARPES spectra of the cuprates explain the mechanism for high-T_c superconductivity?

J. Fink, E. D. L. Rienks, M. Ärrälä, M. Lindroos, F. Roth, W.Tabis, G. Yu, and M.Greven

In the ARPES spectra of the cuprate high-T_c superconductors, various kinks in the band dispersion have been discovered which were analyzed in terms of a coupling of the charge carriers to bosonic excitations possibly mediating high-T_c superconductivity in these materials. In particular, a high-energy anomaly (HEA), i.e., the band bends sharply and seems to proceed almost vertically towards the valence band (see Fig. 1(b)), has been discussed. This phenomenon has been also termed "waterfall". A number of explanation have been suggested including a coupling of the charge carriers to spin fluctuation,

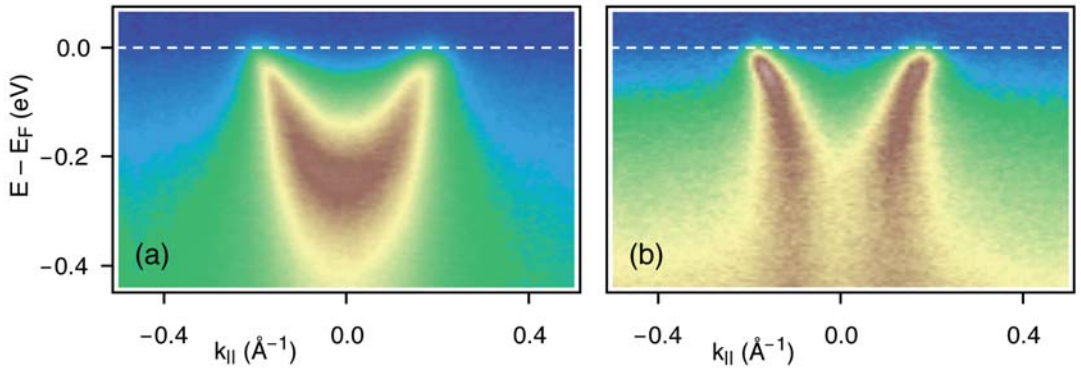

Fig.: ARPES intensity distribution maps of $Nd_{2-x}CuO_4$ x = 0.123 recorded at the antinodal point with **(a)** a photon energy of 120 eV and **(b)** 94 eV.

mediating high-T_c superconductivity, a coupling to phonons, string excitations of spin polarons, a coupling to plasmons, and a transition from a coherent quasi-particle dispersion to an incoherent lower Hubbard band, which should occur in all doped Mott-Hubbard systems. We used angle- and polarization dependent photoemission spectroscopy (ARPES) to study the HEA in the dispersion of $Nd_{2-x}Ce_xCuO_4$. We have found that at particular photon energies and/or photon polarizations gives way to a broad band (see Fig. 1(a)). This clearly shows that the HEA is a matrix element effect (a wipe-out of the intensity in a particular momentum range) and that it is not caused by many-body effects described above. The present results imply strong constraints on theories on high-T_c superconductivity and on the electronic structure of doped Mott-Hubbard insulators. For further details see arXiv 1312.5143.

Cooperations: HZ Berlin; Tampere University of Technology, Finnland; Center for Free-Electron Laser Science, DESY, Hamburg; University of Minesota, USA.
Funding: DFG, Research Unit FOR1154

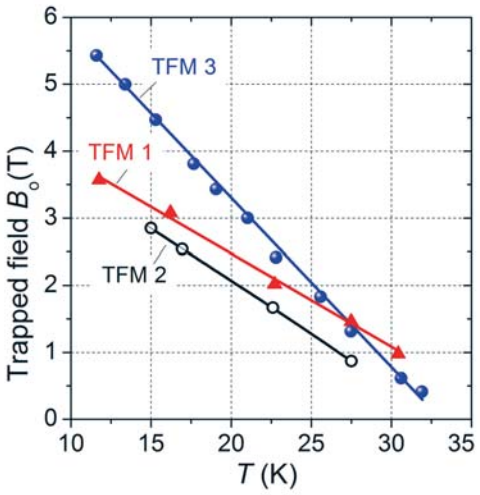

MgB_2 – bulk

G. Fuchs, W. Häßler, J. Scheiter, K. Nenkov, M. Schubert, B. Holzapfel, L. Schultz

The absence of weak-link behaviour in MgB_2 offers the advantage of a relative simple and cost-effective technique for fabrication of large bulks with high trapped fields. Bulk superconducting MgB_2 samples, 20 mm in diameter, were prepared by hot-pressing of high energy ball- milled Mg and B powders using nano-sized boron powders. High maximum trapped fields of B_o = 5.4 T were obtained at 12 K by Hall-probe measurements in one of the investigated trapped field magnets (height 8 mm) at the centre of the bulk surface. For short MgB_2 samples (height ≤ 1.6 mm) trapped fields up to B_o = 3.2 T at 15 K were

Fig.: Temperature dependence of the maximum trapped field B_o of the investigated MgB_2 trapped field magnets measured on the surface of the disc-shaped bulk samples (Ø 20 mm, height 1.6 mm, 1.3 mm and 8 mm for TFM 1, TFM 2 and TFM 3, respectively).

achieved (Fig.). These high trapped fields are related to extremely high critical current densities up to 10^6A/cm^2 at 15 K indicating strong pinning due to nano-crystalline MgB_2 grains.
The measured trapped field of 5.4 T at 12 K is the highest reported so far. By increasing height and/or diameter of these bulk MgB_2 samples, even higher trapped fields are expected which demonstrates the large potential of MgB_2 trapped field magnets in the field of engineering applications at temperatures between 15 and 20 K. For further details see Fuchs, Häßler, Nenkov, Scheiter, Perner, Handstein, Kanai, Schultz, Holzapfel, Supercond. Sci. Technol. 26 (2013) 122002

Cooperation: University of Tokyo
Funding: DFG, Research Unit FOR1154

Observation of strontium segregation in $LaAlO_3/SrTiO_3$ and $NdGaO_3/SrTiO_3$ oxide heterostructures by X-ray photoemission spectroscopy

A. Koitzsch, U. Treske, N. Heming, M. Knupfer, B. Büchner, E. Di Gennaro[1], U. Scotti di Uccio[1], F. Miletto Granozio[1], S. Krause[2]

At the interface between certain insulating metal oxides, $LaAlO_3$ and $SrTiO_3$ for example, a thickness threshold for an insulator to metal phase transition has attracted much interest. A highly mobile two dimensional electron gas is formed at the interface when 4 or more unit cells of $LaAlO_3$ are deposited on a TiO_2-terminated $SrTiO_3$ substrate. The origin of this unexpected behavior has been the subject of passionate debates.
Here, pulsed laser deposition grown $LaAlO_3$ and $NdGaO_3$ on TiO_2-terminated $SrTiO_3$ with different film thicknesses were investigated by soft X-ray photoemission spectroscopy.

The surface sensitivity of the measurements has been tuned by varying photon energy and emission angle. In contrast to the core levels of the other elements, the Sr 3d line shows an unexpected splitting for higher surface sensitivity, signaling the presence of a second strontium component. From our quantitative analysis we conclude that during the growth process Sr atoms diffuse away from the substrate and segregate at the surface of the heterostructure, possibly forming strontium oxide.
Our findings add further insight on the complex picture of oxide heterostructures, both in terms of their growth mechanisms and, possibly, of their electronic properties.

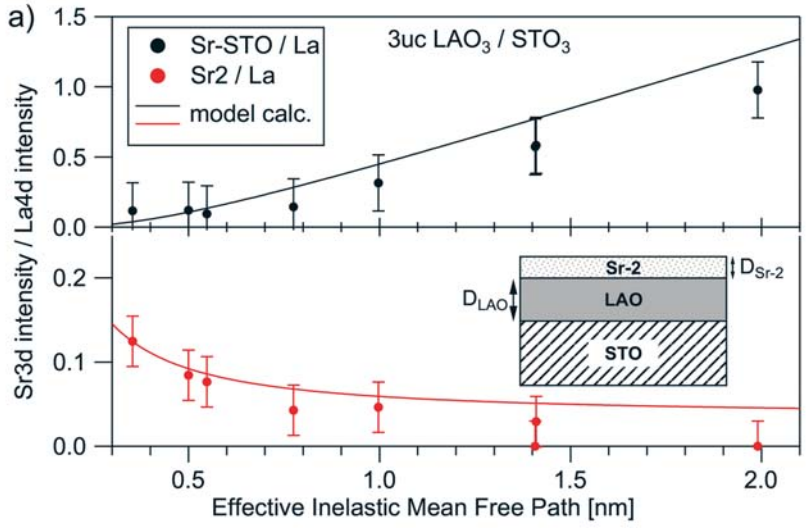

Fig.: Photoemission intensity ratio of La 4d and Sr 3d as a function of effective inelastic mean free path. The two panels correspond to the two strontium components found.
Solid lines: Model calculation. **Inset:** Schematic picture of the heterostructure derived from the model.

Cooperations: [1]CNR-SPIN, Naples, Italy, [2]Helmholtz-Zentrum Berlin

Observation of charge accumulation and onsite Coulomb repulsion at transition metal impurities in the iron pnictides

R. Kraus, V. Bisogni, L. Harnagea, S. Aswartham, S. Wurmehl, G. Levy, I. S. Elfimov, B. Büchner, G. A. Sawatzky, and J. Geck

High-temperature superconductivity (HTS) in the iron pnictides is one of the most intensively studied topics in current condensed matter science. Although research efforts established many properties of these materials, the effects of substituting iron by other transition metals (TMs) such as Co, Ni, or Cu remain a matter of controversy.

We combined valence band photoemission and Auger spectroscopy to study the impact of TM-substitution on the electronic structure of $Ca(Fe,Co)_2As_2$ and $Ba(Fe,TM)_2As_2$ with TM = Ni or Cu. The valence band photoemission data show directly that the TM states move to higher binding energies with increasing atomic number, contributing less and less to the states close to the Fermi level. Furthermore, the $3d^8$ final state of the LVV Auger decay, which is observed for Ni and Cu, unambiguously reveals the accumulation of charge at these impurities (see Fig.). We also showed that the onsite Coulomb interaction on the impurity strongly increases when moving from Co (U_{eff} = 1.4 eV) over Ni (U_{eff} = 1.8 eV) to Cu (U_{eff} = 3 eV). Note that these U_{eff} are strongly reduced from their atomic values due to the screening in the bulk material. Our results quantify the impurity potentials and imply that the superconducting state is rather robust against impurity scattering, which puts constraints on the possible mechanisms of HTS in the iron pnictides.

For further details see Ritschel *et al.* Phys. Rev. B 87, 125135 (2013).

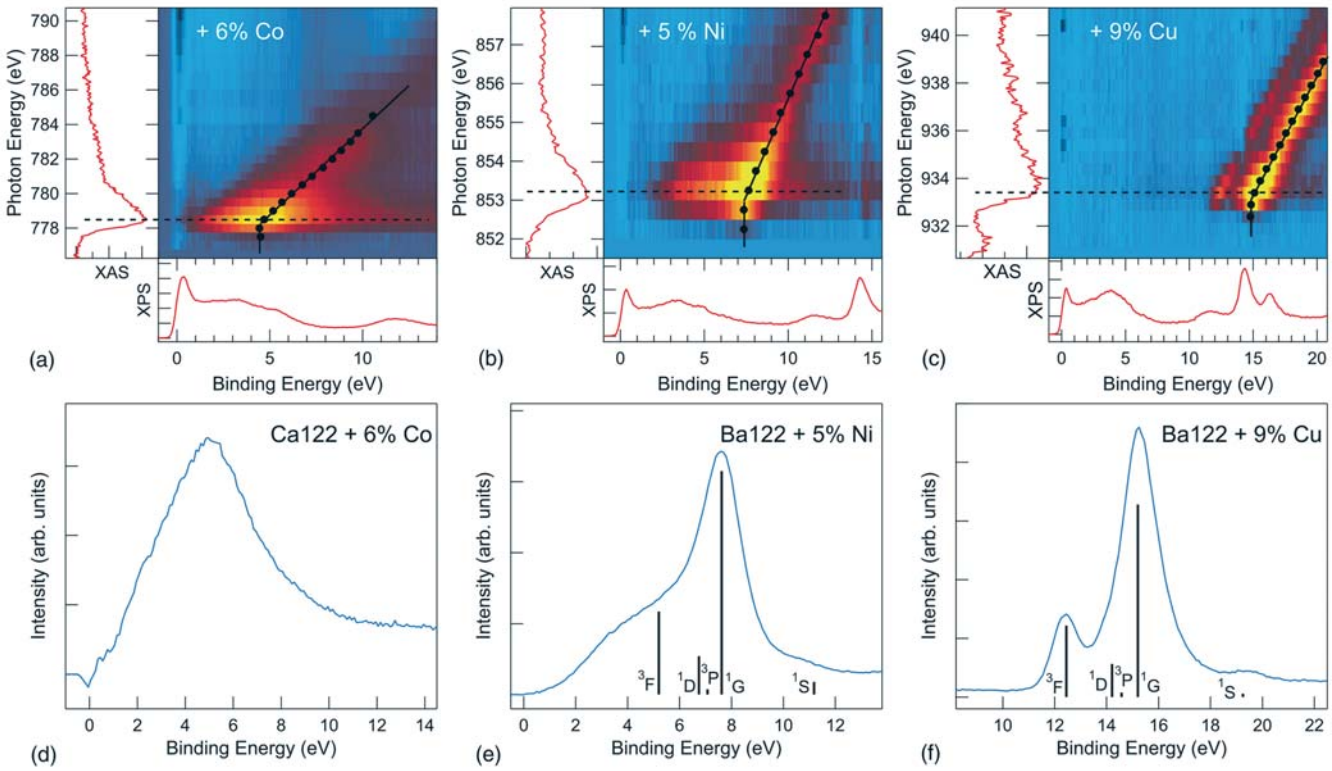

Fig.: Resonant photoemission specroscopy (PES) across the L_3 edge for **(a)** $Ca(Fe,Co)_2As_2$, **(b)** $Ba(Fe,Ni)_2As_2$, and **(c)** $Ba(Fe,Cu)_2As_2$. On the left side of each map in the top row the XAS spectra are displayed. From each map an off-resonance PES spectrum was subtracted, which is shown below each map. The AES peak for each incident photon energy is indicated by black dots, showing the crossover from a resonant Raman (constant binding energy) to the normal AES decay (constant kinetic energy). In the lower panels, the LVV Auger spectra corresponding to the cuts indicated by the dashed lines in the upper panels are presented. Also indicated in the lower panels are the calculated atomic multiplet terms and their AES intensities (vertical bars). The emerging multiplet structure for Ni and Co reveals a $3d^8$ final state for these TMs.

Cooperations: Department of Physics and Astronomy, University of British Columbia, Vancouver, Canada; Institute for Solid State Physics, TU-Dresden, Germany

Funding: DFG through the Emmy Noether Program (Grant No. GE1647/2-1)

Role of in-plane and out-of-plane dilution in CeFeAsO: charge doping versus disorder

G. Prando, O. Vakaliuk, S. Sanna, G. Lamura, T. Shiroka, P. Bonfá, P. Carretta, R. De Renzi, H.-H. Klauss, C. G. F. Blum, S. Wurmehl, C. Hess, B. Büchner

Substituting 10% of O^{2-} ions by F^- leads to a high-T_c superconducting ground state in iron-based 1111 oxypnictides. Although such chemical dilution is realized out of the FeAs layers, it induces charge doping in the Fe bands. Other chemical substitutions involving the dilution of transition metal (TM) elements directly on the FeAs layers also induce superconductivity, even if T_c values are typically lower in these cases. Whether the chemical substitution of Fe by other TM elements effectively induces a charge doping similarly to the case of $O_{1-x}F_x$ is still a controversial and debated topic on both the computational and the experimental sides. At the same time, the perturbation induced by the $Fe_{1-x}TM_x$ substitution is expected to introduce a high degree of in-plane disorder, strongly modifying the physical properties of the electronic ground states across the whole phase diagram.

In Ref. [1], we provide direct evidence for the equivalence of the in-plane $Fe_{1-x}Co_x$ and the out-of-plane $O_{1-x}F_x$ chemical dilutions in CeFeAsO as far as the magnetic properties are concerned. Remarkably, measurements of muon spin spectroscopy show that both these substitutions lead to a quantitatively identical suppression of T_N as a function of x (T_N being the critical transition temperature to the magnetic spin-density-wave phase – see figure). However, the in-plane disorder induced by the $Fe_{1-x}Co_x$ dilution strongly suppresses T_c with respect to what is realized in the case of the $O_{1-x}F_x$ substitution. Finally, a remarkable correlation is reported in the electronic phase diagram among the dome-like features for both T_c and the critical transition temperature for the magnetic phase of the Ce^{3+} sublattice. This suggests an enhancement of the magnetic coupling among Ce^{3+} ions mediated by superconductivity.

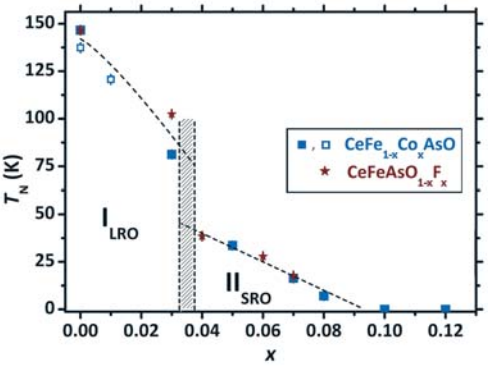

Fig.: Critical transition temperature to the magnetic spin-density-wave phase as a function of x. Solid and open symbols refer to estimates from muon spin spectroscopy and resistivity, respectively.

[1] G. Prando, O. Vakaliuk, S. Sanna, G. Lamura, T. Shiroka, P. Bonfá, P. Carretta, R. De Renzi, H.-H. Klauss, C. G. F. Blum, S. Wurmehl, C. Hess, B. Büchner, *Phys. Rev. B* **87** 174519 (2013)

Cooperations: TU Dresden, Universitá di Pavia – CNISM (Italy), Universitá di Parma – CNISM (Italy), Universitá di Genova – CNR-SPIN (Italy), ETH Zürich (Switzerland)
Funding: Leibniz-DAAD, DFG, Fondazione Cariplo (Italy), FP7 European Project SUPER-IRON

Vortex-glass transition in $Ba(Fe_{1-x}Co_x)_2As_2$ unveiled

G. Prando, R. Giraud, S. Aswartham, O. Vakaliuk, M. Abdel-Hafiez, C. Hess, S. Wurmehl, A. U. B. Wolter-Giraud, B. Büchner

The motion of vortices in high-T_c superconductors is a crucial property for the selection of materials suitable for technological applications. At the same time, studies in this field also lead to fascinating insights about the fundamental physics of an ensemble of flux lines both in mutual interaction among themselves and influenced by the physical parameters of the host material (dimensionality, superconducting anisotropy, but also impurities and defects or, more generally, quenched disorder) as well as by external parameters.

In Ref. [1], we discuss our recent investigation of optimally-doped single crystals of $Ba(Fe_{1-x}Co_x)_2As_2$ by means of magneto-resistivity and magnetic ac susceptibility measurements. The magnetic field-temperature phase diagram is mapped out, identifying the two main regions where flux lines move or not (liquid and glassy phases, respectively). The frequency dependence of the ac susceptibility response allows us to study

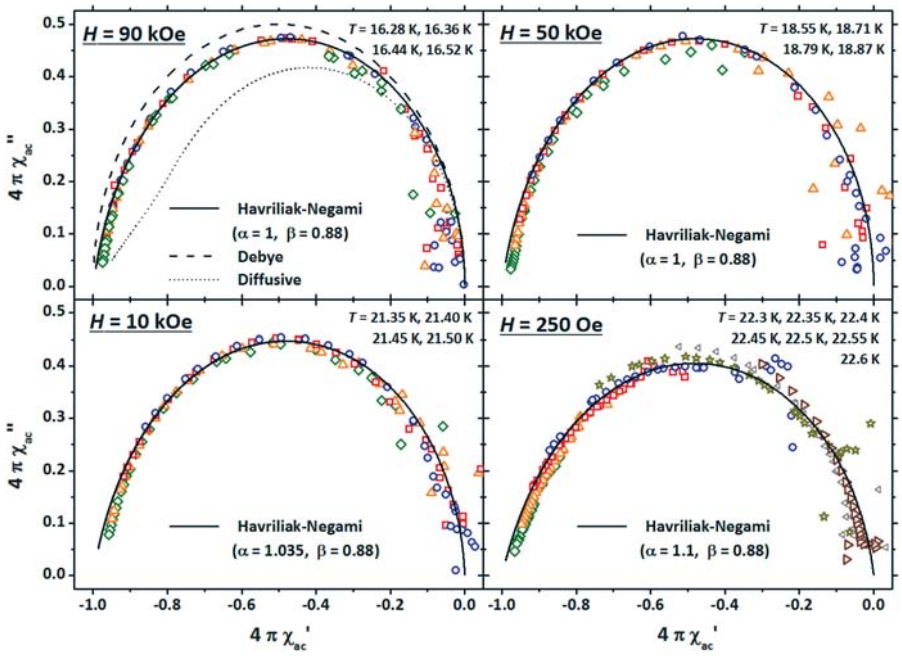

Fig.: Cole-Cole plots for the isothermal magnetic ac susceptibility at different values of polarizing magnetic field.

the dynamical features of the magnetic relaxation in the crossover between these two regions. As a remarkable output, the "diffusive model" typical of high-T_c superconductors is not reproducing our experimental data whereas a Nevriliak-Negami approach yields good agreement (see Fig.). Within this model, information is obtained about the temperature dependence of the correlation time for the ensemble of vortices. Power-law critical divergences are detected, indicative of a thermodynamic phase transition separating the liquid and glassy phases. We analyze our data according to a model previously developed for cuprate superconductors and, remarkably, we deduce that the relatively high concentration of Co (x = 10%) only results in an extremely weak degree of in-plane quenched disorder.

[1] G. Prando, R. Giraud, S. Aswartham, O. Vakaliuk, M. Abdel-Hafiez, C. Hess, S. Wurmehl, A. U. B. Wolter-Giraud, B. Büchner, *J. Phys.: Cond. Matt.* **25** 505701 (2013)

Funding: Leibniz-DAAD, Alexander von Humboldt Stiftung, DFG, BMBF

Pressure dependence of the charge density wave in 1T-TaS_2 and its relation to superconductivity

T. Ritschel, J. Trinkauf, G. Garbarino, M. Hanfland, M. v. Zimmermann, H. Berger, B. Büchner, J. Geck

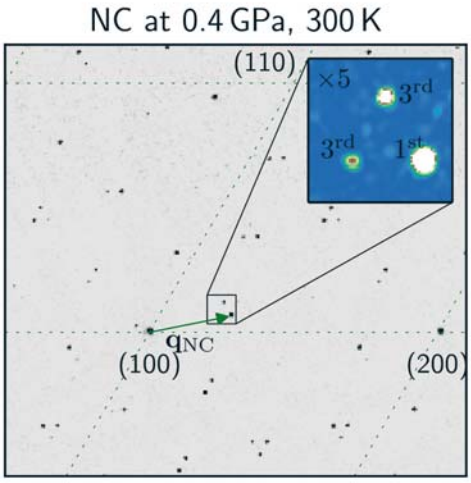

Fig.: Diffraction pattern in the nearly commensurate phase of 1T-TaS_2. The CDW leads to the occurence of superlattice reflections at $\mathbf{q}_{NC}$.

The coexistence of different collective electronic states and the question in how far these states interact is one of the most fascinating and active fields of condensed matter research. In this respect 1T-TaS_2 is an ideal model system: measurements of the electrical resistivity of this material revealed that external pressure stabilizes a superconducting phase, which exists in very close proximity to electronically ordered charge density wave (CDW) phases. Whether and how this superconductivity is related to the CDW on a microscopic level remained, however, unknown from the experimental point of view. This motivated us to perform pressure dependent x-ray diffraction experiments at the beamline ID09A of the ESRF, in order to clarify this issue. Our results prove that the CDW, which we characterize here in terms of wave vector (see Fig.), amplitude and the coherence length, indeed exists in the superconducting region of the phase diagram. The data further imply that the ordered CDW structure as a whole becomes superconducting at low temperatures, i.e, superconductivity and CDW order coexist on a macroscopic scale in real space. This result is fundamentally different from a previously proposed

separation of superconducting and insulating regions in real space and, instead, provides evidence that the superconducting and the CDW gap exist in separate regions of reciprocal space. For further details see Ritschel *et al*. Phys. Rev. B 87, 125135 (2013).

Cooperations: Institute for Solid State Physics, TU-Dresden, Germany; European Synchrotron Radiation Facility (ESRF) Grenoble, France; Hamburger Synchrotronstrahlungslabor (HASYLAB) at Deutsches Elektronensynchrotron (DESY), Germany; Ecole Polytechnique Federale de Lausanne, Switzerland
Funding: DFG through the Emmy Noether Program (Grant No. GE1647/2-1) and the GRK 1621

Thick YBCO layers on highly alloyed Ni-W tapes

M. Sieger, J. Hänisch, K. Iida, U. Gaitzsch, C. Rodig, J. Freudenberger, R. Nast[1], L. Schultz, B. Holzapfel, R. Hühne

The use of high-temperature superconductors for energy applications requires thick superconducting layers on flexible substrates in order to achieve high transport currents in magnetic fields. Non-magnetic substrates are preferred for those so-called coated conductors to reduce ac losses. Therefore, highly cube-textured Ni-W tapes with a W content of up to 9.5 at.% were successfully developed using the Rolling Assisted Biaxially Textured Substrates (RABiTS) approach [1]. Pulsed laser deposition was used to generate $YBa_2Cu_3O_{7-x}$ (YBCO) films with a thickness of more than 1 µm on highly textured Ni-9 at.% W tapes (Fig. a). Additional pinning centers as $BaHfO_3$ or $BaZrO_3$ nanoparticles were incorporated in the YBCO matrix to improve the critical current density J_c in magnetic fields. X-ray diffraction showed an undisturbed transfer of the cube texture from the metallic substrate through the standard $Y_2O_3/YSZ/CeO_2$ buffer architecture to the YBCO layer (Fig. b). A superconducting transition temperature T_c of about 88 K with a small transition width $\Delta T_c \leq 1$ K was determined. Inductive measurements of J_c showed values up to 0.8 MA/cm^2 at 77 K in self-field. The samples were patterned afterwards by laser-cutting to perform transport measurement and to determine the J_c(B) behavior. A significant enhancement of the pinning force density with the doping content was found in these studies.
[1] U. Gaitzsch et al., Supercond. Sci Technol. **26**, 085024 (2013).

Cooperations: [1]KIT Karlsruhe; evico GmbH
Funding: EU (Eurotapes)

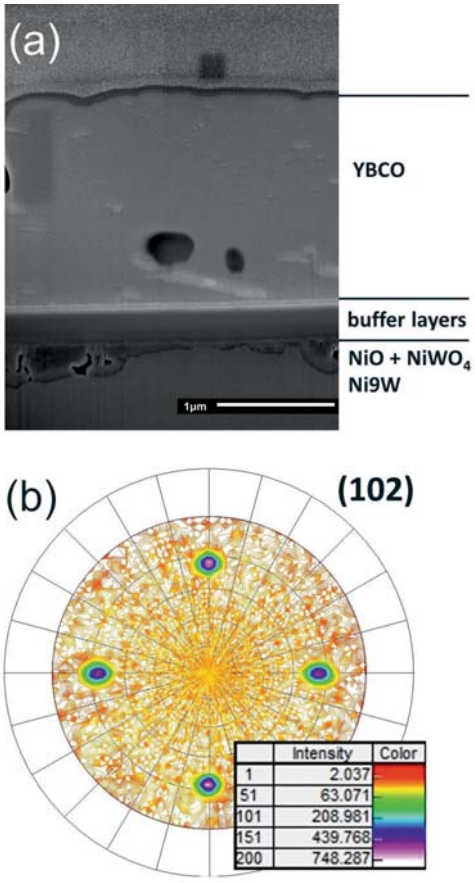

Fig.: (a) FIB cross section of a 1.8 µm thick YBCO layer grown on buffered Ni-9 at.% W substrates; **(b)** (102) pole figure for the YBCO layer

Formation of the coherent heavy fermion liquid at the 'hidden order' transition in URu_2Si_2

S. Chatterjee, J. Trinckauf, T. Hänke, D. E. Shai, J. W. Harter, T. J. Williams, G. M. Luke, K. M. Shen, J. Geck

The interactions between localized and delocalized electrons in the so-called heavy fermion materials result in fascinating and unexpected quantum phenomena that continue to challenge condensed matter researchers. A most notorious example is the enigmatic "hidden order" state of URu_2Si_2. A large loss of entropy at $T_{H0} = 17.5$ K indicates a second order phase transition into an ordered state, but the nature of the underlying microscopic order parameter is still a hotly debated puzzle. We performed a high-resolution angle-resolved photoemission study of the heavy-fermion superconductor URu_2Si_2, in order to investigate the effect of the hidden order on the electronic structure.

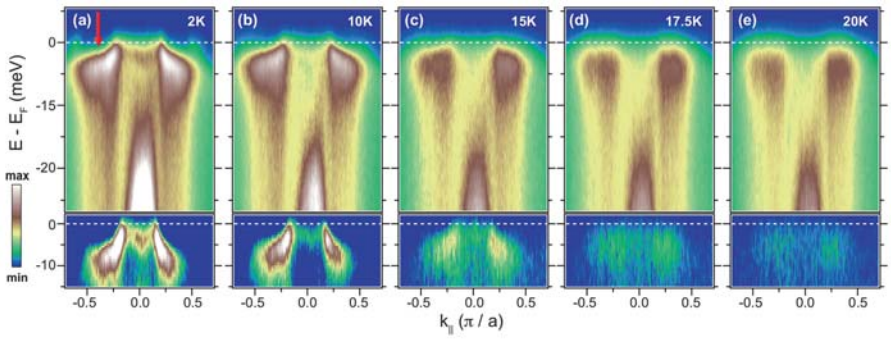

Fig. (a) – (e): Temperature evolution of the ARPES intensity plots of URu_2Si_2 measured along the (100) direction at 31 eV photon energy over the temperature range 2–20 K. In the lower panel, ARPES spectral maps obtained after subtracting the corresponding intensity map at 25 K are shown. The color scale has been adjusted to show only the positive part of the subtracted spectrum. Note that all the spectral maps in the lower panel are plotted keeping the range of the color scale fixed. Below T_{HO} a coherent heavy fermionic band rapidly emerges which simultaneously becomes sharper and more dispersive as the sample is cooled down.

Detailed measurements as a function of both photon energy and temperature allow us to disentangle a variety of spectral features, revealing the evolution of the low-energy electronic structure across the "hidden order" transition. Most significantly, our measurements reveal that already above the hidden order transition heavy quasi particles exist at the Fermi level, which show the characteristics of a Kondo resonance. Upon entering the hidden order phase, these states rapidly hybridize with light conduction band states, the scattering rates of the heavy fermion states rapidly decrease and the system transforms into a coherent heavy fermion liquid. This evolution is in stark contrast with the gradual crossover expected in Kondo lattice systems, which we attribute to the coupling of the Kondo lattice to the hidden order parameter. The onset of coherence seems to be essential for superconductivity in this heavy fermion system, as it emerges only out of the hidden order phase.

For further details see Shouvik Chatterjee, Jan Trinckauf *et al.*, Physical Review Letters **110**, 186401 (2013).

Cooperations: Department of Physics, Cornell University, U.S.A;
Department of Physics and Astronomy, McMaster University, Canada
Funding: DFG through the Emmy Noether Program (Grant No. GE1647/2-1)

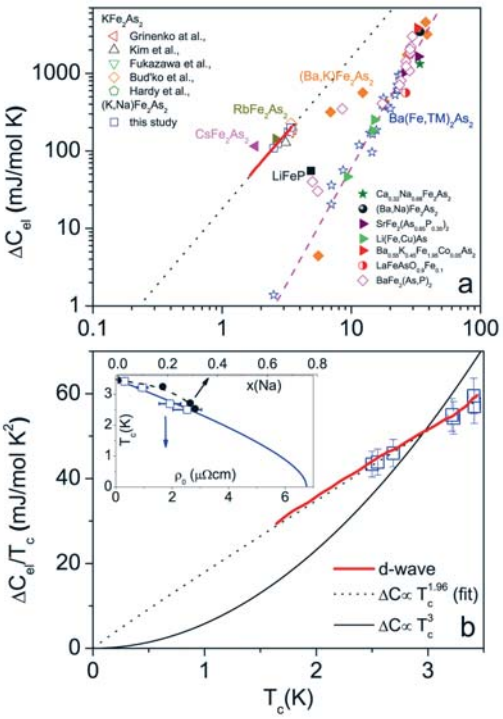

Fig.: (a) The dependence of ΔC_{el} vs. T_c for different iron-pnictide superconductors. Solid line: obtained within Eliashberg theory, and dashed curve: BNC scaling $\Delta C_{el} \propto T_c^3$ for complete bibliography of used compounds see [arXiv:1308.2201]. **(b)** $\Delta C_{el}/T_c$ vs. T_c for $(K,Na)Fe_2As_2$ (a new universality class). Inset: $\Delta C_{el} = T_c$ vs. T_c for $(K,Na)Fe_2As_2$. Inset: T_c vs. residual resistivity ρ_0 and the Na substitution level x. Solid line: fit using the Abrikosov-Gor'kov formula.

Superconducting specific heat jump $\Delta C \propto T_c^{\beta}$ ($\beta \approx 2$) for $K_{1-x}Na_xFe_2As_2$

V. Grinenko, D. V. Efremov, S.-L. Drechsler, S. Aswartham, D. Gruner, M. Roslova, I. Morozov, K. Nenkov, S. Wurmehl, A. U. B. Wolter, B. Holzapfel, and B. Büchner

We found a new universality class for the behavior of the electronic specific heat jump (ΔC_{el}) at the superconducting transition temperature T_c in $K_{1-x}Na_xFe_2As_2$ single crystals. Both T_c and ΔC_{el} monotonously decrease with increasing x. The jump scales approximately with a novel power-law: $\Delta C_{el} \propto T_c$ with an exponent $\beta \approx 2$ determined by the impurity scattering rate as shown in Fig 1. This finding is in sharp contrast to most of all known iron-pnictide superconductors with a cubic Bud'ko-Ni-Caneld (BNC) scaling. Our observations, also, suggests that disorder diminishes the small gaps leading to a partial gapless superconductivity which results in a large residual Sommerfeld coefficient in the superconducting state for $x > 0$. Therefore, both the temperature dependence of $C_{el}(T)$ in the superconducting state and the nearly quadratic scaling of ΔC_{el} at T_c are well described by the Eliashberg-theory for *d*-wave superconductor with weak pair-breaking due to nonmagnetic impurities.

For further details see V. Grinenko et al., arXiv:1308.2201.

Cooperation: Lomonosov Moscow State University
Funding: DFG through the SPP 1458, the E.-Noether program (WU 595/3-1 (S.W.)), and the EU-Japan project (No. 283204 SUPER-IRON), the BMBF for support in the frame of the ERA.Net RUS project FeSuCo No. 245.

Research Area 2
Magnetism and magnetic materials

Magnetic state of pyrochlore $Cd_2Os_2O_7$ emerging from strong competition of ligand distortions and longer-range crystalline anisotropy

N. A. Bogdanov, R. Maurice, I. Rousochatzakis, J. van den Brink, and L. Hozoi

The 5d oxide compounds are at the heart of intensive experimental and theoretical investigations in solid-state physics and materials science. The few different varieties displaying Ir ions in octahedral coordination and tetravalent $5d^5$ valence states, in particular, have set the playground for new insights into the interplay between strong spin-orbit interactions, electronic correlations, and lattice degrees of freedom. Equally intriguing but less studied are pentavalent Os $5d^3$ oxides such as the $S = 3/2$ pyrochlore $Cd_2Os_2O_7$. We have investigated the correlated electronic structure, magnetic interactions, and the role of lattice anisotropy in $Cd_2Os_2O_7$ by *ab initio* quantum chemistry calculations. We find that the magnetic ground state of $Cd_2Os_2O_7$ depends on structural aspects such as the amount of trigonal distortion of the ligand octahedral cages and the anisotropic, ring-like configuration of the adjacent Cd ions. Without trigonal distortions, a large easy-plane magnetic anisotropy develops. Their presence, however, reverses the sign of the zero-field splitting and causes a large easy-axis anisotropy ($D \simeq -6.8$ meV), which in conjunction with the antiferromagnetic exchange interaction ($J \simeq 6.4$ meV) stabilizes an all-in/all-out magnetic order. The competition uncovered here is a generic feature of pyrochlore magnets. For further details, see N. A. Bogdanov *et al.*, Phys. Rev. Lett. **110**, 127206 (2013).

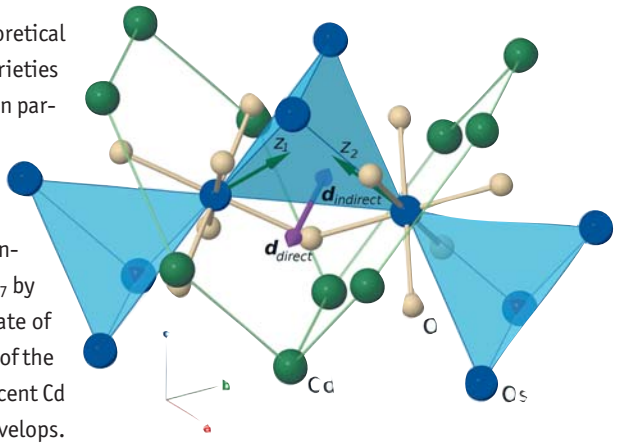

Fig.: Corner-sharing Os_4 tetrahedra (blue color) in $Cd_2Os_2O_7$. O ligands and nearby Cd ions around two adjacent Os sites are shown in beige and green. The two possible orientations of the Dzyaloshinskii-Moriya vector for two nearest-neighbor Os ions are also shown, along with their respective easy axes.

Cooperation: RU Groningen
Funding: DFG, EU's Erasmus Programme

Half-metallic ferromagnetism with unexpectedly small spin splitting in the Heusler compound Co_2FeSi

D. Bombor, C. G. F. Blum, O. Volkonskiy, S. Rodan, S. Wurmehl, C. Hess, and B. Büchner

A crucial ingredient of any kind of spintronics, i.e., the exploitation of spin-dependent electron transport phenomena is the realization of highly spin-polarized materials. Half-metallic ferromagnets (HMF) are considered ideal candidates because they are predicted to possess a 100% spin-polarization at the Fermi level E_F. The complete absence of minority spin states at E_F implies the existence of a gap Δ which separates the occupied majority states from the unoccupied minority states. Since thus spin flip scattering of conduction electrons is exponentially suppressed, one expects also an exponential suppression of the corresponding characteristic T^2 dependence in the electrical resistivity ρ. In a recent Physical Review Letter [1] we presented the electronic transport properties, viz., resistivity, magnetoresistance and Hall effect, of high quality single-crystalline Co_2FeSi which is a prime candidate HMF. We observed an exponentially suppressed $\sim T^2$ behavior of the resistivity at $T \leqslant 100$ K (see Fig.), and observed pronounced changes at ~100 K in the magnetotransport. Our results represent therefore a textbook example of the expected transport behavior for an HMF, however, with an unexpectedly small $\Delta \sim 100$ K.

[1] D. Bombor et al., Phys. Rev. Lett. **110**, 066601 (2013)

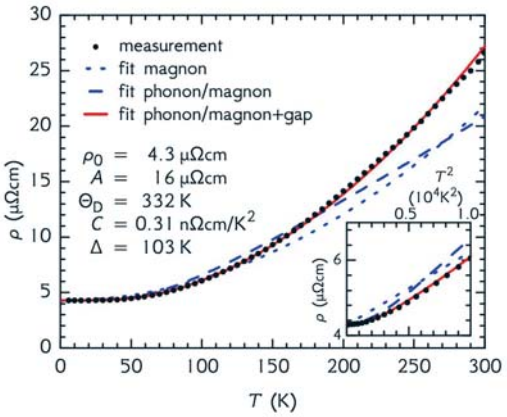

Fig.: Resistivity ρ of Co_2FeSi as a function of temperature T. Measured values are displayed as black dots. Blue chopped lines show fits with magnonic ($\sim T^2$) and magnonic/phononic temperature dependence, where the phononic scattering was accounted for by a fit to the Bloch-Grüneisen formula. The red line shows a fit where an additional Boltzmann factor with a gap Δ was added to the magnonic scattering, the corresponding fitting parameters are displayed, see [1] for details.

Funding: DFG

Controlling competing magnetic phases with electric fields

J. E. Hamann-Borrero, S. Partzsch, S. Valencia, C. Mazzoli, J. Herrero-Martin, R. Feyerherm, E. Dudzik, C. Hess, A. Vasiliev, L. Bezmaternykh, B. Büchner, J. Geck

Materials with a large coupling of ferroelectric and magnetic properties receive large and continued interest. This is not only due the to their potential for future technological applications, but also because they provide a number of unsolved puzzles and challenges for basic research. One prominent example is the strong magneto-electric coupling discovered in some of the rare earth ferroborates. Especially, the material $NdFe_3(BO_3)_4$ generated a lot of excitement, due to its unusually large electric polarization that develops when a magnetic field is applied.

Employing the unique element selectivity of resonant magnetic X-ray diffraction (RMXD), we have identified the magnetic frustration of the Nd- and the Fe-subsystems as the driving force behind the complex behavior of the magnetoelectric (ME) effect in this material. This frustration results in a competition of phases with very similar energies, but still very different properties. In this situation, a small external stimulus (i.e., temperature or magnetic/electric field) is enough to disturb the balance between the competing phases and to induce a large macroscopic response.

For instance, by applying an external magnetic field at low temperatures a ferroelectric phase with an antiferromagnetic (AFM) collinear structure is favored and a helical AFM phase without a ferroelectric polarization is suppressed. The different ferroelectric properties then even allowed us to go one step further and to influence the phase coexistence via an electric field E. Using RMXD we directly observed that, upon increasing E, the ferroelectric phase fraction increases at the expense of the helical phase as clearly shown in the RMXD profiles in figure. The microscopic origin of the huge ME effect in $NdFe_3(BO_3)_4$ therefore lies in the coexistence of phases, providing a new route towards materials with large ME coupling. This may also help to find improved materials for technological applications.

For further details see J. E. Hamann-Borrero *et al.*, Phys. Rev. Lett. **109**, 267202 (2012).

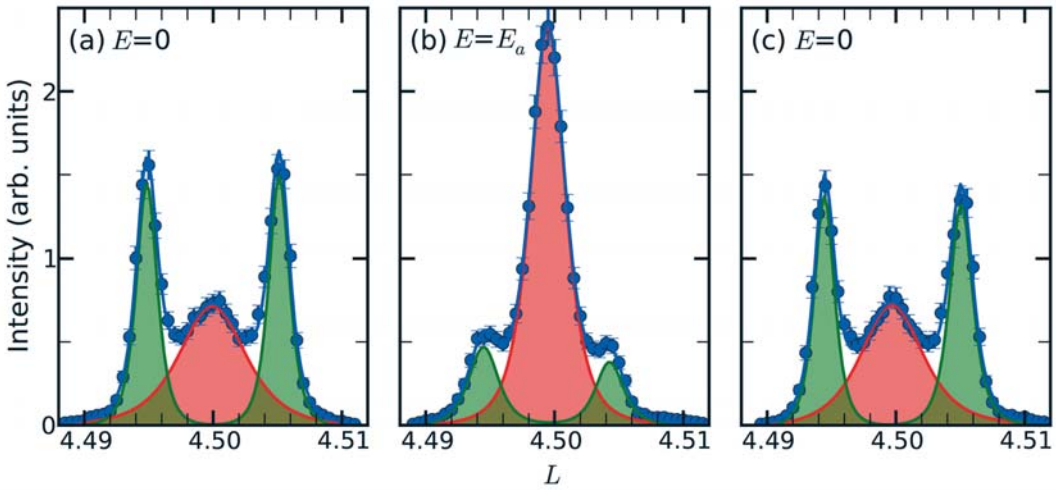

Fig.: L-scan of the (0,0,9/2) magnetic reflection measured at the Nd L_3 edge. **(a)** below T=16K a coexistence of two magnetic phases is observed. A ferroelectric phase with an AFM collinear structure (red) and an AFM helical structure (green). **(b)** after applying an electric field, the collinear phase is enhanced, whereas the helical phase is suppressed. **(c)** once the electric field is switch off, the sample goes back to the initial state where coexistence is observed.

Cooperations: Helmholtz Zentrum Berlin, Germany; Politecnico di Milano e unità CNISM, Italy; European Synchrotron Radiation Facility (ESRF), France; Low Temperature Physics department, Faculty of Physics, Moscow State University, Russia; L.V Kirensky Institute of Physics, Siberian Division, Russian Academy of Sciences, Russia; Institute for Solid State Physics, TU Dresden, Germany

Funding: DFG through the Emmy Noether Program (Grant No. GE1647/2-1)

Fundamental differences among Quantum Spin Hall edge states at Zigzag and Armchair terminations of honeycomb and ruby nets.

L. Cano-Cortes, C. Ortix, and J. van den Brink

Spin-orbit coupling (SOC) in a single plane of graphene leads to a time-reversal invariant Quantum Spin Hall (QSH) state characterized by a bulk energy gap and a pair of topologically protected edge states. The SOC energy scale in graphene, however, is so tiny that it is not possible in practice to establish the existence of a topological order. The recently discovered weak topological insulator $Bi_{14}Rh_3I_9$ provides an entirely novel platform for the actual observation of the QSH effect in graphene-like systems.

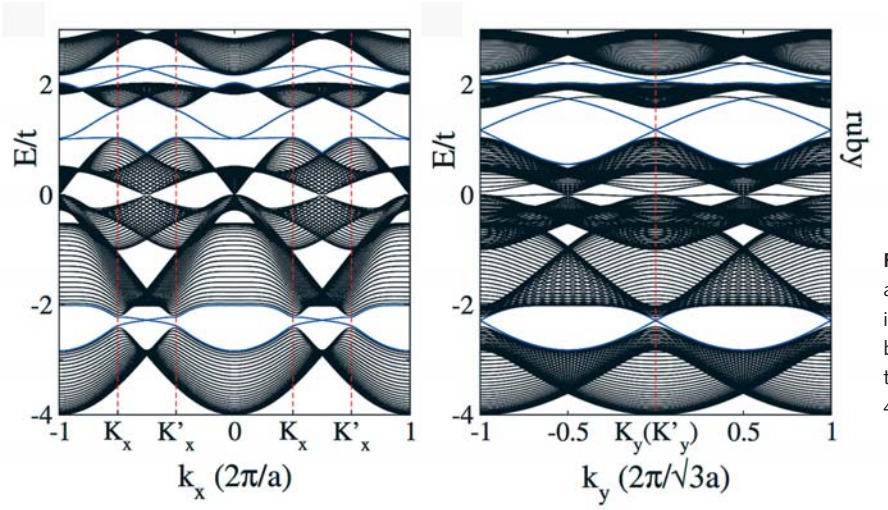

Fig.: Energy bands for ruby zigzag **(left panel)** and armchair **(right panel)** terminated ribbons in presence of spin-orbit coupling. The blue bands correspond to the topologically protected edge states crossing the gap at 1/6, 4/6 and 5/6 fillings.

This material consists of stacks of bismuth-based layers each of which form a honeycomb net composed of $RhBi_8$ cubes with a SOC gap of ~2400 K. These cubes, in turn, form what is commonly referred to as a ruby lattice. In this work [1], we have investigated the electronic characteristics of the topological edge-states in the QSH state of both honeycomb and ruby lattices. In these hexagonal systems there is a dramatic dependence of the edge-state dispersion, decay length and Fermi velocity on the edge geometry. While for a zigzag (ZZ) termination the Fermi velocity of the edge-states critically depends on the size of the spin-orbit gap, armchair (AC) edge-states exhibit a linear dispersion with a velocity that is independent of strength of the SOC. Surprisingly, the edge-state decay lengths at ZZ- and AC-edges depend on the SOC strength in an opposite manner: while the first one grows with the SOC, the other shrinks.
This emphasizes the fundamentally different electronic properties of Quantum Spin Hall edge-states at zig-zag and armchair terminations of hexagonal lattices.
[1] L.Cano-Cortes, C. Ortix, J. van den Brink, Phys. Rev. Lett. 111, 146801 (2013)

First Ba_2YIrO_6 single crystals grown from $BaCl_2$ flux

T. Dey, A. Maljuk, O. Kataeva, F. Steckel, D. Gruner, T. Ritschel, C. G. F. Blum, A. U. B. Wolter, J. Geck, C. Hess, S. Wurmehl, and B. Büchner

Iridates have become an interesting playground for material researchers as they show novel ground states because of competing interactions between crystal field, Coulomb interaction (U) and spin-orbit coupling (SOC).
We have synthesized single crystals of Ba_2YIrO_6 for the first time and studied their structural, magnetic, thermal and electrical transport properties. The Ba_2YIrO_6 crystals clearly crystallize in a cubic double perovskite-type structure, as demonstrated by powder and single crystal x-ray diffractometry. This material could be a good candidate

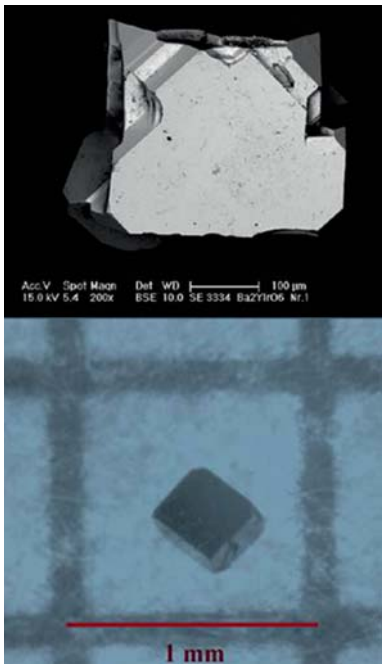

Fig.: (top) Scanning electron microscopy image of one Ba_2YIrO_6 single crystal. **(bottom)** Optical image of a Ba_2YIrO_6 single crystal placed on a millimeter graph paper.

to study the recently proposed novel singlet-triplet gapped excitonic magnetism in $5d^4$ Mott insulators [1] which are generally considered to be non-magnetic. Our magnetic susceptibility and heat capacity measurements confirm the system is highly frustrated. This is originating from the frustrated face-centered-cubic (fcc) lattice formed by the Ir^{5+} ions.

[1] G. Khaliullin, Phys. Rev. Lett. **111**, 197201 (2013)

Funding: DFG (Emmy Noether project WU595/3-1)

Deconfined criticality in the frustrated honeycomb antiferromagnet

R. Ganesh, J. van den Brink, and S. Nishimoto

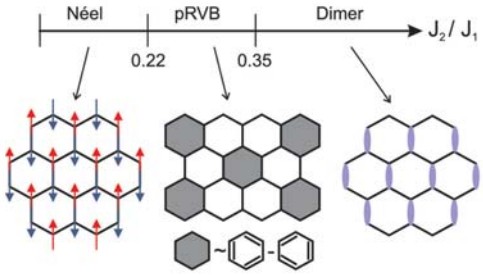

Fig.: Phase diagram of honeycomb lattice antiferromagnet as a function of the frustration parameter J_2/J_1, obtained from DMRG calculations.

Traditional Landau theory dictates that a continuous transition is not possible between two states with different symmetries. The paradigm of deconfined criticality allows for such continuous quantum phase transitions in which the low energy critical excitations are actually the topological defects of either ordered phase. Our study is the first to propose this physics in a realistic model. We consider the Heisenberg antiferromagnet on a honeycomb lattice with frustration arising from next nearest neighbor interactions. We map out the phase diagram of this model using the Density Matrix Renormalization Group (DMRG) procedure generalized to two dimensions. We use clusters with various boundary conditions which act as weak inducing fields favouring different long range orders. Upon tuning the strength of frustration, we find a phase diagram with Néel antiferromagnetism, plaquette order and a 'nematic' dimer order that breaks lattice rotational symmetry. The transition between antiferromagnetism and plaquette order surprisingly seems to be continuous. Subsequent studies have supported the hypothesis of deconfined criticality.

For further details see R. Ganesh et al., Phys. Rev. Lett. **110**, 127203 (2013).

Phase Dynamics and Growth of $Co_2Cr_{1-x}Fe_xAl$ Heusler Compounds: A Key to Understand Their Anomalous Physical Properties

A. Omar, M. Dimitrakopoulou, C. G. F. Blum, H. Wendrock, S. Rodan, S. Hampel, W. Löser, B. Büchner, and S. Wurmehl

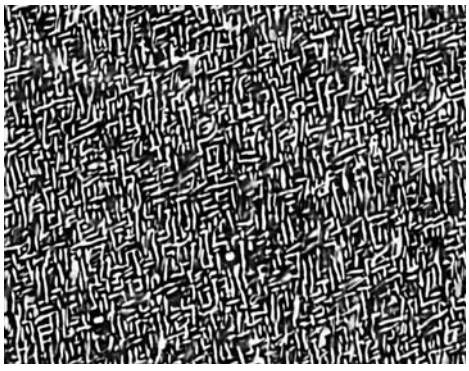

Fig.: SEM (BSE) image of a floating zone grown Co_2CrAl Heusler compound, demonstrating an interconnected basket-weave pattern of a secondary phase in a matrix similar to the microstructure typically observed in the case of a phase transformation via spinodal decomposition.

High-grade samples are the basis to study, e.g., materials with high spin polarization. Each specific material may require a specific technique to yield high-quality samples and crystals. The floating zone technique, as an example, has been proven as the method of choice for the growth of Heusler compounds. We recently used this technique to prove the existence of a phase transformation via spinodal decomposition in the intermetallic Cr-rich samples of the Co-Cr-Fe-Al system. This finding reconciles many controversial experimental results on thin films and bulk samples. This example nicely illustrates, how we can use the floating zone technique to reveal intrinsic materials properties by gaining knowledge about the respective phase dynamics during the growth process with further impact not only on bulk but also on thin film samples. Our study finally enabled us to predict a thermodynamically stable composition in the Co-Cr-Fe-Al system with the desired high spin polarization and high Curie temperature. For further details see Omar et al., Cryst. Growth Des., **13**, 3925 (2013)

Funding: DFG (Emmy Noether project WU595/3-1)

Determining the short-range spin correlations in cuprate chains using resonant inelastic x-ray scattering

C. Monney, V. Bisogni, K.-J. Zhou, R. Kraus, V. N. Strocov, G. Behr, J. Malek, R. Kuzian, S.-L. Drechsler, S. Johnston, A. Revcolevschi, B. Büchner, H. M. Rønnow, J. van den Brink, J. Geck, T. Schmitt

Edge-shared cuprate chains represent a particular class of quantum magnets in which the local geometry gives rise to competing nearest neighbor ferromagnetic (FM) or antiferromagnetic (AFM) exchange coupling J1 and frustrated next-nearest neighbor AFM J2 superexchange couplings. Varying the signs and ratio of J1 and J2 results in rich magnetic properties with ground states spanning FM, AFM, helical, and gapped singlet states. In real materials, the presence of interchain coupling and occasionally coupling to the lattice adds complexity to this behavior, rendering theoretical treatment more difficult. It is therefore desirable to obtain experimental access to nearest neighbor spin correlations both within the ground state probed at very low temperature and in thermally occupied excited spin states as a function of temperature.

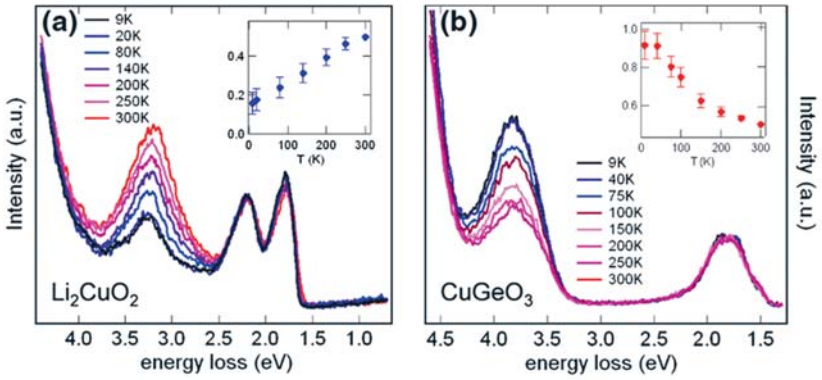

Fig.: (a) Temperature dependent O K-edge RIXS data for **(a)** Li_2CuO_2 and **(b)** $CuGeO_3$. The spectra are plotted as a function of energy loss and have been normalized to the area of the dd excitations. The integrated intensity of the ZRS peaks as a function of temperature is displayed in the corresponding insets. The opposite temperature trends are the result of the different nearest neighbor spin correlation in the ground state of Li_2CuO_2 and $CuGeO_3$.

We performed a high-resolution resonant inelastic soft x-ray scattering (soft RIXS) study of the quantum magnetic spin chain materials Li_2CuO_2 and $CuGeO_3$ with FM and AFM intrachain correlations, respectively. By tuning the incoming photon energy to the oxygen K edge, a strong excitation around 3.5 eV energy loss is clearly resolved for both materials. Comparing the experimental data to many-body calculations, we identify this excitation as a Zhang-Rice singlet (ZRS) exciton on neighboring CuO_4-plaquettes. The results for these two prototype materials demonstrate that the strong temperature dependence of this high-energy exciton enables to probe short-range spin correlations even in the absence of any long range spin order. The Zhang-Rice exciton therefore provides a unique probe to detect novel magnetic ground states such as spin liquids or spin nematic phases. For further details see C. Monney *et al.*, Physical Review Letters **110**, 087403 (2013).

Cooperations: Research Department Synchrotron Radiation and Nanotechnology, Paul Scherrer Institut, Switzerland; Donostia International Physics Center (DIPC), Spain; Laboratoire de Physico-Chimie de l'Etat Solide, ICMMO, Universite' Paris-Sud, France; Department of Physics, TU-Dresden, Germany; Laboratory for Quantum Magnetism, ICMP, Ecole Polytechnique Fe'de'rale de Lausanne (EPFL), Switzerland
Funding: DFG through the Emmy Noether Program (Grant No. GE1647/2-1)

Nucleation study of CuBi alloys in applied magnetic gradient fields

F. Karnbach, K. Tschulik, M. Uhlemann, Ch. Damm, K. Hennig, A. Gebert, J. Eckert

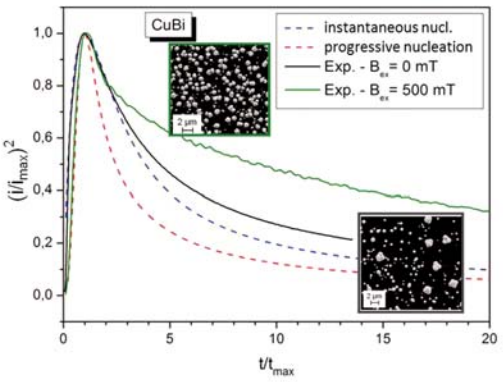

Fig.: Nucleation behavior of CuBi analyzed by the model of Scharifker and Hills and SEM images of nuclei obtained without applied magnetic field and in region of high magnetic field gradient.

Recently it has been demonstrated that structured electrodeposition is possible in applied magnetic gradient fields from electrolytes containing paramagnetic ions [1]. In order to understand the first steps of electrodeposition in magnetic gradient fields, nucleation studies were performed for single metals and CuBi alloy deposited from electrolytes containing strong paramagnetic, electrochemical inert Mn^{2+} ions in addition on glassy carbon. The nucleation mechanism was analyzed electrochemically using the model of Scharifker and Hills, and the morphology, chemical composition and structure were characterized by SEM, ICP-OES and XRD. Due to the local magnetically induced convection caused by the field gradient force overlapped by Lorentz force and gravitational force the nucleation behavior alters depending on the system investigated. The chemical composition of the structured CuBi alloy changes depending on the local magnetic gradient field. In areas of high magnetic gradient field the concentration of Cu is lower than in regions of low magnetic field gradient. This unexpected behavior is attributed to the chosen deposition potential, which leads to charge transfer controlled deposition of Cu and mass transfer controlled deposition of Bi. Despite the diamagnetic Bi^{3+} ions the Bi deposition is enhanced by local convection whereas Cu deposition is unaffected.

[1] M. Uhlemann, K. Tschulik, A. Gebert, G. Mutschke, J. Froehlich, A. Bund, X. Yang, K. Eckert: Structured electrodeposition in magnetic gradient fields, The European Physical Journal - Special Topics 220 (2013) 287-302.

Cooperation: TU Dresden
Funding: DFG (SFB 609)

Nuclear magnetic resonance reveals structural evolution upon annealing in epitaxial Co_2MnSi Heusler films

S. Rodan, A. Alfonsov, M. Belesi, B. Koopmans, H. J. M. Swagten, J. T. Kohlhepp, Y. Sakuraba, S. Bosu, K. Takanashi, B. Büchner, and S. Wurmehl

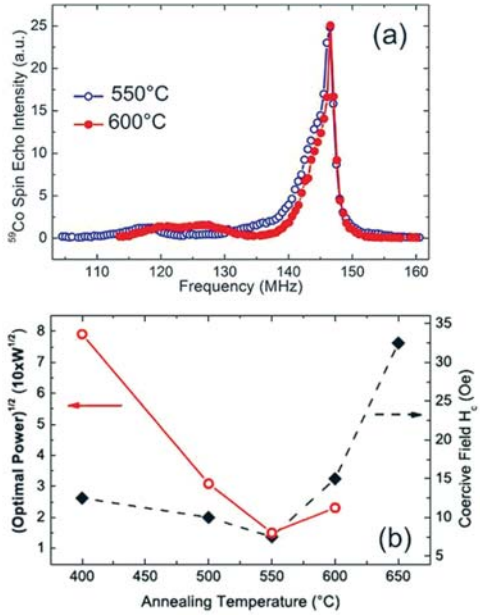

Fig.: ^{59}Co NMR spectra for the films annealed at 550 °C and 600 °C, respectively. The low frequency tail originates in the off-stoichiometry. The linewidth is smaller for the film annealed at higher temperature indicating a higher structural order **(a)**. Square root of the optimal power (proportional to restoring field) for the main line of the ^{59}Co spectrum in different films in comparison with the corresponding coercive fields (H_c) measured by magnetometry **(b)**.

The technological exploitation of high spin polarization in Heusler compounds in spintronics typically requires thin films. Such Co_2MnSi Heusler films were recently reported to show a significant increase in current-perpendicular-to-plane-giant-magnetoresistance upon annealing. We used nuclear magnetic resonance (NMR) to study the impact of annealing as NMR is a powerful tool, sensitive to both magnetic and structural order of such films:

In films which were annealed below 550 °C, no long-range $L2_1$-order is observed, while annealing above 550 °C leads to the formation of the ideal $L2_1$ Heusler structure, however, with a distinct degree of off-stoichiometry. Further evidence from restoring field measurements hints that interdiffusion may account for the drop in magnetoresistance observed for samples annealed above 600 °C. These results show that optimizing films for spintronics involves the identification of the best annealing temperature, high enough for long-range order to emerge, but low enough to maintain smooth interfaces. For details, see Rodan et al. Appl. Phys. Lett. **102**, 242404 (2013).

Cooperations: TU Eindhoven, Netherlands; Tohoku University, Japan
Funding: DFG (Emmy Noether project WU595/3-1)

Dy-free Nd-Fe-B Thick Films with High Coercivity

N. M. Dempsey[1], T. G. Woodcock, H. Sepehri-Amin[2], Y. Zhang[1], H. Kennedy[1], D. Givord[1], K. Hono[2], and O. Gutfleisch[2]

Nd-Fe-B magnets with partial substitution of Dy for Nd, are in great demand for hybrid vehicles and wind turbines. Dy substitution is effective in producing a higher coercivity (H_c) but reduces the magnetisation greatly. In addition, recent fluctuations in the supply of heavy rare earth elements also make Dy substitution undesirable. Achieving high H_c without Dy, requires greater fundamental understanding of coercivity itself. Model systems, *e.g.* thick films, play an important role in meeting this goal. The advantage of thick films as model systems is that they can be produced easily under a range of conditions and with various alloying additions. Here, very high H_c of 2.7 T has been produced in a Nd-Fe-B thick film without Dy. The microstructure of the film has been investigated by high resolution transmission electron microscopy (TEM) and 3D atom probe tomography in order to understand the remarkably high H_c achieved (Fig.).
For further details see N.M. Dempsey, T.G. Woodcock *et al.*, Acta Materialia **61**, 4920-4927 (2013).

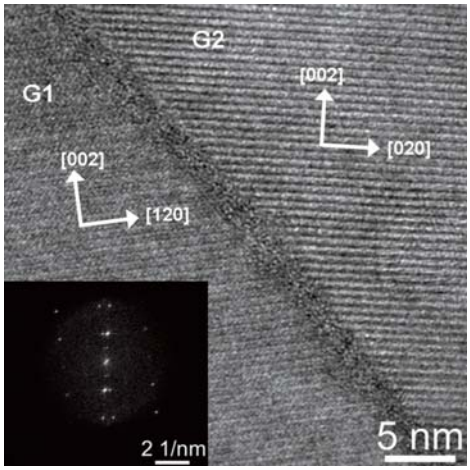

Fig.: High resolution TEM image showing a grain boundary in the Nd-Fe-B thick film, decorated with a 2 nm thick layer of an amorphous, Nd-rich phase, which is thought to be responsible for the high H_c. The orientations of the grains are marked. The inset shows the FFT of the image.

Cooperations: [1]Institut Néel, France; [2]NIMS, Japan; [3]TU Darmstadt, Germany
Funding: Toyota Motor Corporation

Transport study of the SDW material Mn_3Si

F. Steckel, S. Rodan, R. Hermann, C. Blum, S. Wurmehl, B. Büchner, and C. Hess

Electronic ordering such as a spin density wave (SDW) is directly connected with Fermi surface reconstructions in respect to the non-ordered state. Transport properties like the resistivity, the Hall, Seebeck and Nernst coefficients are extremely sensitive to such transitions. The itinerant antiferromagnet Mn_3Si undergoes SDW order at $T_N \sim 21$ K and is therefore an ideal playground to study the effect of a SDW transition on the transport coefficients [1]. While the heat conductivity is phonon dominated and therefore insensitive to the intrinsic electronic ordering, the resistivity, Seebeck and Nernst coefficient (see Fig.) exhibit pronounced anomalies in the vicinity of T_N. Interestingly, these data provide strong evidence for a large fluctuation regime related to the SDW instability which extends up to ~ 200 K.
[1] F. Steckel et al., arXiv:1309.1636.

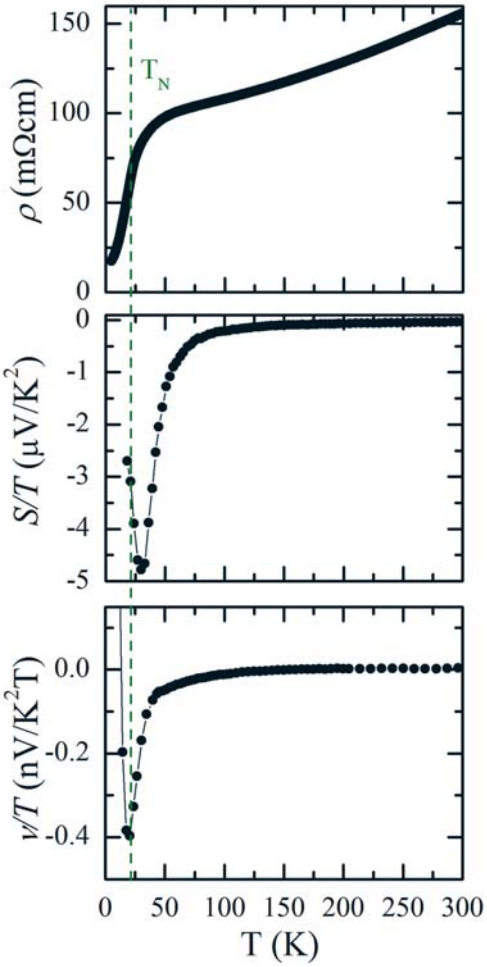

Fig.: Temperature (T) dependence of the resistivity ρ, the Seebeck coefficient S/T and the Nernst coefficient ν/T of single crystalline Mn_3Si. The SDW transition temperature T_N is marked with a dashed line. The pronounced minima in the Seebeck and Nernst coefficient near the transition temperature are clearly visible. The fluctuation regime can be inferred from the deviation from the high-temperature linear (ρ) and constant temperature dependencies (S/T and ν/T).

Funding: DFG

Research Area 3
Molecular nanostructures and molecular solids

Spin density distribution in a Cu(II)-(bis)oxamato complex

A. Aliabadi, A. Petr, M. A. Abdulmalic[1], T. Rüffer[1], T. Hahn[2], J. Kortus[2], Y. Krupskaya, V. Kataev, B. Büchner

Mononuclear Cu(II)-(bis) oxamato complexes are promising starting materials for the synthesis of more complex magnetic molecular structures. For tailoring the desired magnetic properties, it is important to know how the spin density is distributed between the central metal ion and the ligands, because this affects the magnetic superexchange interactions between neighboring ions in the corresponding polymetallic complexes. The spin density distribution of the mononuclear Cu(II)-(bis) oxamato complex containing

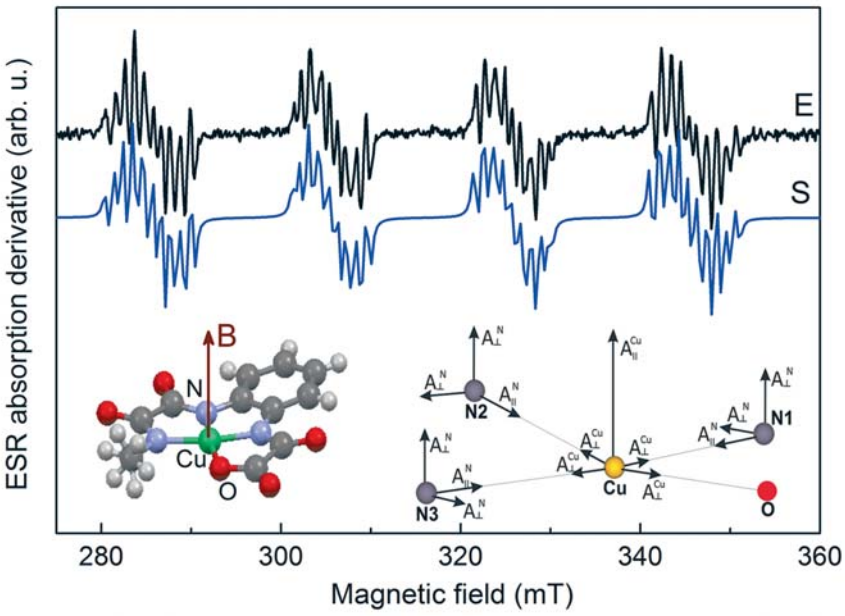

Fig.: Top: Experimental (E) and simulated (S) single crystal ESR spectrum of a Cu(II)-(bis) oxamato complex with three nitrogen ligands ($f = 9.56$ GHz, T = 293 K) for the direction of the external magnetic field perpendicular to the molecular plane. **Bottom:** molecular structure of the studied complex (left) and the scheme of the principal axes of the Cu and N hyperfine tensors (right).

three nitrogen ligands (see Fig.) has been determined using electron spin resonance (ESR) spectroscopy at 10 GHz [1]. The isotropic ESR parameters were obtained from the measurement of liquid solution at $T = 293$ K. The angular dependence of the ESR spectra was studied by rotation of a single crystal in two perpendicular planes. By modelling the spectra (see Fig.), the g-tensor, the Cu hyperfine (HF) coupling tensor, and the N HF coupling tensor were determined. Using these parameters, the spin density on the Cu(II) ion and on N atoms was calculated. Depending on the theoretical model, the spin densities on the Cu ion and per N ligand vary between 51% and 68% (Cu), and 10.5% and 9.5% (N), respectively. Independent DFT quantum chemical calculations yield comparable densities of 53.9% (Cu) and 11.8% (N). A substantial leakage of the spin density to the ligands is favourable for establishing strong superexchange paths in the corresponding multinuclear complexes.

[1] M. A. Abdulmalic et al., Dalton Trans **41**, 14657 (2012).

Cooperations: [1]TU Chemnitz; [2]TU Bergakademie Freiberg
Funding: DFG (FOR 1154)

Structure dependence of charged states in "linear" polyaniline as studied by *in situ* spectroelectrochemistry

A. Kellenberger, E. Dmitrieva, L. Dunsch

By *in situ* ESR/UV-vis-NIR and FTIR spectroelectrochemistry, the formation of charged states in protonated and unprotonated structures of emeraldines was followed [1]. The initial stage of oxidation of the emeraldine base and salt consists of the different charged states. At the early stage of charge injection into the emeraldine salt is preferably the polaron structure, while π-dimers and polaron pairs are formed by oxidation of emeraldine base. The potential dependence of the IR bands during the oxidation of the polymer clearly demonstrates the formation of the different charged polymer structures (π-dimers, polarons, and bipolarons). It is shown that IR bands usually attributed to a semiquinoid polaron lattice correspond in fact to doubly charged species, π-dimers, which are face-to-face complexes of two polarons. IR bands corresponding exclusively to polarons and bipolarons have been identified. The phenazine units in the polymer chains stabilize the charged states in the emeraldines upon p-doping.

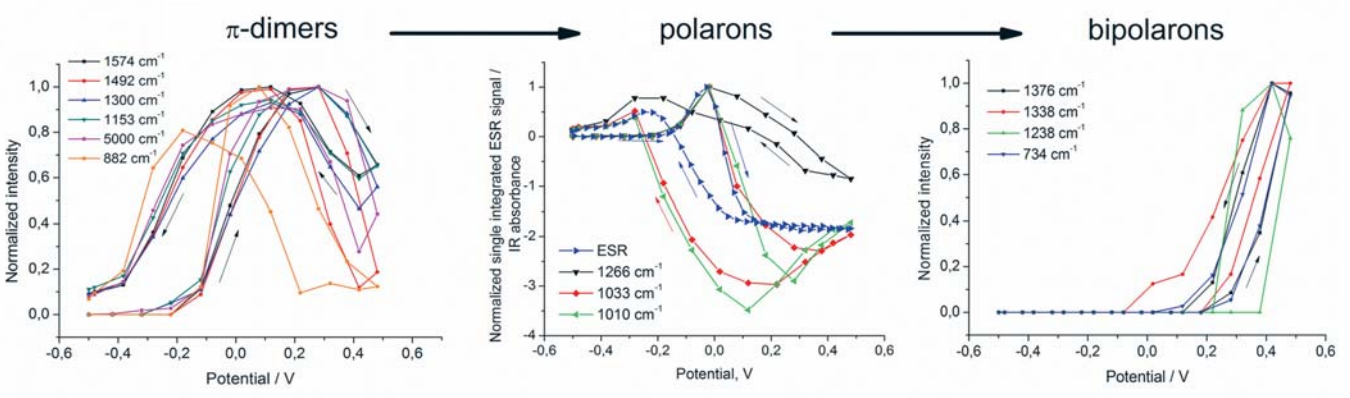

Fig.: Potential dependence of IR bands of emeraldine structure.

[1] A. Kellenberger et. al. *J. Phys. Chem. B*, **2012**, *116*, 4377.

Cooperation: University Politehnica of Timosoara, Romania
Funding: BMBF

The electronic excitation spectrum of calcium-doped picene

F. Roth, E. Müller, B. Rellinghaus, B. Büchner, M. Knupfer

The electronic excitations of Ca-doped picene films have been investigated using electron energy-loss spectroscopy in transmission. We demonstrate that a composition of Ca_3picene can be achieved by evaporation of Ca onto pristine picene films under ultra-high vacuum conditions. The core level excitations indicate a charge transfer of one electron per added Ca to the picene molecules and a hybridization of Ca and picene derived electronic states. Upon doping a new spectral feature is observed at about 2 eV in the electronic excitation spectrum. This new feature does not disperse which signals its localized character. The data analysis using a Kramers-Kronig transformation suggests that Ca_3 picene has a nonmetallic ground state.

For details see: Roth et al., Phys. Rev. B 88, 205105 (2013).

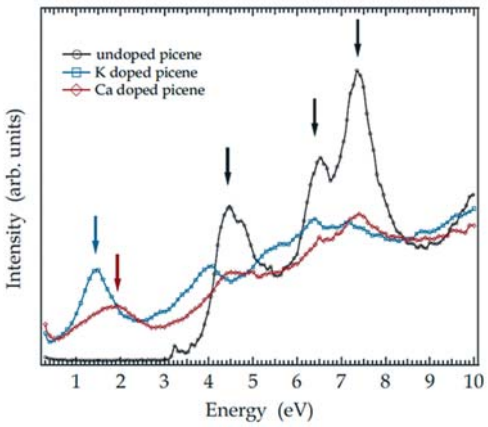

Fig.: Comparison between the loss functions of pristine picene (black circles) as well as potassium- (blue squares) and calcium-intercalated (red diamonds) picene. All measurements have been done with a momentum transfer of 0.1 $Å^{-1}$.

Funding: DFG

Ubiquitous electron-phonon coupling to dopant vibrations in graphene

A. Fedorov, A. Grüneis, M. Knupfer, J. Fink, B. Büchner

Angle-resolved photoemission spectroscopy (ARPES) was carried out to perform a search for an electron donor for graphene, capable of inducing high electron-phonon coupling and potentially superconductivity. We examined the widespread electron donors Cs, Rb, K, Na, Li, Ca and determined for each dopant the full electronic band structure (see Fig.) and the Eliashberg function from the spectral function measured by ARPES. The Eliashberg function has high-energy peaks for the well-known graphene derived optical phonons. Unexpectedly, a new low-energy feature appears for all dopants with an energy and intensity that depend on the dopant atom. By investigating the dopant dependence of this feature we show that it results from a dopant related vibration. The low-energy and high intensity of this peak is crucially important for achieving high electron-phonon coupling and hence also for potential superconductivity. The case of Ca doped graphene yields the highest electron-phonon coupling, which is expected to sustain values of $T_c = 1.5$ K and which supports the expectation of superconductivity in graphene.

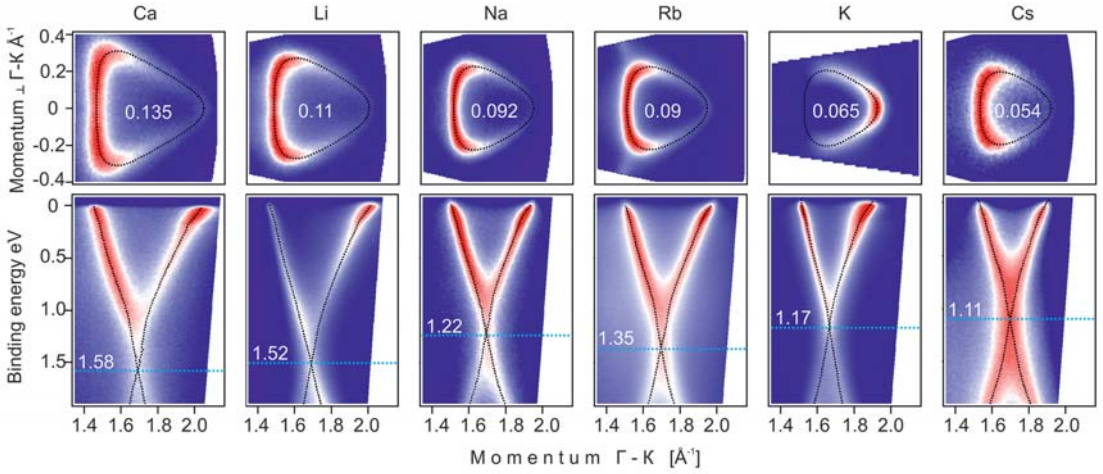

Fig.: ARPES spectra of maximally doped graphene for different dopants. The black dotted line denotes the ARPES intensity maxima. Upper row: Fermi surfaces and electrons transferred per C atom (values inside the contour).

Cooperations: University of Vienna, St. Petersburg State University, Moscow State University, Elettra Sincrotrone Trieste, TU Dresden
Funding: DFG

Analysis of the contact properties of PCBM transistors by combined photoemission spectroscopy, electrical measurements, and numerical simulations

S. Scheinert[1], M. Grobosch, J. Sprogies[1], I. Hörselmann[1], M. Knupfer, G. Paasch

Carrier injection barriers determined by photoemission spectroscopy for organic/metal interfaces are widely accepted to determine the performance of organic field-effect transistors (OFET), which strongly depend on this interface at the source/drain contacts. This assumption is checked here in detail, and a more sophisticated connection is presented. A preparation process has been developed which is essentially the same for PCBM/Au and PCBM/Al samples for characterizing the interface by photoemission and for bottom contacts in OFETs with PCBM as active layer. XPS measurements show that in both cases one has thin contamination layers and in the case of the contact with Al also a thin AlO_x interlayer. UPS measurements yield the energy level alignments at both contacts depicted in the figure. The hole injection barrier is 1.8 eV for both Al and Au contacts. Therefore, the electron injection barriers are also the same. And, one had to expect essentially the same currents in the OFETs. However the measured drain

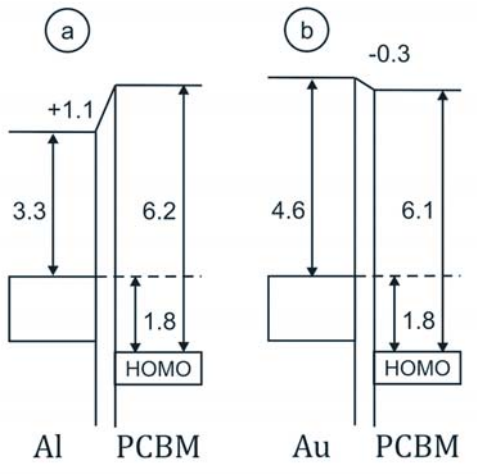

Fig.: Energy level alignment of the PCBM/AlOx/Al system **(a)** and the PCBM/Au system **(b)**. All values given in eV.

currents are orders of magnitude larger for the transistor with the Al contacts than for those with the Au contacts. Comparison of measured current charactersitics with two-dimensional numerical simulations shows, that indeed for these systems the injection is not determined by the barrier but by two other properties measured also by photo-emission, the (reduced) work functions, and the interface dipoles, which have different sign for the two contact materials. For further details see S. Scheinert, M. Grobosch, J. Sprogies, I. Hörselmann, M. Knupfer, G. Paasch, J. Appl. Phys. 113, 174504 (2013)

Cooperation: [1]TU Ilmenau
Funding: DFG

Nanoscale low energy electron induced graphitization in tetrahedral amorphous carbon thin films

F. Klein, T. Mühl

Under ambient or vacuum conditions diamond and related materials like tetrahedral amorphous carbon (ta-C) are in a metastable state. By application of energy the material is able to undergo a phase change to a graphitic or sp^2-hybridised state. We induce local phase changes in ta-C thin films by eV and low keV electron beams in ultrahigh vacuum provided by a scanning tunneling microscope (STM) and a scanning electron microscope (SEM), respectively. These are accompanied by huge changes in many physical properties such as electrical conductivity.

The graphitization is analyzed by STM-based current-distance spectroscopy. The total tip-sample circuit contains the tunneling gap resistance in series with the resistance of the carbon thin film R_{carbon}. An analysis of the STM spectra provides the tunneling barrier height Φ and R_{carbon}.

We observe a decrease of R_{carbon} as well as an increase of Φ in the graphitized areas (see Fig.). However, an expected surface elevation due to a reduction in the material's mass density cannot be seen.

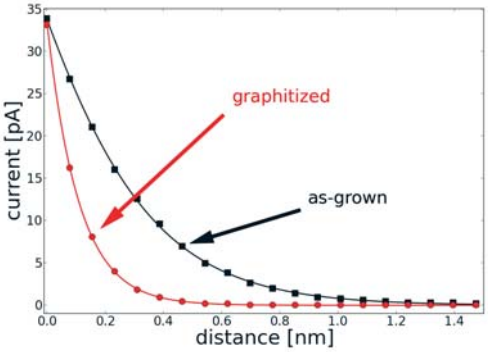

Fig.: Measured STM spectra (points) on as-grown and 4 keV electron beam graphitized ta-C and corresponding fits (lines). Fit-Parameters: R_{carbon} = 44 GΩ, Φ = 0.7 eV (as-grown) and R_{carbon} = 0 GΩ, Φ = 0.9 eV (graphitized).

Cooperations: Fraunhofer IWS Dresden, Helmholtz-Zentrum Dresden-Rossendorf
Funding: DFG

Challenging the nature of low-energy plasmon excitations in CaC_6 using electron energy-loss spectroscopy

F. Roth, A. König, B. Büchner, M. Knupfer

The nature of low-energy plasmon excitations plays an important role in understanding the low-energy electronic properties and coupling mechanism of different superconducting compounds such as CaC_6. Recent *ab initio* studies predict a charge carrier intraband

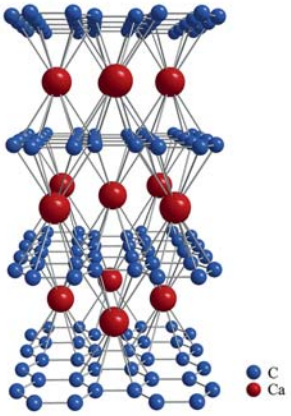

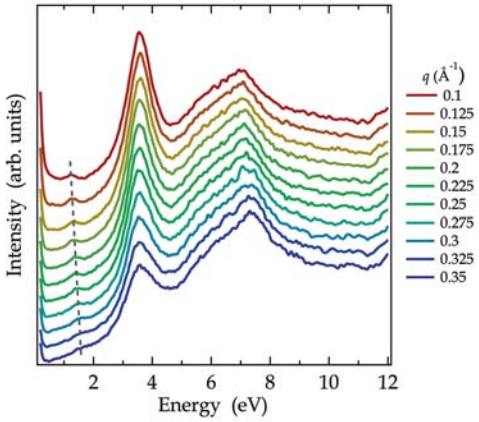

Fig.: Left: Crystal structure of CaC_6.
Right: Momentum dependence of the loss function of CaC_6 demonstrating the negative dispersion of the plasmon around 3.5 eV and the finite energy of the lowest energy feature for small momenta, which contradicts the prediction of an acoustic plasmon.

plasmon in keeping with a low-energy acoustic plasmon. Here, we have studied the low-energy electronic excitations of CaC_6 using high-resolution electron energy-loss spectroscopy in transmission at low temperatures. The analysis of the core level excitations leads to the conclusion that hybridization between graphite and calcium states plays an essential role in this graphite-intercalated compound. Regarding the low-energy plasmon excitations, we observe the formation of an intraband (charge carrier) plasmon with a negative dispersion at about 3.5 eV in sound agreement with theory. Finally, a weak excitation around 1.2 eV with an almost linear dispersion relation can be observed as predicted for an acoustic plasmon that may mediate the superconducting coupling in CaC_6. However its finite energy in the optical limit at ~1 eV challenges the theoretical predictions of an acoustic plasmon. For details see: Roth et al., EPL 102, 17001 (2013).

Cooperation: University of Vienna
Funding: DFG

Strain-Driven Endohedral Redox Couple Ce^{IV}/Ce^{III} in Nitride Clusterfullerenes $CeM_2N@C_{80}$ (M = Sc, Y, Lu)

Y. Zhang, S. Schiemenz, A. A. Popov, and L. Dunsch

Endohedral fullerenes (EMFs) stand for a unique form of fullerenes with atoms, clusters or molecules encapsulated in their interior space. Recently, it was established that not only unusual species can be stabilized inside the fullerene cages, but also that the spin and charge states of such species can be manipulated by endohedral redox processes. The studies of such processes, in which a carbon cage acts as a redox-inert but electron-transparent container, constitute the recently emerged discipline known as *endohedral electrochemistry*. In this work, we have synthesized $CeY_2N@C_{80}$ and performed an NMR spectroscopic and electrochemical study of a series of $CeM_2N@C_{80}$ NCFs (M = Sc, Lu, Y). The unambiguous proof of the endohedral $Ce^{III} \rightarrow Ce^{IV}$ oxidation in these compounds is provided by NMR spectroscopy of the $[CeM_2N@C_{80}]^+$ cations. Although the second cluster metal (Sc, Y, Lu) is not involved in the redox process, the oxidation potential of $CeM_2N@C_{80}$ is a function of the M^{3+} ionic radius and varies in the range of 0.4 V depending on the metal. The large size of the cluster and the limited inner space of the carbon cage result in the inherent strain, and the driving force of the endohedral oxidation of Ce^{III} in $CeM_2N@C_{80}$ is the release of this strain when Ce^{IV} with small ionic radius is formed. For further details see Y. Zhang et al., *The Journal of Physical Chemistry Letters* **4**, 2404 (2013).

Funding: DFG

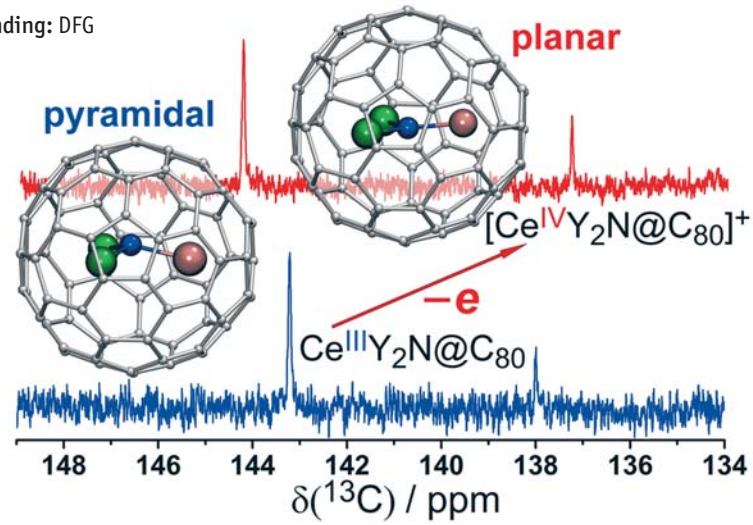

Fig.: Change of the geometry of the nitride cluster in $CeY_2N@C_{80}$ from pyramidal to planar is induced by the one-electron oxidation. The shifts in ^{13}C NMR spectra (blue for neutral compound and red for the cation) prove that oxidation proceeds via removal of $4f^1$ electron from the endohedral Ce^{III} ion.

Research Area 4
Metastable alloys

TiNb-based alloys for implant applications

M. Bönisch, A. Helth, K. Zhuravleva, S. Abdi, H. Attar,
P. F. Gostin, S. Oswald, M. Calin, A. Gebert, J. Eckert

New metallic materials with reduced stiffness and strong surface-tissue bonding are needed to facilitate long-lasting functionality of load-bearing implants. TiNb-based alloys are at the focus of our research because they offer low elastic moduli, high biocompatibility and excellent corrosion resistance in body fluids. However, optimization of the chemical composition, thermo-mechanical processing conditions and surface properties is required. Various manufacturing approaches such as casting, powder metallurgy, selective laser melting and rapid solidification were explored. The phase constitution, microstructure, thermal stability and mechanical properties of bulk Ti-Nb alloys (with Nb content between 14 and 40 wt.%) were investigated by a combination of experimental and theoretical methods. In Ti-Nb alloys the superelastic and shape memory properties can arise due to the thermoelastic martensitic $\beta \rightarrow \alpha''$ phase transformation. We found that the unit cell dimensions and atom positions in TiNb martensites strongly change by Nb addition and heating causes the martensites to decompose into α, β and/or ω phases. The presence of α and ω phases leads to the increase of Young's modulus. At Nb addition of 40 wt.% a metastable single-phase β microstructure with a Young's modulus of ~65 GPa can be formed. For further reduction of the elastic modulus porous structures are required. Porous bodies of β-type Ti-40Nb were prepared by compaction of mechanically alloyed powder mixed with NaCl or Mg particles as space-holder material. The compacts with porosity of 36–80% demonstrated a very low Young's modulus of ~1.5–3 GPa and compression strength of ~10–35 MPa, which are suitable for potential implant applications.

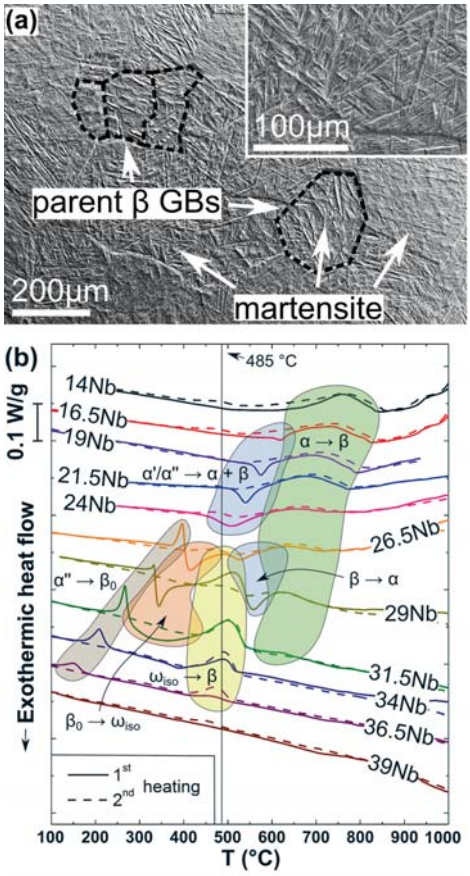

Fig.: (a) Secondary electron SEM image showing the martensitic microstructure in Ti-19Nb. **(b)** Phase reaction sequences in martensitic TiNb alloys revealed by Differential Scanning Calorimetry.

Cooperations: University of Cambridge, UK; University Hospital Giessen and Marburg, Germany; University of Vienna, Austria; Katholieke Universiteit Leuven, Belgium; University of Ioannina, Greece.
Funding: EC ITN BioTiNet, DFG SFB/TRR79

In situ synchrotron studies on battery materials

M. Herklotz, F. Scheiba, L. Giebeler, A.-C. Dippel, H. Ehrenberg, and J. Eckert

Performance loss in novel electrochemical energy storage systems, like lithium ion or lithium sulfur batteries, can be associated with irreversible structural changes in the bulk material. Hence the evolution of phase amounts, lattice parameters, atomic positions, occupation numbers and microstructure formation during the electrochemical cycling has

Fig.: Principle of *in situ* synchrotron diffraction studies on energy storage systems

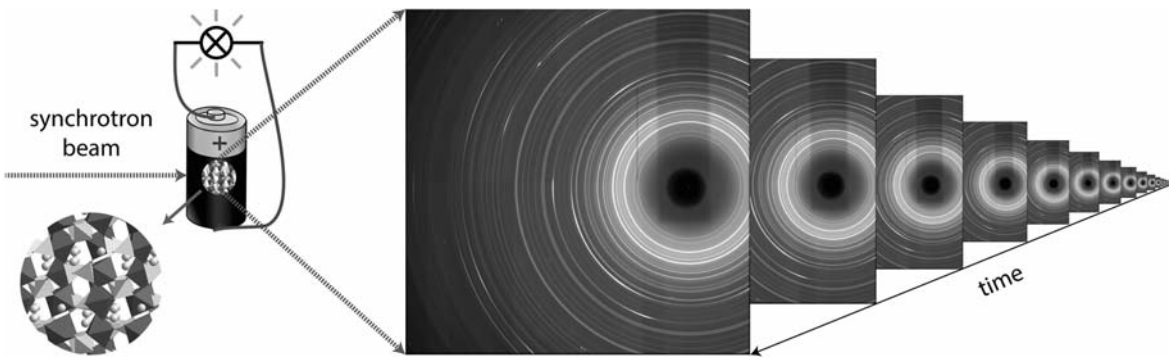

to be investigated in detail. Therefor *in situ* or often called *in operando* synchrotron diffraction studies are used, whose principle is illustrated in the figure.
The new beamline P02.1, PETRA III (DESY Hamburg) was established for *in situ* synchrotron diffraction studies, also on batteries [1]. Thanks to brilliant beam conditions accompanied with an amorphous silicon-based 2D detector and a new *in situ* cell design an excellent performance was achieved. For instance a time resolution in matter of milliseconds per pattern was demonstrated, which enables high current measurements. At medium 2D-detector distances the new setup enables apparent size or strain refinements up to the region of 500 nm or down to 0.01 %, respectively. The performance was exemplified by the *in situ* investigation of monoclinic $Li_3Cr_2(PO_4)_3$, which is handled as a candidate for the next generation of high power cathode materials in lithium ion batteries. New structural phenomena like the formation of chromyl compounds or possible slip planes were revealed.
[1] M. Herklotz, F. Scheiba, M. Hinterstein, et al., "Advances in in situ powder diffraction of battery materials: a case study of the new beamline P02.1 at DESY, Hamburg," *J. Appl. Crystallogr.* 46 (2013) 1117–1127.

Cooperations: Karlsruhe Institute for Technology (KIT), DESY
Funding: The German Ministry of Education and Science (BMBF) within the He-Lion Consortium.

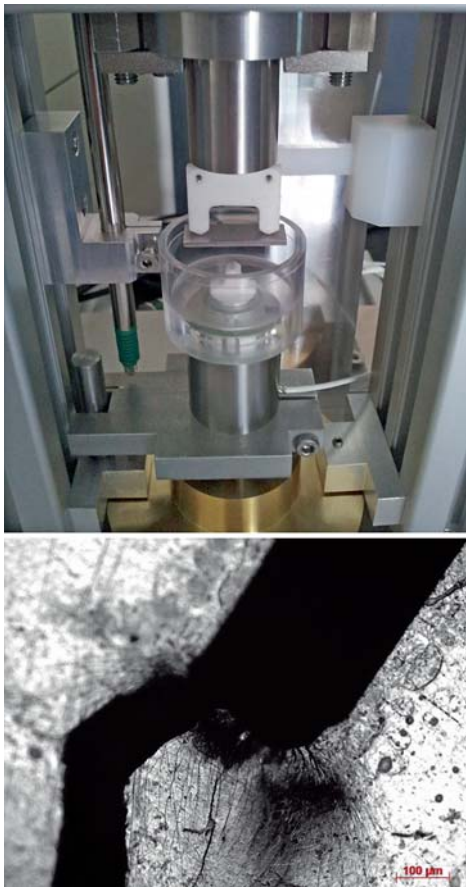

Fig.: (Top) Testing machine for stress corrosion cracking experiments under bending conditions, Research Technology Division of the IFW Dresden; **(Bottom)** Multiple shear bands formed at the notch tip in an amorphous $Zr_{52.5}Cu_{17.9}Al_{10}Ni_{14.6}Ti_5$ (Vit105) sample during quasi-stationary three-point bending.

Stress corrosion cracking and corrosion fatigue of Zr-based bulk metallic glasses

P. F. Gostin, M. Uhlemann, A. Gebert, J. Eckert

For metallic glasses the resistance against crack propagation determining fracture toughness and fatigue resistance is a critical aspect. Moreover, superposition of environmentally induced reactions gives rise to significant stress corrosion cracking and corrosion fatigue phenomena, which are poorly understood at present. We recently demonstrated how shear bands formed ex situ act as preferential sites for local corrosion initiation and propagation, while pre-formed corrosion pits are favourable surface sites to which shear bands are linked [1]. Since cracks initiate and grow along shear bands, present work is focused on studying in situ the interplay of shear bands with corrosive media as well as on clarifying the crack growth behaviour under various mechanical loading conditions (i.e. quasi-static, static and cyclic) and corrosion conditions (i.e. anodic dissolution, passivation-repassivation regimes and cathodic hydrogen charging). For this a custom made bending machine, which enables three point bending testing in corrosive liquid environments, was designed and built by the Research Technology Division of IFW Dresden (see top photo). Microscopic investigations after first bending tests on notched samples of bulk glassy $Zr_{52.5}Cu_{17.9}Al_{10}Ni_{14.6}Ti_5$ alloy (Vit105) revealed the formation of multiple shear bands at the notch tip with subsequent cracking along one of the major shear bands (see bottom image). In the frame of this project, the IFW Dresden is a member of the SPP1594 network.
[1] A. Gebert, P. F. Gostin, M. Uhlemann, J. Eckert, L. Schultz, Interactions Between Mechanically Generated Defects and Corrosion Phenomena of Zr-Based Bulk Metallic Glasses. Acta Materialia 2012, vol. 60, pp. 2300-2309.

Cooperation: TU Kaiserslautern
Funding: DFG

Direct observation of phase separation in ternary Gd-Ti-Co liquids

J. H. Han, N. Mattern, I. Kaban, J. Eckert

According to our recently reported phase diagram [1], the Gd-Ti system is of the monotectic type exhibiting a miscibility gap and liquid-liquid phase separation occurs above the monotectic temperature. This renders Gd-Ti-based multi-component systems appropriate candidates for phase separated glass-glass and glass-crystalline composite materials by rapid quenching the melt e.g. of $Gd_{30}Ti_{30}Co_{30}Al_{10}$. Currently, there is only limited information in the literature about the ternary Gd-Ti-Co phase diagram. Therefore, the phase equilibria and the extension of the miscibility gap in the liquid of the ternary Gd-Ti-Co system have been investigated by combining electrostatic levitation technique with *in situ* high-energy synchrotron X-ray diffraction (XRD) at elevated temperatures [2]. Figure shows XRD patterns of a $Gd_{35}Ti_{35}Co_{30}$ alloy at different temperatures. The coexistence of two liquid phases formed by liquid-liquid phase separation could be directly proven by the two diffuse maxima in the high temperature range (1690 K < T < 1760 K).With increasing temperature both diffuse diffraction maxima shift due to the change in compositions and merge in accordance with a binodal line. The liquid phase of the ternary system exhibits a miscibility gap originating from the binary Gd-Ti subsystem which extends up to 30 at. % Co. Based on the experimental data a thermodynamic description is derived.

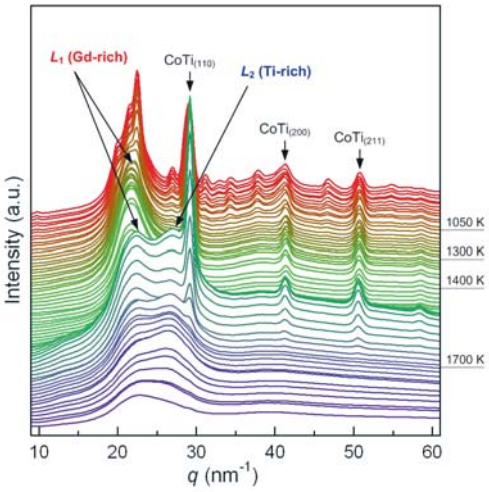

Fig.: *In situ* XRD patterns of $Gd_{35}Ti_{35}Co_{30}$ at different temperatures.

[1] N. Mattern *et al.*, *CALPHAD: Computer Coupling of Phase Diagrams and Thermochemistry* **42** (2013) 19.
[2] J. H. Han et al., *J. Phys.: Condens. Matter* **25** (2013) 245104.

Cooperations: DRL Köln, DESY Hamburg, Yonsei University Seoul
Funding: DFG, GRL Korea

Tuning tensile ductility in composite structured Ti-based alloys

I. V. Okulov, S. Pauly, U. Kühn, T. Marr, J. Freudenberger, L. Schultz,
W. Skrotzki, J. Eckert

The tailoring of composite microstructures is a focus for the current high interest in metals to improve mechanical properties. For example, the ductility of a metallic glass can be significantly improved by crystal precipitates; the strength of Ti-based nano-/ultrafine-dendrite composites (consisting of nano-/ultrafine and coarse grained structures) approaches that of Ti-based metallic glass composites. However, most of Ti-based nano-/ultrafine-dendrite composites are brittle in tensile loading regime. Recently, it was reported that the control of precipitates in the $Ti_{68.8}Nb_{13.6}Al_{6.5}Cu_6Ni_{5.1}$ (Fig. a) and the $Ti_{71.8}Nb_{14.1}Al_{6.7}Cu_4Ni_{3.4}$ (Fig. b) alloys can significantly enhance the tensile ductility and maintaining the high strength [1]. The $Ti_{68.8}Nb_{13.6}Al_{6.5}Cu_6Ni_{5.1}$ alloy exhibits the high yield strength of about 1050 MPa with the tensile ductility of about 5 % already in the as-cast state. The fracture strain of the $Ti_{71.8}Nb_{14.1}Al_{6.7}Cu_4Ni_{3.4}$ alloy is about 14 %. The improvement in ductility is clearly demonstrated by a change of fracture mechanisms from quasi-cleavage (Fig. c) to dimple fracture (Fig. d).

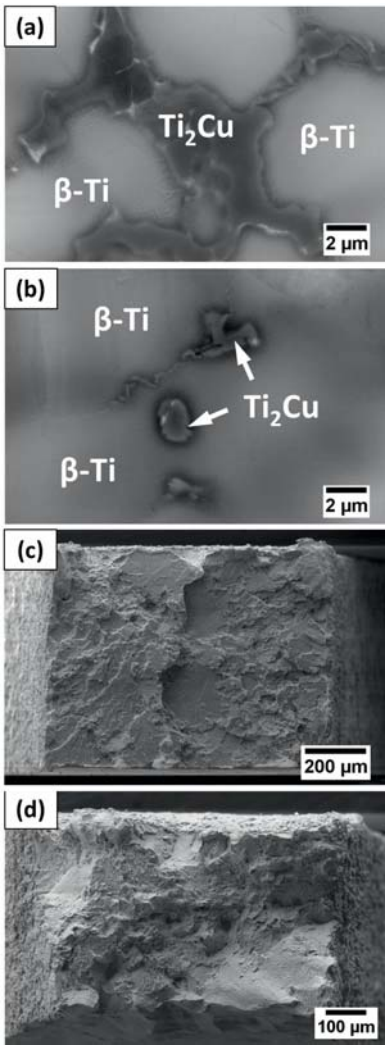

[1] Okulov et al., Materials Science and Engineering C, 33 (2013) 4795–4801.

Fig.: SEM backscattered electron images: microstructure of **(a)** $Ti_{68.8}Nb_{13.6}Al_{6.5}Cu_6Ni_{5.1}$ alloy and **(b)** $Ti_{71.8}Nb_{14.1}Al_{6.7}Cu_4Ni_{3.4}$ alloy; fracture surface of **(c)** $Ti_{68.8}Nb_{13.6}Al_{6.5}Cu_6Ni_{5.1}$ alloy and **(d)** $Ti_{71.8}Nb_{14.1}Al_{6.7}Cu_4Ni_{3.4}$ alloy

Cooperation: TU Dresden
Funding: EU and Free State Saxony (SAB grant no. 13853/2379) within the European Centre for Emerging Materials and Processes Dresden (ECEMP)

Selective laser melting of Al-12Si

K.G. Prashanth, S. Scudino, L. Löber, U. Kühn and J. Eckert

Selective laser melting (SLM) is a powder-based additive manufacturing technique consisting of the exact reproduction of a three dimensional computer model through an additive layer-by-layer strategy. Because of the high degree of freedom offered by the additive manufacturing, parts having almost any possible geometry can be produced by SLM. Another major advantage of SLM compared to conventional techniques is the fast cooling rate during the process, which permits the production of bulk materials with very fine microstructures. This work focuses on the structure-property correlations of Al-12Si samples produced by SLM. The results demonstrate that SLM can be successfully used for the production of parts with an overall superior performance of the mechanical and physical properties with respect to the conventional cast samples. Moreover, the mechanical properties of the SLM samples can be widely tuned *in-situ* by employing suitable hatch styles or *ex-situ* by the proper heat treatment. This might help the development of SLM for the production of innovative high-performance Al-based materials and structures with controlled properties for automotive and aerospace applications. For further details see K. G. Prashanth et al., Mater. Sci. Eng A **590**, 153 (2013).

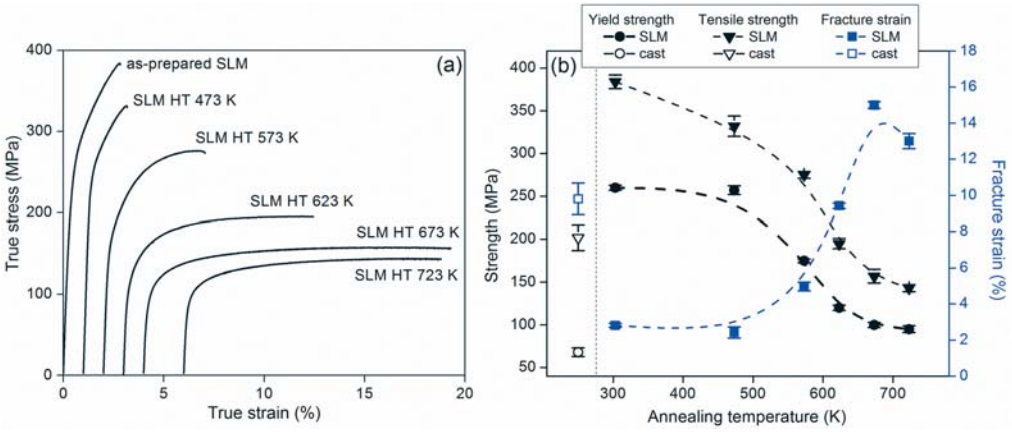

Fig.: (a) Room temperature tensile test curves of the Al-12Si SLM samples annealed at different temperatures and **(b)** corresponding mechanical data.

Cooperations: Indian Institute of Technology, Madras, India; Indian Institute of Science, Bangalore, India; South China University of Technology, China

Coupling of Li motion and structural distortions in olivine $LiMnPO_4$ from ^{7}Li and ^{31}P NMR

C. Rudisch, H.-J. Grafe, J. Geck, S. Partzsch, M. v. Zimmermann[1], N. Wizent, R. Klingeler[2], and B. Büchner

$LiMnPO_4$ is a member of the olivine type lithium phosphate family and features several advantages regarding battery technology such as excellent chemical and thermal stability, nontoxicity, and economic viability and availability of the raw materials. Despite these advantages of $LiMnPO_4$ for battery applications, there are also reports about its poor electrochemical performance. However, the reasons for this currently remain unclear. Therefore, we investigated $LiMnPO_4$ single crystals by ^{7}Li and ^{31}P NMR and diffuse x-ray scattering. The NMR resonance lines shown in the figure are anomalously broadened, and especially for $H_0||b$ show a shoulder in the spectra. Also, we determined the full hyperfine coupling tensor by angle dependent measurements of the resonances. Deviations of the experimentally obtained hyperfine coupling tensors from the calculated tensors and the anomalous broadening of the resonance lines in the paramagnetic phase prove the existence of Mn disorder in the samples. The conclusions from NMR

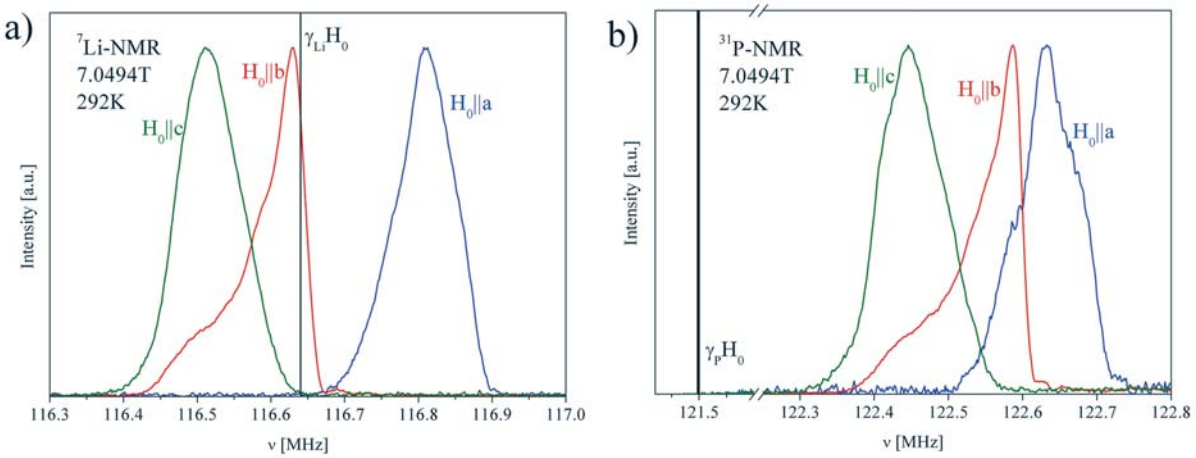

Fig.: (a) Typical ^{7}Li and **(b)** ^{31}P NMR spectra taken at room temperature in single crystalline $LiMnPO_4$ for field orientations H_0||a, b, and c. The unusual broadening and shoulder structure especially for H_0||b are evidence for Mn site disorder which is supported by diffuse x-ray scattering (not shown).

are corroborated by our diffuse x-ray-diffraction (XRD) experiments, which directly reveal the disorder in the Mn sublattice. Our findings provide firm experimental evidence that the movement of Li within $LiMnPO_4$ is strongly coupled to the lattice. Certainly, this also affects the mobility of the Li, and therefore the performance of this material as a battery. Interestingly, our results are perfectly consistent with a recent theoretical study which found a formation of a vacancy-polaron complex by a lithium vacancy and a corresponding hole polaron at the fully lithiated limit owing to lattice distortion and Coulomb interaction between them, thereby explaining the poor electrochemical performance of untreated $LiMnPO_4$.

[1] C. Rudisch et al., Phys. Rev. B **88**, 054303 (2013).

Cooperations: [1]Deutsches Elektronen-Synchrotron DESY, Hamburg,
[2]Kirchhoff-Institut für Physik, Universität Heidelberg
Funding: DFG SPP1473 (Grants No. GR3330/3-1 KL1824/5) and Emmy-Noether Program (Grant No. GE1647/2-1)

Improving visualization of interdiffusion layers in lithium ion batteries

M. Zier, F. Scheiba[1], S. Oswald, J. Thomas, D. Goers[2], T. Scherer[1], M. Klose, H. Ehrenberg[1], and J. Eckert

An osmium tetroxide (OsO_4) staining technique, abundantly used in medicine and biology, has been adopted for electron microscopy studies of graphite and metallic lithium anodes of lithium-ion batteries. OsO_4 shows a coordinated reaction with components of the solid electrolyte interphase (SEI) and the surface of metallic lithium. Scanning electron microscopy (SEM) and high-resolution transmission electron microscopy (HR-TEM) evidenced osmium rich areas by an enhanced elemental contrast where the reaction had taken place. Cross sections of cycled and stained electrodes by focused ion beam (FIB) revealed important information about lithium deposition across the electrode as the highly volatile OsO_4 fume is easily able to penetrate the porous composite electrodes thoroughly. Facilitating the affinity of metallic lithium to react with osmium tetroxide it is possible to localize lithium deposition on graphite electrodes, the lithium dendrite morphology remaining almost untouched by the staining procedure. Furthermore, OsO_4 treatment of lithium plated and subsequently stripped electrodes allows correlating the quantity of osmium detected with the amount of residual ("dead") lithium on the electrode, thus being a practical measure for lithium plating and stripping efficiencies.

To be published

Cooperations: [1]Institute of Applied Materials/ Institute of Nanotechnology, Karlsruhe Institute of Technology, [2]Li-Tec Battery GmbH
Funding: Li-Tec Battery GmbH

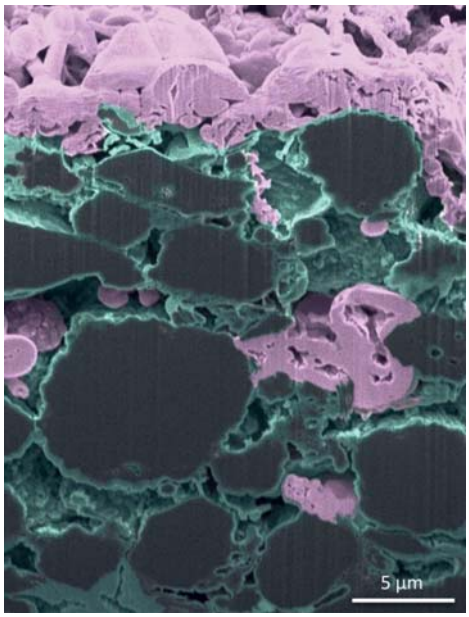

Fig.: Pseudocolor image of the cross section of an aged graphite electrode after osmium tetroxide staining. The increased material contrast due to OsO4-staining enables easy distinction between graphite particles (dark grey) that are covered by a stained SEI (mint) and surrounded by metallic lithium (pink). The electrode surface is located towards the top of the image.

FeCoSiBNbCu bulk metallic glass with large compressive deformability

M. Stoica, I. Kaban, S. Scudino, P. Ramasamy, J. Eckert

By adding 0.5 at.% Cu to the strong but brittle $[(Fe_{0.5}Co_{0.5})_{0.75}Si_{0.05}B_{0.20}]_{96}Nb_4$ bulk metallic glass, fully amorphous rods with diameters up to 2 mm were obtained. The monolithic samples with 1 mm diameter revealed a fracture strain of 3.80 % and a maximum stress of 4143 MPa upon compression, together with a slight work-hardening behavior. SEM micrographs of fractured samples did neither reveal any shear bands on the lateral surface nor the typical vein patterns which characterize ductile fracture. However, some layers appear to have flowed and this phenomenon took place before the brittle final fracture. An estimate of the temperature rise ΔT in the shear plane gives 1039 K, which is large enough to melt a layer of 120 nm. The overall performance and the macroscopic plastic strain depend on the interaction between cleavage-like and viscous flow-like features. Mechanical tests performed in-situ under synchrotron radiation allowed the calculation of the strain tensor components, using the reciprocal-space data and analyzing the shift of the first (the main) and the second broad peak positions in the X-ray diffraction patterns (see Fig.). The results revealed that each atomic shell may have a different stiffness, which may explain the macroscopic compressive plastic deformation. Also, there were no signs of (nano)crystallization induced by the applied stress, but the samples preserve a monolithic amorphous structure until catastrophic failure occurs. For further details see: M. Stoica, S. Scudino, J. Bednarčik, I. Kaban, J. Eckert, "FeCoSiBNbCu bulk metallic glass with large compressive deformability studied by time-resolved synchrotron X-ray diffraction", Journal of Applied Physics, 2014, accepted for publication.

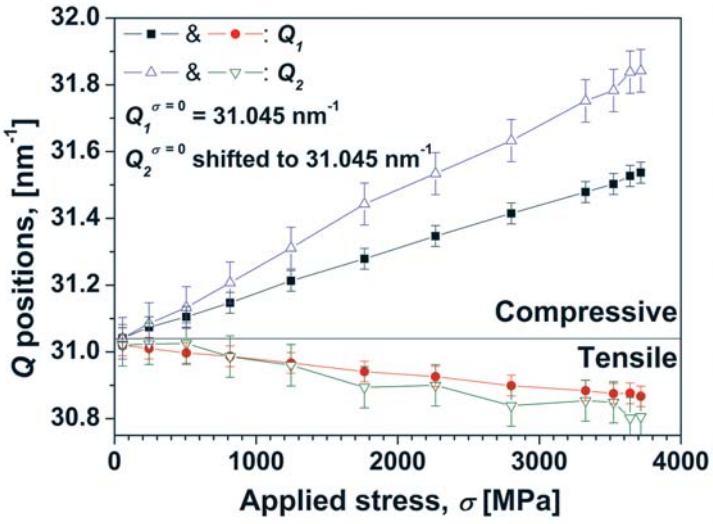

Fig.: Variation of the first (Q_1) and second (Q_2) broad peak positions as a function of the applied stress, along and perpendicular to the direction of mechanical loading. In order to easier trace the differences, the Q_2 positions were shifted down by 21.048 nm^{-1}.

Cooperations: DESY Hamburg, ESRF Grenoble
Funding: DFG

Research Area 5
Stress-driven architectures and phenomena

Propulsion mechanism of catalytic microjet engines

V. M. Fomin, M. Hippler, V. Magdanz, L. Soler, S. Sanchez, and O. G. Schmidt

Microjets have recently shown numerous potential applications in micro- and nanorobotics. There is a lack of accurate theoretical model describing the origin of the motion. A propulsion mechanism is proposed and studied for the catalytic microjet engines fabricated using rolled-up nanotech (Fig., left). The geometric asymmetry of a conical microjet leads to the development of a capillary force, which tends to propel a bubble towards the larger opening of the tube (Fig., right). The calculated bubble velocity ~1 mm/s is in a good agreement with the experiment. Due to this motion in an asymmetric tube, there emerges a momentum transfer to the fluid. In order to compensate this momentum transfer, a jet force acting on the tube occurs. The jet force, counterbalanced by the linear drag force, enables tube velocities ~100 μm/s. The proposed mechanism provides a fundamental explanation for the development of driving forces acting on bubbles in tubular microjets, which is helpful for optimization of microswimmer geometries. For details see V. M. Fomin et al., IEEE Transactions on Robotics **30** (2014); DOI: 10.1109/TRO.2013.2283929.

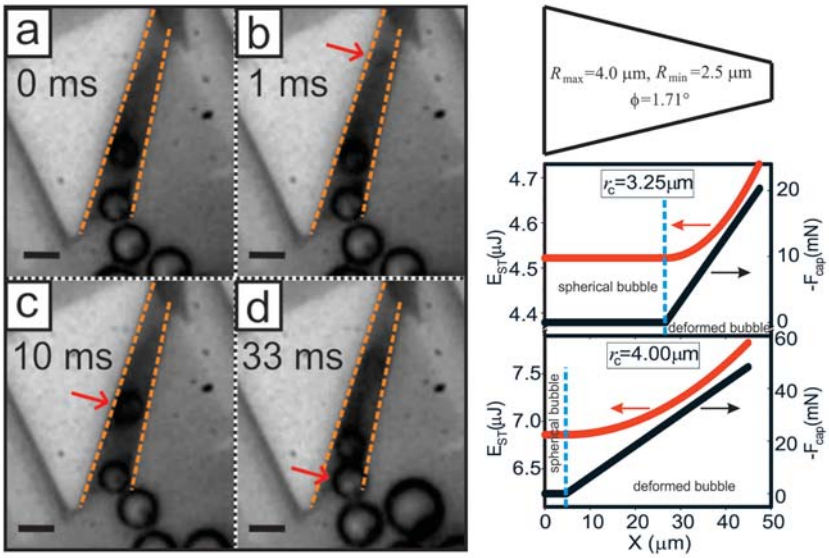

Fig.: (Left) Snapshots of the observed bubble propulsion. Orange dashed lines highlight the walls of a rolled-up tube (scale bar 10 μm). The inner surface of Pt catalyzes the decomposition of H_2O_2 and, consequently, the generation of an O_2 bubble. The bubble grows, moves to the larger opening of the tube and is released. **(Right)** Calculated surface tension energy E_{ST} (red) and capillary force F_{cap} (black) driving a bubble as a function of its position in an asymmetric catalytic microjet. A cross-section of a spherical bubble through the point of its contact with the tube wall has a radius r_c. Blue dashed lines separate the regions of bubbles deformed due to the confinement to the conical tube from those of spherical bubbles.

Cooperation: Max Planck Institute for Intelligent Systems, Stuttgart
Funding: VW foundation grant no. 86362, EU FP7/2007-2013 ERC grant no. 311529

Vertical add-drop filter made from a rolled-up ring resonator

S. Böttner, S. L. Li, M. R. Jorgensen, and O. G. Schmidt

Resonators are important building blocks for on-chip optical data processing systems where signals need to be filtered or routed across photonic circuits. To this end, highly integrated planar silicon or silicon based ring resonators are widely used because they can easily be fabricated in large scales and are compatible with standard fabrication methods. However, as the dimensions of resonators define their resonant properties and quality, the size of these components cannot be made arbitrarily small to achieve a more dense integration. A different approach to decrease the footprint of such optical chips is a vertical stacking of multiple optical layers, to form a three dimensional photonic chip.

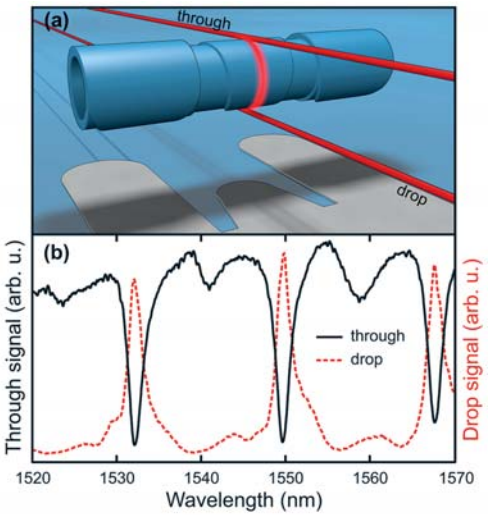

Fig.: a) Lifted rolled-up add-drop filter sandwiched between two tapered fibers (schematic), **b)** transmission and drop spectrum of two coupled fibers.

For an interaction of these layers, vertical interconnects or three dimensional optical components are required to transfer signals. In our recent publication [1] we have proposed and demonstrated that rolled-up ring resonators can be used as three dimensional frequency selective filters and add-drop couplers. These vertical resonators were fabricated by rolling up differentially strained SiO_2 nanomembranes which can, in principle, also be fabricated in large scales on chip. These structures naturally confine light in a vertical plane that can be exploited for an out of plane signal transfer between vertically stacked layers. This has been shown by coupling tapered fibers to a rolled-up ring resonator fabricated with materials that are compatible with industrial fabrication methods. Our resonators work in the widely used telecommunication wavelength range which makes them promising candidates for integration with on-chip silicon waveguides, where they could be used in applications ranging from simple wavelength filtering to the highly interesting vertical add-drop coupler.

[1] S. Böttner et al., Appl. Phys. Lett. **102**, 251119 (2013)

Funding: Volkswagen Foundation (I/84072), U.S. Air Force Office of Scientific Research (MURI) Grant No. FA9550-09-1-0550, DFG research unit FOR 1713, China Scholarship Council, Alexander von Humboldt foundation

Rolled-up nanomembranes as compact 3D architectures for field effect transistors and fluidic sensing applications

D. Grimm, C.C. Bof Bufon, C. Deneke, P. Atkinson, D. J. Thurmer, F. Schäffel, S. Gorantla, A. Bachmatiuk, and O. G. Schmidt

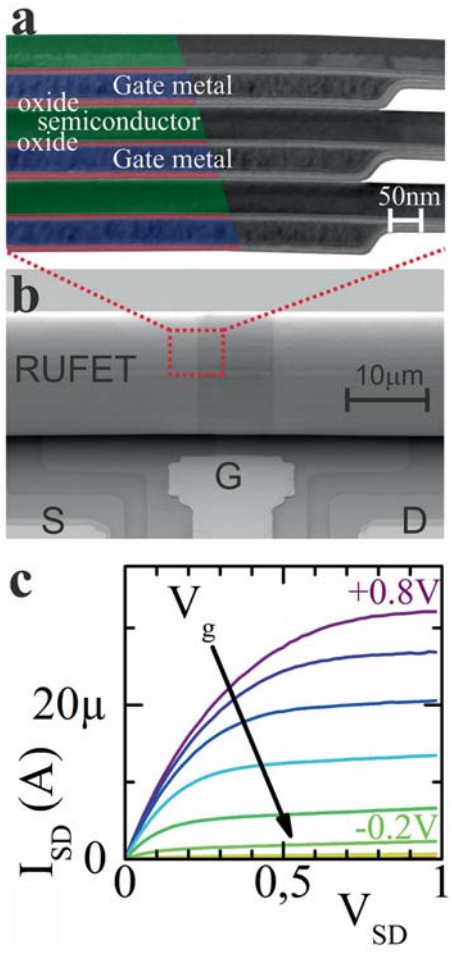

The fabrication of flexible electronic devices recently gained large attention due to attractive applications such as flexible displays, energy harvesters, sensors and artificial muscles. The devices must be able to adopt to highly uneven, rough surfaces and thus require non-standard processing, such as transfer or self-rolling techniques. We could show that active devices such as transistors are able to operate under severe bending conditions in the range of micrometers. The rolled-up metal-oxide-semiconducting field effect transistors (RUFET) are based on III-V semiconductors. Conventional planar MOSFETs incorporating high-k Al_2O_3 dielectrics are processed on top of a 50 nm thin semiconducting nanomembrane. Upon release, the nanomembrane rolls-up, see SEM Fig. (b). The fabricated double-gate like layer system can be clearly identified in the TEM Fig. (a). The obtained very good transfer characteristics with on-off ratios of 100,000 and subthreshold swings of around 160 mV/decade are shown in Fig. (c). The tube radius of the devices can be as small as 5 µm, setting a lower limit to the bending radius of flexible semiconductor transistors. The hollow core of the RUFET can be further explored for fluidic applications. The high capillary forces of the small core suck the testing liquid into the tube. The liquid can be detected millimeter away within seconds by a change of the on-current of the RUFET. The detection response is highly sensitive to the polarity of the introduced liquids. For further details see D. Grimm *et al.*, Nano Letters **13**, 213 (2013).

Fig.: (a) Cross-sectional TEM image of the rolled-up MOSFETs shown in the SEM image **(b)**. The single-crystalline semiconductor (green), amorphous oxide (red) and poly-crystalline Gate metal layers (blue) are color-coded as a guide for the eye. **(c)** Output characteristics of a RUFET with 30 μm channel length. The source-drain current is obtained as function of the applied SD voltage for gate voltages in steps of 0.2 V.

Cooperations: TU Chemnitz, University of Oxford, LNNano – Brazil, UPMC – France
Funding: SMWK, SAB, MURI by AFOSR Grant No. FA9550-09-1-0550.

Growth and characterization of symmetric GaAs quantum dots

Y. Huo, A. Rastelli, O. G. Schmidt

In order to serve as central units in entangled photon-pair sources, quantum dots (QDs) should provide a highly symmetric confinement potential, so that the excitonic fine structure splitting (FSS) is smaller than the intrinsic recombination linewidth of each exciton transition. To achieve this goal, different strategies have been proposed, including post-growth annealing, applying magnetic, electric and strain fields or a combination thereof. However, from a practical point of view it would be desirable to have better growth protocols to provide ensembles of QDs with sufficiently small FSS. Different from reported methods of growing QDs on high-index substrate, we have developed an optimized protocol to grow highly symmetric QDs on GaAs(001) substrates. The sample was grown by filling GaAs in $Al_{0.4}Ga_{0.6}As$ nanoholes etched in-situ using solid state molecular beam epitaxy (MBE). Atomic force microscopy (AFM) images show the nanoholes and hence the GaAs QDs have circular in-plane symmetry. Polarization-dependent micro-photoluminescence measurements reveal a FSS of (3.9 ± 1.8) μeV with random polarization angles. The corresponding linewidth of (23 ± 3) μeV under non-resonant excitation means very good optical quality. These numbers demonstrate that the newly developed QDs might serve as practical sources for entangled photon generation. For further details see Y.H. Huo, A. Rastelli, and O. G. Schmidt Appl. Phys. Lett. **102**, 152105, (2013)

Funding: BMBF project QuaHL-Rep (Contracts no. 01BQ1032 and 01BQ1034), European Union Seventh Framework Programme (FP7/2007-2013) under grant agreement no. 601126 (HANAS)

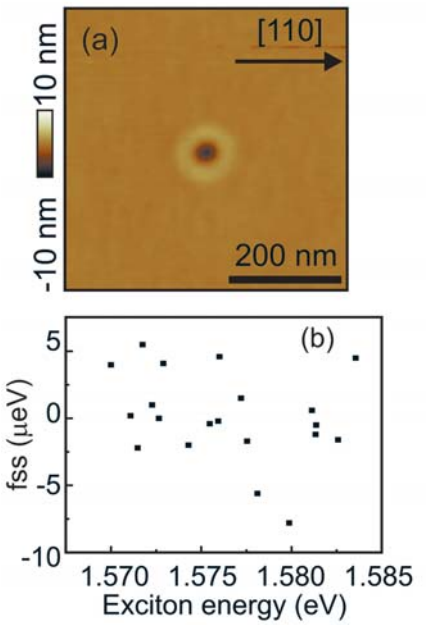

Fig.: (a) Representative topographic AFM image of the circularly symmetric nanoholes etched in $Al_{0.4}Ga_{0.6}As$. **(b)** FSS values of QDs formed by filling GaAs in the nanoholes.

Diamond Lattice Photonic Crystals from Rolled Up Membranes

M. R. Jorgensen, S. Giudicatti, O. G. Schmidt

Many emerging technologies rely on the ability to control light and emitters in novel and precise ways. Strategies allowing light slowing, trapping, and routing, as well as control of spontaneous emission are of fundamental importance for solar energy conversion, lasing, and quantum information processing. These effects can be related to the photonic density of states (DOS) through dispersion relations and Fermi's Golden Rule. Diverse methods to control DOS have been researched including photonic crystals (PCs) – materials with a dielectric periodicity on the order of interacting wavelengths of light – as well as optical cavities and plasmonics. Of these methods, PCs are advantageous because of their broad bandwidth of DOS inhibition, and since modifications are a bulk effect, they are not limited by small cavity volumes.

We proposed and theoretically investigated a novel strategy to fabricate functional PCs using rolled up nanotechnology. If a strained two-dimensional (2D) membrane is patterned using e-beam lithography and plasma or reactive ion etching, a 3D PC would result upon rolling as shown schematically in the figure (a). Due to the many materials – and their combinations – allowed by the rolling process, the control permitted by the deposition process, and the variety of 2D lattices available, a broad family of 3D PCs including <100> and <111> diamond lattices are accessible as shown in figures (b) and (c). For further details see Jorgensen, M. R.; Giudicatti, S.; Schmidt, O. G., *Diamond lattice photonic crystals from rolled up membranes.* Phys. Rev. A. 2013, 87 (4), 041803.

Funding: Alexander von Humboldt foundation

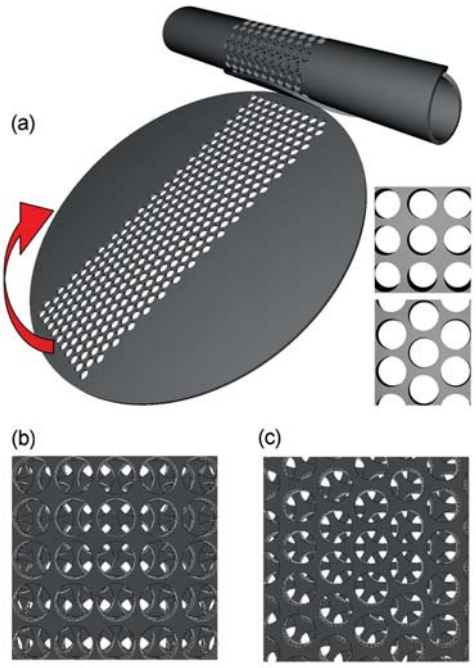

Fig.: (a) A pre-patterned, pre-strained membrane produces a 3D photonic crystal structure on rolling. Due to the flexibility afforded by the fabrication process, a wide variety of crystal structures are available including <100> and <111> diamond lattices shown as **(b)** and **(c)** respectively.

Magnetoresistive Emulsion Analyzer

G. Lin, L. Baraban, L. Han, D. Karnaushenko, D. Makarov, G. Cuniberti, O. G. Schmidt

A substantial part of nanomedicine focuses on drug design and employing magnetic nanomaterials in combination with multifunctional polymers, lipids or proteins. High-throughput drug discovery requires a tool which is able to analyze, manipulate, and sort objects, *e.g.* liposome capsules or emulsions containing known doses of magnetic nanoparticles associated with medications. A promising route relies on the implementation of magnetically-labeled biochemical species in combination with magnetoresistive sensors. In-flow detection based on giant magnetoresistive (GMR) or tunneling magnetoresistive (TMR) sensors has been demonstrated recently, representing first steps towards the integration of magnetic sensor elements into fluidic channels. However, up to date, progress is restrained to the mere sensing and counting of magnetic objects. Advanced and quantitative analysis, which is the main advantage of *e.g.* optical flow cytometry, has not been explored so far with magnetic sensors. Apart from detection and analysis, sorting of species is invaluable in diagnostic devices.
We report a magnetoresistive emulsion analyzer (Fig.) which is capable of detection, multiparametric analysis and sorting of ferrofluid-containing nanoliter-droplets [1]. The operation of the device in a cytometric mode provides high throughput and quantitative information about the dimensions and magnetic content of the emulsion. The method offers important complementarity to conventional optical approaches involving ferrofluids, and paves the way to the development of novel compact tools for diagnostics and nanomedicine including drug design and screening.

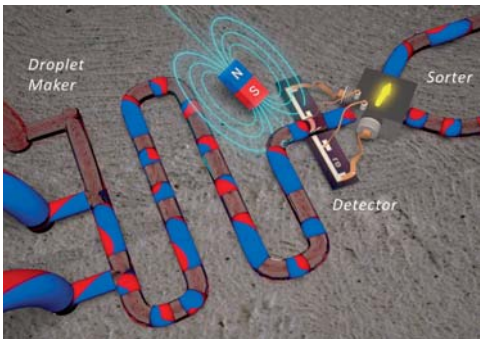

Fig.: Conceptual sketch of the GMR-based emulsion analyzer for multiparametric analysis and sorting.

[1] G. Lin et al., Scientific Reports **3**, 2548 (2013).

Cooperation: Max Bergmann Center of Biomaterials, TU Dresden, Germany
Funding: DFG Research Group For 1713; the European Union's Seventh Framework Programme (FP7/2007-2013)/ERC grant agreement n. 306277

Development of a New Hybrid Tubular Micromotor

V. Magdanz, S. Sanchez, and O. G. Schmidt

Hybrid micromotors comprised of a biological and an artificial part are promising devices for controlled transport, delivery and interaction in physiological environments at the microscale.
We present the approach of integrating motile cells in microdevices fabricated by roll-up technology for the development of micro-bio-robots that are promising for biomedical applications. A new hybrid micromotor comprised of a microtube and a motile cell, in this case a bull spermatozoon, was recently developed in our group.
These micromotors take advantage of the sperm flagellum as the driving force for a magnetic microtube. We illustrated how the motile cell is trapped inside a microtube that is slightly larger than the sperm head and how the cell propels the tube with its

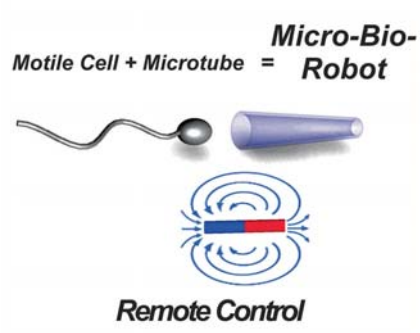

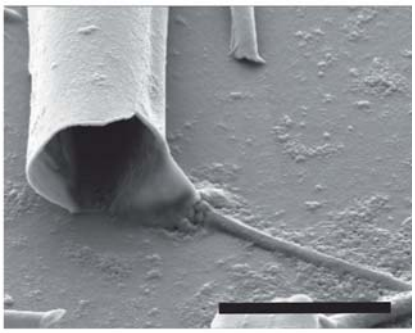

Fig.: Left: Schematic of bovine spermatozoon and metallic microtube that form a micro-bio-robot once the cell is captured. The micro-bio-robot can be remotely controlled by an external magnetic field. **Right:** Scanning Electron Microscopic Image of a bovine spermatozoon at the entrance of a Ti/Fe microtube with a diameter of about 5 µm. Scale bar 10 µm.

flagella motion. The microtube contains a rolled up iron layer for external magnetic control and for improved directionality of its motion. The effects of temperature and relative penetration of the cell inside the tube on the velocity of the micromotor are studied. This micro-bio-robot displays great promise for supported in-vitro and eventually in-vivo fertilization methods. For further details see V. Magdanz, S. Sanchez, O.G. Schmidt, Adv. Mater. 2013, DOI: 10.1002/adma.201302544.

Cooperation: MIRA - Institute for Biomedical Technology and Technical Medicine, University of Twente
Funding: Volkswagen Stiftung #86362.

Magnetic Microstructure of Rolled-Up Single-Layer Ferromagnetic Nanomembranes

R. Streubel, D. Makarov, J. Lee, S.-K. Kim, D. Karnaushenko, L. Han, M.-Y. Im, P. Fischer, R. Schäfer, O. G. Schmidt

Magnetic nanomembranes on stretchable polymer films or in rolled-up tubular architectures have recently enabled novel sensoric devices, spin-wave filters, and remotely controlled micro robotics. Their prospective applications rely on their peculiar magnetic properties, which are currently under thorough investigation both theoretically and experimentally. Due to difficulties to visualize magnetic domain patterns in these truly 3D structures, the magnetization configuration in cylindrical architectures is usually derived from integral measurements, such as magnetoresistance or magnetometry techniques.

In our work, we directly visualize magnetic domain patterns in rolled-up single layer magnetic nanomembranes by means of magnetooptical Kerr microscopy (Fig.). As this technique is surface sensitive and works in reflection, merely signals from the top part of the tube (but not from bottom or sides) are acquired. In this respect, superimposition and mixing in of signals originating from bottom layers are prevented. Our observations show the possibility to tailor the magnetization orientation from longitudinal for positive magnetostrictive materials over spiral-like to azimuthal for negative magnetostrictive materials [1]. All these patterns show a distinct impact on their magnetoelectronic response, which is relevant for sensoric applications.

[1] R. Streubel et al., Adv. Mater. 26, 316 (2014).

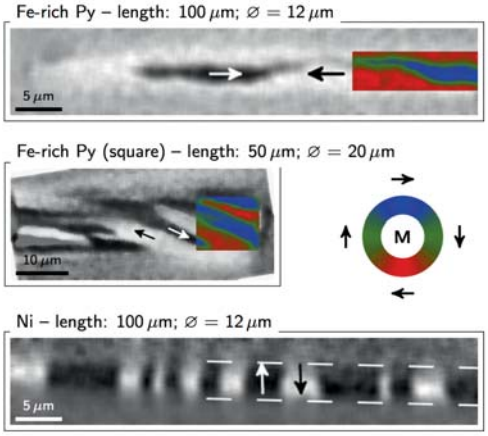

Fig.: Magnetic domain patterns in rolled-up nanomembranes visualized by Kerr microscopy. The magnetization is altered from longitudinal over spiral-like to azimuthal orientation depending on film geometry and magnetostriction constant of the material.

Cooperation: National Creative Research Initiative Center for Spin Dynamics and Spin-Wave Devices, Nanospinics Laboratory, Research Institute for Advanced Materials, Department of Materials Science and Engineering, Seoul National University, South Korea; Center for X-ray Optics, Lawrence Berkeley National Laboratory, CA, USA
Funding: German Science Foundation (DFG) grant MA 5144/2–1; DFG Research Unit 1713; and European Research Council under the European Union's Seventh Framework Programme (FP7/2007–2013)/ERC grant agreement no. 306277

The Institute by numbers

Personnel

End of 2013 the Leibniz Institute for Solid State and Material Research Dresden employed 517 staff members, including 123 doctorate students and additionally 22 apprentices. The quota of female staff was 36%. Furthermore, in 2013, the IFW hosted 69 fellowship holders, who came with their own money to work at the institute. 15 diploma students worked at the IFW and 34 trainees did a practical course at the institute in 2013. Overall, the total number of guest scientists was 145 and 69 fellowship holders.

78.5% of the staff belongs to the five scientific IFW institutes, 9% to the Research Technology Division, 6.5 to Administration, 3% to the Executive Board and Support Staff. The percentage of apprentices amounted to 3%.

Financing

Total budget	39,720 k€
Thereof	
Federal Government of Germany	14,664 k€
Free State of Saxony	14,664 k€
Third party funding (based on expenditure)	10,135 k€
Return on infrastructure, interest, royalties	256 k€
Third-party funding	
by the DFG (German research funding organisation)	3,745 k€
by the EC	3,025 k€
Federal Government	1,217 k€
by Free State of Saxony	541 k€
by industry	1,224 k€
by foundations/others	383 k€
Total	10,135 k€
Expenditure	
Remuneration costs	21,550 k€
Equipment, infrastructure and consumables	10,420 k€
Investment	7,750 k€
Total	**39,720 k€**

Third-party funding granted in 2013

> Third-party funding as a percentage of the total budget

The projects in the "third-party funding" area refer – as does the institutional funding – to the areas of research in the programme budget. Compared to the year 2012 it was possible to increase the funding in 2013 from 11,399 k€ to 12,936 k€. Accordingly, 30% of the IFW's total budget was financed by third-party funding. It is not part of the institute's overall strategy to increase this percentage.

> EU

The IFW was particularly successful in acquiring third-party funding from the EU. In the year 2013 it was possible to increase the acquisition of EU subsidies by 1,037,000 €. Accordingly the share of acquired EU funding rose in 2013 to 30% (3,890 k€) of the total of third-party funding acquired.

The IFW is co-ordinating 8 EU projects and participating in 9 other EU projects. As the EU's 7th framework programme is due to expire, there is a reduction in the number of advertised calls. Nevertheless, the IFW succeeded in further improving its position.
The IFW relates to the thematic structure of the calls in the EU's 7th framework programme, where a lot of calls were thematically oriented towards the "nanotechnology" area for example.
In fundraising for EU projects the emphasis in 2013 lay on the field of nanotechnology and material sciences.

> German Federal Government / Saxon States

A decrease (1.254 TEUR) was observed in the funding from the German Federal Government and the State of Saxony. This decrease was due to the new orientation of calls to the following areas:

- Health
- Life Sciences
- Security
- Environment

In these cases the IFW has had not the possibility to apply for calls.

> DFG

The IFW was also successful in projects sponsored by the DFG whose funding amounted to 37 % of the third-party funding. The IFW will be involved in basic research also in future. In total, DFG funded projects at the IFW in 2012 to the tune of approx. 4,804 k€ in 2013.
The internationality in the research done by the IFW was also reflected in the funding for hosting guest scientists. It was possible to some degree for guest scientists to receive grants from the DFG through the normal process by applying under the "Temporary Position as a Principal Investigator" funding scheme.

> Industry

In addition to funding by the EU and the DFG, the IFW focuses attention on acquiring third-party funding from "industry" to a level of 1,650 k€. In comparison to 2012 it was possible in 2013 to reverse the reduction in intake from industrial funding (due to the slump in the semiconductor industry). In this year, the IFW was able to attract strong partners from industry for co-operation.
Since its foundation in the year 1992, the IFW Dresden has worked very hard on building diverse and close industrial co-operations. In the meantime, numerous co-operations have been established with industry and the IFW has proven to be a high-performing and competent co-operation partner. Within the scope of our research program we work with reputable national and international companies, e.g. from the fields of the motor vehicle supply industry, materials etc.

> Regional

The IFW is also involved on a regional level. Accordingly, 2013 saw a lot of project work done in co-operation with local small and medium-sized enterprises from the fields of Lion-Batteries (energy), research technology, automotive engineering etc.

In 2013 our expertise built up over many years in the areas of carbon nanostructures and materials characterisation was very much in demand by our partners.
From 2012 on, industry was particularly interested in

- the characterisation of micro and nanostructures,
- functional composite materials and
- metallic glass and composites.

BREAKDOWN OF FUNDING BY FUNDING ORGANIZATION*	[k€]
German Federal Government	1,254
State of Saxony	645
DFG	4,804
EU	3,89
Industry	1,650
Others	693
Total	**12,936**

DISTRIBUTION OF FUNDING BY AREAS OF RESEARCH*	[k€]
Superconuctivity & superconductors	2,530
Magnetism & magnetic materials	3,317
Molecular nanostructures & solids	706
Metastable alloys	3,232
Layer & film materials	2,456
Others	695
Total	**12,936**

* Numbers refer to approved projects

DISTRIBUTION OF IFW'S PATENTS AND LICENSES BY COUNTRIES

	Number	Licensed
Europe	**217**	**53**
European Patents	24	3
Germany	139	22
Austria	8	4
Switzerland/ Lichtenstein	10	2
France	9	6
Italy	7	3
Spain	2	2
Belgium	1	0
Netherlands	2	2
Denmark	1	1
Norway	0	0
Sweden	1	1
Great Britain	13	7
North America	**20**	**4**
Canada	0	0
USA	20	4
Asia	**36**	**17**
Japan	15	7
China	11	6
Korea	10	4
PCT-Phase	**7**	**0**
Total	**280**	**74**

Patents

By 31 December 2013, the institute could boast of a total of 139 patents applications filed in Germany and 273 filed abroad. A total of 22 patents were granted in Germany for inventions by the IFW.

DISTRIBUTION OF IFW'S PATENTS BY RESEARCH AREAS

Research area	Number of patents	Share
1. Superconductivity & superconductors	87,5	31,2%
2. Magnetism and magnetic materials	33,0	11,8%
3. Molecular nanostructures and molecular solids	31,9	11,4%
4. Metastable alloys	62,9	22,5%
5. Stress-driven architectures and phenomena	64,7	23,1%
Total	**280,0**	**100%**

Vocational training

In 2013, the IFW trained a total of 28 apprentices in the following professions: physics lab technician, chemical lab technician, electronics technician, technical product designer, management assistant in office communication, specialist for media and information services field: library etc. and additional 2 students of universities of co-operative education in the disciplines of mechanical engineering and electrical engineering. Despite the current competition for good graduates, which is especially noticeable in places of academic excellence like Dresden, the training rate of 3% was maintained. In accordance with the strategy of vocational training of the Leibniz Association, this rate shall be increased up to 5% in the medium term. Since 2012, the Administrative Director of the IFW, Hon.-Prof. Dr. h. c. Rolf Pfrengle is the steering committee's representative for dual vocational education and training of the Leibniz Association and pursues the implementation of the Leibniz strategy of vocational training.

Publications 2013

Monographs and Editorships

B. Schmidt, K. Wetzig, *Ion beams in materials processing and analysis*, Springer-Verl., 2013, 418 S.
J. Thomas, T. Gemming, *Analytische Transmissionselektronenmikroskopie: Eine Einfuehrung fuer den Praktiker*, Springer-Verl., 2013, 363 S.
D. Makarov, C. Ortix, L. Baraban, *Guest Editorial - Functional magnetic nanomembranes*, SPIN 3 (2013) Nr. 3, S. 1302001/1-4.
J.H. Warner, F. Schaeffel, A. Bachmatiuk, M.H. Ruemmeli, (eds.), *Graphene: Fundamentals and emergent applications*, Elsevier, 2013, 450 S.

Journal Papers

1) M. Abdel-Hafiez, V. Grinenko, S. Aswartham, I. Morozov, M. Roslov, Vakaliuk O., S. Johnson, D.V. Efremov, J. van den Brink, H. Rosner, M. Kumar, C. Hess, S. Wurmehl, A.U.B. Wolter, B. Buechner, E.L. Green, J. Wosnitza, P. Vogt, A. Reifenberger, C. Enss, M. Hempel, R. Klingeler, S.-L. Drechsler, *Evidence of d-wave superconductivity in K1-xNaxFe2As2 (x=0,0.1) single crystals from low-temperature specific-heat measurements*, Physical Review B 87 (2013) Nr. 18, S. 180507(R)/1-4.
2) M.A. Abdulmalic, A. Aliabadi, A. Petr, V. Kataev, T. Rueffer, *The formation of overlooked compounds in the reaction of methyl amine with the diethyl ester of o-phenylenebis(oxamic acid) in MeOH*, Dalton Transactions 42 (2013) Nr. 5, S. 1798-1809.
3) A.J. Achkar, F. He, R. Sutarto, J. Geck, H. Zhang, Y.-J. Kim, D.G. Hawthorn, *Resonant X-ray scattering measurements of a spatial modulation of the Cu 3d and O 2p energies in stripe-ordered cuprate superconductors*, Physical Review Letters 110 (2013) Nr. 1, S. 17001/1-5.
4) R. Adam, D. Wadewitz, W. Gruner, V. Klemm, H. Ehrenberg, D. Rafaja, *Phase and microstructure development in the conversion type electrodes for Li-Ion batteries based on the Cu-Fe-O system*, Journal of The Electrochemical Society 160 (2013) Nr. 9, S. A1594-A1603.
5) F. Ali, S. Scudino, S.M. Gorantla, V.C. Srivastava, H.R. Shahid, V. Uhlenwinkel, M. Stoica, G. Vaughan, N.K. Mukhopadhyay, J. Eckert, *Mechanically driven phase transformation in single phase Al62.5Cu25Fe12.5 quasi-crystals: Effect of milling intensity*, Acta Materialia 61 (2013), S. 3819-3830.
6) M.P. Allan, A. Tamai, E. Rozbicki, M.H. Fischer, J. Voss, P.D.C. King, W. Meevasana, S. Thirupathaiah, E. Rienks, J. Fink, D.A. Tennant, R.S. Perry, J.F. Mercure, M.A. Wang, J. Lee, C.J. Fennie, E.-A. Kim, M.J. Lawler, K.M. Shen, A.P. Mackenzie, Z.-X. Shen, F. Baumberger, *Formation of heavy d-electron quasiparticles in Sr3Ru2O7*, New Journal of Physics 15 (2013), S. 63029/1-10.
7) N. Ares, V.N. Golovach, G. Katsaros, M. Stoffel, F. Fournel, L.I. Glazman, O.G. Schmidt, S. De Franceschi, *Nature of tunable hole g factors in quantum dots*, Physical Review Letters 110 (2013), S. 46602/1-5.
8) N. Ares, G. Katsaros, V.N. Golovach, J.J. Zhang, A. Prager, L.I. Glazman, O.G. Schmidt, S. De Franceschi, *SiGe quantum dots for fast hole spin Rabi oscillations*, Applied Physics Letters 103 (2013) Nr. 26, S. 263113/1-3.
9) V.B. Arion, S. Platzer, P. Rapta, P. Machata, M. Breza, D. Vegh, L. Dunsch, J. Telser, S. Shova, T.C.O. Mac Leod, A.J.L. Pombeiro, *Marked stabilization of redox states and enhanced catalytic activity in galactose oxidase models based on transition metal S- methylisothiosemicarbazonates with -SR group in ortho position to the phenolic oxygen*, Inorganic Chemistry 52 (2013) Nr. 13, S. 7524-7540.
10) S.M. Avdoshenko, P. Koskinen, H. Sevincli, A.A. Popov, C.G. Rocha, *Topological signatures in the electronic structure of Graphene spirals*, Scientific Reports 3 (2013), S. 1632/1-6.
11) I. Avigo, R. Cortes, L. Rettig, S. Thirupathaiah, H.S. Jeevan, P. Gegenwart, T. Wolf, M. Ligges, M. Wolf, J. Fink, U. Bovensiepen, *Coherent excitations and electron- phonon coupling in Ba/EuFe2As2 compounds investigated by femtosecond time- and angle-resolved photoemission spectroscopy*, Journal of Physics - Condensed Matter 25 (2013) Nr. 9, S. 94003/1-9.
12) A. Bachmatiuk, R.G. Mendes, C. Hirsch, J. Jaehne, M.R. Lohe, J. Grothe, S. Kaskel, L. Fu, R. Klingeler, J. Eckert, P. Wick, M.H. Ruemmeli, *Few-layer graphene shells and nonmagnetic encapsulates: A versatile and nontoxic carbon nanomaterial*, ACS nano 7 (2013) Nr. 12, S. 10552-10562.
13) S.-H. Baek, L. Harnagea, S. Wurmehl, B. Buechner, H.-J. Grafe, *Anomalous superconducting state in LiFeAs implied by the 75As Knight shift measurement*, Journal of Physics - Condensed Matter 25 (2013) Nr. 16, S. 162204/1-5.
14) N. Balchev, K. Nenkov, V. Antonov, *Vortex pinning energies and H(T) characteristic lines in the MoSr2YCu2O8-delta superconductor*, Journal of Superconductivity and Novel Magnetism 26 (2013) Nr. 1, S. 59-63.
15) L. Baraban, S.M. Harazim, S. Sanchez, O.G. Schmidt, *Chemotactic behavior of catalytic motors in microfluidic channels*, Angewandte Chemie - International Edition 52 (2013) Nr. 21, S. 5552-5556.
16) L. Baraban, D. Makarov, O.G. Schmidt, G. Cuniberti, P. Leiderer, A. Erbe, *Control over janus micromotors by the strength of a magnetic field*, Nanoscale 5 (2013) Nr. 4, S. 1332-1336.
17) L. Baraban, R. Streubel, D. Makarov, L. Han, D. Karnaushenko, O.G. Schmidt, G. Cuniberti, *Fuel-free locomotion of janus motors: Magnetically induced thermophoresis*, ACS nano 7 (2013) Nr. 2, S. 1360-1367.
18) A. Barreiro, F. Boerrnert, S.M. Avdoshenko, B. Rellinghaus, G. Cuniberti, M.H. Ruemmeli, L.M.K. Vandersypen, *Understanding the catalyst-free transformation of amorphous carbon into graphene by current-induced annealing*, Scientific Reports 3:1115 (2013), S. 1-6.

19) J.R. Bautista-Quijano, F. Aviles, J.V. Cauich-Rodrigueza, R. Schoenfelder, A. Bachmatiuk, T. Gemming, M.H. Ruemmeli, *Tensile piezoresistivity and disruption of percolation in singlewall and multiwall carbon nanotube/ polyurethane composites*, Synthetic Metals 185-186 (2013), S. 96-102.
20) M. Beekman, S. Disch, S. Rouvimov, D. Kasinathan, K. Koepernik, H. Rosner, P. Zschack, W.S. Neumann, D.C. Johnson, *Controlling size-induced phase transformations using chemically designed nanolaminates*, Angewandte Chemie - International Edition 52 (2013) Nr. 50, S. 13211-13214.
21) A. Behler, N. Teichert, B. Dutta, A. Waske, T. Hickel, A. Auge, A. Huetten, J. Eckert, *Thickness dependent exchange bias in martensitic epitaxial Ni-Mn-Sn thin films*, AIP Advances 3 (2013) Nr. 12, S. 122112/1-9.
22) E. Benckiser, L. Fels, G. Ghiringhelli, M. Moretti Sala, T. Schmitt, J. Schlappa, V.N. Strocov, N. Mufti, G.R. Blake, A.A. Nugroho, T.T.M. Palstra, M.W. Haverkort, K. Wohlfeld, M. Grueninger, *Orbital superexchange and crystal field simultaneously at play in YVO 3: Resonant inelastic x-ray scattering at the V L edge and the O K edge*, Physical Review B 88 (2013) Nr. 20, S. 205115/1-13.
23) G. Bepete, Z.N. Tetana, S. Lindner, M.H. Ruemmeli, Z. Chiguvare, N.J. Coville, *The use of aliphatic alcohol chain length to control the nitrogen type and content in nitrogen doped carbon nanotubes*, Carbon 52 (2013), S. 316-325.
24) A. Bhaskar, W. Gruner, D. Mikhailova, H. Ehrenberg, *Thermal stability of Li1- delta M0.5Mn1.5O4 (M = Fe, Co, Ni) cathodes in different states of delithiation delta*, RSC Advances 3 (2013) Nr. 17, S. 5909-5916.
25) M. Boenisch, M. Calin, T. Waitz, A. Panigrahi, M. Zehetbauer, A. Gebert, W. Skrotzki, J. Eckert, *Thermal stability and phase transformations of martensitic Ti-Nb alloys*, Science and Technology of Advanced Materials 14 (2013), S. 55004/1-9.
26) F. Boerrnert, A. Bachmatiuk, S. Gorantla, D. Wolf, A. Lubk, B. Buechner, M.H. Ruemmeli, *Retro-fitting an older (S)TEM with two Cs aberration correctors for 80 kV and 60 kV operation*, Journal of Microscopy 249 (2013) Nr. 2, S. 87-92.
27) S. Boettner, S. Li, M.R. Jorgensen, O.G. Schmidt, *Vertically aligned rolled-up SiO2 optical microcavities in add-drop configuration*, Applied Physics Letters 102 (2013) Nr. 25, S. 251119/1-4.
28) N.A. Bogdanov, R. Maurice, I. Rousochatzakis, J. van den Brink, L. Hozoi, *Magnetic state of pyrochlore Cd2Os2O7 emerging from strong competition of ligand distortions and longer-range crystalline anisotropy*, Physical Review Letters 110 (2013) Nr. 12, S. 127206/1-5.
29) D. Bombor, C.G.F. Blum, O. Volkonskiy, S. Rodan, S. Wurmehl, C. Hess, B. Buechner, *Half-metallic ferromagnetism with unexpectedly small spin splitting in the Heusler compound Co2FeSi*, Physical Review Letters 110 (2013) Nr. 6, S. 66601/1-5.
30) C. Bonatto Minella, I. Lindemann, P. Nolis, A. Kiessling, M. Dolors Barod, M. Klose, L. Giebeler, B. Rellinghaus, J. Eckert, L. Schultz, O. Gutfleisch, *NaAlH4 confined in ordered mesoporous carbon*, International Journal of Hydrogen Energy 38 (2013), S. 8829-8837.
31) E. Bonera, M. Bollani, D. Chrastina, F. Pezzoli, A. Picco, O.G. Schmidt, D. Terziotti, *Substrate strain manipulation by nanostructure perimeter forces*, Journal of Applied Physics 113 (2013) Nr. 16, S. 164308/1-5.
32) S. Borisenko, *Fewer atoms, more information*, nature materials 12 (2013), S. 600-601.
33) M. Brasse, L. Chioncel, J. Kunes, A. Bauer, A. Regnat, C.G.F. Blum, S. Wurmehl, C. Pfleiderer, M.A. Wilde, D. Grundler, *de Haas-van Alphen effect and Fermi surface properties of single-crystal CrB2*, Physical Review B 88 (2013) Nr. 15, S. 155138/1-7.
34) N. Brun, K. Sakaushi, L. Yu, L. Giebeler, J. Eckert, M.M. Titirici, *Hydrothermal carbon-based nanostructured hollow spheres as electrode materials for high-power lithium-sulfur batteries*, Physical Chemistry Chemical Physics 15 (2013), S. 6080-6087.
35) M. Calin, A. Gebert, A.C. Ghinea, P.F. Gostin, S. Abdi, C. Mickel, J. Eckert, *Designing biocompatible Ti-based metallic glasses for implant applications*, Materials Science and Engineering C 33 (2013) Nr. 2, S. 875-883.
36) L. Cano-Cortes, C. Ortix, J. van den Brink, *Fundamental differences between quantum spin Hall Edge states at zigzag and Armchair terminations of honeycomb and ruby nets*, Physical Review Letters 111 (2013) Nr. 14, S. 146801/1-5.
37) C. Cao, C.G.F. Blum, T. Ritschel, S. Rodan, L. Giebeler, D. Bombor, S. Wurmehl, W. Loeser, *Peculiarities of anisotropic electrical resistivity in Lu2PdSi3 single crystals*, CrystEngComm 15 (2013), S. 9052-9056.
38) K.P. Castro, Y. Jin, J.J. Rack, S.H. Strauss, O.V. Boltalina, A.A. Popov, *Perfluoroalkyl [70]- fullerenes as robust highly-luminescent fluorocarbons, or position of one CF3 group matters*, Journal of Physical Chemistry Letters 4 (2013), S. 2500-2507.
39) S. Chatterjee, J. Trinckauf, T. Haenke, D.E. Shai, J.W. Harter, T.J. Williams, G.M. Luke, K.M. Shen, J. Geck, *Formation of the coherent heavy fermion liquid at the hidden order transition in URu2Si2*, Physical Review Letters 110 (2013) Nr. 18, S. 186401/1-5.
40) A.K. Chaubey, S. Scudino, M. Samadi Khoshkhoo, K.G. Prashanth, N.K. Mukhopadhyay, B.K. Mishra, J. Eckert, *Synthesis and characterization of nanocrystallineMg-7.4%Al powders produced by mechanical alloying*, Metals 3 (2013) Nr. 1, S. 58-68.
41) P. Chen, N.A. Katcho, J.P. Feser, W. Li, M. Glaser, O.G. Schmidt, D.G. Cahill, N. Mingo, A. Rastelli, *Role of surface-segregation-driven intermixing on the thermal transport through planar Si/Ge superlattices*, Physical Review Letters 111 (2013) Nr. 11, S. 115901/1-6.
42) Y. Chen, C. Yan, O.G. Schmidt, *Strain-driven formation of multilayer graphene/GeO2 tubular nanostructures as high-capacity and very long-life anodes for Lithium-ion batteries*, Advanced Energy Materials 3 (2013), S. 1269-1274.
43) Y.Z. Chen, N. Bovet, F. Trier, D.V. Christensen, F.M. Qu, N.H. Andersen, T. Kasama, W. Zhang, R. Giraud, J. Dufouleur, T.S. Jespersen, J.R. Sun, A. Smith, J. Nygard, L. Lu, B. Buechner, B.G. Shen, S. Linderoth, N. Pryds, *A high-mobility two-dimensional electron gas at the spinel/ perovskite interface of Y- Al2O3/SrTiO3*, nature communications 4 (2013), S. 1371/1-6.
44) A.E. Chivu, S. Ciuca, D. Bojin, G.E. Stan, A. Gebert, J. Eckert, *Electrochemical deposited hydroxyapatite on pre-treated Cp-Ti surfaces*, Metalurgia International 18 (2013) Nr. Special Issue, 1, S. 34.
45) G. Cirillo, T. Caruso, S. Hampel, D. Haase, F. Puoci, M. Ritschel, A. Leonhardt, M. Curcio, F. Iemma, V. Khavrus, M. Grobosch, N. Picci, *Novel carbon nanotube composites by grafting reaction with water-compatible redox initiator system*, Colloid and Polymer Science 291 (2013) Nr. 3, S. 699-708.

46) G. Cirillo, O. Vittorio, S. Hampel, F. Iemma, P. Parchi, M. Cecchini, F. Puocia, N. Picci, *Quercetin nanocomposite as novel anticancer therapeutic: Improved efficiency and reduced toxicity*, European Journal of Pharmaceutical Sciences 49 (2013), S. 359-365.

47) G. Cirillo, O. Vittorio, S. Hampel, U.G. Spizzirri, N. Picci, F. Iemma, *Incorporation of carbon nanotubes into a gelatin–catechin conjugate: Innovative approach for the preparation of anticancer materials*, International Journal of Pharmaceutics 446 (2013) Nr. 1-2, S. 176-182.

48) T.T. Clikeman, S.H.M. Deng, S. Avdoshenko, X.-B. Wang, A.A. Popov, S.H. Strauss, O.V. Boltalina, *Fullerene "Superhalogen" radicals: The substituent effect on electronic properties of 1,7,11,24,27-C60X5*, Chemistry - A European Journal 19 (2013) Nr. 45, S. 15404-15409.

49) T.T. Clikeman, I.V. Kuvychko, N.B. Shustova, Y.-S. Chen, A.A. Popov, O.V. Boltalina, S.H. Strauss, *Regioselective sequential additions of nucleophiles and electrophiles to perfluoroalkylfullerenes: Which cage C atoms are the most reactive and why?*, Chemistry - A European Journal 19 (2013) Nr. 16, S. 5070-5080.

50) J.W. Cui, M. Calin, J. Eckert, Z.F. Zhang, *Tensile fracture dynamics and intrinsic plasticity of metallic glasses*, Applied Physics Letters 102 (2013) Nr. 3, S. 31908/1-4.

51) J. Cwik, N. Kolchugina, K. Nenkov, *Effect of partial Ho-substitution on the magnetic and magnetocaloric properties of polycrystalline DyCo2-based solid solutions*, Journal of Alloys and Compounds 560 (2013), S. 72-79.

52) J. Cwik, K. Nenkov, T. Palewski, *Effect of Sc on magnetic properties and heat capacity of R1-xScxNi2 (R = Gd, Tb, Dy, Ho) solid solutions: Comparative analysis*, Intermetallics 32 (2013), S. 109-118.

53) M. Daghofer, M. Haque, *Viewpoint: Toward fractional quantum hall physics with cold atoms*, Physics 6 (2013), S. 49/1-3.

54) A.N. Darinskii, M. Weihnacht, H. Schmidt, *Resonant reflection of a surface acoustic wave from strip waveguides*, Wave Motion 50 (2013), S. 1185-1196.

55) A.N. Darinskii, M. Weihnacht, H. Schmidt, *Mutual conversion of bulk and surface acoustic waves in gratings of finite length on half-infinite substrates. II. FE analysis of bulk wave generation*, Ultrasonics 53 (2013), S. 1004-1011.

56) A.N. Darinskii, M. Weihnacht, H. Schmidt, *Mutual conversion of bulk and surface acoustic waves in gratings of finite length on half-infinite substrates. I. FE analysis of surface wave generation*, Ultrasonics 53 (2013), S. 998-1003.

57) A.N. Darinskii, M. Weihnacht, H. Schmidt, *Anisotropy effects in the reflection of surface acoustic waves from obstacles*, IEEE Transaction on Ultrasonics, Ferroelectrics, and Frequency Control 60 (2013) Nr. 1, S. 235-242.

58) F. de Clippel, A.L. Khan, A. Cano-Odena, M. Dusselier, K. Vanherck, L. Peng, S. Oswald, L. Giebeler, S. Corthals, B. Kenens, J.F.M. Denayer, P.A. Jacobs, I.F.J. Vankelecom, B.F. Sels, *CO2 reverse selective mixed matrix membranes for H2 purification by incorporation of carbon-silica fillers*, Journal of Materials Chemistry A 1 (2013), S. 945-953.

59) Y. Demidenko, D. Makarov, O.G. Schmidt, V. Lozovski, *Magneto-optical Kerr effect in corrugated magnetoplasmonic heterostructures*, Journal of the Optical Society of America B 30 (2013) Nr. 8, S. 2053-2058.

60) N.M. Dempsey, T.G. Woodcock, H. Sepehri-Amin, Y. Zhang, H. Kennedy, D. Givord, K. Hono, O. Gutfleisch, *High-coercivity Nd-Fe-B thick films without heavy rare earth additions*, Acta Materialia 61 (2013), S. 4920-4927.

61) J. Deng, H. Ji, C. Yan, J. Zhang, W. Si, S. Baunack, S. Oswald, Y. Mei, O.G. Schmidt, *Naturally rolled-up C/Si/C trilayer nano-membranes as stable anodes for lithium-ion batteries with remarkable cycling performance*, Angewandte Chemie/ International Edition 52 (2013) Nr. 8, S. 2326-2330.

62) J. Deng, C. Yan, L. Yang, S. Baunack, S. Oswald, H. Wendrock, Y. Mei, O.G. Schmidt, *Sandwich-stacked SnO2/Cu hybrid nanosheets as multichannel anodes for Lithium Ion batteries*, ACS nano 7 (2013) Nr. 8, S. 6948-6954.

63) A. Diestel, V. Neu, A. Backen, L. Schultz, S. Faehler, *Magnetic domain pattern in hierarchically twinned epitaxial Ni-Mn-Ga films*, Journal of Physics - Condensed Matter 25 (2013), S. 266002/1-11.

64) N. Du, Y. Shuai, W. Luo, C. Mayr, R. Schueffny, O.G. Schmidt, H. Schmidt, *Practical guide for validated memristance measurements*, Review of Scientific Instruments 84 (2013) Nr. 2, S. 23903/1-7.

65) J. Dufouleur, L. Veyrat, A. Teichgraeber, S. Neuhaus, C. Nowka, S. Hampel, J. Cayssol, J. Schumann, B. Eichler, O.G. Schmidt, B. Buechner, R. Giraud, *Quasiballistic transport of dirac fermions in a Bi2Se3 nanowire*, Physical Review Letters 110 (2013) Nr. 18, S. 186806/1-5.

66) D.V. Efremov, A.A. Golubov, O.V. Dolgov, *Manifestations of impurity-induced s±) s ++ transition: multiband model for dynamical response functions*, New Journal of Physics 15 (2013), S. 13002/1-15.

67) B. Elliott, A.D. Pykhova, J. Rivera, C.M. Cardona, L. Dunsch, A.A. Popov, L. Echegoyen, *Spin density and cluster dynamics in Sc3N@C80 - upon [5,6] exohedral functionalization: An ESR and DFT study*, Journal of Physical Chemistry C 117 (2013), S. 2344-2348.

68) J. Ellison, K. Tschulik, E.J.E. Stuart, K. Jurkschat, D. Omanovic, M. Uhlemann, A. Crossley, R.G. Compton, *Get more out of your data: A new approach to agglomeration and aggregation studies using nanoparticle impact experiments*, Chemistry open online first (2013), S. 1-8.

69) J. Engelmann, V. Grinenko, P. Chekhonin, W. Skrotzki, D.V. Efremov, S. Oswald, K. Iida, R. Huehne, J. Haenisch, M. Hoffmann, F. Kurth, L. Schultz, B. Holzapfel, *Strain induced superconductivity in the parent compound BaFe2As2*, nature communications 4 (2013), S. 2877/1-6.

70) J. Engelmann, K. Iida, F. Kurth, C. Behler, S. Oswald, R. Huehne, B. Holzapfel, L. Schultz, S. Haindl, *Fe/Ba(Fe1-xCox)2As2 multilayers and quasi-multilayers with Tc = 29 K*, Physica C 494 (2013), S. 185-188.

71) D.V. Evtushinsky, V.B. Zabolotnyy, L. Harnagea, A.N. Yaresko, S. Thirupathaiah, A.A. Kordyuk, J. Maletz, S. Aswartham, S. Wurmehl, E. Rienks, R. Follath, B. Buechner, S.V. Borisenko, *Electronic band structure and momentum dependence of the superconducting gap in Ca1-xNaxFe2As2 from angle-resolved photoemission spectroscopy*, Physical Review B 87 (2013) Nr. 9, S. 94501/1-6.

72) F.S. Fedorov, J. Linnemann, K. Tschulik, L. Giebeler, M. Uhlemann, A. Gebert, *Capacitance performance of cobalt hydroxide-based capacitors with utilization of near-neutral electrolytes*, Electrochimica Acta 90 (2013), S. 166-170.

73) F.S. Fedorov, I. Moench, C. Mickel, K. Tschulik, B. Zhao, M. Uhlemann, A. Gebert, J. Eckert, *Electrochemical deposition of Co(Cu)/Cu multilayered nanowires*, Journal of the Electrochemical Society 160 (2013), S. D13-D19.

74) E. Fidiani, P.M.F.J. Costa, A.U.B. Wolter, D. Maier, B. Buechner, S. Hampel, *Magnetically active and coated Gadolinium-filled carbon nanotubes*, The Journal of Physical Chemistry C 117 (2013), S. 16725-16733.

75) J. Fink, E. Schierle, E. Weschke, J. Geck, *Resonant elastic soft x-ray scattering*, Reports on Progress in Physics 76 (2013) Nr. 5, S. 56502/1-59.

76) V.M. Fomin, E.J. Smith, D.D. Karnaushenko, D. Makarov, O.G. Schmidt, *Asymmetric drag in oscillatory motion: Ratchet effect without an asymmetric potential*, Physical Review E 87 (2013) Nr. 5, S. 52122/1-5.

77) J. Fornell, E. Pellicer, N. Van Steenberge, S. Gonzalez, A. Gebert, S. Surinach, M.D. Baro, J. Sort, *Improved plasticity and corrosion behavior in Ti-Zr-Cu-Pd metallic glass with minor addition of Nb: An alloy composition intended for biomedical applications*, Materials Science and Engineering A 559 (2013), S. 159-164.

78) F. Forte, J. van den Brink, M. Cuoco, *Evolution of spinon Fermi surface and magnetic response of hyperkagome spin liquids*, Physical Review B 88 (2013) Nr. 14, S. 144422/1-5.

79) R. Friedrich, S. Lindner, T. Hahn, C. Loose, S. Liebing, M. Knupfer, J. Kortus, *Systematic theoretical investigation of the phthalocyanine based dimer: MnPcd+/F16CoPc-delta-*, Physical Review B 87 (2013) Nr. 11, S. 115423/1-10.

80) D.-W. Fu, H.-L. Cai, Y. Liu, Q. Ye, W. Zhang, Y. Zhang, X.-Y. Chen, G. Giovannetti, M. Capone, J. Li, R.-G. Xiong, *Diisopropylammonium bromide is a high-temperature molecular ferroelectric crystal*, Science 339 (2013) Nr. 6118, S. 425-428.

81) G. Fuchs, W. Haessler, K. Nenkov, J. Scheiter, O. Perner, A. Handstein, T. Kanai, L. Schultz, B. Holzapfel, *High trapped fields in bulk MgB2 prepared by hot-pressing of ball-milled precursor powder*, Superconductor Science and Technology 26 (2013) Nr. 12, S. 122002/1-5.

82) U. Gaitzsch, J. Haenisch, R. Huehne, C. Rodig, J. Freudenberger, B. Holzapfel, L. Schultz, *Highly alloyed Ni-W substrates for low AC loss applications*, Superconductor Science and Technology 26 (2013) Nr. 8, S. 85024/1-6.

83) R. Ganesh, S. Nishimoto, J. van den Brink, *Plaquette resonating valence bond state in a frustrated honeycomb antiferromagnet*, Physical Review B 87 (2013) Nr. 5, S. 54413/1-8.

84) R. Ganesh, J. van den Brink, S. Nishimoto, *Deconfined criticality in the frustrated Heisenberg honeycomb antiferromagnet*, Physical Review Letters 110 (2013) Nr. 12, S. 127203/1-5.

85) P. Gargarella, S. Pauly, K.K. Song, J. Hu, N.S. Barekar, M. Samadi Khoshkhoo, A. Teresiak, H. Wendrock, U. Kuehn, C. Ruffing, E. Kerscher, J. Eckert, *Ti-Cu-Ni shape memory bulk metallic glass composites*, Acta Materialia 61 (2013) Nr. 1, S. 151-162.

86) M. Gellesch, M. Dimitrakopoulou, M. Scholz, C.G.F. Blum, M. Schulze, J. van den Brink, S. Hampel, S. Wurmehl, B. Buechner, *Facile nanotube-assisted synthesis of ternary intermetallic nanocrystals of the ferromagnetic Heusler phase Co2FeGa*, Crystal Growth and Design 13 (2013), S. 2707-2710.

87) P. Gentile, M. Cuoco, C. Ortix, *Curvature-induced Rashba spin-orbit interaction in strain-driven nanostructures*, SPIN 3 (2013), S. 1340002/1-6.

88) C. Georgi, A. Hildebrandt, A. Tuchscherer, S. Oswald, H. Lang, *Hexacarbonyl (Trimethylsilyl Ethyne) dicobalt as MOCVD precursor for thin cobalt layer formation*, Zeitschrift für anorganische und allgemeine Chemie 639 (2013) Nr. 14, S. 2532-2535.

89) M. Goettlicher, M. Rohnke, A. Helth, T. Leichtweiss, T. Gemming, A. Gebert, J. Eckert, J. Janek, *Controlled surface modification of Ti-40Nb implant alloy by electrochemically assisted inductively coupled RF plasma oxidation*, Acta Biomaterialia 9 (2013), S. 9201-9210.

90) M. Gogebakan, C. Kursun, J. Eckert, *Formation of new Cu-based nanocrystalline powders by mechanical alloying technique*, Powder Technology 247 (2013), S. 172-177.

91) M. Golecki, J. Lach, A. Jeremies, F. Lungwitz, M. Fronk, G. Salvan, D.R.T. Zahn, J. Park, Y. Krupskaya, V. Kataev, R. Klingeler, B. Buechner, B. Mahns, M. Knupfer, P.F. Siles, D. Grimm, O.G. Schmidt, A. Reis, W.R. Thiel, D. Breite, B. Abel, B. Kersting, *Chemisorption of exchange-coupled (Ni2L(dppba)) complexes on gold by using ambidentate 4- (Diphenylphosphino)benzoate Co-Ligands*, Chemistry - A European Journal 19 (2013), S. 7787-7801.

92) H. Gong, P. Chen, Y. Ma, L. Wang, A. Rastelli, O.G. Schmidt, Z. Zhong, *Formation and characterization of multilayer GeSi nanowires on miscut Si (001) substrates*, Journal of Nanoscience and Nanotechnology 13 (2013), S. 834-838.

93) R.S. Gonnelli, M. Tortello, D. Daghero, P. Pecchio, S. Galasso, V.A. Stepanov, Z. Bukowski, N.D. Zhigadlo, J. Karpinski, K. Iida, B. Holzapfel, *The order-parameter symmetry and fermi surface topology of 122 Fe-based superconductors: A point-contact Andreev-reflection study*, Journal of Superconductivity and Novel Magnetism 26 (2013) Nr. 4, S. 1331-1337.

94) D.I. Gorbunov, A.V. Andreev, M.D. Kuzmin, *Magnetization study of a GdFe5Al7 single crystal*, Journal of the Korean Physical Society 62 (2013) Nr. 10, S. 1517-1520.

95) D.I. Gorbunov, A.V. Andreev, Y. Skourski, M.D. Kuzmin, *High-field magnetization of a DyFe5Al7 single crystal*, Journal of Alloys and Compounds 553 (2013), S. 358-363.

96) P.F. Gostin, A. Helth, A. Voss, R. Sueptitz, M. Calin, J. Eckert, A. Gebert, *Surface treatment, corrosion behavior, and apatite-forming ability of Ti-45Nb implant alloy*, Journal of Biomedical Materials Research Part B 101 (2013) Nr. 2, S. 269-278.

97) H. Gretarsson, J.P. Clancy, X. Liu, J.P. Hill, E. Bozin, Y. Singh, S. Manni, P. Gegenwart, J. Kim, A.H. Said, D. Casa, T. Gog, M.H. Upton, H.-S. Kim, J. Yu, V.M. Katukuri, L. Hozoi, J. van den Brink, Y-J. Kim, *Crystal-field splitting and correlation effect on the electronic structure of A2Ir03*, Physical Review Letters 110 (2013), S. 76402/1-5.

98) D. Grimm, C.C. Bof Bufon, C. Deneke, P. Atkinson, D.J. Thurmer, F. Schaeffel, S. Gorantla, Bachmatiuk A., O.G. Schmidt, *Rolled-up nanomembranes as compact 3D architectures for field effect transistors and fluidic sensing applications*, Nano Letters 13 (2013) Nr. 1, S. 213-218.

99) V. Grinenko, S.-L. Drechsler, M. Abdel-Hafiez, S. Aswartham, A.U.B. Wolter, S. Wurmehl, C. Hess, K. Nenkov, G. Fuchs, D.V. Efremov, B. Holzapfel, J. van den Brink, B. Buechner, *Disordered magnetism in superconducting KFe2As2 single crystals*, Physica Status Solidi B 250 (2013) Nr. 3, S. 593-598.

100) V. Grinenko, G. Fuchs, K. Nenkov, B. Holzapfel, *An efficient method for AC loss reduction of YBCO pancake coils wound from parallel tapes*, Superconductor Science and Technology 26 (2013) Nr. 3, S. 35002/1-10.

101) T. Gross, L. Giebeler, C. Hess, *Novel in situ cell for Raman diagnostics of lithium-ion batteries*, Review of Scientific Instruments 84 (2013) Nr. 7, S. 73109/1-6.

102) O. Gutfleisch, K. Gueth, T.G. Woodcock, L. Schultz, *Recycling used Nd-Fe-B sintered magnets via a hydrogen-based route to produce anisotropic, resin bonded magnets*, Advanced Energy Materials 3 (2013) Nr. 2, S. 151-155.

103) D. Haberer, L. Petaccia, A.V. Fedorov, C.S. Praveen, S. Fabris, S. Piccinin, O. Vilkov, D.V. Vyalikh, A. Preobrajenski, N.I. Verbitskiy, H. Shiozawa, J. Fink, M. Knupfer, B. Buechner, A. Grueneis, *Anisotropic Eliashberg function and electron-phonon coupling in doped graphene*, Physical Review B 88 (2013) Nr. 8, S. 81401/1-5.

104) M. Haertel, J. Richter, O. Goetze, D. Ihle, S.-L. Drechsler, *Thermodynamics of the two-dimensional frustrated J1-J2 Heisenberg ferromagnet in the collinear stripe regime: Susceptibility and correlation length*, Physical Review B 87 (2013) Nr. 5, S. 54412/1-6.

105) W. Haessler, H. Hermann, M. Herrmann, C. Rodig, A. Aubele, L. Schmolinga, B. Sailer, B. Holzapfel, *Influence of the milling energy transferred to the precursor powder on the microstructure and the superconducting properties of MgB2 wires*, Superconductor Science and Technology 26 (2013) Nr. 2, S. 25005/1-7.

106) F. Haidu, A. Fechner, G. Salvan, O.D. Gordan, M. Fronk, D. Lehmann, B. Mahns, M. Knupfer, D.R.T Zahn, *Influence of film thickness and air exposure on the transport gap of manganese phthalocyanine*, AIP Advances 3 (2013) Nr. 6, S. 62124/1-7.

107) S. Haindl, M. Kidszun, F. Onken, A. Mietke, T. Thersleff, *Lessons from oxypnictide thin films*, International Journal of Modern Physics B 27 (2013) Nr. 4, S. 1330001/1-13.

108) F. Hammerath, U. Graefe, T. Kuehne, H. Kuehne, P.L. Kuhns, A.P. Reyes, G. Lang, S. Wurmehl, B. Buechner, P. Carretta, H.-J. Grafe, *Progressive slowing down of spin fluctuations in underdoped LaFeAs01-xFx*, Physical Review B 88 (2013) Nr. 10, S. 104503/1-9.

109) J.H. Han, N. Mattern, I. Kaban, D. Holland-Moritz, J. Bednarcik, R. Nowak, N. Sobczak, D.H. Kim, J. Eckert, *Phase separation in ternary Co-Gd-Ti liquids*, Journal of Physics - Condensed Matter 25 (2013) Nr. 24, S. 245104/1-7.

110) J. He, N. Mattern, J. Tan, J.Z. Zhao, I. Kaban, Z. Wang, L. Ratke, D.H. Kim, W.T. Kim, J. Eckert, *A bridge from monotectic alloys to liquid-phase-separated bulk metallic glasses: Design, microstructure and phase evolution*, Acta Materialia 61 (2013), S. 2102-2112.

111) A. Heinzig, T. Mikolajick, J. Trommer, D. Grimm, W.M. Weber, *Dually active silicon nanowire transistors and circuits with equal electron and hole transport*, Nano Letters 13 (2013), S. 4176-4181.

112) A. Helth, U. Siegel, U. Kuehn, T. Gemming, W. Gruner, S. Oswald, T. Marr, J. Freudenberger, J. Scharnweber, C.-G. Oertel, W. Skrotzki, L. Schultz, J. Eckert, *Influence of boron and oxygen on the microstructure and mechanical properties of high-strength Ti66Nb13Cu8Ni6.8Al6.2 alloys*, Acta Materialia 61 (2013) Nr. 9, S. 3324-3334.

113) A. Herklotz, E.-J. Guo, M.D. Biegalski, H.-M. Christen, L. Schultz, K. Doerr, *Strain-controlled switching kinetics of epitaxial PbZr0.52Ti0.4803 films*, New Journal of Physics 15 (2013), S. 73021/1-7.

114) A. Herklotz, M. Kataja, K. Nenkov, M.D. Biegalski, H.-M. Christen, C. Deneke, L. Schultz, K. Doerr, *Magnetism of the tensile-strain-induced tetragonal state of SrRu03 films*, Physical Review B 88 (2013) Nr. 14, S. 144412/1-8.

115) M. Herklotz, F. Scheiba, M. Hinterstein, K. Nikolowski, M. Knapp, A.-C. Dippel, L. Giebeler, J. Eckert, H. Ehrenberg, *Advances in in situ powder diffraction of battery materials: a case study of the new beamline P02.1 at DESY, Hamburg*, Journal of Applied Crystallography 46 (2013), S. 1117-1127.

116) H. Hermann, A. Elsner, D. Stoyan, *Surface area and volume fraction of random open-pore systems*, Modelling and Simulation in Materials Science and Engineering 21 (2013), S. 85005/1-17.

117) R. Hermann, H. Wendrock, S. Rodan, U.K. Roessler, C.G.F. Blum, S. Wurmehl, B. Buechner, *Single crystal growth of antiferromagnetic Mn3Si by a two-phase RF floating-zone method*, Journal of Crystal Growth 363 (2013), S. 1-6.

118) C. Hess, S. Sykora, T. Haenke, R. Schlegel, D. Baumann, V. B. Zabolotnyy, L. Harnagea, S. Wurmehl, J. van den Brink, B. Buechner, *Interband quasiparticle scattering in superconducting LiFeAs reconciles photoemission and tunneling measurements*, Physical Review Letters 110 (2013) Nr. 1, S. 17006/1-5.

119) J. Hosko, I. Janotova, P. Svec, G. Vlasak, I. Matko, D. Janickovic, T. Gemming, M. Stoica, Svec Sr., P., *Magnetostriction behavior of pseudobulk CoFeBSiNb(Ga) systems*, Journal of Superconductivity and Novel Magnetism 26 (2013) Nr. 4, S. 797-800.

120) C. Hotta, S. Nishimoto, N. Shibata, *Grand canonical finite size numerical approaches in one and two dimensions: Real space energy renormalization and edge state generation*, Physical Review B 87 (2013) Nr. 11, S. 115128/1-19.

121) J. Hufenbach, K. Kunze, L. Giebeler, T. Gemming, H. Wendrock, C. Baldauf, U. Kuehn, W. Hufenbach, J. Eckert, *The effect of boron on microstructure and mechanical properties of high-strength cast FeCrVC*, Materials Science and Engineering A 586 (2013), S. 267-275.

122) Y.H. Huo, A. Rastelli, O.G. Schmidt, *Ultra-small excitonic fine structure splitting in highly symmetric quantum dots on GaAs (001) substrate*, Applied Physics Letters 102 (2013) Nr. 15, S. 152105/1-4.

123) J. Hwang, M. Kim, D. Campbell, H.A. Alsalman, J.Y. Kwak, S. Shivaraman, A.R. Woll, A.K. Singh, R.G. Hennig, S. Gorantla, M.H. Ruemmeli, M.G. Spencer, *van der Waals epitaxial growth of graphene on sapphire by chemical vapor deposition without a metal catalyst*, ACS Nano 7 (2013) Nr. 1, S. 385-395.

124) E.M.M. Ibrahim, S. Hampel, R. Kamsanipally, J. Thomas, K. Erdmann, S. Fuessel, C. Taeschner, V.O. Khavrus, T. Gemming, A. Leonhardt, B. Buechner, *Highly biocompatible superparamagnetic Ni nanoparticles dispersed in submicron-sized C spheres*, Carbon 63 (2013), S. 358-366.

125) I. Ibrahim, Y. Zhang, A. Popov, L. Dunsch, B. Buechner, G. Cuniberti, M.H. Ruemmeli, *Growth of all-carbon horizontally aligned single-walled carbon nanotubes nucleated from fullerene-based structures*, Nanoscale Research Letters 8 (2013), S. 265/1-6.

126) K. Iida, J. Haenisch, E. Reich, F. Kurth, R. Huehne, L. Schultz, B. Holzapfel, A. Ichinose, M. Hanawa, I. Tsukuda, M. Schulze, S. Aswartham, S. Wurmehl, S. Buechner, *Intrinsic pinning and the critical current scaling of clean epitaxial Fe(Se,Te) thin films*, Physical Review B 87 (2013) Nr. 10, S. 104510/1-6.

127) K. Iida, S. Haindl, F. Kurth, J. Haenisch, L. Schulz, B. Holzapfel, *BaFe2As2/Fe bilayers with [001]- tilt grain boundary on MgO and SrTiO3 bicrystal substrates*, Physics Procedia 45 (2013), S. 189-192.

128) K. Iida, J. Hanisch, C. Tarantini, F. Kurth, J. Jaroszynski, S. Ueda, M. Naito, A. Ichinose, I. Tsukada, E. Reich, V. Grinenko, L. Schultz, B. Holzapfel, *Oxypnictide SmFeAs(O,F) superconductor: A candidate for high-field magnet applications*, Scientific Reports 3 (2013), S. 2139.

129) D. Iselt, A. Funk, L. Schultz, H. Schloerb, *Electrodeposition of Fe-Ga alloys: From thin films to nanowires*, ECS Electrochemistry Letters 2 (2013) Nr. 3, S. D13-D15.

130) I. Janotova, J. Hosko, P. Svec, I. Matko, D. Janickovic, P. Svec Sr, T. Gemming, M. Stoica, *The study of structure of Fe-B-P based metallic glasses*, Applied Surface Science 269 (2013), S. 102-105.

131) T. Jaumann, E.M.M. Ibrahim, S. Hampel, D. Maier, A. Leonhardt, B. Buechner, *The synthesis of superparamagnetic cobalt nanoparticles encapsulated in carbon through high-pressure CVD*, Chemical Vapor Deposition 19 (2013), S. 228-234.

132) A. Jedrzejewska, A. Bachmatiuk, I. Ibrahim, H. Srekova, C. Nganou, F. Schuechner, E. Borowiak-Palen, T. Gemming, G. Cuniberti, B. Buechner, M.H. Ruemmeli, *A systematic and comparative study of binary metal catalysts for carbon nanotube fabrication using CVD and laser evaporation*, Fullerenes, Nanotubes and Carbon Nanostructures 21 (2013), S. 273-285.

133) K.D. Joens, P. Atkinson, M. Mueller, M. Heldmaier, S.M. Ulrich, O.G. Schmidt, P. Michler, *Triggered indistinguishable single photons with narrow line widths from site-controlled quantum dots*, Nano Letters 13 (2013) Nr. 1, S. 126-130.

134) M.R. Jorgensen, S. Giudicatti, O.G. Schmidt, *Diamond lattice photonic crystals from rolled-up membranes*, Physical Review A 87 (2013) Nr. 4, S. 41803/1-5.

135) P. Jovari, A. Piarristeguy, R. Escalier, I. Kaban, J. Bednarcik, A. Pradel, *Short range order and stability of amorphous GexTe100-x alloys ...*, Journal of Physics - Condensed Matter 25 (2013) Nr. 19, S. 195401/1-9.

136) P. Jovari, Y. Sutou, I. Kaban, Y. Saito, J. Koike, *Fourfold coordinated Te atoms in amorphous GeCu2Te3 phase change material*, Scripta Materialia 68 (2013), S. 122-125.

137) I. Kaban, P. Jovari, V. Kokotin, O. Shuleshova, B. Beuneu, K. Saksl, N. Mattern, J. Eckert, A.L. Greer, *Local atomic arrangements and their topology in Ni–Zr and Cu–Zr glassy and crystalline alloys*, Acta Materialia 61 (2013) Nr. 7, S. 2509-2520.

138) T. Kaspar, J. Fiedler, I. Skorupa, D. Buerger, A. Muecklich, M. Fritzsche, O.G. Schmidt, H. Schmidt, *Persistent current reduction in metal-semiconductor FETs with a ZnCoO channel in an external magnetic field*, IEEE Electron Device Letters 34 (2013) Nr. 10, S. 1271-1273.

139) J. Kasprzak, S. Portolan, A. Rastelli, L. Wang, J.D. Plumhof, O.G. Schmidt, W. Langbein, *Vectorial nonlinear coherent response of a strongly confined exciton-biexciton system*, New Journal of Physics 15 (2013) Nr. 5, S. 55006/1-27.

140) A. Kauffmann, J. Freudenberger, H. Klauss, V. Klemm, W. Schillinger, V. Subramanya Sarma, L. Schultz, *Properties of cryo-drawn copper with severely twinned microstructure*, Materials Science and Engineering A 588 (2013), S. 132-141.

141) S. Kauffmann-Weiss, B. Erkartal, L. Schultz, L. Kienle, S. Faehler, *Influence of kinetics on the phase formation in epitaxial Fe–Pd films*, Scripta Materialia 68 (2013) Nr. 6, S. 412-415.

142) S. Kauffmann-Weiss, A. Kauffmann, R. Niemann, J. Freudenberger, L. Schultz, S. Faehler, *Twinning phenomena along and beyond the bain path*, metals 4 (2013), S. 319-336.

143) I.S.M. Khalil, V. Magdanz, S. Sanchez, O.G. Schmidt, S. Misra, *Three-dimensional closed-loop control of self-propelled microjets*, Applied Physics Letters 103 (2013), S. 172404/1-5.

144) D.H. Kim, W.T. Kim, E.S. Park, N. Mattern, J. Eckert, *Phase separation in metallic glasses*, Progress in Materials Science 58 (2013) Nr. 8, S. 1103-1172.

145) K.C. Kim, K.R. Lim, E.S. Lee, W.T. Kim, A. Gebert, J. Eckert, D.H. Kim, *Thermal stability of amorphous oxide in Al87Ni3Y10 metallic glass*, Corrosion Science 77 (2013), S. 1-5.

146) S.Y. Kim, S.J. Kim, S.S. Jee, J.M. Park, K.H. Park, S.C. Park, E.A. Cho, J.H. Lee, I.Y. Song, S.M. Lee, I.T. Han, K.R. Lim, W.T. Kim, J.C. Park, J. Eckert, D.H. Kim, E.-S. Lee, *Capillary flow of amorphous metal for high performance electrode*, Scientific Reports 3 (2013), S. 2185/1-7.

147) F. Kirtschig, J. Rijnbeek, J. van den Brink, C. Ortix, *Quantum collapses and revivals of matter wave in dynamics of symmetry breaking*, Physical Review B 87 (2013) Nr. 1, S. 14304/1-.
148) P. Klaer, H.C. Herper, P. Entel, R. Niemann, L. Schultz, S. Faehler, H.J. Elmers, *Electronic structure of the austenitic and martensitic state of magnetocaloric Ni-Mn-In Heusler alloy films*, Physical Review B 88 (2013) Nr. 17, S. 174414/1-8.
149) E. Knauer, J. Freudenberger, T. Marr, A. Kauffmann, L. Schultz, *Grain refinement and deformation mechanisms in room temperature Ssvere plastic deformed Mg-AZ31*, metals 3 (2013), S. 283-297.
150) A. Koenig, R. Schuster, M. Knupfer, B. Buechner, H. Berger, *Doping dependence of the plasmon dispersion in 2H-TaSe2*, Physical Review B 87 (2013) Nr. 19, S. 195119/1-5.
151) J. Koenig, K. Tschulik, L. Buettner, M. Uhlemann, J. Czarske , *Analysis of the electrolyte convection inside the concentration boundary layer during structured electrodeposition of copper in high magnetic gradient fields*, Analytical Chemistry 85 (2013), S. 3087-3094.
152) A. Koitzsch, T.K. Kim, U. Treske, M. Knupfer, B. Buechner, M. Richter, I. Opahle, R. Follath, E.D. Bauer, J.L. Sarrao, *Band-dependent emergence of heavy quasiparticles in CeCoIn5*, Physical Review B 88 (2013) Nr. 3, S. 35124/1-5.
153) A.A. Kordyuk, V.B. Zabolotnyy, D.V. Evtushinsky, A.N. Yaresko, B. Buechner, S.V. Borisenko, *Electronic band structure of Ferro-Pnictide superconductors from ARPES experiment*, Journal of Superconductivity and Novel Magnetism 26 (2013) Nr. 9, S. 2837-2841.
154) K. Kosiba, P. Gargarella, S. Pauly, U. Kuehn, J. Eckert, *Predicted glass-forming ability of Cu-Zr-Co alloys and their crystallization behavior*, Journal of Applied Physics 113 (2013), S. 123505/1-4.
155) P. Kovac, L. Kopera, T. Melisek, M. Rindfleisch, W. Haessler, I. Husek, *Behaviour of filamentary MgB2 wires subjected to tensile stress at 4.2 K*, Superconductor Science and Technologie 26 (2013), S. 105028/1-8.
156) C. Kramberger, T. Thurakitseree, S. Maruyama, M. Knupfer, *Pi and Pi plus delta plasmon localization in single-walled carbon nanotube meta-materials*, Nanotechnology 24 (2013), S. 405202/1-6.
157) R. Kraus, V. Bisogni, L. Harnagea, S. Aswartham, S. Wurmehl, G. Levy, I.S. Elfimov, B. Buechner, G.A. Sawatzky, J. Geck, *Observation of charge accumulation and onsite Coulomb repulsion at transition metal impurities in the iron pnictides*, Physical Review B 87 (2013) Nr. 13, S. 134516/1-7.
158) S. Kumar, L. Harnagea, S. Wurmehl, B. Buechner, A.K. Sood, *Gap-dependent quasiparticle dynamics and coherent acoustic phonons in CaFe2As2 across spin density wave phase transition*, Journal of the Physical Society of Japan 87 (2013) Nr. 22, S. 44715/1-9.
159) N.V. Kuratieva, M. Banki, A.A. Tsirlin, J. Eckert, Ehrenberg H., D. Mikhailova, *New lithium copper borates with BO3 triangles: Li6CuB4O10, Li3CuB3O7, Li8Cu7B14O32, and Li2Cu9B12O28*, Inorganic Chemistry 52 (2013), S. 13974-13983.
160) F. Kurth, K. Iida, S. Trommler, J. Haenisch, K. Nenkov, J. Engelmann, S. Oswald, J. Werner, L. Schultz, B. Holzapfel, S. Haindl, *Electronic phase diagram of disordered Co doped BaFe2As2-delta*, Superconductor Science and Technology 26 (2013) Nr. 2, S. 25014/1-7.
161) F. Kurth, E. Reich, J. Haenisch, A. Ichinose, I. Tsukuda, R. Huehne, S. Trommler, J. Engelmann, L. Schultz, B. Holzapfel, K. Iida, *Versatile fluoride substrates for Fe-based superconducting thin films*, Applied Physics Letters 102 (2013) Nr. 14, S. 142601/1-5.
162) I.V. Kuvychko, C. Dubceac, S.H.M. Deng, X.-B. Wang, A.A. Granovsky, A.A. Popov, M.A. Petrukhina, S.H. Strauss, O.V. Boltalina, *C20H4 (C4F8) 3: A fluorine-containing annulated corannulene that is a better electron acceptor than C60*, Angewandte Chemie-International Edition 125 (2013) Nr. 29, S. 7653-7656.
163) N. Kyzyltas-Yavuz, M. Herklotz, A.H. Hashem, H.M. Abuzeid, B. Schwarz, H. Ehrenberg, A. Mauger, C.M. Julien, *Synthesis, structural, magnetic and electrochemical properties ofLiNi1/3Mn1/3Co1/3O2prepared by a sol-gel method using table sugar aschelating agent*, Electrochimica Acta 113 (2013), S. 313-321.
164) D. Lahiri, P.K. Gill, S. Scudino, C. Zhang, V. Singh, J. Karthikeyan, N. Munroe, S. Seal, A. Agarwal, *Cold sprayed aluminum based glassy coating: Synthesis, wear and corrosion properties*, Surface and Coatings Technology 232 (2013), S. 33-40.
165) B.W. Larson, J.B. Whitaker, X.-B. Wang, A.A. Popov, G. Rumbles, N. Kopidakis, S.H. Strauss, O.V. Boltalina, *Electron affinity of phenyl-C61-butyric acid methyl ester (PCBM)*, Journal of Physical Chemistry C 117 (2013), S. 14958-14964.
166) D. Leberl, R. Ummethala, A. Leonhardt, B. Hensel, S.F. Tedde, O. Schmidt, O. Hayden, *Characterization of carbon nanotube field emitters in pulsed operation mode*, Journal of Vacuum Science and Technology B 31 (2013) Nr. 1, S. 12204/1-6.
167) W.S. Lee, S. Johnston, B. Moritz, J. Lee, M. Yi, K.J. Zhou, T. Schmitt, L. Patthey, V. Strocov, K. Kudo, Y. Koike, J. van den Brink, T.P. Devereaux, Z.X. Shen, *Role of lattice coupling in establishing electronic and magnetic properties in quasi-one-dimensional cuprates*, Physical Review Letters 110 (2013) Nr. 26, S. 265502/1-5.
168) K. Leistner, J. Wunderwald, N. Lange, S. Oswald, M. Richter, H. Zhang, L. Schultz, S. Faehler, *Electric-field control of magnetism by reversible surface reduction and oxidation reactions*, Physical Review B 87 (2013) Nr. 22, S. 224411/1-7.
169) P.V. Leksin, A.A. Kamashev, N.N. Garifyanov, I.A. Garifullin, Y.V. Fominov, J. Schumann, C. Hess, V. Kataev, B. Buechner, *Peculiarities of performance of the spin valve for the superconducting current*, JETP Letters 97 (2013) Nr. 8, S. 478-482.
170) M. Lepple, R. Adam, D.M. Cupid, P. Franke, T. Bergfeldt, D. Wadewitz, D. Rafaja, H.J. Seifert, *Thermodynamic investigations of copper oxides used as conversion type electrodes in lithium ion batteries*, Journal of Materials Science 48 (2013) Nr. 17, S. 5818-5826.
171) C.J. Li, J. Tan, G. Wang, J. Bednarcik, X.K. Zhu, Y. Zhang, M. Stoica, U. Kuehn, J. Eckert, *Enhanced strength and transformation-induced plasticity in rapidly solidified Zr-Co- (Al) alloys*, Scripta Materialia 68 (2013) Nr. 11, S. 897-900.
172) C.J. Li, J. Tan, X.K. Zhu, Y. Zhang, M. Stoica, U. Kuehn, J. Eckert, *On the transformation-induced work-hardening behavior of Zr47.5Co47.5Al5 ultrafine-grained alloy*, Intermetallics 35 (2013), S. 116-119.

173) S. Li, L. Ma, S. Boettner, Y. Mei, M.R. Jorgensen, S. Kiravittaya, O.G. Schmidt, *Angular position detection of single nanoparticles on rolled-up optical microcavities with lifted degeneracy*, Physical Review A 88 (2013) Nr. 3, S. 33833/1-8.

174) K.R. Lim, J.M. Park, S.S. Jee, S.Y. Kim, S.J. Kim, E.-S. Lee, W.T. Kim, A. Gebert, J. Eckert, D.H. Kim, *Effect of thermal stability of the amorphous substrate on the amorphous oxide growth on Zr–Al–(Cu,Ni) metallic glass surfaces*, Corrosion Science 73 (2013), S. 1-6.

175) K.R. Lim, J.M. Park, S.J. Kim, E.-S. Lee, W.T. Kim, A. Gebert, J. Eckert, D.H. Kim, *Enhancement of oxidation resistance of the supercooled liquid in Cu-Zr-based metallic glass by forming an amorphous oxide layer with high thermal stability*, Corrosion Science 66 (2013), S. 1-4.

176) G. Lin, L. Baraban, L. Han, D. Karnaushenko, D. Makarov, G. Cuniberti, O.G. Schmidt, *Magnetoresistive emulsion analyzer*, Scientific Reports 3 (2013), S. 2548/1-4.

177) I. Lindemann, A. Borgschulte, E. Callini, A. Zuettel, L. Schultz, O. Gutfleisch, *Insight into the decomposition pathway of the complex hydride Al3Li4(BH4)13*, International Journal of Hydrogen Energy 38 (2013), S. 2790-2795.

178) S Lindner, U. Treske, M. Knupfer, *The complex nature of phthalocyanine/gold interfaces*, Applied Surface Science 267 (2013), S. 62-65.

179) S. Lindner, B. Mahns, A. Koenig, F. Roth, M. Knupfer, R. Friedrich, T. Hahn, J. Kortus, *Phthalocyanine dimers in a blend: Spectroscopic and theoretical studies of MnPc delta +/F16CoPc delta-*, The Journal of Chemical Physics 138 (2013) Nr. 2, S. 24707/1-4.

180) C.D. Ling, S. Schmid, P.E.R. Blanchard, V. Petricek, G.J. McIntyre, N. Sharma, A. Maljuk, A.A. Yaremchenko, V.V. Kharton, M. Gutmann, R.L. Withers, *A (3 + 3)- dimensional "Hypercubic" oxide-ionic conductor: Type II Bi2O3-Nb2O5*, Journal of the American Chemical Society 135 (2013), S. 6477-6484.

181) X. Liu, A. Grueneis, D. Haberer, A.V. Fedorov, O. Vilkov, W. Strupinski, T. Pichler, *Tunable interface properties between pentacene and graphene on the SiC substrate*, The Journal of Physical Chemistry C 117 (2013), S. 3969-3975.

182) L. Loeber, C. Flache, R. Petters, U. Kuehn, J. Eckert, *Comparison of different post processing technologies for SLM generated 316l steel parts*, Rapid Prototyping Journal 19 (2013) Nr. 3, S. 173-179.

183) U. Loew, S. Zvyagin, M. Ozerov, U. Schaufuss, V. Kataev, B. Wolf, B. Luethi, *Magnetization, magnetic susceptibility and ESR in Tb3Ga5O12*, European Physical Journal B 86 (2013), S. 87/1-6.

184) Y.M. Lu, Z.J. Liu, C.Y. Bai, F. Fan, R. Zhao, Z.Y. Liu, R. Huehne, B. Holzapfel, C.B. Cai, *Epitaxial growth of Gd2 Zr2O7/Y2O3 buffer layers for YBa2Cu3O7-delta coated conductors*, Physica C 485 (2013), S. 15-19.

185) V. Lukes, P. Rapta, K. Haubner, M. Rosenkranz, H. Hartmann, L. Dunsch, *Combined spectroelectrochemical and theoretical study of electron-rich dendritic 2,5-diaminothiophene derivatives: N,N,N Œ,N Œ.Tetrakis-(4-diphenylamino-phenyl)-thiophene-2,5-diamine*, The Journal of Physical Chemistry A 117 (2013), S. 6702-6711.

186) Q. Luo, B. Schwarz, N. Mattern, J. Shen, J. Eckert, *Roles of hydrogenation, annealing and field in the structure and magnetic entropy change of Tb-based bulk metallic glasses*, AIP Advances 3 (2013), S. 32134/1-17.

187) G.Z. Ma, K.K. Song, B.A. Sun, Z.J. Yan, U. Kuehn, D. Chen, J. Eckert, *Effect of cold-rolling on the crystallization behavior of a CuZr-based bulk metallic glass*, Journal of Materials Science 48 (2013), S. 6825-6832.

188) G.Z. Ma, B.A. Sun, S. Pauly, K.K. Song, U. Kuehn, D. Chen, J. Eckert, *Effect of Ti substitution on glass-forming ability and mechanical properties of a brittle Cu–Zr–Al bulk metallic glass*, Materials Science and Engineering A 563 (2013), S. 112-116.

189) L. Ma, S. Li, V.A. Bolanos Quinones, L. Yang, W. Xi, M. Jorgensen, S. Baunack, Y. Mei, S. Kiravittaya, O.G. Schmidt, *Dynamic molecular processes detected by microtubular opto-chemical sensors self-assembled from prestrained nanomembranes*, Advanced Materials 25 (2013) Nr. 16, S. 2357-2361.

190) P. Ma, C.M. Zou, H.W. Wang, S. Scudino, K.K. Song, M. Samadi Khoshkhoo, Z.J. Wei, U. Kuehn, J. Eckert, *Structure of GP zones in Al-Si matrix composites solidified under high pressure*, Materials Letters 109 (2013), S. 1-4.

191) H. Maeter, A.A. Zvyagin, H. Luetkens, G. Pascua, Z. Shermadini, R. Saint-Martin, A. Revcolevschi, C. Hess, B. Buechner, H.-H. Klauss, *Low temperature ballistic spin transport in the S= 1/2 antiferromagnetic Heisenberg chain compound SrCuO2*, Journal of Physics - Condensed Matter 25 (2013) Nr. 36, S. 365601/1-8.

192) V. Magdanz, S. Sanchez, O.G. Schmidt, *Development of a sperm-flagella driven micro-bio-robot*, Advanced Materials 25 (2013), S. 6581-6588.

193) D. Makarov, D. Karnaushenko, O.G. Schmidt, *Printable magnetoelectronics*, ChemPhysChem 14 (2013), S. 1771-1776.

194) D. Makarov, C. Ortix, L. Baraban, *Guest Editorial - Functional magnetic nanomembranes*, SPIN 3 (2013) Nr. 3, S. 1302001/1-4.

195) S. Makharza, G. Cirillo, A. Bachmatiuk, I. Ibrahim, N. Ioannides, B. Trzebicka, S. Hampel, M.H. Ruemmeli, *Graphene oxide-based drug delivery vehicles: Functionalization, characterization, and cytotoxicity evaluation*, Journal of Nanoparticle Research 15 (2013) Nr. 12, S. 2099/1-26.

196) S. Makharza, G. Cirillo, A. Bachmatiuk, O. Vittorio, R.G. Mendes, S. Oswald, S. Hampel, M.H. Ruemmeli, *Size-dependent nanographene oxide as a platform for efficient carboplatin release*, Journal of Materials Chemistry B 1 (2013), S. 6107-6114.

197) Maletz, J., V.B. Zabolotnyy, D.V. Evtushinsky, A.N. Yaresko, A.A. Kordyuk, Z. Shermadini, H. Luetkens, K. Sedlak, R. Khasanov, A. Amato, A. Krzton-Maziopa, K. Conder, E. Pomjakushina, H.-H. Klauss, E.D.L. Rienks, B. Buechner, S.V. Borisenko, *Photoemission and muon spin relaxation spectroscopy of the iron-based Rb 0.77 Fe 1.61 Se 2 superconductor: Crucial role of the cigar-shaped Fermi surface*, Physical Review B 88 (2013), S. 134501/1-7.

198) T. Marr, J. Freudenberger, A. Kauffmann, J. Romberg, I. Okulov, R. Petters, J. Scharnweber, A. Eschke, C.-G. Oertel, U. Kuehn, J. Eckert, W. Skrotzki, L. Schultz, *Processing of intermetallic titanium aluminide wires*, metals 3 (2013), S. 188-201.

199) P. Marra, S. Sykora, K. Wohlfeld, J. van den Brink, *Resonant inelastic X-Ray scattering as a probe of the phase and excitations of the order parameter of superconductors*, Physical Review Letters 110 (2013) Nr. 11, S. 117005/1-5.

200) N. Mattern, J. Bednarcik, H.-P. Liermann, J. Eckert, *Structural behaviour of Pd40Cu30Ni10P20 metallic glass under high pressure*, Intermetallics 38 (2013), S. 9-13.

201) N. Mattern, J. Bednarcik, M. Stoica, J. Eckert, *Temperature dependence of the short-range order of Cu65Zr35 metallic glass*, Intermetallics 32 (2013), S. 51-56.

202) N. Mattern, J.H. Han, O. Fabrichnaya, M. Zinkevich, W. Loeser, J. Werner, R. Nowak, I. Kaban, O. Shuleshova, D. Holland-Moritz, J. Bednarcik, N. Sobczak, J. Eckert, *Experimental and thermodynamic assessment of the Gd-Ti system*, CALPHAD: Computer Coupling of Phase Diagramsand Thermochemistry 42 (2013), S. 19-26.

203) M. Melzer, A. Kopylov, D. Makarov, O.G. Schmidt, *Stretchability and self-healing of wrinkled GMR multilayers on elastomeric membranes*, SPIN 3 (2013) Nr. 3, S. 1340005/1-6.

204) R.G. Mendes, A. Bachmatiuk, B. Buechner, G. Cuniberti, M.H. Ruemmeli, *Carbon nanostructures as multi-functional drug delivery platforms*, Journal of Materials Chemistry B 1 (2013), S. 401-428.

205) S. Miao, T. Yang, S.G. Hickey, V. Lesnyak, B. Rellinghaus, J. Xu, A. Eychmueller, *Emissive Zn0@Zn3P2 nanocrystals: Synthesis, optical, and optoelectrochemical properties*, Small 9 (2013) Nr. 20, S. 3415-3422.

206) D. Mikhailova, A. Thomas, S. Oswald, W. Gruner, N.N. Bramnik, A.A. Tsirlin, D.M. Trots, A. Senyshyn, J. Eckert, H. Ehrenberg, *Structural changes in the LiCrMn04 cathode material during electrochemical Li extraction and insertion*, Journal of the Electrochemical Society 160 (2013), S. A3082-A3089.

207) P. Milde, R. Schoenfelder, A. Koitzsch, K. Haubner, U. Zerweck-Trogisch, E. Jaehne, L.M. Eng, *In situ self-assembled organic interface layers for the controlled growth of oligothiophene thin films on ferroelectric Pb(Zr0.2Ti0.8)03.*, The Journal of Chemical Physics 139 (2013) Nr. 21, S. 214702/1-5.

208) M. Minola, L. Hozoi, D. Di Castro, R. Felici, M. Moretti Sala, A. Tebano, G. Balestrino, G. Ghiringhelli, J. van den Brink, L. Braicovich, *Measurement of the effect of lattice strain on magnetic interactions and orbital splitting in CaCu02 using resonant inelastic x-ray scattering*, Physical Review B 87 (2013) Nr. 8, S. 85124/1-7.

209) V. Mishev, W. Seeboeck, M. Eisterer, K. Iida, F. Kurth, J. Haenisch, E. Reich, B. Holzapfel, *One-dimensional pinning behavior in Co-doped BaFe2As2 thin films*, Applied Physics Letters 103 (2013) Nr. 23, S. 232601/1-4.

210) C. Monney, V. Bisogni, K.-J. Zhou, R. Kraus, V.N. Strocov, G. Behr, J. Malek, R. Kuzian, S.-L. Drechsler, S. Johnston, A. Revcolevschi, B. Buechner, H.M. Ronnow, J. van den Brink, J. Geck, T. Schmitt, *Determining the short-range spin correlations in the spin-chain Li2Cu02 and CuGe03 compounds using resonant inelastic X-Ray scattering*, Physical Review Letters 110 (2013) Nr. 8, S. 87403/1-5.

211) M. Montagnese, M. Otter, X. Zotos, D.A. Fishman, N. Hlubek, O. Mityashkin, C. Hess, R. Saint-Martin, S. Singh, A. Revcolevschi, P.H.M. van Loosdrecht, *Phonon-magnon interaction in low dimensional quantum magnets observed by dynamic heat transport measurements*, Physical Review Letters 110 (2013) Nr. 14, S. 147206/1-5.

212) J.D. Moore, D. Klemm, D. Lindackers, S. Grasemann, R. Traeger, J. Eckert, L. Loeber, S. Scudino, M. Katter, A. Barcza, K.P. Skokov, O. Gutfleisch, *Selective laser melting of La(Fe,Co,Si)13 geometries for magnetic refrigeration*, Journal of Applied Physics 114 (2013) Nr. 4, S. 43907/1-8.

213) M. Moore, R. Sueptitz, A. Gebert, L. Schultz, O. Gutfleisch, *Impact of magnetization state on the corrosion of sintered Nd-Fe-B magnets for e-motor applications*, Materials and Corrosion 64 (2013), S. online first.

214) A.S. Moskvin, E. Vavilova, S.-L. Drechsler, V. Kataev, B. Buechner, *7Li NMR study of the ordering phenomena in the intrinsic two-component magnetoelectric material Li2ZrCu04*, Physical Review B 87 (2013) Nr. 5, S. 54405/1-5.

215) N.K. Mukhopadhyay, F. Ali, S. Scudino, M. Samadi Khoshkhoo, M. Stoica, V.C. Srivastava, V. Uhlenwinkel, G. Vaughan, C. Suryanarayana, J. Eckert, *Grain size softening effect in Al62.5Cu25Fe12.5 nanoquasicrystals*, Applied Physics Letters 103 (2013) Nr. 20, S. 201914/1-5.

216) F.M. Muntyanu, A. Gilewski, K. Nenkov, A.J. Zaleski, T. Palewski, V. Chistol, *High-field peculiarities of galvanomagnetic quantum oscillations in Bi bicrystals with nano-width superconducting crystallite interfaces*, Solid State Communications 158 (2013), S. 9-12.

217) F. Napolitano, A.L. Soldati, J. Geck, D.G. Lamas, A. Serquis, *Electronic and structural properties of La0.4Sr0.6Ti1LyCoy03±d electrode materials for symmetric SOFC studied by hard X-ray absorption spectroscopy*, International Journal of Hydrogen Energy 38 (2013), S. 8965-8973.

218) R. Nath, A.A. Tsirlin, P. Khuntia, O. Janson, T. Foerster, M. Padmanabhan, J. Li, Y. Skourski, M. Baenitz, H. Rosner, I. Rousochatzakis, *Magnetization and spin dynamics of the spin S=1/2 hourglass nanomagnet Cu-5(OH)(2)(NIPA)(4) center dot 10H(2)O*, Physical Review B 87 (2013) Nr. 21, S. 214417/1-15.

219) E. Nazarova, K. Buchkov, K. Nenkov, S. Terzieva, *Doping dependence of magnetoresistivity in polycrystalline Y(Ca) BC0*, Journal of Optoelectronics and Advanced Materials 15 (2013) Nr. 1-2, S. 66-68.

220) V. Neu, C. Schulze, M. Faustini, J. Lee, D. Makarov, D. Suess, S.-K. Kim, D. Grosso, L. Schultz, M. Albrecht, *Probing the energy barriers and magnetization reversal processes of nanoperforated membrane based percolated media*, Nanotechnology 24 (2013) Nr. 14, S. 145702/1-6.

221) F. Nickel, D.M. Gottlob, I.P. Krug, H. Doganay, S. Cramm, A.M. Kaiser, G. Lin, D. Makarov, O.G. Schmidt, C.M. Schneider, *Time-resolved magnetic imaging in an aberration-corrected, energy-filtered photoemission electron microscope*, Ultramicroscopy 130 (2013), S. 54-62.

222) S. Nishimoto, S. Ejima, H. Fehske, *Anderson localization versus charge-density-wave formation in disordered electron systems*, Physical Review B 87 (2013) Nr. 4, S. 45116/1-5.

223) S. Nishimoto, N. Shibata, C. Hotta, *Controlling frustrated liquids and solids with an applied field in a kagome Heisenberg antiferromagnet*, nature communications 4 (2013), S. 2287/1-.

224) S. Niyomsoan, P. Gargarella, M. Stoica, M.S. Khoshkoo, U. Kuehn, J. Eckert, *Phase formation in rapid solidified Ag-Y alloys*, Journal of Applied Physics 113 (2013) Nr. 10, S. 104308/1-9.

225) I.V. Okulov, S. Pauly, U. Kuehn, P. Gargarella, T. Marr, J. Freudenberger, L. Schultz, J. Scharnweber, C.-G. Oertel, W. Skrotzki, J. Eckert, *Effect of microstructure on the mechanical properties of as-cast Ti–Nb–Al–Cu–Ni alloys for biomedical application*, Materials Science and Engineering C 33 (2013), S. 4795-4801.

226) A. Omar, M. Dimitrakopoulou, C.G.F. Blum, H. Wendrock, S. Rodan, S. Hampel, W. Loeser, B. Buechner, S. Wurmehl, *Phase dynamics and growth of Co2Cr1-xFexAl Heusler compounds: A key to understand their anomalous physical properties*, Crystal Growth and Design 13 (2013), S. 3925-3934.

227) P. Pahlke, S. Trommler, B. Holzapfel, L. Schultz, R. Huehne, *Dynamic variation of biaxal strain in optimally doped and underdoped YBa2Cu3O7-delta thin films*, Journal of Applied Physics 113 (2013) Nr. 12, S. 123907/1-6.

228) S.K. Pal, K. Gueth, T.G. Woodcock, L. Schultz, O. Gutfleisch, *Properties of isolated single crystalline and textured polycrystalline nano/sub-micrometre Nd2Fe14B particles obtained from milling of HDDR powder*, Journal of Physics D 46 (2013) Nr. 37, S. 375004/1-8.

229) S.K. Pal, L. Schultz, O. Gutfleisch, *Effect of milling parameters on SmCo5 nanoflakes prepared by surfactant-assisted high energy ball milling*, Journal of Applied Physics 113 (2013) Nr. 1, S. 13913/1-6.

230) Y.D. Panov, A.S. Moskvin, N.S. Fedorova, S.-L. Drechsler, *Nonstoichiometry effect on magnetoelectric coupling in cuprate multiferroics*, Ferroelectrics 442 (2013) Nr. 1, S. 27-41.

231) P.D. Parchi, O. Vittorio, L. Andreani, N. Piolanti, G. Cirillo, F. Iemma, S. Hampel, M. Lisanti, *How nanotechnology can really improve the future of orthopedic implants and scaffolds for bone and cartilage defects*, Nanomedicine and Biotherapeutic Discovery 3 (2013) Nr. 2, S. 1000114/1-16.

232) A. Paris, N. Verbitskiy, A. Nefedov, Y. Wang, A. Fedorov, D. Haberer, M. Oehzelt, L. Petaccia, D. Usachov, D. Vyalikh, H. Sachdev, C. Woell, M. Knupfer, B. Buechner, L. Calliari, L. Yashina, S. Irle, A. Grueneis, *Kinetic isotope effect in the hydrogenation and deuteration of graphene*, Advanced Functional Materials 23 (2013), S. 1628-1635.

233) S. Pauly, L. Loeber, R. Petters, M. Stoica, S. Scudino, U. Kuehn, J. Eckert, *Processing metallic glasses by selective laser melting*, Materials Today 16 (2013) Nr. 1-2, S. 37-41.

234) V. Pavlyuk, G. Dmytriv, I. Chumakc, O. Gutfleisch, I. Lindemann, H. Ehrenberg, *High hydrogen content super-lightweight intermetallics from the Li-Mg-Si system*, International Journal of Hydrogen Energy 38 (2013), S. 5724-5737.

235) P. Pecchio, D. Daghero, G.A. Ummarino, R.S. Gonnelli, F. Kurth, B. Holzapfel, K. Iida, *Doping and critical-temperature dependence of the energy gaps in Ba(Fe1-xCox)2As2 thin films*, Physical Review B 88 (2013) Nr. 17, S. 174506/1-9.

236) D.C. Peets, J.-H. Kim, P. Dosanjh, M. Reehuis, A. Maljuk, N. Aliouane, C. Ulrich, B. Keimer, *Magnetic phase diagram of Sr3Fe2O7-delta*, Physical Review B 87 (2013) Nr. 21, S. 214410/1-8.

237) O. Penzin, G. Paasch, L. Smith, *Nonparabolic multivalley quantum correction model for InGaAs double-gate structures*, IEEE Transactions on Electron Devices 60 (2013) Nr. 7, S. 2246-2250.

238) B. Peters, A. Alfonsov, C.G.F. Blum, S.J. Hageman, P.M. Woodward, S. Wurmehl, B. Buechner, F.Y. Yang, *Epitaxial films of Heusler compound Co2FeAl0.5Si0.5 with high crystalline quality grown by off-axis sputtering*, Applied Physics Letters 103 (2013) Nr. 16, S. 162404/1-5.

239) K. Pinkert, L. Giebeler, M. Herklotz, S. Oswald, J. Thomas, A. Meier, L. Borchardt, L. Kaskel, H. Ehrenberg, J. Eckert, *Functionalised porous nanocomposites: Amultidisciplinary approach to investigate designed structures for supercapacitor applications*, Journal of Materials Chemistry A 1 (2013) Nr. 5, S. 4904-4910.

240) T. Plecenik, M. Gregor, R. Sobota, M. Truchly, L. Satrapinskyy, F. Kurth, B. Holzapfel, K. Iida, P. Kus, A. Plecenik, *Surface transport properties of Fe-based superconductors: The influence of degradation and inhomogeneity*, Applied Physics Letters 103 (2013) Nr. 5, S. 52601/1-4.

241) J.D. Plumhof, R. Trotta, V. Krapek, E. Zallo, P. Atkinson, S. Kumar, A. Rastelli, O.G. Schmidt, *Tuning of the valence band mixing of excitons confined in GaAs/AlGaAs quantum dots via piezoelectric-induced anisotropic strain*, Physical Review B 87 (2013), S. 75311/1-5.

242) G. Pollefeyt, S. Rottiers, P. Vermeir, P. Lommens, R. Huehne, K. De Buysser, I. van Driessche, *Feasibility study of the synthesis of YBiO3 thin films by aqueous chemical solution deposition as an alternative for CeO2 buffer layers in coated conductors*, Journal of Materials Chemistry A 1 (2013), S. 3613-3619.

243) A.A. Popov, Yang S., L. Dunsch, *Endohedral fullerenes*, Chemical Reviews 113 (2013), S. 5989-6113.

244) A.K. Pramanik, S. Aswartham, A.U.B. Wolter, S. Wurmehl, V. Kataev, B. Buechner, *Flux dynamics and avalanches in the 122 pnictide superconductor Ba0:65Na0:35Fe2As2*, Journal of Physics - Condensed Matter 25 (2013) Nr. 49, S. 495701/1-9.

245) G. Prando, P. Bonfa, G. Profeta, R. Khasanov, F. Bernardini, M. Mazzani, E.M. Bruening, A. Pal, V.P.S. Awana, H.-J. Grafe, B. Buechner, R. De Renzi, P. Carretta, S. Sanna, *Common effect of chemical and external pressures on the magnetic properties of RCoPO (R = La, Pr)*, Physical Review B 87 (2013) Nr. 6, S. 64401/1-11.

246) G. Prando, R. Giraud, S. Aswartham, O. Vakaliuk, M. Abdel-Hafiez, C. Hess, S. Wurmehl, A.U.B. Wolter, B. Buechner, *Evidence for a vortex-glass transition in superconducting Ba.Fe0:9Co0:1/2As2*, Journal of Physics - Condensed Matter 25 (2013) Nr. 50, S. 505701/1-10.

247) G. Prando, S. Sanna, G. Lamura, T. Shiroka, M. Tropeano, A. Palenzona, H.-J. Grafe, B. Buechner, P. Carretta, R. De Renzi, *Phase separation at the magnetic–superconducting transition in La0.7Y0.3FeAs01xFx*, Physica Status Solidi B 250 (2013) Nr. 3, S. 599-602.

248) G. Prando, O. Vakaliuk, S. Sanna, G. Lamura, T. Shiroka, P. Bonfa, P. Carretta, R. De Renzi, H.-H. Klauss, C.G.F. Blum, S. Wurmehl, C. Hess, B. Buechner, *Role of in-plane and out-of-plane dilution in CeFeAs0: Charge doping versus disorder*, Physical Review B 87 (2013) Nr. 17, S. 174519/1-8.

249) I. Presniakov, I. Morozov, A. Sobolev, M. Roslova, A. Boltalin, V. Son, O. Volkova, A. Vasiliev, S. Wurmehl, B. Buechner, *Local structure and hyperfine interactions of 57Fe in NaFeAs studied by Moessbauer spectroscopy*, Journal of Physics - Condensed Matter 25 (2013) Nr. 34, S. 346003/1-12.

250) F. Puoci, S. Hampel, O.I. Parisi, A. Hassan, G. Cirillo, N. Picci, *Imprinted microspheres doped with carbon nanotubes as novel electroresponsive drug-delivery systems*, Journal of Applied Polymer Science 130 (2013) Nr. 2, S. 829-834.

251) L. Rademaker, S. Johnston, J. Zaanen, J. van den Brink, *Determinant quantum Monte Carlo study of exciton condensation in the bilayer Hubbard model*, Physical Review B 88 (2013) Nr. 23, S. 235115/1-9.

252) L. Rademaker, J. van den Brink, H. Hilgenkamp, J. Zaanen, *Enhancement of spin propagation due to interlayer exciton condensation*, Physical Review B 88 (2013) Nr. 12, S. 121101(R)/1-5.

253) L. Rademaker, J. van den Brink, J. Zaanen, H. Hilgenkamp, *Exciton condensation in strongly correlated electron bilayers*, Physical Review B 88 (2013) Nr. 23, S. 235127/1-21.

254) M. Rafique, A. Herklotz, E.-J. Guo, R. Roth, L. Schultz, K. Doerr, S. Manzoor, *Annealing control of magnetic anisotropy and phase separation in CoFe2O4-BaTiO3 nanocomposite films*, Journal of Applied Physics 114 (2013) Nr. 23, S. 233910/1-5.

255) B. Rasche, A. Isaeva, M. Ruck, S. Borisenko, V. Zabolotnyy, B. Buechner, K. Koepernik, C. Ortix, M. Richter, J. van den Brink, *Stacked topological insulator built from bismuth-based graphene sheet analogues*, nature materials 12 (2013), S. 422-425.

256) L. Ratkai, I. Kaban, T. Wagner, J. Kolar, I. Valkova, B. Beuneu, P. Jovari, *Silver environment and covalent network rearrangement in GeS3-Ag glasses*, Journal of Physics - Condensed Matter 25 (2013), S. 454210/1-7.

257) L. Rehm, D. Henrich, M. Hofherr, S. Wuensch, P. Thoma, A. Scheuring, K. Ilin, M. Siegel, S. Haindl, K. Iida, F. Kurth, B. Holzapfel, L. Schultz, *Infrared photo-response of Fe-shunted Ba-122 thin film microstructures*, IEEE Transactions on Applied Superconductivity 23 (2013) Nr. 3, S. 7501105/1-5.

258) L. Reichel, S. Faehler, L. Schultz, K. Leistner, *Initial preorder as condition for L10 ordering in ultrathin CoPt films*, Journal of Applied Physics 114 (2013) Nr. 9, S. 93909/1-6.

259) L. Reichel, S. Oswald, S. Faehler, L. Schultz, K. Leistner, *Electrochemically driven variation of magnetic properties in ultrathin CoPt films*, Journal of Applied Physics 113 (2013), S. 143904/1-7.

260) L. Rettig, R. Cortes, H.S. Jeevan, P. Gegenwart, T. Wolf, J. Fink, U. Bovensiepen, *Electron-phonon coupling in 122 Fe pnictides analyzed by femtosecond time-resolved photoemission*, New Journal of Physics 15 (2013) Nr. 8, S. 83023/1-11.

261) E.D.L. Rienks, T. Wolf, K. Koepernik, I. Avigo, P. Hlawenka, C. Lupulescu, T. Arion, F. Roth, W. Eberhardt, U. Bovensiepen, J. Fink, *Electronic structure and quantum criticality in Ba(Fe1-x-yCoxMny)2As2, an ARPES study*, epl 103 (2013), S. 47004/1-7.

262) T. Ritschel, J. Trinckauf, G. Garbarino, M. Hanfland, M. v. Zimmermann, H. Berger, B. Buechner, J. Geck, *Pressure dependence of the charge density wave in 1T-TaS2 and its relation to superconductivity*, Physical Review B 87 (2013) Nr. 12, S. 125135/1-5.

263) X. Rocquefelte, K. Schwarz, P. Blaha, S. Kumar, J. van den Brink, *Room-temperature spin-spiral multiferroicity in high-pressure cupric oxide*, nature communications 4 (2013), S. 2511/1-7.

264) S. Rodan, A. Alfonsov, M. Belesi, F. Ferraro, J.T. Kohlhepp, H.J.M. Swagten, B. Koopmans, Y. Sakuraba, S. Bosu, K. Takanashi, B. Buechner, S. Wurmehl, *Nuclear magnetic resonance reveals structural evolution upon annealing in epitaxial Co2MnSi Heusler films*, Applied Physics Letters 102 (2013), S. 242404/1-4.

265) J. Romberg, J. Freudenberger, J. Scharnweber, U. Gaitzsch, T. Marr, A. Eschke, U. Kuehn, C.-G. Oertel, I. Okulov, R. Petters, W. Skrotzki, J. Eckert, L. Schultz, *Metallographic preparation of Aluminium-Titanium composites*, Praktische Metallographie 50 (2013) Nr. 11, S. 739-753.

266) J. Romberg, C. Huerrich, M. Poetschke, S. Kauffmann-Weiss, U. Gaitzsch, S. Roth, P. Muellner, L. Schultz, *Geometric factors on magnetically driven actuation behaviour for polycrystalline Ni–Mn–Ga and its composites*, Journal of Alloys and Compounds 577S (2013), S. S344-S347.

267) M.V. Roslova, O.I. Lebedev, I.V. Morozov, S. Aswartham, S. Wurmehl, B. Buechner, A.V. Shevelkov, *Diversity of microstructural phenomena in superconducting and non-superconducting RbxFe2-ySe2: A transmission electron microscopy study at the atomic scale*, Inorganic Chemistry 52 (2013), S. 14419-14427.

268) F. Roth, P. Cudazzo, B. Mahns, M. Gatti, J. Bauer, S. Hampel, M. Nohr, H. Berger, M. Knupfer, A. Rubio, *Loss spectroscopy of molecular solids: combining experiment and theory*, New Journal of Physics 15 (2013) Nr. 12, S. 125024/1-18.

269) F. Roth, A. Koenig, C. Kramberger, T. Pichler, B. Buechner, M. Knupfer, *Challenging the nature of low-energy plasmon excitations in CaC6 using electron energy-loss spectroscopy*, epl 102 (2013), S. 17001/1-6.

270) F. Roth, B. Mahns, S. Hampel, M. Nohr, H. Berger, B. Buechner, M. Knupfer, *Exciton properties of selected aromatic hydrocarbon systems*, The European Physical Journal B 86 (2013) Nr. 66, S. 1-5.

271) F. Roth, E. Mueller, B. Rellinghaus, B. Buechner, M. Knupfer, *Electronic excitation spectrum of calcium-doped picene: Electron energy-loss spectroscopy study*, Physical Review B 88 (2013) Nr. 20, S. 205105/1-5.

272) S.A. Rounaghi, H. Eshghi, A.R. Kiani Rashid, J. Vahdati Khaki, M. Samadi Khoshkhoo, S. Scudino, J. Eckert, *Synthesis of nanostructured AlN by solid state reaction of Al and diaminomaleonitrile*, Journal of Solid State Chemistry 198 (2013), S. 542-547.

273) I. Rousochatzakis, R. Moessner, J. van den Brink, *Frustrated magnetism and resonating valence bond physics in two-dimensional kagome-like magnets*, Physical Review B 88 (2013) Nr. 19, S. 195109/1-11.

274) C. Rudisch, H.-J. Grafe, J. Geck, S. Partzsch, M. v. Zimmermann, N. Wizent, R. Klingeler, B. Buechner, *Coupling of Li motion and structural distortions in olivine LiMnPO4 from 7Li and 31P NMR*, Physical Review B 88 (2013) Nr. 5, S. 54303/1-9.

275) M.H. Ruemmeli, S. Gorantla, A. Bachmatiuk, J. Phieler, N. Geissler, I. Ibrahim, J. Pang, J. Eckert, *On the role of vapor trapping for Chemical Vapor Deposition (CVD) grown graphene over copper*, Chemistry of Materials 25 (2013), S. 4861-4866.

276) M.H. Ruemmeli, M. Zeng, S. Melkhanova, S. Gorantla, A. Bachmatiuk, L. Fu, C. Yan, S. Oswald, R.G. Mendes, D. Makarov, O. Schmidt, J. Eckert, *Insights into the early growth of homogeneous single-layer graphene over Ni-Mo binary substrates*, Chemistry of Materials 25 (2013), S. 3880-3887.

277) S.F. Rus, A. Herklotz, R. Roth, L. Schultz, K. Doerr, *Thickness dependence of the magnetoelastic effect of CoFe2O4 films grown on piezoelectric substrates*, Journal of Applied Physics 114 (2013), S. 43913/1-5.

278) F.N. Rybakov, A.B. Borisov, A.N. Bogdanov, *Three-dimensional skyrmion states in thin films of cubic helimagnets*, Physical Review B 87 (2013) Nr. 9, S. 94424/1-4.

279) K. Sakaushi, E. Hosono, G. Nickerl, T. Gemming, H. Zhou, S. Kaskel, J. Eckert, *Aromatic porous-honeycomb electrodes for a sodium-organic energy storage device*, nature communications 4 (2013), S. 1485/1-7.

280) K. Sakaushi, G. Nickerl, H.C. Kandpal, L. Cano-Cortes, T. Gemming, J. Eckert, S. Kaskel, J. van den Brink, *Polymeric frameworks as organic semiconductors with controlled electronic properties*, The Journal of Physical Chemistry Letters 4 (2013), S. 2977-2981.

281) K. Sakaushi, J. Thomas, S. Kaskel, J. Eckert, *Aqueous solution process for the synthesis and assembly of nanostructured one-dimensional alpha-MoO3 electrode materials*, Chemistry of Materials 25 (2013), S. 2557-2563.

282) M. Samadi Khoshkhoo, S. Scudino, J. Thomas, T. Gemming, H. Wendrock, J. Eckert, *Size evaluation of nanostructured materials*, Materials Letters 108 (2013), S. 343-345.

283) S. Sawatzki, I. Dirba, L. Schultz, O. Gutfleisch, *Electrical and magnetic properties of hot-deformed Nd-Fe-B magnets with different DyF3 additions*, Journal of Applied Physics 114 (2013) Nr. 13, S. 133902/1-5.

284) M. Schaepers, A.U.B. Wolter, S.-L. Drechsler, S. Nishimoto, K.-H. Mueller, M. Abdel-Hafiez, W. Schottenhamel, B. Buechner, J. Richter, B. Ouladdiaf, M. Uhlarz, R. Beyer, Y. Skourski, J. Wosnitza, K.C. Rule, H. Ryll, B. Klemke, K. Kiefer, M. Reehuis, B. Willenberg, S. Suellow, *Thermodynamic properties of the anisotropic frustrated spin-chain compound linarite PbCuSO4(OH)2*, Physical Review B 88 (2013) Nr. 18, S. 184410/1-17.

285) M. Scheffler, L. Smykalla, D. Baumann, R. Schlegel, T. Haenke, M. Toader, B. Buechner, M. Hietschold, C. Hess, *Structural study of monolayer cobalt phthalocyanine adsorbed on graphite*, Surface Science 608 (2013), S. 55-60.

286) S. Scheinert, M. Grobosch, J. Sprogies, I. Hoerselmann, M. Knupfer, G. Paasch, *Organic [6,6] -phenyl-C61-butyric-acid-methyl-ester field effect transistors: Analysis of the contact properties by combined photoemission spectroscopy and electrical measurements*, Journal of Applied Physics 113 (2013) Nr. 17, S. 174504/1-10.

287) A. Scheuring, P. Thoma, J. Day, K. Il'in, J. Haenisch, B. Holzapfel, M. Siegel, *Thin Pr-Ba-Cu-O film antenna-coupled THz bolometers for room temperature operation*, IEEE Transactions on Terahertz Science and Technology 3 (2013), S. 103-109.

288) H. Schloerb, M. Uhlemann, V. Haehnel, D. Iselt, A. Gebert, *Electrodeposition of Fe-based magnetic alloy nanowires*, Zeitschrift fuer Physikalische Chemie 227 (2013), S. 1071-1082.

289) H. Schmidt, S. Habicht, S. Feste, A.-D. Mueller, O.G. Schmidt, *Kelvin probe force microscopy for characterizing doped semiconductors for future sensor applications in nano- and biotechnology*, Applied Surface Science 281 (2013), S. 24-29.

290) S. Schmidt, S. Doering, F. Schmidl, V. Tympel, S. Haindl, K. Iida, F. Kurth, B. Holzapfel, P. Seidel, *Bicrystalline grain boundary and hybrid sns junctions based on Ba-122 thin films*, IEEE Transactions on Applied Superconductivity 23 (2013) Nr. 3, S. 7300104/1-4.

291) S. Schmitz, W. Loeser, H. Klauss, C. Mickel, B. Buechner, *Effects of Re microalloying on glass formation and mechanical properties of Zr-Cu-Al alloys*, Philosophical Magazine 93 (2013) Nr. 7, S. 847-857.

292) R. Schoenfelder, F. Aviles, M. Knupfer, J.A. Azamar-Barrios, P.I. Gonzalez-Chi, M.H. Ruemmeli, *Influence of architecture on the raman spectra of acid-treated carbon nanostructures*, Journal of Experimental Nanoscience online first (2013).

293) B. Schwarz, N. Mattern, O. Shuleshova, J. Eckert, *Liquid- liquid demixing and microstructure of CoeCueZr alloys with low Zr content*, Intermetallics 32 (2013), S. 250-258.

294) S. Scudino, J.Y. Kim, K.G. Prashanth, M.H. Lee, B.S. Kim, U. Kuehn, J. Eckert, *Production of customized hybrid porous structures by powder metallurgy of Ni59Zr20Ti16Si2Sn3 glassy powders*, Journal of Materials Research 28 (2013) Nr. 17, S. 2490-2498.

295) M. Seifert, L. Schultz, R. Schaefer, V. Neu, S. Hankemeier, S. Roessler, R. Froemter, H.P. Oepen, *Domain evolution during the spin-reorientation transition in epitaxial NdCo5 thin films*, New Journal of Physics 15 (2013) Nr. 1, S. 13019/1-12.

296) A. Seifoddini, M. Stoica, M. Nili-Ahmadabadi, S. Heshmati-Manesh, U. Kuehn, J. Eckert, *New (Fe0.9Ni0.1)77Mo5P9C7.5B1.5 glassy alloys with enhanced glass-forming ability and large compressive strain*, Materials Science and Engineering A 560 (2013), S. 575-582.

297) H. Shiozawa, A. Bachmatiuk, A. Stangl, D.C. Cox, S.R.P. Silva, M.H. Ruemmeli, T. Pichler, *Microscopic insight into the bilateral formation of carbon spirals from a symmetric iron core*, Scientific Reports 3 (2013), S. 1840/1-7.

298) Y. Shuai, X. Ou, W. Luo, A. Muecklich, D. Buerger, S. Zhou, C. Wu, Y. Chen, W. Zhang, M. Helm, T. Mikolajick, O.G. Schmidt, H. Schmidt, *Key concepts behind forming-free resistive switching incorporated with rectifying transport properties*, Scientific Reports 3 (2013), S. 2208/1-6.

299) W. Si, C. Yan, Y. Chen, S. Oswald, L. Han, O.G. Schmidt, *On chip, all solid-state and flexible micro-supercapacitors with high performance based on MnOx/Au multilayers*, Energy and Environmental Science 6 (2013), S. 3218-3223.

300) P.F. Siles, M. de Pauli, C.C. Bof Bufon, S. O Ferreira, J. Bettini, O.G. Schmidt, A. Malachias, *Tuning resistive switching on single-pulse doped multilayer memristors*, Nanotechnology 24 (2013) Nr. 3, S. 35702/1-8.

301) G. Simutis, S. Gvasaliya, M. Mansson, A.L. Chernyshev, A. Mohan, S. Singh, C. Hess, A.T. Savici, A.I. Kolesnikov, A. Piovano, T. Perring, I. Zaliznyak, B. Buechner, A. Zheludev, *Spin pseudogap in Ni-doped SrCu02*, Physical Review Letters 111 (2013), S. 67204/1-5.

302) K. Sitarama Raju, V. Subramanya Sarma, A. Kauffmann, Z. Hegedus, J. Gubicza, M. Peterlechner, J. Freudenberger, G. Wilde, *High strength and ductile ultrafine-grained Cu-Ag alloy through bimodal grain size, dislocation density and solute distribution*, Acta Materialia 61 (2013) Nr. 1, S. 228-238.

303) Y. Skourski, J. Bartolome, M.D. Kuzmin, K.P. Skokov, M. Bonilla, O. Gutfleisch, J. Wosnitza, *High-field transitions in ErFe11Ti and HoFe11Ti single crystals*, Journal of Low Temperature Physics 170 (2013), S. 307-312.

304) E.P. Smirnova, A.V. Sotnikov, H. Schmidt, M. Weihnacht, *Temperature dependence of the elastic moduli of multiferroic PbFe2/3W1/3O3 ceramics*, Technical Physics Letters 39 (2013) Nr. 3, S. 277-279.

305) L. Soler, V. Magdanz, V.M. Fomin, S. Sanche, O.G. Schmidt, *Self-propelled micromotors for cleaning polluted water*, ACS nano 7 (2013) Nr. 11, S. 9611-9620.

306) L. Soler, C. Martínez-Cisneros, A. Swiersy, S. Sanchez, O.G. Schmidt, *Thermal activation of catalytic microjets in blood samples using microfluidic chips*, Lab on a Chip 13 (2013), S. 4299-4303.

307) A. Solovev, S. Sanchez, O.G. Schmidt, *Collective behaviour of self-propelled catalytic micromotors*, Nanoscale 5 (2013) Nr. 4, S. 1284-1293.

308) K.K. Song, S. Pauly, B.A. Sun, J. Tan, M. Stoica, U. Kuehn, J. Eckert, *Correlation between the microstructures and the deformation mechanisms of CuZr based bulk metallic glass composites*, AIP Advances 3 (2013), S. 12116/1-8.

309) K.K. Song, S. Pauly, Z. Wang, U. Kuehn, J. Eckert, *Effect of TaW particles on the microstructure and mechanical properties of metastable Cu47.5Zr47.5Al5 alloys*, Materials Science and Engineering A 587 (2013), S. 372-380.

310) K.K. Song, S. Pauly, Y. Zhang, B.A. Sun, J. He, G.Z. Ma, U. Kuehn, J. Eckert, *Thermal stability and mechanical properties of Cu46Zr46Ag8 bulk metallic glass and its composites*, Materials Science and Engineering A 559 (2013), S. 711-718.

311) M. Spindler, B. Uhlig, S.B. Menzel, C. Huck, T. Gemming, J. Eckert, *Local temperature determination in power loaded surface acoustic wave structures using Raman spectroscopy*, Journal of Applied Physics 114 (2013), S. 164317/1-5.

312) U.G. Spizzirri, S. Hampel, G. Cirillo, F.P. Nicoletta, A. Hassan, O. Vittorio, N. Picci, F. Iemma, *Spherical gelatin/ CNTs hybrid microgels as electro-responsive drug delivery systems*, International Journal of Pharmaceutics 448 (2013), S. 115-122.

313) V.C. Srivastava, K.B. Surreddi, S. Scudino, M. Schowalter, V. Uhlenwinkel, A. Schulz, J. Eckert, A. Rosenauer, H.-W. Zoch, *Microstructural characteristics of spray formed and heat treated Al–(Y, La)-Ni-Co system*, Journal of Alloys and Compounds 578 (2013), S. 471-480.

314) R. Streubel, D. Koehler, R. Schaefer, L.M. Eng, *Strain-mediated elastic coupling in magnetoelectric nickel/barium-titanate heterostructures*, Physical Review B 87 (2013) Nr. 5, S. 54410/1-6.

315) R. Streubel, D. Makarov, J. Lee, C. Mueller, M. Melzer, R. Schaefer, *Rolled-up permalloy nanomembranes with multiple windings*, SPIN 3 (2013) Nr. 3, S. 1340001/1-7.

316) S. Stute, L. Goetzke, D. Meyer, M.L. Merroun, P. Rapta, O. Kataeva, W. Seichter, K. Gloe, L. Dunsch, K. Gloe, *Molecular structure, UV/Vis spectra, and cyclic voltammograms of Mn(II), Co(II), and Zn(II) 5,10,15,20-Tetraphenyl-21-oxaporphyrins*, Inorganic Chemistry 52 (2013), S. 1515-1524.

317) R. Sueptitz, P. Dunne, K. Tschulik, M. Uhlemann, J. Eckert, A. Gebert, *Electrochemical micromachining of passive electrodes*, Electrochimica Acta 109 (2013), S. 562-569.

318) R. Sueptitz, S. Sawatzki, M. Moore, M. Uhlemann, O. Gutfleisch, A. Gebert, *Effect of DyF3 on the corrosion behavior of hot-pressed Nd-Fe-B permanent magnets*, Materials and Corrosion online first (2013).

319) R. Sueptitz, K. Tschulik, M. Uhlemann, J. Eckert, A. Gebert, *Retarding the corrosion of iron by inhomogeneous magnetic fields*, Materials and Corrosion 63 (2013) Nr. online first.

320) B.A. Sun, S. Pauly, J. Hu, W.H. Wang, U. Kuehn, J. Eckert, *Origin of intermittent plastic flow and instability of shear band sliding in bulk metallic glasses*, Physical Review Letters 110 (2013) Nr. 22, S. 225501/1-5.

321) A.L. Svitova, A.A. Popov, L. Dunsch, *Gd-Sc-based mixed-metal nitride cluster fullerenes: Mutual influence of the cage and cluster size and the role of scandium in the electronic structure*, Inorganic Chemistry 52 (2013), S. 3368-3380.

322) S. Sykora, K.W. Becker, *Heavy fermion properties of the Kondo Lattice model*, Scientific Reports 3 (2013), S. 2691/1-6.

323) A.H. Taghvaei, M. Stoica, F. Mazaleyrat, K.G. Prashanth, M. Samadi Khoshkhoo, K. Janghorban, J. Eckert, *Microstructure and magnetic properties of soft magnetic composites based on silicon resin coated Co40Fe22Ta8B30 glassy powders*, Intermetallics 43 (2013), S. 1-7.

324) A.H. Taghvaei, M. Stoica, K.G. Prashanth, J. Eckert, *Fabrication and characterization of bulk glassy Co40Fe22Ta8B30 alloy with high thermal stability and excellent soft magnetic properties*, Acta Materialia 61 (2013), S. 6609-6621.

325) A.M. Taghvaei, M. Stoica, M.S. Khoshkhoo, I. Kaban, J. Bednarcik, P. Jovari, K. Janghorban, J. Eckert, *DSC, XRD and TEM characterization of glassy Co40Fe22Ta8B30 alloy with very high thermal stability*, Materials Letters 93 (2013), S. 322-325.

326) Y. Talanov, N. Beisengulov, G. Kornilov, T. Shaposhnikova, E. Vavilova, C. Nacke, S. Wurmehl, N. Panarina, C. Hess, V. Kataev, B. Buechner, *Microwave absorption study of pinning regimes in Ba.(Fe1-xCox)2As2 single crystals*, Superconductor Science and Technology 26 (2013) Nr. 4, S. 45015/1-7.

327) J. Tan, F.S. Pan, C.J. Li, J.F. Wang, J. Eckert, *Effect of Fe on crystallization process of Zr-Co-Al-(Fe) bulk metallic glasses*, Materials Science Forum 745-746 (2013), S. 734-739.

328) S.V. Taskaev, V.D. Buchelnikov, A.P. Pellenen, M.D. Kuzmin, K.P. Skokov, D.Y. Karpenkov, D.S. Bataev, O.G. Gutfleisch, *Influence of thermal treatment on magnetocaloric properties of Gd cold rolled ribbons*, Journal of Applied Physics 113 (2013) Nr. 17, S. 17A933/1-3.

329) S.V. Taskaev, M.D. Kuzmin, K.P. Skokov, D.Y. Karpenkov, A.P. Pellenen, V.D. Buchelnikov, O. Gutfleisch, *Giant induced anisotropy ruins the magnetocaloric effect in gadolinium*, Journal of Magnetism and Magnetic Materials 331 (2013), S. 33-36.

330) M. Taut, K. Koepernik, M. Richter, *Electronic structure of stacking faults in hexagonal graphite*, Physical Review B 88 (2013) Nr. 20, S. 205411/1-10.

331) S. Thirupathaiah1, T. Stuerzer, V.B. Zabolotnyy, D. Johrendt, B. Buechner, S.V. Borisenko, *Why T c of (CaFeAs) 10 Pt 3.58 As 8 is twice as high as (CaFe 0.95 Pt 0.05 As) 10 Pt 3 As 8*, Physical Review B 88 (2013) Nr. 14, S. 140505(R)/1-5.

332) D. Thomas, M. Abdel-Hafiez, T. Gruber, R. Huettl, J. Seidel, A.U.B. Wolter, B. Buechner, J. Kortus, F. Mertens, *The heat capacity and entropy of lithium silicides over the temperature range from (2 to 873) K*, The Journal of Chemical Thermodynamics 64 (2013), S. 205-225.

333) J. Thomas, J. Ramm, T. Gemming, *Density measurement of thin layers by electron energy loss spectroscopy (EELS)*, Micron 50 (2013), S. 57-61.

334) F. Thoss, L. Giebeler, J. Thomas, S. Oswald, K. Potzger, H. Reuther, H. Ehrenberg, J. Eckert, *Amorphous Li-Al-based compounds: A novel approach for designing high performance electrode materials for Li-Ion batteries*, Inorganics 1 (2013), S. 14-31.

335) Y.Z. Tian, J. Freudenberger, R. Pippan, Z.F. Zhang, *Formation of nanostructure and abnormal annealing behavior of a Cu–Ag–Zr alloy processed by high-pressuretorsion*, Materials Science and Engineering A 568 (2013), S. 184-194.

336) J. Torrens-Serra, P. Bruna, M. Stoica, S. Roth, J. Eckert, *Glass forming ability, thermal stability, crystallization and magnetic properties of [(Fe,Co,Ni)0.75Si0.05B0.20]95Nb4Zr1 metallic glasses*, Journal of Non-Crystalline Solids 367 (2013), S. 30-36.

337) J. Torrens-Serra, M. Stoica, J. Bednarcik, J. Eckert, S. Kustov, *Elastic and anelastic properties close to the curie temperature of Fe-based bulk metallic glass*, Applied Physics Letters 102 (2013) Nr. 4, S. 41904/1-4.

338) R. Trotta, E. Zallo, E. Magerl, O.G. Schmidt, A. Rastelli, *Independent control of exciton and biexciton energies in single quantum dots via electroelastic fields*, Physical Review B 88 (2013) Nr. 15, S. 155312/1-5.

339) S. Tsuchiya, R. Ganesh, T. Nikuni, *Higgs mode in a superfluid of Dirac fermions*, Physical Review B 88 (2013) Nr. 1, S. 14527/1-8.

340) M. Uhlemann, K. Tschulik, A. Gebert, G. Mutschke, J. Froehlich, A. Bund, X. Yang, K. Eckert, *Structured electrodeposition in magnetic gradient fields*, The European Physical Journal - Special Topics 220 (2013) Nr. 1, S. 287-302.

341) A.N. Vasiliev, T.M. Vasilchikova, O.S. Volkova, A.A. Kamenev, A.R. Kaul, T.G. Kuzmova1, D.M. Tsymbarenko, K.A. Lomachenko, A.V. Soldatov, S.V. Streltsov, J.-Y. Lin, C.-N. Kao, J.-M. Chen, M. Abdel-Hafiez, A. Wolter, R. Klingeler, *Spin-State Transition, Magnetism and Local Crystal Structure in Eu1-xCaxCoO3-delta*, Journal of the Physical Society of Japan 82 (2013) Nr. 4, S. 44714/1-8.

342) F. Virot, R. Hayn, M. Richter, J. van den Brink, *Engineering topological surface states: HgS, HgSe, and HgTe*, Physical Review Letters 111 (2013) Nr. 14, S. 146803/1-5.

343) D. Wadewitz, W. Gruner, M. Herklotz, M. Klose, L. Giebeler, A. Voss, J. Thomas, T. Gemming, J. Eckert, H. Ehrenberg, *Investigation of copper-cobalt-oxides as model systems for composite interactions in conversion-type electrodes for Lithium-Ion batteries*, Journal of the Electrochemical Society 160 (2013) Nr. 8, S. A1333-A1339.

344) J. Wang, M. Zeng, L. Tan, B. Dai, Y. Deng, M. Ruemmeli, H. Xu, Z. Li, S. Wang, L. Peng, J. Eckert, L. Fu, *High-mobility graphene on liquid p-block elements by ultra-low-loss CVD growth*, Scientific Reports 3 (2013), S. 2670/1-7.

345) M. Wang, L. Fu, L. Gan, C. Zhang, M. Ruemmeli, A. Bachmatiuk, K. Huang, Y. Fang, Z. Liu, *CVD Growth of large area smooth-edged graphene nanomesh by nanosphere lithography*, Scientific Reports 3:1238 (2013), S. 1-6.

346) X. Wang, S. Scudino, J. Eckert, *Production and characterization of Al 2024 matrix composites reinforced with beta-Al3Mg2 complex metallic alloy particles*, Materials Research Society Symposium, in: MRS Proceedings, **1517**, 1-11 (2013).

347) Y. Wang, A. Kreisel, V.B. Zabolotnyy, S.V. Borisenko, B. Buechner, T.A. Maier, P.J. Hirschfeld, D.J. Scalapino, *Superconducting gap in LiFeAs from three-dimensional spin-fluctuation pairing calculations*, Physical Review B 88 (2013) Nr. 17, S. 174516/1-12.

348) A. Waske, B. Schwarz, N. Mattern, J. Eckert, *Magnetocaloric (Fe–B)-based amorphous alloys*, Journal of Magnetism and Magnetic Materials 329 (2013), S. 101-104.

349) S. Wei, F. Yang, J. Bednarcik, I. Kaban, A. Meyer, R. Busch, *Polyamorphous transformation in bulk metallic glassforming liquid and its implication to strong liquids*, in: AIP Conference Proceedings, **1518**, 260-265 (2013).

350) S. Wei, F. Yang, J. Bednarcik, I. Kaban, O. Shuleshova, A. Meyer, R. Busch, *Liquid-liquid transition in a strong bulk metallic glass-forming liquid*, nature communications 4 (2013), S. 2083/1-9.

351) S. Wicht, V. Neu, L. Schultz, D. Weller, O. Mosendz, G. Parker, S. Pisana, B. Rellinghaus, *Atomic resolution structure-property relation in highly anisotropic granular FePt-C films with near-Stoner-Wohlfarth behaviour*, Journal of Applied Physics 114 (2013), S. 63906/1-8.

352) M.N. Wilson, E.A. Karhu, D.P. Lake, A.S. Quigley, S. Meynell, A.N. Bogdanov, H. Fritzsche, U.K. Roessler, T.L. Monchesky, *Discrete helicoidal states in chiral magnetic thin films*, Physical Review B 88 (2013) Nr. 21, S. 214420/1-6.

353) K. Wohlfeld, S. Nishimoto, M.H. Haverkort, J. van den Brink, *Microscopic origin of spin-orbital separation in Sr 2 CuO 3*, Physical Review B 88 (2013) Nr. 19, S. 195138/1-21.

354) W.B. Wu, N. Hiraoka, D.J. Huang, S.W. Huang, K.D. Tsuei, M. van Veenendaal, J. van den Brink, Y. Sekio, T. Kimura, *Effective orbital symmetry of CuO: Examination by nonresonant inelastic X-ray scattering*, Physical Review B 88 (2013) Nr. 20, S. 205129/1-6.
355) S. Wurmehl, A. Alfonsov, J.T. Kohlhepp, H.J.M. Swagten, B. Koopmans, M. Wojcik, B. Balke, V. Ksenofontov, C.G.F. Blum, B. Buechner, *55 Mn NMR study of quaternary half-metallic ferromagnetic Co2Mn1-xFexSi Heusler compounds*, Physical Review B 88 (2013) Nr. 13, S. 134424/1-8.
356) W. Xi, A. Solovev, A.N. Ananth, D.H. Gracias, S. Sanchez, O.G. Schmidt, *Rolled-up magnetic microdrillers: Towards remotely controlled minimally invasive surgery*, Nanoscale 5 (2013) Nr. 4, S. 1294-1297.
357) X. Xi, Y.M. Dai, C.C. Homes, M. Kidszun, S. Haindl, G.L. Carr, *Evidence of a full gap in LaFeAsO1-xFx thin films from infrared spectroscopy*, Physical Review B 87 (2013) Nr. 18, S. 180509/1-5.
358) Xu, N., P. Richard, X.-P. Wang, X. Shi, A. van Roekeghem, T. Qian, E. Ieki, K. Nakayama, T. Sato, E. Rienks, S. Thirupathaiah, J. Xing, H.-H. Wen, M. Shi, T. Takahashi, H. Ding, *Angle-resolved photoemission observation of isotropic superconducting gaps in isovalent Ru-substituted Ba(Fe 0.75 Ru 0.25) 2 As 2*, Physical Review B 87 (2013) Nr. 9, S. 94513/1-5.
359) W. Xu, D.P. Edwards, X. Wu, M. Stoica, M. Calin, U. Kuehn, J. Eckert, K. Xia, *Promoting nano/ultrafine-duplex structure via accelerated alpha precipitation in a beta-type titanium alloy severely deformed by high-pressure torsion*, Scripta Materialia 68 (2013) Nr. 1, S. 67-70.
360) C. Yan, W. Xi, W. Si, J. Deng, O.G. Schmidt, *Highly conductive and strain-released hybrid multilayer Ge/Ti nanomembranes with enhanced lithium-ion-storage capability*, Advanced Materials 25 (2013) Nr. 4, S. 539-544.
361) Z. Yan, W. Hao, Y. Hu, K. Song, M. Stoica, S. Scudino, J. Eckert, *Evidence for viscous flow nature in Zr60Al15Ni25 metallic glass subjected to cold rolling*, Applied Physics Letters 103 (2013), S. 21907/1-5.
362) L. Yang, S. Wang, J. Mao, J. Deng, Q. Gao, Y. Tang, O.G. Schmidt, *Hierarchical MoS 2 /polyaniline nanowires with excellent electrochemical performance for lithium-ion batteries*, Advanced Materials 25 (2013) Nr. 8, S. 1180-1184.
363) L. Yu, N. Brun, K. Sakaushi, J. Eckert, M.M. Titirici, *Hydrothermal nanocasting: Synthesis of hierarchically porous carbon monoliths and their application in lithium–sulfur batteries*, Carbon 61 (2013), S. 245-253.
364) Y. Yu, C. Yan, L. Gu, X. Lang, K. Tang, L. Zhang, Y. Hou, Z. Wang, M.W. Chen, O.G. Schmidt, J. Maier, *Three-dimensional (3D) bicontinuous Au/Amorphous-Ge thin films as fast and high-capacity anodes for lithium-ion batteries*, Advanced Energy Materials 3 (2013) Nr. 3, S. 281-285.
365) G.S. Zakharova, C. Taeschner, T. Kolb, C. Jaehne, A. Leonhardt, B. Buechner, R. Klingeler, *Morphology controlled NH4V3O8 microcrystals by hydrothermal synthesis*, Dalton Transactions 42 (2013), S. 4897-4902.
366) S. Zapf, B. Gorshunov, D. Wu, E. Zhukova, V.S. Nozdrin, S. Haindl, K. Iida, M. Dressel, *Intra-gap absorption in superconducting Ba(Fe1-xCox)2As2 thin films studied by a Fabry–Perot resonant technique*, Journal of Superconductivity and Novel Magnetism 26 (2013) Nr. 4, S. 1227-1231.
367) R. Zaripov, E. Vavilova, V. Miluykov, I. Bezkishko, O. Sinyashin, K. Salikhov, V. Kataev, B. Buechner, *Boosting the electron spin coherence in binuclear Mn complexes by multiple microwave pulses*, Physical Review B 88 (2013) Nr. 9, S. 94418/1-8.
368) J. Zhang, F. Ding, E. Zallo, R. Trotta, B. Hoefer, L. Han, S. Kumar, Y. Huo, A. Rastelli, O.G. Schmidt, *A nanomembrane-based wave length-tunable high-speed single-photon-emitting diode*, Nano letters 13 (2013), S. 5808-5813.
369) J.J. Zhang, A. Rastelli, O.G. Schmidt, D. Scopece, L. Miglio, F. Montalenti, *Self-organized evolution of Ge/Si(001) into intersecting bundles of horizontal nanowires during annealing*, Applied Physics Letters 103 (2013) Nr. 8, S. 83109/1-5.
370) J.J. Zhang, O.G. Schmidt, *Strain-induced self-assembly of Ge nanodashes, nanodumbbells, and dot chains on Si(001)*, Applied Physics Letters 103 (2013) Nr. 14, S. 143112/1-5.
371) Y. Zhang, N. Mattern, J. Eckert, *Strong correlation of atomic thermal motion in the first coordination shell of a Cu-Zr metallic glass*, Applied Physics Letters 102 (2013) Nr. 8, S. 81901/1-4.
372) Y. Zhang, S. Schiemenz, A.A. Popov, L. Dunsch, *Strain-driven endohedral redox couple CeIV/CeIII in nitride clusterfullerenes CeM2N@C80 (M = Sc, Y, Lu)*, Journal of Physical Chemistry Letters 4 (2013), S. 2404-2409.
373) G. Zhao, S. Sanchez, O.G. Schmidt, M. Pumera, *Poisoning of bubble propelled catalytic micromotors: The chemical environment matters*, Nanoscale 5 (2013), S. 2909-2914.
374) G. Zhao, H. Wang, S. Sanchez, O.G. Schmidt, M. Pumera, *Artificial micro-cinderella based on self-propelled micromagnets for the active separation of paramagnetic particles*, Chemical Communications 49 (2013) Nr. 45, S. 5147-5149.
375) H.L. Zhen, G.S. Huang, S. Kiravittaya, S.L. Li, Ch. Deneke, D.J. Thurmer, Y.F. Mei, O.G. Schmidt, W. Lu, *Light-emitting properties of a strain-tuned microtube containing coupled quantum wells*, Applied Physics Letters 102 (2013) Nr. 4, S. 41109/1-5.
376) K.-J. Zhou, Y.-B. Huang, C. Monney, X. Dai, V.N. Strocov, N.-L. Wang, Z.-G. Chen, C. Zhang, P. Dai, L. Patthey, J. van den Brink, H. Ding, T. Schmitt, *Persistent high-energy spin excitations in iron-pnictide superconductors*, nature communications 4 (2013), S. 1470/1-6.
377) P. Zhu, J. Cao, Y. Zhu, J. Geck, Y. Hidaka, S. Pjerov, T. Ritschel, H. Berger, Y. Shen, R. Tobey, J.P. Hill, X.J. Wang, *Dynamic separation of electron excitation and lattice heating during the photoinduced melting of the periodic lattice distortion in 2H-TaSe2*, Applied Physics Letters 103 (2013), S. 71914/1-5.
378) K. Zhuravleva, M. Boenisch, K.G. Prashanth, U. Hempel, A. Helth, T. Gemming, M. Calin, S. Scudino, L. Schultz, J. Eckert, A. Gebert, *Production of porous beta-type Ti-40Nb alloy for biomedical applications: Comparison of selective laser melting and hot pressing*, materials 6 (2013), S. 5700-5712.

379) K. Zhuravleva, A. Chivu, A. Teresiak, S. Scudino, M. Calin, L. Schultz, J. Eckert, A. Gebert, *Porous low modulus Ti40Nb compacts with electrodeposited hydroxyapatite coating for biomedical applications*, Materials Science and Engineering C 33 (2013) Nr. 4, S. 2280-2287.

380) K. Zhuravleva, S. Scudino, M.S. Khoshkhoo, A. Gebert, M. Calin, L. Schultz, J. Eckert, *Mechanical alloying of beta- Type Ti-Nb for biomedical applications*, Advanced Engineering Materials 15 (2013) Nr. 4, S. 262-268.

Contributions to Conference proceedings and monographs

1) S.V. Biryukov, H. Schmidt, M. Weihnacht, *Resonance properties of APTUDT on SAW vs. Electrode track apertures*, 2013 Joint UFFC, EFTF and PFM Symposium; IEEE International Ultrasonics Symposium, in: Proceedings, 1073-1076 (2013).
2) A.N. Darinskii, M. Weihnacht, H. Schmidt, *SAW resonance excitation of acoustic strip waveguide modes*, 2013 Joint UFFC, EFTF and PFM Symposium; IEEE International Ultrasonics Symposium, in: Proceedings, 1065-1068 (2013).
3) G. Doerfel, R. Tobies, *Elektronenroehrenforschung nach 1945- Telefunkenforscher in Ost und West und das Scheitern des Konzepts der „Gnom-Roehren" in Erfurt*, in: Physik im Kalten Krieg; Beitraege zur Physikgeschichte waehrend des Ost-West-Konflikts, Springer Spektrum, 2013, Christian Forstner ; Dieter Hoffmann (Hrsg.) , 91-112 (2013).
4) M.S. Khatri, H. Schloerb, S. Faehler, L. Schultz, *Ageing effect of the electrolyte on structure and magnetic properties of Co-rich Co-Pt films*, International Conference on Recent Trends in Applied Physics and Material Science (RAM), 1.-2.2.13, Bikaner/ India, in: AIP Conference Proceedings, 1536, 1246 (2013).
5) A. Sotnikov, H. Schmidt, M. Weihnacht, O. Buzanov, S. Sakharov, *Material parameters of Ca3TaGa3Si2O14 single crystal revisited*, 2013 Joint UFFC, EFTF and PFM Symposium; IEEE International Ultrasonics Symposium, in: Proceedings, 1488-1491 (2013).
6) J. Tan, C.J. Li, Y.H. Jiang, R. Zhou, J. Eckert, *Correlation between internal states and strength in bulk metallic glasses*, Pacific Rim International Congress on Advanced Materials and Processing (PRICM-8), Waikaloa, Hawaii/ USA, 4.-9.8.13, in: Proceedings, Fernand Marquis (Ed.), 3199- (2013).
7) X. Wang, S. Scudino, J. Eckert, *Production and characterization of Al 2024 matrix composites reinforced with beta-Al3Mg2 complex metallic alloy particles*, Materials Research Society Symposium, in: MRS Proceedings, 1517, 1-11 (2013).
8) S. Wei, F. Yang, J. Bednarcik, I. Kaban, A. Meyer, R. Busch, *Polyamorphous transformation in bulk metallic glassforming liquid and its implication to strong liquids*, in: AIP Conference Proceedings, 1518, 260-265 (2013).
9) S. Wurmehl, J.T. Kohlhepp, *Local structure of highly spin polarized Heusler compounds revealed by nuclear magnetic resonance spectroscopy*, in: Spintronics, G.H. Fecher ; C. Felser (eds.), Dordrecht: Springer Verl., S. 205-220 (2013).

Invited talks

1) S. Aswartham, *Crystal growth and physical properties of Fe-based superconductors*, Trilateral Workshop on Hot Topics in HTSC: Fe-Based Superconductors, Zvenigorod, Moscow/ Russia, 1.10.13 (2013).
2) A. Backen, S.R. Yeduru, S. Kauffmann-Weiss, R. Niemann, A. Diestel, C. Behler, L. Schultz, M. Kohl, S. Faehler, *Thin Ni-Mn-Ga films for microsystem applications: From epitaxial growth to training of freestanding films*, Energy Materials Nanotechnology (EMN) Spring Meeting 2013, Orlando, Florida/ USA, 8.-11.4.13 (2013).
3) C.C. Bof Bufon, C. Vervacke, M.E. Navarro Fuente, D.J. Thurmer, C. Mueller, M. Fronk, G. Salvan, D.R.T. Zahn, O.G. Schmidt, *Nanomembrane based electrodes for contacting ultra-thin organic layers*, DPG-Fruehjahrstagung, Regensburg, 10.-15.3.13 (2013).
4) S. Borisenko, *Fermiology and order parameter of iron-based superconductors from ARPES*, DPG Spring Meeting, Regensburg/ Germany, 11.-15.3.13 (2013).
5) S. Borisenko, *ARPES with 1-cubed facility*, Workshop „Spectroscopy of Novel Materials", Flumserberg/ Switzerland, 7.-11.3.13 (2013).
6) S. Borisenko, *ARPES in cuprates and iron-based superconductors*, Italian National Conference on Condensed Matter Physics (FisMat2013), Politecnico di Milano/ Italy, 9.-13.9.13 (2013).
7) S. Borisenko, *Superconductivity from the Fermiology*, 2013 Montauk Conference on High Temperature Superconductors, Montauk, Long Island, New York/ USA, 2.-6.9.13 (2013).
8) S. Borisenko, *Momentum and orbital anisotropy of the gap functions in iron-based superconductors*, Spectroscopy on Novel Superconductors (SNS2013), Berkeley, California/ USA, 24.-28.6.13 (2013).
9) S. Borisenko, *Symmetry of the order parameter in the iron based superconductors from ARPES. Workshop on recent developments in iron-based superconductivity*, Riverhead, Long Island/ USA, 3.-6.9.13 (2013).
10) S. Borisenko, *ARPES of iron-based superconductors*, Quantum in Complex Matter, Superstripes 2013 Konferenz, Ischia/ Italy, 27.5.-1.6.13 (2013).
11) S. Borisenko, *Materials architecture: Correlations and topology*, Festkoerperkolloquium, TU Muenchen, 28.11.13 (2013).
12) S. Borisenko, *Fermi surface topology and order parameter of iron-based superconductors from ARPES*, Energy Materials Nanotechnology (EMN) West Meeting, Houston/ USA, 7.-10.1.13 (2013).
13) M. Brehm, *Hybrid and ordered SiGe nanostructures*, Institute Seminar, IHP GmbH Innovations for High Performance Microelectronics, Frankfurt (Oder)/ Germany, 17.10.13 (2013).
14) M. Brehm, *MBE growth and investigation of SiGe nanostructures*, Seminar, Institut fuer Angewandte Photophysik, Dresden/ Germany, 29.5.13 (2013).

15) M. Brehm, *Growth and characterization of hybrid and ordered SiGe nanostructures*, Workshop on Ordered Island Growth in Group-IV Systems, University of Stuttgart/ Germany, 3.7.13 (2013).
16) B. Buechner, *Electron spin resonance studies of iridates*, Workshop - Electronic Properties of Spin-Orbit Driven Oxides, Dresden, 4.-7.9.13 (2013).
17) B. Buechner, *Phase diagrams of Fe based superconductors*, Eingeladener Vortrag, Universitaet Zuerich/ Schweiz, 27.2.13 (2013).
18) B. Buechner, *Tunable sub-THz spectroscopy of complex transition metal oxides*, Strongly Correlated Transition Metal Compounds - A Farewell to CRC 608, Koeln, 6.-8.3.13 (2013).
19) B. Buechner, *Phase diagrams of Fe based superconductors*, Gordon Conferences Superconductivity 2013, Les Diableretes/ Schweiz, 12.-17.5.13 (2013).
20) B. Buechner, *FeSc ferromagnetism and superconductivity in doped LiFeAs*, 2013 EMN Workshop on Iron-based Superconductors, Houston/ USA, 7.-10.1.13 (2013).
21) B. Buechner, *Tunable high field ESR spectroscopy of complex transition metal oxides*, Symposium anlaesslich des 70ten Geburtstags von Gernot Guentherodt, RWTH Aachen, 3.-4.5.13 (2013).
22) B. Buechner, *Phase diagrams of Fe based superconductors*, SUPERSTRIPES Workshop, Ischia/ Italien, 28.-30.5.13 (2013).
23) B. Buechner, *The iron age of high temperature superconductivity*, Colloqium on Solid-State Physics at TU Muenchen, 4.7.13 (2013).
24) B. Buechner, *Tunable sub-THz ESR spectroscopy of complex transition metal oxides*, Telluride Workshop: Enhanced Functionalities in 5d Transition Metal Compounds from large Spin-orbit Coupling, Telluride, Colorado/ USA, 15.-19.7.13 (2013).
25) M. Calin, M. Boenisch, A. Helth, K. Zhuravleva, S. Abdi, A. Panigrahi, M., Gebert, A. Zehetbauer, J. Eckert, *Enhancing the biomechanical capacity of Ti-Nb-based metastable alloys for implant applications*, International Conference EUROMAT 2013, Sevilla/ Spain, 8.-13.9.13 (2013).
26) M. Calin, N. Zheng, S. Abdi, P.F. Gostin, C. Damm, M.D. Baro, P. Rizzi, A. Gebert, J. Eckert, *Biocompatible Ti-based metallic glasses for implant applications*, ISMANAM 2013 Conference, Turin/ Italy, 30.6.-5.7.13 (2013).
27) M. Calin, N. Zheng, A. Helth, M. Boenisch, S. Abdi, A. Gebert, J. Eckert, *Titanium-based amorphous alloys as prospective biomaterials*, Conference „Advanced Materials and Structures „- AMS 2013, Timisoara/ Romania, 24.-25.10.13 (2013).
28) M. Daghofer, *Spontaneous fractional quantum-Hall state in strongly correlated multiorbital systems*, Workshop „Flat Bands: Design, Topology, and Correlations“, Dresden, 4.-8.3.13 (2013).
29) M. Daghofer, *Multi-orbital models for Pnictide superconductors*, Workshop „Tuning Superconductivity in Doped Semiconductors“, Jacob-Univ. Bremen, 11.-12.9.13 (2013).
30) M. Daghofer, *Correlations and topology in multi-orbital models*, Seminar, Stanford Institute for Materials and Energy Sciences, Stanford/ USA, 25.3.13 (2013).
31) M. Daghofer, *The spin-orbit coupled j =1=2 antiferromagnet in iridates*, Workshop „Electronic Properties of Spin-Orbit Driven Oxides“, Dresden, 4.-7.9.13 (2013).
32) M. Daghofer, *Spin-orbit coupling and correlations in iridates*, Seminar, Univ. Tenn., Knoxville/ USA, 1.4.13 (2013).
33) M. Daghofer, *Z2-vortex phase in the triangular-lattice Kitaev-Heisenberg model*, MPI-FKF Stuttgart, 17.4.13 (2013).
34) M. Daghofer, *Topologically nontrivial and nearly at bands in multi-orbital models*, Seminar, Salerno/ Italy, 20.01.13 (2013).
35) F. Ding, *Triggered single-photon emission from a wavelength-tunable quantum LED*, 1st International Workshop on Engineering of Quantum Dot Emission Properties, Linz/ Austria, 9.-10.12.13 (2013).
36) J. Dufouleur, *Quasi-ballistic transport of Dirac fermions in a Bi2Se3 nanowire*, Complex Nano-Materials, Dresden 21.11.13 (2013).
37) J. Dufouleur, *Quantum transport in Bi2Se3 topological insulators*, DFG Research Unit 912 Meeting, Frankfurt/ Germany, 6.2.13 (2013).
38) L. Dunsch, *Clusterfullerenes: Exciting nanostructures in endohedral electrochemistry and magnetic states*, XXVII International Winterschool on Electronic Properties of Novel Materials, Kirchberg/ Austria, 2.-9.3.13 (2013).
39) J. Eckert, *Heterogeneity and phase transformations as ways to tailor the deformability of high-strength metastable materials*, China-Germany Workshop on „Microstructure-Driven Design and Performance of Advanced Metals“, Shenyang/ PR China, 14.4.13 (2013).
40) J. Eckert, *Mechanical properties of metallic glasses and composites*, 20th International Symposium on Metastable, Amorphous and Nanostructured Materials (ISMANAM 2013), Turin/ Italy, 2.7.13 (2013).
41) J. Eckert, *Metallic glasses - Structure, properties and perspectives*, Kolloquium on „Current Challenges in Materials Physics“, Universitaet Goettingen, 24.5.13 (2013).
42) J. Eckert, *Application of amorphous alloys: Potential and challenges to overcome*, Res Metallica 2013 Workshop on „Amorphous Alloys and Bulk Metallic Glasses“, KU Leuven/ Belgien, 8.5.13. (2013).
43) J. Eckert, K.K. Song, S. Pauly, B.A. Sun, Y. Zhang, R. Li, S. Gorantla, T. Gemming, U. Kuehn, *Deformation mechanisms in metastable CuZrAl composites*, 2013 TMS Annual Meeting and Exhibition, Symposium „Bulk Metallic Glasses (X)“, San Antonio/ USA, 5.3.13 (2013).
44) D. Evtushinsky, *ARPES on iron-based superconductors*, Trilateral Workshop on hot Topics in HTSC: Fe-Based Superconductors, Moscow-Zvenigorod/ Russia, 29.9.-2.10.13 (2013).
45) D. Evtushinsky, *ARPES on iron-based superconductors: leading role of 3d_xz/yz orbitals*, Electronic Structure and Electron Spectroscopies, Kiev/ Ukraine, 20.-23.5.13 (2013).
46) S. Faehler, *The material is the machine*, TU Chemnitz, Physikalisches Kolloquium, Chemnitz, 3.7.13 (2013).

47) S. Faehler, *Interfaces in multiferroic magnetic shape memory alloys*, Donostia International Conference on Magnetism, San Sebastian/ Spain, 9.-13.9.13 (2013).
48) S. Faehler, *Unpacking the martensitic matryoshka*, Fourth International Conference on Ferromagnetic Shape Memory Alloys, Boise, Idaho/ USA, 3.-7.5.13 (2013).
49) S. Faehler, *Nanostrukturierte multifunktionale Materialien: Neue Perspektiven fuer energieeffiziente Anwendungen*, Eingeladener Vortrag, Duisburg, 2.5.13 (2013).
50) S. Faehler, *Caloric effects in ferroic materials: New concepts for cooling*, ECo MaTech European Conference on Materials and Technologies for Sustainable Growth, Bled/ Slovenia, 19.-21.9.13 (2013).
51) S. Faehler, M.E. Gruner, R. Niemann, U. Roessler, *Ergodicity by ordering nanotwins*, International Symposium on Non-ergodic behavior in Martensites, Duisburg, 19.1.13 (2013).
52) J. Fink, *Investigations of the electronic structure of ferropnictides using angle- and femtosecond time-resolved photoemission spectroscopy*, Quantum in Complex Matter, Superstripes 2013 Konferenz, Ischia/ Italy, 27.5.-1.6.13 (2013).
53) J. Fink, *Zum Mechanismus der Hochtemperatursupraleitung – Untersuchungen mit winkel- und zeitaufgeloester Photoemissionsspektroskopie*, Kolloquiumsvortrag, TU Ilmenau, 9.4.13 (2013).
54) J. Fink, *Fermiology and charge carrier dressing in ferropnictides by angle- and femtosecond time-resolved photoemission spectroscopy*, Workshop „Advances in Electron Spectroscopy-Experiment and Theory" (AESET 2013), Goettingen, 23.-25.5.13 (2013).
55) J. Fink, *Angle-resolved photoemission spectroscopy on unconventional superconductors*, Seminarvortrag, Universitaet Duisburg-Essen, 24.4.13 (2013).
56) J. Fink, *ARPES and tr-ARPES, two complementary techniques for the investigation of unconventional superconductors*, Short-time Dynamics in Strongly Correlated Systems and Novel Superconductors, Bochum, 18.-21.2.13 (2013).
57) V.M. Fomin, *Physics of quantum rings*, Seminar of the Department of Physics and Engineering, State University of Moldova Kishinev/ Republic of Moldova, 18.4.13 (2013).
58) V.M. Fomin, *Electronic properties of Moebius microrings*, Seminar, Department of Theoretical Physics, National Research Tomsk State University Tomsk/ Russian Federation, 24.4.13 (2013).
59) V.M. Fomin, *Theoretical modeling of electronic and optical properties of nanostructures: From the non-adiabaticity of semiconductor nanocrystals to the geometric and topological effects in quantum rings*, Seminar Physical Chemistry and Electrochemistry, TU Dresden, 9.4.13 (2013).
60) V.M. Fomin, *Superconducting micro- and nanotubes*, 10th International Conference „Perspectives of Advancement in Fundamental Sciences" Tomsk/ Russian Federation, 23.-26.4.13 (2013).
61) V.M. Fomin, *Impact of topology on electronic properties of solid-state micro- and nanostructures*, Seminar on Condensed Matter Physics, Moscow State Lomonosov University, Moscow/ Russia, 30.10.13 (2013).
62) V.M. Fomin, *Novel manifestations of the Aharonov-Bohm effect in quantum rings and Moebius rings*, 2nd International Conference on Nanotechnologies and Biomedical Engineering Kishinev/ Republic of Moldova, 18.-20.4.13 (2013).
63) V.M. Fomin, *Dynamics of vortices in planar and tubular microstructured superconductors*, Humboldt Kolleg and International Symposium „NANO-2013", Kishinev/ Republic of Moldova, 13.-16.9.13 (2013).
64) V.M. Fomin, *Electronic structure and the Aharonov-Bohm effect in inhomogeneous Moebius rings*, Nanophysics Group Seminar, Ludwig-Maximilians-Universitaet, Muenchen/ Germany, 13.5.13 (2013).
65) J. Freudenberger, *Werkstoffwissenschaft - interdisziplinaere Forschung*, MINT-Woche, Werner-Heisenberg-Gymnasium Riesa, Riesa, 3.12.13 (2013).
66) J. Freudenberger, T. Marr, J. Romberg, E. Knauer, D. Seifert, H. Klauss, L. Schultz, U. Martin, H. Watanabe, H. Bauder, J. Scharnweber, C.-G. Oertel, W. Skrotzki, I. Okulov, U. Kuehn, J. Eckert, *Damaszen-Technik fuer Verbundwerkstoffe*, 4. Dresdner Werkstoffsymposium, Dresden, 18.-19.11.13 (2013).
67) A. Gebert, A. Helth, K. Zhuravleva, S. Abdi, P.F. Gostin, M. Calin, U. Hempel, R. Medda, A. Cavalcanti-Adam, J. Eckert, *Tailoring the surfaces of metastable beta-type Ti-based alloys at the nano-scale for biomedical applications*, ISMANAM 2013, Turin/ Italien, 30.5.-5.6.13 (2013).
68) A. Gebert, R. Sueptitz, M. Uhlemann, J. Eckert, *Electrochemical micromachining of bulk metallic glasses*, TMS Annual Spring Meeting, San Antonio, Texas/ USA, 3.-7.3.13 (2013).
69) J. Geck, *Correlated electron physics in the light of DORIS*, Symposium, DESY Hamburg, 15.5.13 (2013).
70) J. Geck, *Determining the short-range spin correlations in cuprate chain materials with resonant inelastic x-ray scattering*, MAMA-Trend: Trends, Challenges and Emergent new Phenomena in Multi-functional Materials, Sorrento/ Italy, 20.-23.5.13 (2013).
71) J. Geck, *Two current issues with the interpretation of REXS and RIXS in the cuprates*, IXS-Konferenz, Standford/ USA, 12.-16.8.13 (2013).
72) J. Geck, *Magnetic frustration, phase competition, and the magnetoelectric effect in NdFe3(BO3)4*, Quantum in Complex Matter, Superstripes 2013 Konferenz, Ischia/ Italy, 27.5.-1.6.13 (2013).
73) R. Giraud, *Quantum transport of spin-chiral Dirac fermions in Bi2Se3 nanostructures*, Workshop on Mesoscopic Physics, Aussois/ France, 9.-12.12.13 (2013).
74) D. Grimm, *Rolled Electronics: Active, passive, thermo-electric and molecular devices*, Semiconductor Physics Group Meeting, Karlovy Vary/ Czech Republic, 29.9.-2.10.13 (2013).

75) D. Grimm, P.F. Siles, *Investigating the magnetoresistance of thin molecular films: From local to integrative approaches*, TMS Winterschool 2013, Zakopane/ Poland, 25.2.-1.3.13 (2013).
76) M. Grydlik, *Strictly ordered SiGe quantum dots and their optical response*, Seminar, Institut fuer Angewandte Photophysik, Dresden/ Germany, 29.5.13 (2013).
77) M. Grydlik, *Optical response and growth of perfectly ordered Ge quantum dots on Si(001) substrates*, Workshop on Ordered Island Growth in Group-IV Systems, University of Stuttgart/ Germany, 3.7.13 (2013).
78) M. Grydlik, *Perfectly site-controlled Ge quantum dots: Fabrication conditions and optical properties*, Institute Seminar, IHP GmbH Innovations for High Performance Microelectronics, Frankfurt (Oder)/ Germany, 17.10.13 (2013).
79) J. Haenisch, *Critical current anisotropy in clean superconducting pnictide thin films*, CEC-ICMC 2013, Anchorage/ USA, 17.-21.6.13 (2013).
80) S. Haindl, *A scaling approach to determine the Hc2-anisotropy of oxypnictides*, 2013 EMN Conference, Houston/ USA, 7.-10.1.13 (2013).
81) S. Hampel, *Chemical modification of carbon nanostructures for medical application especially for the therapy of non-muscle invasive bladder cancer*, Dienstagsseminar der Med. Fakultaet, Universitaet Duisburg-Essen, 3.12.13 (2013).
82) S. Hampel, *Carbon nanostructures: physicochemical and technological characterization and application in the treatment of solid cancers*, Summer School 2013 „Materials for Pharmaceutical Applications: Physico-chemical and technological Characterization", University of Calabria/ Italy, 9.-12.9.13 (2013).
83) M. Herklotz, F. Scheiba, N.K. Yavuz, D. Wadewitz, M. Hinterstein, A.-C. Dippel, J. Eckert, H. Ehrenberg, *In operando / In situ studies on battery materials - capabilities of the beamline P02.1 and recent results*, Workshop: Structural and in situ material science at Beamline P02.1 et PETRA III, DESY Hamburg, 12.-13.9.13 (2013).
84) H. Hermann, *Simulation of low-k insulators for application in semiconducting devices*, Workshop Computational exploration of atomistic structures and their Interrelation with Physical Properties; Dresden, 4.-8.11.13 (2013).
85) C. Hess, *Quasiparticle interference as a probe for the unconventional superconductivity in LiFeAs*, Eingeladener Vortrag, Universitaet Hannover, 9.4.13 (2013).
86) C. Hess, *Unconventional superconductivity in LiFeAs as seen by scanning tunneling microscopy and spectroscopy*, SFB/TRR 49 Colloquium, University of Frankfurt, Frankfurt/ Germany, 7.11.13 (2013).
87) C. Hess, *Heat transport in low-dimensional quantum magnets*, Eingeladener Vortrag, LMU Muenchen, 10.7.13 (2013).
88) C. Hess, *Unconventional superconductivity in LiFeAs as seen by STM/STS and transport experiments*, Trilateral Workshop on Hot Topics in HTSC: Fe-Based Superconductors (Fall of 2013), Zvenigorod City, near Moscow/ Russia, 29.9.-2.10.13 (2013).
89) C. Hess, *Quasiparticle interference as a probe for the unconventional superconductivity in LiFeAs*, Invited Seminar, TU Muenchen, Muenchen, 29.11.13 (2013).
90) V. Hoffmann, *Progress and demands in analytical glow discharges*, Colloquium Spectroscopicum Internationale XXXVIII, Tromsoe/ Norwegen, 17.-20.6.13 (2013).
91) V. Hoffmann, *Plasma diagnostics on analytical glow discharges*, International Workshop „Diagnostic Systems for Plasma Processes" Lichtenwalde, Chemnitz, 24.9.13 (2013).
92) R. Huehne, *Introduction to Pulsed Laser Deposition as a versatile preparation method*, 537th Wilhelm and Else Heraeus Seminar „Physics of Ionized and Ion-Assisted PVD: Principles and Current Trends", HZDR Dresden-Rossendorf, 26.-28.8.13 (2013).
93) R. Huehne, *Pulsed laser deposition as a versatile preparation method for functional thin films*, Seminarvortrag, Helmholtz-Zentrum Berlin, Institut fuer Solare Brennstoffe, Berlin, 5.11.13 (2013).
94) Y.H. Huo, *A light-hole exciton in a quantum dot: Fabrication and fine structure*, Seminar, European Synchrotron Radiation Facility (ESRF), Grenoble/ France, 20.9.13 (2013).
95) Y.H. Huo, *Highly symmetric GaAs quantum dots with light-hole ground state*, Seminar, Centre de Recherche sur l'HétéroEpitaxie et ses Applications (CRHEA), CNRS, Sophia Antipolis/ France, 23.9.13 (2013).
96) Y.H. Huo, *Symmetric GaAs quantum dots with light-hole ground state: Fabrication and characterization*, 1st International Workshop on Engineering of Quantum Dot Emission Properties, Linz/ Austria, 9.-10.12.13 (2013).
97) K. Iida, *Fabrication of Fe-based superconducting films by employing Fe-buffer layer (Lecture will be given in Japanese)*, Lecture for Post Graduate, Hiroshima/ Japan, 14.11.13 (2013).
98) K. Iida, *High field transport properties of epitaxial Fe-based superconducting films*, Seminar talk, Universitaet Stuttgart, Stuttgart/ Germany, 3.12.13 (2013).
99) K. Iida, J. Haenisch, F. Kurth, V. Grinenko, L. Schultz, B. Holzapfel, C. Tarantini, J. Jaroszynski, S. Ueda, M. Naito, A. Ichinose, I. Tsukada, *Experimental evidence for the dimensional crossover in epitaxial SmFeAs(O,F) thin films*, IUMRS-ICAM 2013, Qingdao/ China, 22.-28.9.13 (2013).
100) K. Iida, F. Kurth, J. Engelmann, S. Trommler, J. Haenisch, T. Thersleff, R. Huehne, V. Grinenko, E. Reich, L. Schultz, B. Holzapfel, P. Chekhonin, W. Skrotzki, *Generic Fe-buffer layers for epitaxial Fe-based superconducting thin films*, Solid State Surfaces and Interfaces, Smolenice Castle/ Slovakia, 24.-28.11.13 (2013).
101) M.R. Jorgensen, *Photonic crystals: From biology to rolled-up nanotechnology*, Seminar, Utah State University Logan, Utah/ USA, 25.10.13 (2013).
102) M.R. Jorgensen, *Rolled-up nanotechnology and photonics*, Seminar, University of Utah, Salt Lake City/ USA, 29.10.13 (2013).
103) I. Kaban, *Structural studies of CuZr and CuZrAl metallic glasses in relation to their GFA and mechanical properties*, Institutsseminar, Institut fuer Materialphysik im Weltraum, DLR Koeln, 17.12.13 (2013).

104) D. Karnaushenko, *Printable magnetoelectronics*, International Conference „5th Printing Future Days 2013“, Chemnitz/ Germany, 10.-12.9.13 (2013).
105) D. Karnaushenko, *Printable magnetoelectronics*, Dresden School on Functional Nanomaterials, Dresden/ Germany, 1.-3.10.13 (2013).
106) D. Karnaushenko, *Printable magnetoelectronics*, Colloquium of the Institute for Print and Media Technology, Chemnitz/ Germany, 19.11.13 (2013).
107) V. Kataev, *Uncovering a complex interplay of spins, orbitals and charges in LaSrMnO4 by sub-THz spectroscopy in ultra-strong magnetic fields*, International Conference Modern Development of Magnetic Resonance, 2013, Kazan/ Russland, 24.-28.9.13 (2013).
108) V. Kataev, *Sub-THz spectroscopy of the layered manganite LaSrMnO4 in ultra-strong magnetic fields*, XV. International Feofilov Symposium, Kazan/ Russland, 16.-20.9.13 (2013).
109) M. Knupfer, *Electronic properties of undoped and doped, hydrocarbon based molecular solids*, ICTP Conference on Mechanisms and Developments in light-element based and other Novel Superconductors, Trieste/ Italien, 24.-26.9.13 (2013).
110) M. Knupfer, *Electronic properties of undoped and doped, hydrocarbon based molecular solids*, Kolloquium des SFB/TRR 49, Universitaet Frankfurt, 16.5.13 (2013).
111) M. Knupfer, *Electronic properties of undoped and doped hydrocarbon based molecular solids*, Seminar, Kirchhoff-Institut, Universitaet Heidelberg, 1.2.13 (2013).
112) A. Koitzsch, *Soft x-ray spectroscopy studies of LaAlO3/SrTiO3, NdGaO3/SrTiO3 and LaGaO3/SrTiO3 interfaces*, MAMA Trend Conference, Sorrento/ Italy, 20.-23.5.13 (2013).
113) A. Koitzsch, *Band dependent emergence of heavy quasiparticles in CeCoIn5*, F-ARPES Workshop, MPI-PKS Dresden, 27.- 30.5.13 (2013).
114) S. Kumar, *Tuning of single semiconductor quantum dots and their host structures via strain and in situ laser processing*, Seminar Institute of Photonics and Quantum Sciences, Herio-Watt University Edinburgh, Scotland/ UK, 24.4.13 (2013).
115) G. Lin, *Magnetoresistive emulsion analyzer*, 526. Heraeus Seminar „Functional Magnetic Nanomembranes“, Bad Honnef/ Germany, 6.3.13 (2013).
116) W. Loeser, T. Volkmann, D.M. Matson, *Effect of microgravity on solidification processes in Fe-based undercooled melts*, TMS 2013, San Antonio, Texas/ USA, 2.-7.3.13 (2013).
117) D. Makarov, *Shapeable magnetic sensorics*, Leibniz-Doktoranden-Forum der Sektion D, Berlin/ Germany, 7.6.13 (2013).
118) D. Makarov, *Magnetism in curved nanomembranes*, Seminar, Universite du Maine, Le Mans/ France, 21.3.13 (2013).
119) D. Makarov, *Shapeable magnetoelectronics*, 58th Annual Magnetism and Magnetic Materials (MMM) Conference, Denver, CO/ USA, 4.-9.11.13 (2013).
120) D. Makarov, *Magnetic nanomembranes*, Seminar, Peter Gruenberg Institute (PGI-6), FZ Juelich, Juelich/ Germany, 4.2.13 (2013).
121) D. Makarov, *Magnetism in curved surfaces*, ALS/ CXRO Seminar, ALS Berkeley, Berkeley/ USA, 2.10.13 (2013).
122) D. Makarov, *Ultraduenne formbare Magnetfeldsensorik*, INNOMAG Mitgliederversammlung, Fraunhofer-Institut fuer Integrierte Schaltungen Dresden/ Germany, 1.3.13 (2013).
123) D. Makarov, *Shapeable magnetoelectronics*, Group Seminar of the Electronic Laboratory, ETH Zurich/ Switzerland, 23.9.13 (2013).
124) M. Melzer, *Stretchable magnetoelectronics*, 526. Heraeus Seminar „Functional Magnetic Nanomembranes“, Bad Honnef/ Germany, 6.3.13 (2013).
125) S.B. Menzel, E. Brachmann, A. Winkler, C. Strobel, M. Albert, M. Fahland, T. Gemming, *Mechanical testing of thin film p-i-n silicon solar cells on flexible polymer substrates*, 28th EU PVSEC, Paris/ France, 30.9.-4.10.13 (2013).
126) V. Neu, *Tailoring energy densities around 450 kJ/m3 in exchange coupled SmCo5/Fe multilayers*, Workshop on Energy and Materils Criticality, Santorini/ Greece, 22.-25.8.13 (2013).
127) V. Neu, *Epitaxial Sm-Co thin films and multilayer: magnetism and more*, Physikalisches Kolloquium des Instituts fuer Physik, Technische Universitaet Chemnitz, 4.12.13 (2013).
128) V. Neu, *Introduction to magnetic materials*, Guest Lecture, Dpt. of Physics and Astronomy, Uppsala University, Uppsala/ Schweden, 24.4.13 (2013).
129) V. Neu, M. Kopte, S. Sawatzki, C. Damm, L. Schultz, *Tailoring energy densities above 450 kJ/m3 in exchange coupled SmCo/Fe multilayers*, 5th Seeheim Conference on Magnetism, Frankfurt/Main, 29.9.-3.10.13 (2013).
130) R. Niemann, H. Seiner, C. Behler, A. Backen, S. Kauffmann-Weiss, U. Roessler, O. Heczko, L. Schultz, S. Faehler, *Nucleation and microstructure of martensite in magnetic shape memory alloys*, Donostia International Conference on Nanoscaled Magnetism and Applications, San Sebastian/ Spain, 9.-13.9.13 (2013).
131) M. Niethammer, R. Pfrengle, *Zukunft der Chemie- und Umweltbranche als Gestaltungsaufgabe - Herausforderungen an berufliche Bildung und Arbeit*, 17. Hochschultage Berufliche Bildung 2013 „Arbeit der Zukunft - Zukunft der Arbeit. Berufliche Bildung, Qualifikation und Fachkraeftebedarf im Zeichen des demographischen Wandels“, FT07 - Chemie- und Umwelttechnik, Essen, 13.-15.3.13 (2013).
132) S. Oswald, *Depth profiling in the nm-thickness range: A critical evaluation of angle-resolved XPS*, Universitaet Wuerzburg, Kolloqium Experimentelle Physik 7, Wuerzburg, 11.12.13 (2013).
133) P. Pahlke, S. Trommler, B. Holzapfel, L. Schultz, R. Huehne, *Dynamic variation of biaxial strain in optimally and underdoped YBCO thin films*, Seminarvortrag, Paul Scherrer Institut, Villingen/ Schweiz , 7.6.13 (2013).
134) S. Partzsch, *Resonant soft X-ray diffraction studies on multiferroic YMn2O5 with six circle diffractometer and CCD-camera*, Seminar bei ALBA CELLS (spanische Synchrotron), Cerdanyola del Valles/ Spain, 10.12.13 (2013).

135) R. Pfrengle, *Empfehlungen der Leibniz-Gemeinschaft fuer Mitarbeiterausgruendungen*, 46. Sitzung des Verwaltungsausschusses sowie Jahrestagung der Leibniz-Gemeinschaft, Berlin, 27.-28.11.13 (2013).
136) R. Pfrengle, *Fachkraeftesicherung in der Chemie-Branche im demografischen Wandel*, Regionalveranstaltung des Demografie-Netzwerks Sachsen, Dresden, 22.4.13 (2013).
137) R. Pfrengle, *Valide Berichtsdaten fuer eine effiziente Steuerung*, MACH-Workshop Berichtswesen, Berlin, 23.4.13 (2013).
138) R. Pfrengle, K. Backhaus-Nousch, *Brauchen wir die duale Ausbildung fuer die ausseruniversitaere Forschung?*, 17. Hochschultage Berufliche Bildung 2013, Essen, 14.3.13 (2013).
139) R. Pfrengle, K. Backhaus-Nousch, *The German research and funding landscape*, Vorlesungen an der Slovak University of Technology in Bratislava (Akademisches Jahr 2012/2013), Trnava/ Slovakia, 15.4.13 (2013).
140) R. Pfrengle, K. Backhaus-Nousch, *Project management in practice: The EU project DIVERSITY*, Vorlesungen an der Slovak University of Technology Bratislava, Trnava/ Slovakia, 16.4.13 (2013).
141) R. Pfrengle, K. Backhaus-Nousch, *Die Leibniz-Gemeinschaft - Starker Partner im DRESDEN-concept*, Helmholtz-Referent/innentreffen, Dresden, 19.-20.6.13 (2013).
142) R. Pfrengle, K. Backhaus-Nousch, *Administrative Aspekte des Wissens- und Technologietransfers (WTT)*, Wissens- und Technologietransfer am AIP-Potsdam, Postdam, 19.2.13 (2013).
143) D. Pohl, A. Surrey, B. Bieniek, U. Wiesenhuetter, E. Mohn, F. Schaeffel, L. Schultz, B. Rellinghaus, *Segregation phenomena in nanoscopic systems studied by aberration-corrected HRTEM*, ICSS 2013, Las Vegas/ USA, 15.-18.12.13 (2013).
144) A.A. Popov, *The endohedral magnetism: Lanthanide ions in the nitride clusterfullerenes*, 223rd Electrochemical Society Meeting, Toronto/ Canada, 12.-16.5.13 (2013).
145) A.A. Popov, *Endohedral fullerenes: An inside story*, Swiss Molecule-on-Surfaces (MolCH) Meeting, Bern/ Switzerland, 11.6.13 (2013).
146) A.A. Popov, *Reaction mechanisms of organic structures at electrodes as studied by spectroelectrochemistry*, XIV European Symposium on Organic Reactivity, Prague/ Czech Republic, 1.-6.9.13 (2013).
147) A.A. Popov, *Endohedral transition metal and rare-earth redox couples inside the carbon cage: Fullerene as an innocent ligand*, 46th Heyrovsky Discussion - Molecular Electrochemistry in Organometallic Science, Castle Trest/ Czech Republic, 23.-27.6.13 (2013).
148) A.A. Popov, *Endohedral electrochemistry*, 223rd Electrochemical Society Meeting, Toronto/ Canada, 12.-16.5.13 (2013).
149) A.A. Popov, *Endohedral electrochemistry: Tuning the charge and spin states of metal atoms inside the carbon cage*, 1st International Symposium on Nanocarbons, Heifei/ China, 16.-21.6.13 (2013).
150) A.A. Popov, *Endohedral electrochemistry: Tuning the charge and spin states of metal atoms inside the carbon cage*, New Processes and Materials Based on Electrochemical Concepts at the Microscopic Level - MicroEchem 2013, Queretaro/ Mexico, 16.-19.9.13 (2013).
151) A.A. Popov, *Endohedral electrochemistry and the role of ESR spectroelectrochemistry*, XXV International EPR Seminar, Casta-Papiernicka/ Slovakia, 10.-12.4.13 (2013).
152) A.A. Popov, *Electrochemistry and spectroelectrochemistry of empty and endohedral fullerenes and their derivatives*, AKK Fachausschuss-Sitzung, Freiberg, 15.10.13 (2013).
153) B. Rellinghaus, *Potential and limitations of aberration-corrected transmission electron microscopy*, HGST - A Western Digital Company, San Jose/ USA, 28.3.13 (2013).
154) B. Rellinghaus, *Phase stability at small length scales: Segregation tendencies in nanoparticles of binary metallic alloys*, Keynote Lecture, 3rd Int. Conference on Nanotek and Expo, Las Vegas, NV/ USA, 2.-4.12.13 (2013).
155) B. Rellinghaus, *How stable are binary metallic alloys at small length scales?*, Seminar of the Institute for Scattering Methods, JCNS-2/PGI-4, Juelich Center for Neutron Science, FZ Juelich, 17.10.13 (2013).
156) B. Rellinghaus, E. Mohn, D. Pohl, S. Wicht, D. Weller, L. Schultz, *Structure-property relations in high anisotropy nanomagnets*, 3rd International Conference on Nanotek and Expo, Las Vegas/ USA, 2.-4.12.13 (2013).
157) B. Rellinghaus, D. Pohl, E. Mohn, S. Wicht, L. Schultz, *Phase stabilities at small length scales and their relevance to magnetic nanoparticles*, International Workshop on Amorphous and Nanostructured Magnetic Materials, ANMM'2013, Sendai/ Japan, 1.-3.10.13 (2013).
158) M. Richter, *Theoretische Physik in der Materialforschung: Von Kuehlschraenken ueber Festplatten zu ultraschneller Elektronik*, „Tag der Wissenschaften" am Schiller-Gymnasium Bautzen, Bautzen, 8.6.13 (2013).
159) A. Saicharan, *Crystal growth and physical properties of Fe-based superconductors*, Trilateral Workshop on Hot Topics in HTSC: Fe-Based Superconductors (Fall of 2013), Zvenigorod City, near Moscow/ Russia, 29.9.-2.10.13 (2013).
160) S. Sanchez, *Tubular nanojet engines: Smart design for smart nanorobots*, Small Scale Robotics Workshop, IEEE International Conference on Robotics and Automation 2013, Karlsruhe/ Germany, 6.5.13 (2013).
161) S. Sanchez, *Bubble-propelled microswimmers: From single to collective motion*, Ringberg Meeting „Active particles and micro-swimmers", Tegernsee/ Germany, 8.-12.7.13 (2013).
162) S. Sanchez, *How to fabricate and design self-propelled micromotors*, Invited Lecture, BuildMoNa Module University Leipzig, Leipzig/ Germany, 28.5.13 (2013).
163) S. Sanchez, *Potential applications, challenges and future of micromotors: From individual motors to collective behaviour*, Invited Lecture, BuildMoNa Module University Leipzig, Leipzig/ Germany, 28.5.13 (2013).
164) S. Sanchez, *Nanorobots*, Remote Lecture, California NanoSystems Institute - NanoLab, UCLA, Los Angeles/ USA, 30.7.13 (2013).

165) S. Sanchez, *Small and smart rolled-up tubes for biomaterials in cell biology and nanorobotics*, Seminar, CIC-BiomaGUNE, San Sebastian/ Spain, 26.2.13 (2013).
166) S. Sanchez, *Engineering smart microtubes for nano-bio-sciences*, Invited Lecture, KIST Europe, Saarbruecken, 1.3.13 (2013).
167) R. Schaefer, *Magneto-optical analysis of magnetic microstructure*, Seminar, IEEE Distinguished Lecture, Moscow State University, Moskau/ Russland, 30.9.13 (2013).
168) R. Schaefer, *Magneto-optical analysis of magnetic microstructure*, Seminar, IEEE Distinguished Lecture, University of Zaragoza, Inst. of Nanoscience, Zaragoza/ Spanien, 19.9.13 (2013).
169) R. Schaefer, *Magneto-optical analysis of magnetic microstructure*, Seminar, IEEE Distinguished Lecture, BCMaterials and Univ. del Pais Vasco, Bilbao/ Spanien, 20.9.13 (2013).
170) R. Schaefer, *Magneto-optical analysis of magnetic microstructure*, Seminar, IEEE Distinguished Lecture, Data Storage Institute, Singapur/ Singapur, 6.9.13 (2013).
171) R. Schaefer, *Magneto-optical analysis of magnetic microstructure*, Seminar, IEEE Distinguished Lecture, Inst. de Ciencia de Materiales, CSIC, Madrid/ Spanien, 17.9.13 (2013).
172) R. Schaefer, *Magneto-optical analysis of magnetic microstructure*, Semina, IEEE Distinguished Lecture, Inst. de Nanociencia i Nanotecnologia, Barcelona/ Spanien, 18.9.13 (2013).
173) R. Schaefer, *Magneto-optical analysis of magnetic microstructure*, Seminar, IEEE Distinguished Lecture, Ural Federal University, Ekaterinburg/ Russland, 2.10.13 (2013).
174) R. Schaefer, *Magneto-optical analysis of magnetic microstructure*, Seminar, IEEE Distinguished Lecture, Russian Accademy of Science, Inst. of Metall Physics, Ekaterinburg/ Russland, 3.10.13 (2013).
175) R. Schaefer, *Magneto-optical analysis of magnetic microstructure*, Seminar, IEEE Distinguished Lecture, Nanyang Technological University, Singapur/ Singapur, 6.9.13 (2013).
176) R. Schaefer, *Magneto-optical analysis of magnetic microstructure*, Seminar, IEEE Distinguished Lecture, Univ. of Colorado and NIST, Boulder, Colorado/ USA, 10.10.13 (2013).
177) R. Schaefer, *Domains and magnetization processes in soft magnetic materials*, Donostia International Conference on Nanoscaled Magnetism and Applications (ICNMA), San Sebastian/ Spanien, 13.9.13 (2013).
178) R. Schaefer, *Magneto-optical analysis of magnetic microstructure*, Seminar, IEEE Distinguished Lecture, Univ. of Colorado Springs, Colorado Springs/ USA, 11.10.13 (2013).
179) R. Schaefer, *Magneto-optical analysis of magnetic microstructure*, Seminar, IEEE Distinguished Lecture, University of Wyoming, Laramie/ USA, 15.10.13 (2013).
180) R. Schaefer, *Magneto-optical analysis of magnetic microstructure*, Seminar, IEEE Distinguished Lecture, Seagate, Minneapolis/ USA, 16.10.13 (2013).
181) R. Schaefer, *Magneto-optical analysis of magnetic microstructure*, Seminar, IEEE Distinguished Lecture, University of Minnesota, Minneapolis/ USA, 16.10.13 (2013).
182) R. Schaefer, *Magneto-optical analysis of magnetic microstructure*, Seminar, IEEE Distinguished Lecture, University of California, Center of Magnetic Recording, San Diego/ USA, 18.10.13 (2013).
183) R. Schaefer, *Magneto-optical analysis of magnetic microstructure*, Kolloquium, IEEE Distinguished Lecture, Technische Universitaet Darmstadt, Darmstadt, 21.10.13 (2013).
184) R. Schaefer, *Magneto-optical analysis of magnetic microstructure*, Seminar, IEEE Distinguished Lecture, Ningbo Institute of Materials Technology, Ningbo/ China, 30.10.13 (2013).
185) R. Schaefer, *The analysis of Hidden and internal magnetic domains*, 58th Annual Conference on Magnetism and Magnetic Materials, Denver, Colorado/ USA, 4.-8.11.13 (2013).
186) R. Schaefer, *Magneto-optical analysis of magnetic microstructure*, Seminar, IEEE Distinguished Lecture, IBM Research Center, Yorktown Heights/ USA, 11.11.13 (2013).
187) R. Schaefer, *Magneto-optical analysis of magnetic microstructure*, Seminar, IEEE Distinguished Lecture, University of Delaware, Newark/ USA, 12.11.13 (2013).
188) R. Schaefer, *Magneto-optical analysis of magnetic microstructure*, Seminar, IEEE Distinguished Lecture, Ames Lab, Iowa, Ames/ USA, 13.11.13 (2013).
189) R. Schaefer, *Magneto-optical analysis of magnetic microstructure*, Seminar, IEEE Distinguished Lecture, MINT Center, University of Alabama, Tuscaloosa/ USA, 15.11.13 (2013).
190) R. Schaefer, *Magneto-optical analysis of magnetic microstructure*, Seminar, IEEE Distinguished Lecture, Colorado State University, Fort Collins/ USA, 14.10.13 (2013).
191) R. Schaefer, *Magneto-optical analysis of magnetic microstructure*, Seminar, IEEE Distinguished Lecture, Universidad del Valle, Cali/ Columbien, 29.11.13 (2013).
192) R. Schaefer, *Magneto-optical analysis of magnetic microstructure*, Seminar, IEEE Distinguished Lecture, National Autonomous Univ. of Mexico, Mexico City/ Mexico, 26.11.13 (2013).
193) R. Schaefer, *Magneto-optical analysis of magnetic microstructure*, Seminar, IEEE Distinguished Lecture, Tohoku University, Sendai/ Japan, 30.8.13 (2013).
194) R. Schaefer, *Magneto-optical analysis of magnetic microstructure*, Vortrag, IEEE Distinguished Lecture, Workshop „Nanomagnetism“, Chuo-University Tokyo, Tokyo/ Japan, 29.8.13 (2013).

195) R. Schaefer, *Magneto-optical analysis of magnetic microstructure*, Seminar, IEEE Distinguished Lecture, Nippon Steel and Sumitomo Metal Corporation, Electric Steel Sheet Res. Lab, Chiba/ Japan, 28.8.13 (2013).
196) R. Schaefer, *Magneto-optical analysis of magnetic microstructure*, Seminar, IEEE Distinguished Lecture, University of Hongkong, Dep. Electrical and Electronic Engeneering, Hongkong/ China, 23.8.13 (2013).
197) R. Schaefer, *Magneto-optical Kerr microscopy*, Seminar am IMDEA Nanosciencia, Madrid/ Spanien, 25.7.13 (2013).
198) R. Schaefer, *Analysis of complex domains patterns in bulk ferromagnets*, SIAM Conference on Mathematical Aspects of Materials Science (MSI13), Philadelphia/ USA, 10.7.13 (2013).
199) R. Schaefer, *Magneto-optical analysis of magnetic microstructure*, Plenarvortrag, Annual Meeting on Advanced Spintronic, Materials and Transport Phenomena, Dresden, 5.7.13 (2013).
200) R. Schaefer, *Magneto-optical analysis of magnetic microstructure*, Vorlesung, IEEE Distinguished Lecture, IEEE Summer School, Assisi/ Italien, 13.6.13 (2013).
201) R. Schaefer, *Magneto-optical analysis of magnetic microstructure*, Seminar, IEEE Distinguished Lecture, NIST and Goerge Washington University, Gaithersburg/ USA, 7.6.13 (2013).
202) R. Schaefer, *Magneto-optical analysis of magnetic microstructure*, Seminar, IEEE Distinguished Lecture, Univ. Complutense de Madrid, Madrid/ Spanien, 16.9.13 (2013).
203) R. Schaefer, *Magneto-optical analysis of magnetic microstructure*, Seminar, IEEE Distinguished Lecture, University of Washington, Seattle/ USA, 3.6.13 (2013).
204) R. Schaefer, *Magneto-optical analysis of magnetic microstructure*, Seminar, IEEE Distinguished Lecture, Universidade Federal Fluminense, Niteroi/ Brasilien, 2.12.13 (2013).
205) R. Schaefer, *Magneto-optical analysis of magnetic microstructure*, Seminar, IEEE Distinguished Lecture, Centro Brasileiro de Pesquisas Fisicas, Rio/ Brasilien, 3.12.13 (2013).
206) R. Schaefer, *Magneto-optical analysis of magnetic microstructure*, Seminar, IEEE Distinguished Lecture, Fed. Univ. of Rio Grande del Soul, Porto Alegre/ Brasilien, 4.12.13 (2013).
207) R. Schaefer, *Magneto-optical analysis of magnetic microstructure*, Seminar, IEEE Distinguished Lecture, Centre Atomico Bariloche, Bariloche/ Argentinien, 6.12.13 (2013).
208) R. Schaefer, *Magneto-optical analysis of magnetic microstructure*, Seminar, IEEE Distinguished Lecture, American University of Beirut, Beirut/ Libanon, 12.12.13 (2013).
209) R. Schaefer, *Magneto-optical analysis of magnetic microstructure*, Seminar, IEEE Distinguished Lecture, Notre Dame University, Beirut/ Libanon, 13.12.13 (2013).
210) R. Schaefer, *Magneto-optical analysis of magnetic microstructure*, Seminar, IEEE Distinguished Lecture, Simon Fraser University, Burnaby/ Kanada, 31.5.13 (2013).
211) R. Schaefer, *Magneto-optical analysis of magnetic microstructure*, Seminar, IEEE Distinguished Lecture, Berkeley, Berkeley/ USA, 29.5.13 (2013).
212) R. Schaefer, *Magneto-optical analysis of magnetic microstructure*, Seminar, IEEE Distinguished Lecture, Santa Clara Chapter, Western Digital, San Jose/ USA, 28.5.13 (2013).
213) R. Schaefer, *Magneto-optical analysis of magnetic microstructure*, Seminar, IEEE Distinguished Lecture, Stanford University, Stanford/ USA, 28.5.13 (2013).
214) R. Schaefer, *Magneto-optical analysis of magnetic microstructure*, Seminar, IEEE Distinguished Lecture, Institute of Molecular Physics, Polish Academy of Science, Poznan/ Polen, 17.5.13 (2013).
215) R. Schaefer, *Magneto-optical analysis of magnetic microstructure*, Seminar, IEEE Distinguished Lecture, Faculty of Physics, AGH University of Science and Technology, Krakau/ Polen, 15.5.13 (2013).
216) R. Schaefer, *Magneto-optical analysis of magnetic microstructure*, Vortrag, IEEE Distinguished Lecture, Annual Meeting of Magnetics Society Japan, Sapporo/ Japan, 3.9.13 (2013).
217) R. Schaefer, *Magneto-optical analysis of magnetic microstructure*, Seminar, IEEE Distinguished Lecture, Faculty of Physics, University of Bialystok, Bialystok/ Polen, 14.5.13 (2013).
218) R. Schaefer, *Magneto-optical analysis of magnetic microstructure*, Seminar, IEEE Distinguished Lecture, Institute of Physics, Polish Academy of Science, Warschau/ Polen, 13.5.13 (2013).
219) R. Schaefer, *Magneto-optical analysis of magnetic microstructure*, Seminar, IEEE Distinguished Lecture, DL Talk at Tongji University, Shanghai/ China, 3.5.13 (2013).
220) R. Schaefer, *Magneto-optical analysis of magnetic microstructure*, Seminar, IEEE Distinguished Lecture, Oregon State University, Corvallis/ USA, 5.6.13 (2013).
221) R. Schaefer, *Magneto-optical analysis of magnetic microstructure*, Seminar, IEEE Distinguished Lecture, DL Talk at Southeast University, Nanjing/ China, 2.5.13 (2013).
222) R. Schaefer, *Magneto-optical analysis of magnetic microstructure*, Seminar, IEEE Distinguished Lecture, Nanjing University, Nanjing/ China, 1.5.13 (2013).
223) R. Schaefer, *Magneto-optical analysis of magnetic microstructure*, Seminar, IEEE Distinguished Lecture, Tsinghua University, Peking/ China, 29.4.13 (2013).
224) R. Schaefer, *Magneto-optical analysis of magnetic microstructure*, Seminar, IEEE Distinguished Lecture, National PingTung University of Education, Pingtung/ Taiwan, 26.4.13 (2013).
225) R. Schaefer, *Magneto-optical analysis of magnetic microstructure*, Seminar, IEEE Distinguished Lecture, National University of Kaohsiung, Kaohsiung/ Taiwan, 25.4.13 (2013).

226) R. Schaefer, *Magneto-optical analysis of magnetic microstructure*, Seminar, IEEE Distinguished Lecture, National Tsing Hua University, Hsinchu/ Taiwan, 24.4.13 (2013).
227) R. Schaefer, *Magneto-optical analysis of magnetic microstructure*, Seminar, IEEE Distinguished Lecture, National Taiwan University, Taipei/ Taiwan, 23.4.13 (2013).
228) R. Schaefer, *Magneto-optical analysis of magnetic microstructure*, Seminar, IEEE Distinguished Lecture, National Taiwan Normal University and Academia Sinica, Taipei/ Taiwan, 22.4.13 (2013).
229) R. Schaefer, *Magneto-optical Kerr microscopy*, Seminar bei Tungsten Steel, Xiamen/ China, 19.4.13 (2013).
230) R. Schaefer, *Magneto-optical Kerr microscopy and magnetic domains*, 2-taegige Blockvorlesung bei der Firma Precise, Peking/ China, 16.-17.4.13 (2013).
231) R. Schaefer, *Dynamic aspects of magnetic domains, observed by stroboscopic Kerr microscopy*, Domain Microstructure and Dynamics in Magnetic Elements, Heraklion, Kreta/ Greece, 8.-11.4.13 (2013).
232) R. Schaefer, *Magneto-optical analysis of magnetic microstructure*, Seminar, IEEE Distinguished Lecture, University of Sheffield, Sheffield, England/ GB, 19.3.13 (2013).
233) R. Schaefer, *Magneto-optical analysis of magnetic microstructure*, Seminar, IEEE Distinguished Lecture, Glasgow University, Glasgow/ Schottland/ GB, 22.3.13 (2013).
234) R. Schaefer, *Magneto-optical analysis of magnetic microstructure*, Seminar, IEEE Distinguished Lecture, University of Manchester, Manchester, England/ GB, 21.3.13 (2013).
235) R. Schaefer, *Magneto-optical analysis of magnetic microstructure*, Seminar, IEEE Distinguished Lecture, University of York, England/ GB, 20.3.13 (2013).
236) R. Schaefer, *Magneto-optical analysis of magnetic microstructure*, Seminar, Wolfson Centre for Magnetics, Cardiff, England/ GB, 18.3.13 (2013).
237) R. Schaefer, *Magneto-optical Kerr microscopy*, Instituts Seminar am Institute Vinca, Belgrad/ Serbien, 31.1.13 (2013).
238) R. Schaefer, *Magneto-optical analysis of magnetic microstructure*, Seminar, IEEE Distinguished Lecture, Institut fuer Physik, Universitaet Mainz, Mainz, 18.12.13 (2013).
239) R. Schaefer, *Magneto-optical analysis of magnetic microstructure*, Seminar, IEEE Distinguished Lecture, National Institute for Materials Science, Tsukuba/ Japan, 27.8.13 (2013).
240) R. Schaefer, *Magneto-optical analysis of magnetic microstructure*, International Symposium on Electrodynamics and Mechatronic Systems (SELM 2013), IEEE Distinguished Lecture, Zawiercie/ Polen, 16.5.13 (2013).
241) H. Schloerb, *Electrodeposition of magnetic nanowires within nanoporous templates*, Seminar des Instituts fuer Fluiddynamik, TU Dresden, 24.4.13 (2013).
242) H. Schmidt, *Microacoustic fluid actuators*, 5th International Workshop on Novel Developments and Applications in Sensor and Actuator Technology; ISAT, Coburg, 18.-20.9.13 (2013).
243) O.G. Schmidt, *Strain-tunable nanomembrane-based single quantum dot devices*, Sino-Germany Solid-State Quantum Information Symposium, Wuerzburg/ Germany, 16.-20.9.13 (2013).
244) O.G. Schmidt, *Rolled-up integrative bioanalytic microsystem for a single cell*, Kuratoriumssitzung VW Stiftung, Schloss Herrenhausen, Hannover/ Germany, 4.7.13 (2013).
245) O.G. Schmidt, *Nanomembranes: Shaping a new nanoworld*, Seminar, The Hongkong Polytechnic University, Hongkong/ China, 7.5.13 (2013).
246) O.G. Schmidt, *Rolled-up nanotechnology*, International Conference on Ultimate Integration on Silicon (ULIS), University of Warwick/ England, 19.-21.3.13 (2013).
247) O.G. Schmidt, *Stretching and shaping inorganic nanomembranes: From tunable single photon sources to nanorobotics*, Colloquium „Optik und Kondensierte Materie“, University of Bonn/ Germany, 18.6.13 (2013).
248) O.G. Schmidt, *Nanomembranes for electronic, magnetoelectronic and photonic applications*, The Ninth International Nanotechnology Conference on Communication and Cooperation, Berlin/ Germany, 14.-17.5.13 (2013).
249) O.G. Schmidt, *Forschungsneubau MAIN*, Hauptversammlung, Kompetenznetzwerk für Nanosystemintegration, Chemnitz/ Germany, 12.11.13 (2013).
250) O.G. Schmidt, *Nanomembrane science and technologies*, Joint Symposium of the DFG Research Units FOR 1497, 1713, and 1154 Chemnitz/ Germany, 19.4.13 (2013).
251) O.G. Schmidt, *Nanomembranes: Shaping a new nanoworld*, Physikalisches Kolloquium, University of Leipzig, Leipzig/ Germany, 16.7.13 (2013).
252) O.G. Schmidt, *Thermal conductivity in Ge/Si and nanomembrane superlattices*, International CECAM Workshop „Nanophononics“, Bremen/ Germany, 19.-23.8.13 (2013).
253) O.G. Schmidt, *Shaping nanomembranes into a new nanoworld*, 6th NTT-BRL School, Atsugi, Kanagawa/ Japan, 24.-26.11.13 (2013).
254) O.G. Schmidt, *Electro-elastic single quantum dot devices*, International Symposium on Nanoscale Transport and Technology, NTT Atsugi R and D Center, Kanagawa/ Japan, 26.-29.11.13 (2013).
255) O.G. Schmidt, *Photonics with deformable nanomembranes*, International Workshop of Functional Nanomaterials, City University of Hongkong, Hongkong/ China, 6.-9.5.13 (2013).
256) O.G. Schmidt, *Quantum dots: From growth to quantum devices*, 6th NTT-BRL School, Atsugi, Kanagawa/Japan, 24.-26.11.13 (2013).
257) L. Schultz, *Superconducting levitation on a permanent magnet track - The SupraTrans Test Facility*, Half Plenary Talk, Joint European Magnetic Symposia (JEMS 2013), Rhodes/ Greece, 25.-30.8.13 (2013).

258) L. Schultz, *Von der Schwebenden Dampflok zu SupraTrans II - Die supraleitende Schwebetechnologie und moegliche Anwendungen*, 34. Adelbodener Werkstoffseminar des Instituts fuer Angewandte Materialien, Karlsruher Institut fuer Technologie (KIT), Adelboden/ Switzerland, 21.3.13 (2013).
259) L. Schultz, *High temperature superconductors for magnetic suspension - The SupraTrans Test Facility*, Kolloquium „Aktuelle Herausforderungen in der Materialphysik", Universitaet Goettingen, Goettingen, 24.5.13 (2013).
260) L. Schultz, *Bulk YBaCuO high temperature superconductors for superconducting suspension*, Plenary Talk, 3rd International Conference on Rare Earth Materials (REMAT 2013), Wroclaw/ Poland, 26.-28.4.13 (2013).
261) L. Schultz, *Schweben auf Magnetfeldern*, Innovationslunch Supraleitung, Verkehrshaus der Schweiz, Luzern/ Switzerland, 8.2.13 (2013).
262) L. Schultz, *Schweben auf Magnetfeldern - Supraleitende Schwebetechnik fuer den Transport von Personen und Guetern*, Institutsseminar, Institut fuer Foerdertechnik und Kunststoffe, TU Chemnitz, Chemnitz, 11.01.13 (2013).
263) L. Schultz, D. Berger, *SupraTrans II - Die supraleitende Schwebetechnologie und moegliche Anwendungen*, 11. Dresdner Sensor-Symposium, Dresden, 9.-10.12.13 (2013).
264) L. Schultz, D. Berger, *SupraTrans II - Die supraleitende Schwebetechnologie und moegliche Anwendungen*, Veranstaltung „Wissenschaft trifft Industrie", Bundesverband mittelstaendische Wirtschaft e.V., Dresden, 1.10.13 (2013).
265) L. Schultz, D. Berger, *The SupraTrans Test Facility at Dresden - Superconducting suspension for urban transportation*, Sonderveranstaltung des Netzwerks Korea der Stadt Dresden, Dresden, 24.7.13 (2013).
266) L. Schultz, S. Fleischer, *Die supraleitende Schwebebahn*, Sonderveranstaltung „After Dark -Mathe, Musik und Cocktails", Phaeno Wolfsburg, Wolfsburg, 23.5.13 (2013).
267) L. Schultz, S. Fleischer, *Die wundersame Welt der Supraleitung - Die supraleitende Schwebetechnologie und moegliche Anwendungen*, Internes Seminar, Phaeno Wolfsburg, Wolfsburg, 23.5.13 (2013).
268) L. Schultz, A. Kirchner, *Energy-efficient transportation by superconducting suspension*, 2nd International Conference on Materials for Energy 2013, Plenary Talk, Karlsruhe, 12.-16.5.13 (2013).
269) L. Schultz, A. Kirchner, *Vom Schweben auf Magnetfeldern - die supraleitende Schwebetechnologie und moegliche Anwendungen*, Colloquium Humanum e.V., Forum für Internationale Begegnung, Wissenschaftszentrum Bonn, Bonn, 20.6.13 (2013).
270) L. Schultz, A. Kirchner, *Zum Schweben auf Magnetfeldern - Die wundersame Welt der Supraleitung*, 10. Industriegespraech Chemnitz / Jena, DPG-Arbeitskreis Industrie und Wirtschaft, Jena, 4.9.13 (2013).
271) L. Schultz, J. Thielsch, *Supraleitende Schwebesysteme*, Verein Johannstadthalle, Dresden, 24.10.13 (2013).
272) M. Stoica, *Soft magnetic Fe-based amorphous and (nano)composite alloys with very good mechanical properties*, Eingeladener Vortrag bei TMS Tagung, San Antonio/ USA, 3.-7.3.13 (2013).
273) M. Stoica, *Fe-based bulk metallic glasses, properties and possible applications*, Soft Magnetic Materials Conference (SMM 21), Budapest/ Hungary, 1.-4.9.13 (2013).
274) M. Stoica, J. Bednacik, G. Vaughan, I. Kaban, J. Eckert, *Fe-based bulk metallic glasses with enhanced plastic deformation*, ISMANAM 2013, Torino/ Italy, 30.6.-5.7.13 (2013).
275) M. Stoica, I. Kaban, J. Bednarcik, G. Vaughan, J. Eckert, *Fe-based bulk metallic glasses with enhanced plastic deformation*, The 8th International Conference on Processing and Manufacturing of Advanced Materials THERMEC 2013, Las Vegas/ USA, 2.-6.12.13 (2013).
276) M. Stoica, A.H. Tagvaei, P. Kollar, J. Fuezer, J. Eckert, *FeNiMoPCB and CoFeTaB bulk metallic glasses and composites, preparation and properties*, Amorphous and Nanocrystalline Magnetic Materials (ANMM), Sendai/ Japan, 30.9.-4.10.13 (2013).
277) S. Vock, *Revealing local magnetization structures by quantitative magnetic force microscopy*, Seminarvortrag in der Arbeitsgruppe Materialphysik, Universitaet Uppsala/ Schweden, 3.6.13 (2013).
278) T. Volkmann, W. Loeser, J. Gao, J. Strohmenger, S. Reutzel, *Phase selection in undercooled Nd-Fe-B alloy melts*, TMS 2013, San Antonio, Texas/ USA, 2.-7.3.13 (2013).
279) S. Wicht, V. Neu, L. Schultz, B. Rellinghaus, *Influence of the local atomic structure on the magnetic properties of particulate FePt-X films*, HGST - A Western Digital Company, San Jose/ USA, 28.3.13 (2013).
280) U. Wolff, K. Zuzek Rozman, S. Arshad, N. Kostevsek, S. Kobe, V. Neu, *Magnetization behaviour in CoPt nanowires and -tubes*, Facultad de Ingenieria de la Universidad de Buenos Aires/ Argentina, 8.-21.3.13 (2013).
281) A.U.B. Wolter, *Magnetic frustration in a quantum spin chain: The case of linarite PbCuSO4(OH)2*, DPG Tagung 2013, Regensburg, 11.-15.3.13 (2013).
282) T.G. Woodcock, G. Hrkac, Q. Ramasse, T. Schrefl, O. Gutfleisch, *Interfaces at the atomic scale in Nd-Fe-B permanent magnets*, Symposium: Magnetic Materials for Energy Applications III at theTMS Annual Meeting 2013, San Antonio/ USA, 4.-7.3.13 (2013).
283) S. Wurmehl, *Thermoelectric Heusler materials*, Universitaet Hamburg, Hamburg, 22.8.13 (2013).
284) S. Wurmehl, *Single crystal growth and characterization of superconducting LiFeAs and its substitution variants*, JEMS, Rhodos/ Greece, 26.-30.8.13 (2013).
285) S. Wurmehl, *Single crystal growth and characterization of superconducting LiFeAs and its substitution variants*, 3CG Conference 2013, Cancun/ Mexico, 10.-15.6.13 (2013).
286) C. Yan, *Nanomembranes for energy storage*, Seminar, Soochow University, Suzhou/ China, 7.9.13 (2013).
287) E. Zallo, *Strain-induced active tuning of the coherent tunneling in quantum dot molecules*, Seminar, University of Rome Tor Vergata, Rome/ Italy, 11.10.13 (2013).

Calls and Awards

Calls on Professorships

Prof. Dr. Bernhard Holzapfel	KIT Karlsruhe
Dr. Jens Freudenberger	TU BA Freiberg
Dr. Sabine Wurmehl	Univ. Cologne

Appointments as Adjunct, Honorary, Deputy and Associated Professorships

Prof. Dr. Mark Rümmeli	Sungkyunkwan Univ., Seoul, Korea (Adjunct Professorship)
Prof. Dr. Arnulf Möbius	TU Chemnitz (Adjunct Professorship)
Prof. Dr. h. c. Rolf Pfrengle	STU Bratislava (Honorary Professorship)
Prof. Dr. Martin Knupfer	TU Dresden, (Deputy Professorship)
Prof. Dr. Jens Freudenberger	Bergakademie TU Freiberg, (Deputy Professorship)
Ass. Prof. Dr. Mariana Calin	Univ. Timisoara, Rumania (Associated Professorship)
Ass. Prof. Dr. Mariana Calin	Univ. Bucharest, Rumania (Associated Professorship)
Ass. Prof. Dr. Mihai Stoica	Univ. Timisoara, Rumania (Associated Professorship)

Awards

Prof. Dr. Jürgen Eckert	ERC Advanced Grant
Dr. Carmine Ortix	ERC FET young researcher grant
Dr.-Ing. David Geißler	Manfred Hirschvogel Prize of the Frank Hirschvogel Foundation
Johannes Gleinig	Winner of the MatWerk Short Film Competition of the DGM Junior Forum 2013 in Bochum
Jan Engelmann	Best young researchers presentation at EUCAS 2013 in „Materials“
Dr. Kristina Tschulik	Junior Research Award of the Leibniz Association for the outstanding PhD thesis on „Electrochemical Deposition of Metallic Layers and Structures in Magnetic Gradient Fields“
Christin Scheunert	Best graduation as chemical laboratory assistant in Saxony 2012/13
Marco Naumann	Best graduation as physical laboratory assistant in Saxony 2012/13
Marco Naumann	German wide best graduation as physical laboratory assistant
IFW Dresden	Appreciation award as Distinguished Professional Training Company 2013

IFW Awards

Dr. Jochen Geck	IFF Research Award 2013
Dr. Heike Schlörb	IMW Research Award 2013
Dr. Margitta Uhlemann	IKM Research Award 2013
Dr. Chenglin Yan	IIN Research Award 2013
Dr. Maria Daghofer	ITF Research Award 2013
Dr. Maria Sparing	Tschirnhaus-Medal of the IFW for excellent PhD theses 2013

Patents 2013

Issues of Patents (Publication date of the issue)

DE 10 2012 213 837.4	Seltenerdfreie und korrosionsbeständige Permanent- oder Weichmagnete (28.11.2013) *Inventors:* Markus Gellesch, Silke Hampel, Sabine Wurmehl, Bernd Büchner
DE 10 2012 220 124.6	Multikristallanalysatordetektorsystem für 60 keV (02.10.2013) *Inventors:* Alexander Horst, Andreas Berghäuser, Manuel Hinterstein, Michael Knapp
DE 10 2008 043 751.4	Verfahren zur Herstellung von großen Vesikeln aus selbstorganisierenden, membranbildenden Molekülen (26.09.2013) *Inventors:* Laura Florentiona Steller, Petra Schwille, Heiko Keller, Hagen Schmidt
DE 10 2007 047 874.9	Poröser Formkörper aus Metalloxiden und Verfahren zu seiner Herstellung (08.08.2013) *Inventors:* Min Ha Lee, Kyung Tae Kim, Jürgen Eckert, Daniel Sordelet
DE 10 2011 077 907.8	Verfahren zur Herstellung von gedruckten magnetischen Funktionselementen für Widerstandssensoren und gedruckte magnetische Funktionselemente (11.07.2013) *Inventors:* Daniil Karnaushenko, Denys Makarov, Oliver G. Schmidt
DE 10 2006 024 358.7	Hochfeste, bei Raumtemperatur plastisch verformbare Formkörper aus Eisenlegierungen *Inventors:* Uta Kühn, Ludwig Schultz, Katarzyna Werniewicz
DE 10 2008 054 522.8	Verfahren zur Beschichtung der Oberfläche eines magnetischen Legierungsmaterials sowie ein solches Legierungsmaterial (21.11.2013) *Inventors:* Julia Lyubina, Oliver Gutfleisch, Miheala Buschbeck
US 8,614,534	Transducer having natural unidirectionality for surface acoustic waves (24.12.2013) *Inventors:* Günter Martin, Manfred Weihnacht, Sergey Biryukov, Alexander Darinski, Bert Wall
JP 2007-546060	Semifinished product based on nickel and having a cubic texture and method for the production thereof (06.09.2013) *Inventors:* Jörg Eickemeyer, Bernhard Holzapfel, Horst Wendrock, Dietmar Selbmann
US 8,465,605	Method for the production and use of semi-finished products on the basis of nickel, having a recrystallization cube texture (18.06.2013) *Inventors:* Jörg Eickemeyer, Dietmar Selbmann, Horst Wendrock, Bernhard Holzapfel
EP 2010878	Method for pyrometrically measuring the temperature of the melt material in monocrystal cultivation systems (08.05.2013) *Inventors:* Günter Behr, Friedrich Fischer, Rolf Morgner, Ralf Voigtländer, Alexander Horst
US 8,391,936	Magnetic levitation device (05.03.2013) *Inventors:* Christoph Beyer, Ludwig Schultz, Oliver de Haas, Torsten Riederich
KR 1231936	Nickel-based semifinished product having a cube recrystallization texture, corresponding method of production and use (04.02.2013) *Inventors:* Jörg Eickemeyer, Bernhard Holzapfel, Ralph Opitz, Dietmar Selbmann

Priority Patent Applications

11225 Verfahren und Vorrichtung zur Präparation von Proben für transmissionselektronenmikroskopische Untersuchungen
Inventors: Volker Hoffmann, Vavara Efimova, Jürgen Thomas, Thomas Gemming, Samuel Grasemann, Alexander Horst, Steffen Grundkowski, Ralf Voigtländer, Swen Marke, Michael Analytis

11302 Seltenerdmetallfreie permanentmagnetische Materialien
Inventors: Hannes Stummer, Sabine Wurmehl, Bernd Büchner

11303 Schichtsystem zur Ermittlung von Eigenschaften der Materialien von Funktionsschichten und Verfahren zu seiner Herstellung
Inventors: Sandra Kaufmann-Weiß, Sven Hamann, Sebastian Fähler, Ludwig Reichel, Alfred Ludwig

11307 Dispergatoren und Verfahren zur Abwasseraufbereitung
Inventors: Lluís Soler Turu, Veronika Magdanz, Samuel Sanchez Ordonez, Oliver G. Schmidt

11309 Wellenleiter-Resonator-Bauelement und Verfahren zu seiner Herstellung
Inventors: Stefan Böttner, Oliver G. Schmidt

11313 Wärmetauscher mit Wabenhohlstruktur in Rohrform
Inventors: Tom Marr, Jens Freudenberger, Volker Schubert, Torsten Enders

11314 Akustisches Oberflächenwellenbauelement mit vorwiegend in Ausbreitungsrichtung polarisierten Oberflächenwellen
Inventors: Manfred Weihnacht, Hagen Schmidt, Alexander Darinski

11315 Schweißwerkstoff und Schweißverbindung
Inventors: Jürgen Eckert, Uta Kühn, Julia Kristin Hufenbach, Gunnar Bürkner, Alexander Fröhlich

11320 Messsonde und Verfahren zu deren Herstellung
Inventors: Volker Neu, Tina Sturm, Denis Pelekhov

11325 Thermoelektrischer Formkörper und Verfahren zu seiner Herstellung
Inventors: Marcel Haft, Markus Gellesch, Silke Hampel, Sabine Wurmehl, Bernd Büchner

11352 Magnetoptik mit strukturierten, unmagnetischen Metallen
Inventors: Robert Brunner, Tim Kaspar, Oliver G. Schmidt, Heidemarie Schmidt

11354 Möbius Resonator Bauelement
Inventors: Shilong Li, Libo Ma, Stefan Böttner, Oliver G. Schmidt

11364 Verfahren zur Herstellung von massiven Kalibrationsproben für die analytische Spektrometrie
Inventors: Volker Hoffmann, Sven Donath, Harald Merker

PhD and diploma/master theses

PhD theses

Anja Backen	Epitaktische Schichten der Formgedächtnislegierung Ni-Mn-Ga für die Anwendung in Mikrosystemen, TU Dresden
Denise Beitelschmidt	Verformungsinduzierte Erhöhung der Plastizität einer amorphen quaternären Zirkonbasislegierung, TU Dresden
Ganna Butenko	Phenomenological theory of chiral states in magnets with Dzyaloshinskii-Moriya interactions, TU Dresden
Claudia Hengst	Magnetisierungsdynamik weichmagnetischer Dünnschichten mit modifizierter magnetischer Mikrostruktur, TU Dresden
Andreas König	Charge-Density Waves and Collective Dynamics in the Transition-Metal Dichalcogenides: An Electron Energy-Loss Study, TU Dresden
Santosh Kumar	Tuning of single semiconductor quantum dots and their host structures via strain and in situ laser processing, TU Chemnitz
Oleg Mityashin	Magnetic heat transport in low-dimensional quantum spin systems, TU Dresden
Stefan Philippi	The Mechanical Response of Individual Ferromagnetic Nanowires in Applied Fields, TU Dresden
Darius Pohl	Untersuchung der oberflächennahen Gitterstruktur und Grenzflächen metallischer Nanopartikel mittels aberrationskorrigierter hochauflösender Transmissionselektronenmikroskopie, TU Dresden
Friedrich Roth	Electronic structure of selected aromatic hydrocarbon systems investigated with electron energy-loss spectroscopy, TU Dresden
Christian Rudisch	Nucleaar Magnetic Resonance on Selected Lithium Based Compounds, TU Dresden
Ken Sakaushi	On Design for Electrochemical Energy Storage MaterialsChemistry, TU Dresden
KaiKai Song	Synthesis, microstructure and deformation mechanisms of CuZr-based bulk metallic glass composites, TU Dresden
Maria Sparing	Integration von gasphasenkondensierten Nanopartikeln in YBa2Cu3O7 -Multilagen, TU Dresden
Anna Svitova	Mixed-Metal Clusterfullerenes: New Structures and New Challenges, Univ. Jena
Franziska Thoss	Amorphe, Al-basierte Anodenmaterialien für Li-Ionen-Batterien, TU Dresden
Uhland Weißker	Synthesis and mechanical properties of iron-filled carbon nanotubes, TU Dresden
Yang Zhang	Metal Nitride Cluster as a Template to Tune the Electronic and Magnetic Properties of Rare-Earth Metal Containing Endohedral Fullerenes, Univ. Jena
Na Zheng	Ni-free Ti-based Bulk Metallic Glasses: Glass Forming Ability and Mechanical Behavior, TU Dresden
Markus Herklotz	Elektrochemische und strukturelle Untersuchungen von Li3Cr2(PO4)3 als Hochvolt-Kathodenmaterial in Lithiumionenbatterien, TU Dresden

Habilitation

Jens Freudenberger	Hochfeste Leitermaterialien auf Kupferbasis

Diploma and Master theses

Florian Bittner	Einfluss der Zusammensetzung auf Eigenschaften und Gefügeentwicklung von Cu-Ag-Zr-Legierungen, TU Dresden
Fabian Dittrich	Mikrostrukturelle, magnetische und mechanische Charakterisierung von metallischen Gläsern auf Co-, Fe- und FeNi-Basis, TU Dresden
Christoph Flache	Konzeption einer Anlage zur Herstellung von metallischem Glas in Granulatform in geschützter Gasatmosphäre, HTW Dresden
Johannes Gleinig	Einfluss verschiedener Abkühlbedingungen auf das Gefüge und die mechanischen Eigenschaften eines Fe-Cr-V-C-Gusswerkstoffes, TU Dresden
Daniel Gruner	Aufbau eines AC-Suszeptometers zur Charakterisierung neuartiger Hochtemperatursupraleiter, TU Dresden
Patrick Herre	Dekoration der Oberflächen von Ti-Nb-Legierungen mit Au-Nanopartikeln zur Steigerung der Biofunktionalität, TU Dresden
Abd-ur-Rehman Jalil	Study of Electrical Properties in Metal CoPc Structures by means of CS-AFM, TU Chemnitz
Toni Jaumann	Synthese und Charakterisierung von intermetallischen kohlenstoffumhüllten Nanopartikeln, TU Dresden
Jiaqi Jia	Herstellung und Charakterisierung amorpher Si-Legierungen für Li-Ionen-Batterien, TU Dresden
Varun John	Evaluation of electrically active defects in Vanadium dioxide-Silicon dioxide-p-Silicon diodes, TU Chemnitz
Franziska Karnbach	Elektrochemische Abscheidung von Bu und CuBi-Legierungen in überlagerten magnetischen Gradientenfeldern
Kati Kühnel	Elektrochemische Präparation von Absorptionsschichten für pyroelektrische Infrarotdetektoren, TU Dresden
Michael Mietschke	Korrelation zwischen strukturellen und ferroelektrischen Eigenschaften epitaktischer PMN-PT Schichten, TU Dresden
Theresa Moebus	Photoelektronenspektroskopie an dotierten Strontiumtitanat-Oberflächen, TU Bergakademie Freiberg
Ioannis Paschos	Scanning Tunneling Microscopy of Topological Insulators, TU Dresden
Laura Restrepo Perez	Trapping biofunctionalized micromotors fort he transport and confinement of biological targets, TU Chemnitz
Stefan Pilz	Thermomechanische Behandlung von Ti-40Nb zur Verbesserung der Biofunktionalität, TU Dresden
Fabian Rhein	Direkte Bestimmung physikalischer Eigenschaften supraleitender Materialien mittels Entfaltung magnetkraftmikroskopischer Bilddaten, TU Dresden
Jan Sander	Herstellung sowie strukturelle und mechanische Charakterisierung von magnesiumbasierten Glasmatrix-AlSi Verbunden, TU Dresden
Benjamin Schleicher	Dünne epitaktische DyCo-Schichten mit magnetischer Kompensation, TU Dresden
Frank Schmidt	Optimierung des Lichtofens für das optische Heizen von Nanopartikeln im Flug und seine Anwendung bei der Herstellung von Nd-Fe-B-Partikeln, TU Dresden
Maik Scholz	Mn3Ga gefüllte CNT: Synthese und Charakterisierung, TU Dresden
Max Sieger	Einfluss von PLD-Prozessparametern auf die supraleitenden und strukturellen Eigenschaften dotierter YBa2Cu3O7-d-Schichten, TU Dresden
Holger Schwab	Charakterisierung von Titan und der Legierung Ti-45Nb hergestellt mittels selektiven Laserstrahlschmelzens, TU Dresden
Wei Wan	Materialwissenschaftliche Untersuchung von Al-Ge Legierungsschmelzen: Dichte, Oberflächenspannung und Benetzungsverhalten an keramischen Substraten, TU Dresden

Scientific conferences and IFW colloquia

Conferences

526. WE Heraeus Seminar "Functional Magnetic Nanomembranes", March 4-6, 2013, Bad Honnef, Germany
BioTiNet Workshop „Biomaterials for Orthopaedic Applications", June 26-28, 2013, Neuchâtel, Switzerland
Summer School Spectroelectrochemistry 2013, August 23-30, 2013, IFW Dresden, Germany
Workshop „Electronic properties of spin-orbit driven oxides" September 4 -7, 2013, IFW Dresden
B1.II symposium "Metallic Glasses and their Composites", September 8-13, 2013, EUROMAT in Seville, Spain
International LOTHERM Workshop quantum magnets, September 9-13, 2013, Kolymbari, Crete
Workshop „Bridging the Scale in Glasses II" October 21-23, 2013, Dresden, Germany
International Workshop „Computational exploration of atomistic structures and interrelation with physical properties" and Tutorial „hands-on-FPLO", November 4-8, 2013, IFW Dresden, Germany

IFW Colloquium 2013

Prof. Dr. C. James Kirkpatrick, Institute of Pathology University Medical Center Johannes Gutenberg University, 17.01.2013, Cell-biomaterial interactions in Regenerative Medicine: a major challenge for the life sciences

Prof. Dr. Jens Gutzmer, Helmholtz-Zentrum Dresden-Rossendorf, 31.01.2013, Geometallurgy - how to efficiently use complex materials

Prof. O./J. Moravcik/ Janovec, Slovakisch Technische Universität Trnava, 05.12.2013, Ion Beam Technology - a New Facility of Materials Research at MTF STU

Prof. Joerg Weißmüller, TU Hamburg-Harburg, 12.12.2013, Hybrid Nanomaterials for Strength and Function

Prof. Markus Antonietti, Max-Planck-Institut für Kolloid- und Grenzflächenforschung Potsdam-Golm, 19.12.2013, Porous C, N - Materials for Energy Application

IFF Seminar

Dr. Matthias Frontzek, Paul Scherrer Institut, 16.01.2013, The multiferroic, geometric frustrated CuCrO2 compound: interlayer exchange and chirality

Prof. Lambert Alff, TU Darmstadt, 16.01.2013, Novel and metastable arsenic free pnictide superconductors synthesized by reactive molecular beam epitaxy

Dr. Francis Avilés, Yucatan Center for Scientific Research, 14.02.2013, Strain and damage sensing in carbon nanotube/ polymer composites

Dr. Nenad Lazarevic, Center for Solid State Physics and New Materials University of Belgrade, 18.03.2013, Raman scattering study of KxFe2-ySe2 single crystals

Prof. Andrea Damascelli, University of British Columbia, 07.03.2013, From p-wave supercounductors to relativistic-Mott insulators via spin-orbit interaction in solids

Dr. Thomas Lorenz, Universität zu Köln, 12.04.2013, Monopole heat transport and anomalous hysteresis effects in spin ice

Prof. Dr. Ingrid Mertig, Martin-Luther-Universität Halle-Wittenberg, 29.04.2013, Spin Hall and Spin Nernst Effect

Prof. Oliver Rader, Helmholtz-Zentrum Berlin, 06.05.2013, Band gap opening in graphene and topological insulators

Dr. Bastien Dassonneville, LPS Orsay, 15.05.2013, Probing the Dynamics of Andreev States in a Coherent Normal metal/ Superconducting ring

Dr. Giuseppe Cirillo, Università della Calabria, 03.06.2013, Functional hybrid nanomaterials: Innovative therapeutics with high efficiency and biocompatibility

Dr. Andreas Heinrich, IBM Research, 10.06.2013, The quantum and classical properties of spins on surfaces

Prof. Dr. Elke Dopp, Universität Duisburg-Essen, 01.07.2013, Toxicological aspects of carbon nanotubes

Prof. Maria Kavallaris, Children's Cancer Institute Australia for Medical Research Lowy Cancer Research Centre, UNSW, 06.09.2013, Nanomedicine strategies for cancer

Dr. Kinshuk Dasgupta, Bhabha Atomic Research Centre, 16.09.2013, Fluidized bed synthesis of carbon nanotubes

Dr. Nikolai Zhigadlo, Laboratory for Solid State Physics ETH Zurich, 19.12.2013, Crystal growth under extreme conditions

IMW Seminar

Prof. Markus Rettenmayr, Institut für Materialwissenschaft und Werkstofftechnologie, 10.01.2013, Legierungsentwicklung mit modernen Werkzeugen

Prof. Petr Šittner, Institute of Physics of the ASCR, 24.01.2013, Revealing deformation mechanisms in Shape Memory Alloys by in-situ X-ray and neutron diffraction methods

Prof. Uwe Glatzel, Metallische Werkstoffe Universität Bayreuth, 31.01.2013, Modeling the Influence of Oxidation on Single Crystal Thin-Walled Specimens

Prof. Norbert Esser, Leibniz - Institut für Analytische Wissenschaften, 11.04.2013, Surface Structure Analysis by Optical Spectroscopy: Semiconductor Surfaces, Atomic Nanowires

Prof. Alexander Brosius, TU Dresden, Professur „Formgebende Fertigungsverfahren", 25.04.2013, Moderne Umformtechnik – von ungewöhnlichen Verfahren bis zur Werkstoffcharakterisierung

Prof. Horst Hahn, Institute for Nanotechnology Karlsruhe Institute of Technology, 30.05.2013, Nanogläser

Prof. Koki Takanashi, Tohoku University, 01.07.2013, Advanced spintronic materials for generation and control of spin current

Prof. Frank Mücklich, Lehrstuhl für Funktionswerkstoffe Universität des Saarlandes, 04.07.2013, Wie wir das Werkstoffgefüge besser verstehen - Strukturieren und Charakterisieren auf der Mikro-, Nano- und atomaren Skala

Prof. Matthias Beller, Leibniz-Institut für Katalyse, 11.07.2013, Katalyse - Eine Zukunftstechnologie für nachhaltige chemische Produktion und umweltfreundliche Energietechnologien

Prof. Georg Schmidt, Institut für Physik Martin-Luther-Universität Halle-Wittenberg, 12.07.2013, Tuneable tunnel barriers at interfaces between organic semiconductors and La0.7Sr0.3MnO3

Prof. Michael E. McHenry, Carnegie Mellon University, 19.08.2013, Nanocomposite Magnets for Energy Applications

Prof. Reinhard Pippan, Erich Schmid Institute of Materials Science, 24.10.2013, Mechanical alloying by Severe Plastic Deformation

Prof. Klaus Leifer, Laboratory of Electron Microscopy and Nanoengineering Uppsala University, 21.11.2013, Analysing dichroism in magnetic samples in the TEM

Prof. Adekunle Adeyeye, National University of Singapore, 11.12.2013, Artificial Ferromagnetic Nanostructures: An Experimental Platform for Magnonics

Dr. Jens Freudenberger, IFW Dresden, 19.12.2013, Weihnachtsvorlesung

IKM Seminar

Dr. Joao Amaral, Universidade de Aveiro, 30.01.2013, Thermodynamic models in the study of non-equilibrium and disorder effects in giant magnetocaloric materials

Prof. Dr. Ingrid Fritsch, University of Arkansas, 26.03.2013, Redox-Magnetohydrodynamic Microfluidics

Dr. Sascha Gruner, Institut für Physik TU Chemnitz, 05.04.2013, Methodische Aspekte der Viskositätsmessung mit dem Schwingtiegelverfahren

Prof. Steffen Strehle, Universität Ulm, 29.05.2013, Exploring Life at the Nanoscale with Silicon Nanoprobe Devices

Dr. Jan Macak, Department of General and Inorganic Chemistry University of Pardubice, 20.06.2013, Nanostructured anodic templates for advanced materials

Prof. Dr. Ulrich Häussermann, Department of Materials and Environmental Chemistry Stockholm University, 17.07.2013, Materials from high pressure synthesis - challenges and opportunities

Dr. Jiri Orava, University of Cambridge and Tohoku University, 11.09.2013, Chalcogenide glasses: applications in photonics and solid-state memory

Prof. J. Dutkiewicz, University of Kraków, 10.10.2013, Structure of aluminum matrix composites strengthened with Al base or CuZr base amorphous particles

Dr. L. Rogal, Institute of Metallurgy and Materials Science Polish Academy of Science, 10.10.2013, Semi-solid processing technology of X210CrW12 tool steel and its effect on deformation mechanism and mechanical properties

Prof. Dietrich Stoyan, TU Bergakademie Freiberg, 22.10.2013, On two conjectures for random close packing of spheres

Dr. Bernd Müller, Friedrich-Schiller-Universität Jena, 23.10.2013, Symmetrie und Topologie als Brücken zwischen den Skalen kondensierter Materie"

Prof. Upadrasta Ramamurty, Indian Institute of Science Bangalore, 22.11.2013, Fracture in amorphous alloys

IIN Seminar

Dr. Mark Rümmeli, IFW Dresden, 18.01.2013, Engineering sp2 carbon nanostructures with electrons

Dr. Leonid Ionov, Leibniz-Institut für Polymerforschung Dresden, 01.02.2013, Soft microorigami: shape-programmed folding of stimuli-responsive polymer films

Prof. Dr. Arno Ehresmann, Institut für Physik und Centre for Interdisciplinary Nanostructure Science and Technology, 22.02.2013, Static and dynamic local magnetic fields for positioning and controlled movement of small objects

Prof. Val Zwiller, TU Delft, 01.03.2013, Quantum Optics with Nanowires

Dr. Sven M. Ulrich, Universität Stuttgart, 15.03.2013, Resonance Fluorescence of a Single Quantum Dot: Photon Statistics and Coherence Properties of 'Dressed State' Emission"

Dr. Sven Höfling, Universität Würzburg, 28.03.2013, An electrically pumped polariton laser

Dr. Peter Fischer, Lawrence Berkeley national Laboratory, 04.06.2013, Soft-X-ray microscopy:
Facing the mesoscale challenge in magnetism

Dr. Moussa Barhoum, University of Utah, 12.04.2013, Rapid and Versatile Fabrication of High-Quality Thin Fiom One-Dimensional Optical Band Gap Materials on Planar and Curved Substrates using Sol-Gel Chemnistry

Dr. Klaus Mathwig, Nanoionics Group MESA+Instittue for Nanotechnology University of Twente, 17.04.2013,
Electrical Spectroscopy in Nanofluidic Channels

Prof. Dr. Mathias Kläui, Institut für Physik Johannes Gutenberg-Universität Mainz, 26.04.2013, Ultra-fast domain wall dynamics

Natalia Ares, CEA-INAC/UJF-Grenoble, 03.05.2013, SiGe self-assembled nanostructures for quantum spintronics

Dr. Lifeng Liu, International Iberian Nanotechnology Laboratory, 24.05.2013, Nanostructures for Solar Hydrogen Production and Electrochemical Energy Storage

Dr. Yongheng Huo, IFW Dresden, 21.06.2013, Growth of Novel GaAs QDs in AlGaAs Matrix

Dr. Lothar Ratschbacher, Institut für Angewandte Physik Universität Bonn, 17.07.2013, Cavity QED with single atoms and small atomic ensembles

Prof. Ferdinand Scholz, Institut für Optoelektronik Universität Ulm 07.08.2013, Semipolar GaN for optoelectronic applications

Svetlana Zakharchenko, Leibniz Institute of Polymer Research Dresden, 30.08.2013, Self-rolled polymer tubes for cell encapsulation and potential bio-applications

Dr. Ingrid Graz, Soft Matter Physics Johannes Kepler University, 06.09.2013, Approaches to electronic skin

Prof. Nicola Pinna, Humboldt-Universtität Berlin, 20.09.2013, Non-aqueous Sol-gel Routes to Nanostructured Functional Materials

Dr. Weibo Gao, Quantum Photonics Group ETH Zürich, 11.10.2013, Quantum Teleportation from a Propagating Photon to a Solid-State Spin Qubit

Prof. Dr. Roger Wördenweber, Peter Grünberg Institute and JARA-Fundamentals of Future Information Technology FZ Jülich, 18.10.2013, Functional Oxides: From Multiferroic to Fluxonic Concepts

Prof. Dr. Jochen Guck, TU Dresden, 25.10.2013, The mechanical properties of cells and tissues – does soft matter?

Dr. Rainer F. Mahrt, IBM Research Zurich, 08.11.2013, Bose-Einstein condensation of exciton-polaritons in a polymer filled microcavity at room temperature

Dr. Andrii Chumack, TU Kaiserslautern, 29.11.2013, Magnons as an alternative to a charge current

ITF Seminar

Dr. Alexander Yaresko, Max-Planck-Institut für Festkörperforschung, 28.01.2013, Unexpected behaviour of magneto-crystalline anisotropy in Fe-pnictides

Dr. Valerii Vinokour, Argonne National Laboratory, 31.01.2013, Superconductor-Superinsulator Duality: Experiment and Theory

Ekaterina Plotnikova, Moscow Institute of Physics and Technology, 06.02.2013, Magnetization processes in hard magnetic crystals and exchange-coupled composite nanostructures

Prof. Jürgen Kübler, TU Darmstadt, 01.03.2013, The Berry Curvature: Challenges in Electronic Structure

Dumitru-Claudiu Sergentu, Zernike Institute for Advanced Materials University of Groningen, 25.03.2013, Revisiting the Intersystem Crossing in Benzophenone

Prof. Dr. Maxim Mostovoy, Zernike Institute for Advanced Materials University of Groningen, 10.04.2013, Stripe domain states and Yukawa forces in frustrated magnets

Prof. Dr. Alexei Bogdanov, IFW Dresden, 06.05.2013, Why do skyrmions exist in nanolayers of cubic helimagnets?:
Theory of confined chiral modulations

Dr. Mike E. Zhitomirsky, CEA Grenoble, 17.05.2013, Multipolar phases in frustrated magnets

Dr. Masaaki Nakamura, Max-Planck-Institut for Solid State Research, 31.05.2013, One-dimensional lattice model with an exact matrix-product ground state describing the Laughlin wave function

Eugen Wolf, TU Dresden, 03.07.2013, Transport in Graphene

Dr. Peter Barmettler, Dept. of Theoretical Physics University of Geneva, 15.07.2013, Quantum dynamics far from equilibrium:
Spreading and relaxation of correlations in a bosonic Mott insulator

Dr. Jasper van Wezel, University of Bristol, 16.07.2013, NbSe2 as a prototypical strong-coupling charge ordered material

Dr. Jasper van Wezel, University of Bristol, 18.07.2013, Chiral charge order

Prof. Dr. Giniyat Khaliullin, Max-Planck-Institut for Solid State Research, 14.10.2013, Excitonic Magnetism in Van Vleck-type d4 Mott Insulators

Alexander Lau, TU Dresden, 13.11.2013, Topological Surface States in Paramagnetic and Antiferromagnetic Iron Pnictides

Prof. Zvi Ovadyahu, Racah Institute of Physics the Hebrew University, 02.12.2013, Aging and memory effects in the Electron-Glass

Guests and Scholarships

Guest scientists (stay of 4 weeks and more)

Name	Home Institute	Home country
Dr. Apostu, Mircea-Odin	Alexandru Ioan Cuza Univ.	Rumania
Dr. Arayanarakool, Rerngchai	BIOS, Inst. of Nanotechnology Twente	Thailand
Dr. Audebert, Fernando E.	Univ. of Buernos Aires	Argentina
Dr. Bachmatiuk, Alicja	Wroclaw Research Centre EIT	Poland
Dr. Bezkishko, Ilya	A.E. Arbuzov Institute Kazan	Russia
Bonatto Minella, Christian	Helmholtz-Zentrum Geesthacht	Italy
Brzezicki, Wojciech	Jagiellonian Univ. Krakow	Poland
Prof. Cao, Chongde	Northwestern Polytechn. Univ. Xian	China
Dr. Chen, Yao		China
Dr. Chumak, Ihor	Karlsruhe Institute for Technology	Ukraine
Dr. Cirillo, Giuseppe	Univ. of Calabria	Italy
Dr. da Costa, Pedro Miguel Ferreira J.	CICEDO Univ. of Aveiro	Portugal
Dr. Darinskiy, Alexander	Institute for Crystallography Moscow	Russia
Dr. Dey, Tusharkanti	Indian Institute of Technology Bombay	India
Enachi, Mihai	Technical Univ. of Moldova, Chisinau	Moldavia
Gaididei, Yuri	Inst. for Theoretical Physics, Kiev	Ukraine
Dr. Galano, Marina	Univ. Oxford	Italy
Dr. Gammer, Christoph	Univ. Wien	Austria
Prof. Dr. Garifullin, Ilgiz	Zavoisky Physical-Technical Inst. Kazan	Russia
Giussani, Ester	Center for Nanoscience and Techn. Milano	Italy
Dr. Grüneis, Alexander	Univ. Wien	Austria
Dr. Guix Noguera, Maria	Catalan Inst. of Nanotechnology (ICN)	Spain
Dr. Haindl, Silvia	Univ. Tübingen	Austria
Prof. Dr. Hirschfeld, Peter Joseph	Univ. of Florida	USA
Hynowska, Anna Paulina	Univ. Autonoma de Barcelona	Spain
Dr. Jiang, Chongyun	Inst. of Semiconductors Beijing	China
Dr. Johnston, Steven S.	Univ. of British Columbia	Canada
Jung, Hyoyun	Yonsei Univ.	South Korea
Dr. Jung, Hyoyun	Yonsei Univ.	South Korea
Dr. Jung, Kyubong	Univ. of Tokyo, Japan	Japan
Dr. Kataeva, Olga	A.E. Arbuzov Inst. Kazan	Russia
Prof. Dr. Kikoin, Konstantin	Univ. Tel-Aviv	Israel
Dr. Kim, Hee Dae	Univ. of Oxford	South Korea
Kravchuk, Volodymyr	Bogolyubov Institute for Theoretical Physics Kiev	Ukraine
Dr. Kvitnytska, Oksana	Inst. for Low Temperature Physics & Engineering Kharkov	Ukraine
Lamrani, Sabrina	Nuclear Research Centre of Algiers	Algeria
Dr. Leksin, Pavel	Kazan Physical Technical Institute	Russia
Prof. Lishchynskyy, Igor	Precarpathian National University Ivano-Frankivsk	Ukraine
Dr. Liu, Xianghong	Nankai Univ. Shandong	China
Dr. Liu, Zhonghao	Renmin Univ. Beijing	China
Dr. Lukes, Vladimir	Slov. Univ. of Technology Bratislava	Slovakia
Machata, Peter	Slov. Univ. of Technology, Bratislava	Slovakia
Dr. Martinez C., Cynthia S.		Mexico
Melchiors Gilberto	Federal Univ. of Rio Grande do Norte	Brazil
Dr. Miao, Shiding	Hefei Univ. of Technology	China
Dr. Mohamed, M. Abdelhafez		Egypt
Dr. Morozov, Igor	Moscow State Univ.	Russia

Moscoso, L. Oscar	From Univ. des Buenos Aires	Columbia
Dr. Naidyuk, Yurii	Inst. for Low Temperature Physics & Engineering Kharkov	Ukraine
Panigrahi, Ajit	Univ. Wien	India
Dr. Rapta, Peter	Slov. Univ. of Technology, Bratislava	Slovakia
Dr. Reja, Sahinur		India
Dr. Romhanyi, Judit	Eötvös Univ. Budapest	Hungary
Roslova, Mariia	State Univ. Moskau	Russia
Rounaghi, Seyyed Amin	Ferdowsi Univ. of Mashhad, Iran	Iran
Rozenberg, Silvia Mirta	Univ.de Buenos Aires	Argentina
Rus, Stefania	Uni. Politehnica Din Timisoara	Rumania
Dr. Seiner, Hanus	Inst. of Thermomechanics, Prag	Czech Rep.
Prof. Dr. Sheka, Denys	Taras Shevchenko National Univ. of Kyiv	Ukraine
Dr. Shima, Toshiyuki	Tohoku Gakuin Univ.	Japan
Prof. Dr. Sidorov, Verlerii	Ural State Pedagogical Univ.	Russia
Dr. Soler Turu, Lluis		Spain
Dr. Vavilova, Evgeniya	Physical-Technical Inst. Kazan	Russia
Volkov, Oleksii	Taras Shevchenko National Univ. of Kyiv	Ukraine
Prof. Dr. Yan, Zhijie	Taiyuan Univ. of Science and Technology	China
Dr. Yao, Xiaoyan	Southeast Univ. Nanjing	China
Dr. Yerin, Yuriy	Institute for Low Temperature Physics & Engineering Kharkov	Ukraine
Dr. Yushankhai, Victor	Joint Inst. for Nuclear Research Dubna	Russia
Dr. Zhang, Lin		China
Dr. Zhang, Yang	Hong Kong Polytechnic University	China
Zhang, Yuan	Fudan Univ. Shanghai	China
Zhu, Bao	Fudan Univ., Shanghai	China
Dr. Zhu, Feng		China

Scholarships

Name	Home country	Donor
Dr. Prando, Giacomo	Italy	AvH Foundation
Prof. Dr. He, Jie	China	AvH Foundation
Dr. Jorgensen, Matthew	USA	AvH Foundation
Fedorchenko, Oleksii	Ukraine	AvH Foundation
Cocemasov, Alexandr	Moldavia	DAAD
Crismari, Dmitrii	Moldavia	DAAD
Prof. Dr. Yakhvarov, Dmitry	Russia	DAAD
Dr. Prando, Giacomo	Italy	DAAD
Dr. Zhao, Jiong	China	DAAD
Ramasamy, Parthiban	India	DAAD
Nowak, Rafal	Poland	DAAD
Kolay, Santa	India	DAAD
Dr. Singh, Shiv Jee	India	DAAD
Dusaev, Renat	Russia	BMBF
Romero da Silva, Murillo	Brazil	CAPES Foundation Brazil
A. Basilio, Leonardo	Brazil	CAPES Foundation Brazil
Wolf, Witor	Brazil	CAPES Foundation Brazil
Yuan, Feifei	China	China Scholarship Council
Prof. Dai, Fuping	China	China Scholarship Council
Dr. Huang, Gaoshan	China	China Scholarship Council

Dr. Wang, Jiao	China	China Scholarship Council
Dr. Mei, Yongfeng	China	China Scholarship Council
Prof. Dr. Yan, Zhijie	China	China Scholarship Council
Ma, Guozhi	China	China Scholarship Council
Zhang, Jiaxiang	China	China Scholarship Council
Pang, Jinbo	China	China Scholarship Council
Song, Kaikai	China	China Scholarship Council
Li, Kefeng	China	China Scholarship Council
Xi, Lixia	China	China Scholarship Council
Lil, Menglin	China	China Scholarship Council
Ma, Pan	China	China Scholarship Council
Ma, Pan	China	China Scholarship Council
Li, Shilong	China	China Scholarship Council
Sun, Xiaolei	China	China Scholarship Council
Lu, Xueyi	China	China Scholarship Council
Yin, Yin	China	China Scholarship Council
Dr. Kim, Beom Hyun	China	China Scholarship Council
Dr. Chang, Ching-Hao	Taiwan	Nat. Science Council of China
Rafique, Mohsin	Pakistan	COMSATS Institute Islamabad
Dr. Zilic, Dijana	Croatia	Croatian Science Foundation
Prof. Dr., Takeshi Tayagaki	Japan	Kyoto Univ.
Rodriguez L., Oscar A.	Columbia	Colciencias
Surrey, Alexander	Germany	Reiner Lemoine Foundation
Auckett, Josie Elise	Australia	Univ. Sydney
Gadgil, Bhushan	India	Aalto Univ.
Hassan, A. Hamdy	Egypt	Egypt

Guest stays of IFW members at other institutes

Stefanos Kourtis	25.03.–26.04.2013, Boston University, Research stay on fractional Chern insulators with strong interactions far exceeding bandgaps
Ritschel Tobias	19.04.–17.05.2013, Brookhaven National Laboratory New York, Brookhaven, USA, Measuring time
Fedorov Alexander	16.05.–17.06.2013, HZB Berlin, Measuring time
Bezkishko Ilya	01.07.–28.08.2013, Univ. Leipzig, research cooperation
Kataev Vladislav	19.04.–12.05.2013, Russian Academy of Sciences Kazan, Russia, Measuring time and research cooperation with the Physical Technical Institute
Fedorov Alexander	18.02.–11.03.2013, Elettra Sincrotrone Trieste, Italy, Measuring time
Dr. Zhonghao Liu	01.10.2013–31.08.2014, HZB Berlin am Bessy II, Deutschland
Dr. Silvia Haindl	09.12.2013–04.01.2014, Tokyo Inst. of Technology, Japan
Dr. Franziska Hammerath	01.07.2012–30.11.2013, Univ. Pavia, Italy, PostDoc stay
Dr. Yulia Krupskaya	01.07.2013–30.06.2015, DPMC Univ. of Geneva, Switzerland
Dr. Carola Langer	15.10.2013–31.01.2014, German Embassy Brasilia, Brazil, Scientific Work Shadowing Program of Leibniz and Foreign Office
Matthias Bönisch	26.05.–22.06.2013, Kath. Univ. Leuven, Belgium, Research stay
Jin Young Kim	09.03.–31.03.2013, Korea Institute of Industrial Technology Seoul, South Korea, Research stay
Dr. Norbert Mattern	15.09.–15.11.13, Institute for Materials Research, Tohoku Univ. Sendai, Japan, Research stay
Jinbo Pang	15.10.–33.11.13, Wuhan Univ., China, Research stay
Lixia Xi	03.04.–02.05.2013; 23.11.–22.12.2013, Foundry Research Institute Krakow, Poland, Research stay
Jan Romberg	22.01.–29.01.2013, research cooperation with Carl Wezel KG, Mühlacker
Robert Niemann	25.02.–08.03.2013, European School of Magnetism, Cargese, Corse
Ludwig Reichel	25.02.–08.03.2013, European School of Magnetism, Cargese, Corse
Dr. Ulrike Wolff	01.06.–10.06.2013, mounting and introduction of a measuring apparatus, Ljubljana, Slowenien
Robert Niemann	08.09.–20.09.2013, research cooperation with the University of Barcelona, Spain
Dr. Ulrike Wolff	07.03.–23.03.2013, cooperation with the University of Buenos Aires, Argentina
Fritz Kurth	02.03.–05.04.2013, stay within the framework of the IronSea project, Nagoya, Japan
Dr. Bernd Rellinghaus	26.03.–07.04.2013, project coordination meetings, San Francisco, USA
Dr. Kazumasa Iida	09.06.–17.06.2013, measurements, Tallahassee, USA
Fritz Kurth	09.06.–17.06.2013, measurements, Tallahassee, USA
Dr. Jens Freudenberger	all-the-year partial deputation to the TU Bergakademie Freiberg
Prof. Rudolf Schäfer	all-the-year lecture tour for IEEE as Distinguished Lecturer, e.g. Taiwan, China, USA, Argentina, Beirut, Russia

Board of trustees

Joachim Linek, Saxonian Ministry of Science and Art - Head -
Dr. Herbert Zeisel, Federal Ministry of Education and Research
Prof. Dr. Bernd Kieback, TU Dresden
Prof. Dr. Konrad Samwer, Univ. Göttingen

Scientific Advisory Board

Up to September 2013
Prof. Dr. Reiner Kirchheim, Univ. Göttingen, Germany -Head-
Prof. Dr. Dominique Givord, Laboratoire Louis Néel, Grenoble, France
Prof. Dr. Alan Lindsay Greer, Univ. of Cambridge, U.K.
Prof. Dr. Rudolf Gross, Walter Meißner Institute Garching, Germany
Prof. Dr. Rolf Hellinger, Siemens AG Erlangen, Germany
Prof. Dr. Max Lagally, Univ. of Wisconsin-Madison, U.S.A.
Prof. Dr. Xavier Obradors Berenguer Univ. Autònoma de Barcelona, Spain
Prof. Dr. Stuart Parkin, IBM Almaden Research Center, San Jose, USA
Prof. Dr. Eberhardt Umbach, Karlsruhe Institute of Technology, Germany
Prof. Dr. Gertrud Zwicknagl, TU Braunschweig, Germany

Starting from October 2013
Prof. Dr. Maria-Roser Valenti, Univ. Frankfurt, Germany -Head-
Prof. Dr. Philippe M. Fauchet, Vanderbilt Univ., USA
Prof. Dr. Matthias Göken, Univ. Erlangen-Nürnberg, Germany
Prof. Dr. Alan Lindsay Greer, Univ. of Cambridge, U.K.
Prof. Dr. Rudolf Gross, Walter Meißner Institute Garching, Germany
Prof. Dr. Rolf Hellinger, Siemens AG Erlangen, Germany
Prof. Dr. Xavier Obradors Berenguer Univ. Autònoma de Barcelona, Spain
Prof. Dr. Roberta Sessoli, Univ. di Firenze, Italy
Prof. Dr. Eberhardt Umbach, Karlsruhe Institute of Technology, Germany

IFW's Research Program 2013

1. Superconductivity and superconductors
1.1 Electronic structure and fundamentals
1.2 Superconducting materials
1 P1 Superconducting transport systems and magnetic bearings
1 P2 YBCO tape conductors

2. Magnetism and magnetic materials
2.1 Theoretical and experimental fundamentals
2.2 Magnetic materials
2.3 Magnetic microstructures
2 P1 High magnetic fields
2 P2 Energy efficient cooling with magnetocaloric materials (Pakt 2010)

3. Molecular nanostructures and molecular solids
3.1 Fullerenes, nanotubes and graphene
3.2 Conducting polymers and organic molecular solids
3.3 Molecular Magnets

4. Metastable alloys
4.1 Phase formation in complex systems
4.2 Corrosion and hydrogen
4.3 Bulk amorphous metals and composite materials
4.4 Electrochemical energy storage systems / Lithium-ion batteries
4 P1 Electrochemical energy storage in autonomous microsystems (Pakt 2011)

5. Stress-driven architectures and phenomena
5.1 3D micro/nanoarchitectures
5.2 Quantum dots
5.3 SAW systems